The role of WASP family members in *Dictyostelium discoideum* cell migration

By Andrew J. Davidson

Submitted in fulfillment of the requirements for the degree of Doctor of Philosophy

The Beatson Institute for Cancer Research

College of Medical, Veterinary and Life Sciences

University of Glasgow

February 2014

Abstract

The WASP family of proteins are nucleation-promoting factors that dictate the temporal and spatial dynamics of Arp2/3 complex recruitment, and hence actin polymerisation. Consequently, members of the WASP family, such as SCAR/WAVE and WASP, drive processes such as pseudopod formation and clathrin-mediated endocytosis, respectively. However, the nature of functional specificity or overlap of WASP family members is controversial and also appears to be contextual. For example, some WASP family members appear capable of assuming each other's roles in cells that are mutant for certain family members. How the activity of each WASP family member is normally limited to promoting the formation of a specific subset of actin-based structures and how they are able to escape these constraints in order to substitute for one another, remain unanswered questions. Furthermore, how the WASP family members collectively contribute to complex processes such as cell migration is yet to be addressed.

To examine these concepts in an experimentally and genetically tractable system we have used the single celled amoeba *Dictyostelium discoideum*. The regulation of SCAR via its regulatory complex was investigated by dissecting the Abi subunit. Abi was found to be essential for complex stability but not for its recruitment to the cell cortex or its role in pseudopod formation. The roles of WASP A were examined by generating a *was*A null strain. Our results contradicted previous findings suggesting that WASP A was essential for pseudopod formation and instead demonstrated that WASP A was required for clathrin-mediated endocytosis. Unexpectedly, WASP A – driven clathrin-mediated endocytosis was found to be necessary for efficient uropod retraction during cell migration and furrowing during cytokinesis. Finally, we created a double *scr*A/*was*A mutant, and found that it was unable to generate pseudopodia. Therefore, we were able to confirm that SCAR is the predominant driver of pseudopod formation in wild-type *Dictyostelium* cells, and that only WASP A can assume its role in the *scr*A null. Surprisingly, the double mutant was also deficient in bleb formation, showing that these proteins are also necessary for this alternative, Arp2/3 complex-independent mode of motility. This implies that there exists interplay between the different types of actin-based protrusions and the molecular pathways that underlie their formation.

Table of Contents

List of Figures

Supplementary Movies

Movie 1: The localisation of the SCAR complex in starved *abi*A nulls co-expressing HSPC300-GFP (green channel) and either full length WT Abi or the ΔAbiΔ fragment. Cells were visualised by TIRF and DIC microscopy.

Movie 2: Arp2/3 complex and F-actin dynamics in wild-type and *was*A null cells chemotaxing towards folate in the under-agarose assay. Cells were co-expressing GFP-ArpC4 (Arp2/3 complex, green channel) and Lifeact-mRFP (F-actin, red channel) and were visualised using spinning disc confocal microscopy

Movie 3: WASP A and CCP dynamics in a cell undergoing cytokinesis. GFP-WASP A (green channel) and CLC-mRFP (Red channel) were co-expressed in the *was*A null. Cells were compressed under an agarose slab and imaged using TIRF and DIC microscopy.

Movie 4: The aggregation of CCPs in the cleavage furrow of the *was*A null. CLC-mRFP (Red channel) was expressed in wild-type and *was*A null cells stably expressing GFP-PCNA (nuclear marker, green channel). Mitotic cells were identified using the GFP-PCNA marker (visualised by epifluorescence) and CCPs were observed using TIRF microscopy. White arrows highlight extreme CCP aggregation co-inciding with impaired furrowing in the *was*A nulls.

Movie 5: Distribution of active Rac in chemotaxing *was*A nulls. The GFP-tagged GBD of PakB (green channel) was co-expressed with CLC-mRFP (Red channel) in wild-type and *was*A nulls. Cells were then imaged using TIRF and DIC microscopy, whilst chemotaxing towards folate in the under-agarose assay.

Movie 6: Arp2/3 complex and F-actin dynamics in control, *scr*A mutant and double *scr*A/*was*A mutant cells chemotaxing towards folate in the under-agarose assay. Cells were co-expressing GFP-ArpC4 (Arp2/3 complex, green channel) and Lifeact-mRFP (F-actin, red channel) and visualised using spinning disc confocal microscopy

Movie 7: Arp2/3 complex and F-actin dynamics in severely compressed control, *scr*A mutant and *was*A mutant cells chemotaxing towards folate in the under-agarose assay. Under such conditions cells move primarily through blebs. Cells were co-expressing GFP-ArpC4 (Arp2/3 complex, green channel) and Lifeact-mRFP (F-actin, red channel) and visualised using spinning disc confocal microscopy.

Movie 8: Cortical FRAP of control and double *scr*A/*was*A mutant cells. GFP-actin was expressed in cells and a region of the cortex was photobleached (white box number 1., white circle indicates timing of bleach) and its fluorescence recovery was compared to a non-bleached region (white box number 2.) FRAP and visualisation of GFP-actin was conducted using spinning disc confocal microscopy.

Movie 9: Arp2/3 complex and F-actin dynamics in a severely compressed double *scr*A/*was*A mutant cell. Cells were compressed under an agarose slab with a weight placed on top of it and this induced robust blebbing. Cells were co-expressing GFP-ArpC4 (Arp2/3 complex, green channel) and Lifeact-mRFP (F-actin, red channel) and visualised using spinning disc confocal microscopy.

Acknowledgements

I'd like to thank Robert Insall for giving me the opportunity to work with him in his lab, and for giving me the freedom to to follow my own interests. I will always be grateful for his patience and his guidance and for our long discussions about my projects and science in general.

I thank Peter Thomason for his tireless proofreading of not only this thesis, but of all my scientific writing. He has always been there to listen to my problems, and to encourage me when I have failed and for that I am eternally grateful.

I'd like to acknowledge Douwe Veltman, Seiji Ura and Jason King. Together with Robert and Peter, they have taught me everything I know. I will always remember our time together in the lab fondly.

So much of this thesis has its roots in the work of Douwe and my success owes much to the experiments he undertook whilst in the Insall lab.

The vast majoity of the data generated during the course of my PhD was derived through microscopy, which just wouldn't have been possible without the help of the support staff in the BAIR facility. Margret O'Prey in particular was of great help with getting me started on the spinning disc confocal microscope.

There are many so many other people at the Beatson who have helped me and I have not thanked here individually. For this I can only appologise and offer an encompassing thank you.

I am grateful to my family and friends for sticking bye me, I owe you all more of my time than I have been able to give you in the last four years.

Lastly, I would not have achieved this with out the support of Fiona, to whom I simply give my thanks and my love.

Author's Declaration

I declare that, except where explicit reference is made to the contribution of others, that this dissertation is the result of my own work and has not been submitted for any other degree at the University of Glasgow or any other institution.

Some data and text excerpts presented here have been previously published as part of the following paper:

'*Abi is required for modulation and stability of the SCAR/WAVE complex, but not localization or activity.*'

Davidson, A. J., Ura, S., Thomason, P. A., Kalna, G. and Insall R. H.

(PMID: 24036345)

Abbreviations

Abi	Abelson tyrosine kinase interactor
Arp	Actin-related protein
ATP/ADP	Adenosine triphosphate/diphosphate
Ax2/3	Axenic strain 2/3
cAMP	Cyclic adenosine monophosphate
cAR1	cAMP receptor 1
CCP	Clathrin-coated pit
Cdc42	Cell division control protein 42
CME	Clathrin-mediated endocytosis
Cobl	Cordon-bleu
CRIB	Cdc42/Rac interactive binding domain
DNA	Deoxyribonucleic acid
DOX	Doxycycline
DRF	Diaphanous related formin
E. coli	*Escherichia coli*
F-actin	Filamentous actin
FH1/2/3	Formin homology domain 1/2/3
FRAP	Fluorescence recovery after photobleaching
G-actin	Globular actin
GBD	GTPase binding domain
GTP/GDP	Guanosine triphosphate/disphosphate
HSPC300	haematopoietic stem/progenitor cell protein 300
JMY	Junction mediating and regulatory protein
Lat. A	Latrunculin A
MHC	Myosin heavy chain
MLC	Myosin light chain
mRNA	messenger ribonucleic acid
N-/C-terminus	Amino/carboxyl terminus
NPF	Nucleation promoting factor
Nap1	Nucleosome assembly protein 1
PCR	Polymerase chain reaction
PIR121	p53 inducible protein 121

N-WASP	Neuronal Wiskott Aldrich syndrome protein
Rac	Ras-related C3 botulinum toxin substrate 1
REMI	Restriction enzyme-mediated integration
SCAR/WAVE	Suppressor of cAMP of receptor/WASP family verprolin homologous protein
SHD	SCAR homology domain
SIKO	SCAR inducible knockout
TIRF	Total internal reflection fluorescence
VCA	Verprolin homology, connecting region and acidic region domain
WASH	WASP and SCAR homologue protein
WASP	Wiskott Aldrich syndrome protein
WH1/2	WASP homology domain 1/2
WHAMM	WASP homologue associated with actin, membranes and microtubules
WIKO	WASP A inducible knockout
WIP	WASP-interacting protein

Chapter 1

Introduction

1.1 *Dictyostelium dicoideum* as a model organism

1.1.1 Introduction to *Dictyostelium dicoideum*

Dictyostelium discoideum (henceforth often simply referred to as '*Dictyostelium*') is a free-living amoeba that is found in forest soils where it feeds on bacteria and yeast (Raper, 1935). As a model organism, *Dictyostelium discoideum* has many advantages. First and foremost, it is a simple eukaryote that exhibits many of the same cellular behaviours as higher eukaryotic cells such as those found in mammals. Examples include cell motility and cell division, both of which are more comparable to mammalian cells than in simpler models such as budding yeast. It has a relatively small, haploid genome that is divided between six chromosomes and has been fully sequenced (Cox, Vocke, Walter, Gregg, & Bain, 1990, Eichinger et al., 2005). Such factors, combined with the availability of a wide range of molecular tools, makes *Dictyostelium* very amenable to genetic manipulation, especially in comparison to slow growing, diploid mammalian cell lines.

Dictyostelium discoideum has been used to study a wide range of cell biology. However, this thesis shall focus on the use of *Dictyostelium* to investigate the actin cytoskeleton during processes such as cell migration and cytokinesis.

1.1.2 The lifecycle of *Dictyostelium discoideum*

In the presence of plentiful food, *Dictyostelium* exists in a single-celled, vegetative state during which it reproduces asexually. *Dictyostelium* can also undergo sexual reproduction, which is initiated when two different mating types fuse to initiate macrocyst formation (Saga & Yanagisawa, 1983). Recently, it has been shown that variation at a single genetic locus underlies the three different mating types in *Dictyostelium* (Bloomfield, Skelton, Ivens, Tanaka, & Kay, 2010).

The aggregation of *Dictyostelium* during multicellular development is one of the best-studied aspects of the *Dictyostelium* lifecycle. This process is initiated by starvation and accumulates in the formation of resistant spores secured within a fruiting body or

'sorocarp'. The sorocarp consists of the stalk (or "sorophore"), which supports the spore containing head or ('sorus') (Raper, 1935). Nutrient deprivation promotes the cells to produce and secrete pulses of cyclic adenosine monophosphate (cAMP, Gerisch & Wick, 1975). This coincides with the starvation-induced expression of the cAMP receptor 1 (cAR1), which upon binding cAMP transiently stimulates adenylate cyclase to produce and release more cAMP (Klein, Vaughan, Borleis, & Devreotes, 1987, Dinauer, MacKay, & Devreotes, 1980). In a monolayer of cells, the pulsatile release of cAMP stimulates neighbouring cells to secrete cAMP and so forth, resulting in waves of cAMP production travelling through the monolayer (Tomchik & Devreotes, 1981). Since starved cells are also highly chemotactic towards cAMP, this drives the aggregation of the *Dictyostelium* (Konijn, Van De Meene, Bonner, & Barkley, 1967, Barkley, 1969). Once aggregated, the *Dictyostelium* undergo differentiation and morphogenesis to first form a migratory slug or 'pseudoplasmodium' and then the final fruiting body.

1.1.3 *Dictyostelium* laboratory strains

Up until the isolation of laboratory strains that could grow in liquid culture, *Dictyostelium* could only be grown in the presence of bacteria. Cells were initially selected to grow in an aseptic, undefined medium (Sussman & Sussman, 1967). Repeated subculture of these cells allowed the more complex components of this medium to be diluted out and yielded cells with more efficient growth in liquid growth (Watts & Ashworth, 1970). This 'axenic' strain was named 'Ax2' and remains one of the major laboratory strains used by the *Dictyostelium* research community. An alternative, widely used strain strain was optimised to grow in liquid culture by mutagenesis and is known as 'Ax3' (Loomis, 1971).

Although the isolation of axenic strains was a key advance in the history of *Dictyostelium* research, the harsh selection or mutagenesis used to derive these cells has resulted in dramatic genomic rearrangements (Bloomfield, Tanaka, Skelton, Ivens, & Kay, 2008). This undoubtedly underlies the numerous phenotypic discrepancies that exist between different axenic strains and between the axenic strains and the original NC4 isolate from the soil. An example of this is the low vegetative motility of the axenic strains compared to the non-axenic *Dictyostelium*

isolates (Pollitt, Blagg, Ibarra, & Insall, 2006). Efforts have been made to create axenic cells through less severe selection and one such cell line derived from NC4 was NC4A2 (Morrison & Harwood, 1992, Shelden & Knecht, 1995). The authenticity of NC4A2 has been called into question due to it possessing identical duplications to Ax3 (Bloomfield et al., 2008). However, NC4A2 retains the high vegetative motility of non-axenic cell isolates, making it useful for motility studies (Pollitt et al., 2006).

1.1.4 *Dictyostelium* chemotaxis

Dictyostelium are highly motile cells and their movement is similar to that observed in other migratory cells such as human neutrophils (Devreotes & Zigmond, 1988, Andrew & Insall, 2007). As vegetative cells they are capable of robust chemotaxis towards folic acid, which is commonly released from their bacterial prey (Pan, Hall, & Bonner, 1972). As described in the previous section, starved *Dictyostelium* secrete and become sensitive to cAMP (Konijn et al., 1967, Barkley, 1969). Chemotaxis can be induced experimentally by introducing vegetative or starved cells to a gradient of folic acid or cAMP respectively. Cell motility is driven by the formation of cellular protrusions, which shall be introduced in later sections. Such properties have made *Dictyostelium* a powerful model for the study of chemotaxis and cell migration. There are currently two fundamentally different models to explain chemotaxis in *Dictyostelium* and eukaryotic cells in general. The chemotactic compass model proposes that the detection of chemoattractants (e.g. cAMP) via a transmembrane receptor (e.g. cAR1) initiates intracellular signaling, which ultimately leads to the extension of cellular protrusions towards the source of the chemoattractant to create a leading edge (Weiner, 2002a & 2002b). Alternatively, it has been suggested that motile cells perpetually generate protrusions at the front of the cell and then those protrusions that best orient the cell towards the chemoattractant are favoured (Andrew & Insall, 2007). Which of these two models is correct remains to be established, however the use of *Dictyostelium* as a simple model for the study of chemotaxis has a lot to offer the debate.

1.1.5 *Dictyostelium* cell division

Dictyostelium cytokinesis is remarkably similar to that observed in higher eukaryotes. However, its cytokinesis is extremely robust to the point that different aspects of *Dictyostelium* division can compensate for one another and are even often referred to as different modes of cytokinesis in their own right (Nagasaki, de Hostos, & Uyeda, 2002). Cytokinesis A acts to pinch the cell in two through the formation of a cleavage furrow. In suspension, cytokinesis A is entirely dependent on the action of myosin-II, whereas on a substratum myosin-II plays a nonessential supportive role and helps stabilise the furrow during ingression (De Lozanne & Spudich, 1987, Zang et al., 1997, Neujahr, Heizer, & Gerisch, 1997). Cytokinesis B acts independently of cleavage furrow formation, whereby the newly formed daughter cells migrate in opposite directions to help physically pull themselves apart (King, Veltman, Georgiou, Baum, & Insall, 2010, Nagasaki et al., 2002). Finally, cytokinesis C or traction-mediated cytofission acts as a failsafe to tear up multinucleate cells independently of mitosis (De Lozanne & Spudich, 1987, Nagasaki et al., 2002). Both cytokinesis B and C are entirely dependent on adhesion, meaning myosin-II is essential for cell division in suspension. The growth of mutants with severely defective cytokinesis A can be maintained by culturing them in the presence of a substratum, offering a unique opportunity to isolate and study the different aspects of eukaryote cytokinesis.

1.2 The actin cytoskeleton

1.2.1 Globular actin

Monomeric or globular (G) actin is the fundamental unit of the actin cytoskeleton. The importance of actin can be surmised from its extremely high conservation and its sheer abundance within all eukaryotic cells. For instance, the *Dictyostelium* genome encodes 41 actin and actin-related proteins (Arps) (Joseph et al., 2008). 34 of these genes encode conventional actins, of which 17 are identical in amino acid sequence. Mammalian actins are classed as α-, β- or γ-actins and are either involved in muscle

contraction (α-actin isoforms and γ2-actin) or are ubiquitously expressed in non-muscle cells (γ1-actin and β-actin) (Vandekerckhove & Weber, 1978).

The crystal structure of G-actin revealed it to be a square or cushion-shaped molecule composed of two similar domains each formed of two subdomains (Kabsch, Mannherz, Suck, Pai, & Holmes, 1990). A loop with exposed hydrophobic residues was suggested to mediate actin-actin interactions during polymerisation and this was supported by the subsequent resolution of the crystal structure of actin dimers (Holmes, Popp, Gebhard, & Kabsch, 1990, Kudryashov et al., 2005).

G-actin binds adenosine triphosphate (ATP), which was found to bind a cleft between two of the domains in the crystal structure (Kabsch et al., 1990). G-actin has a very low rate of ATP hydrolysis, which is greatly increased following polymerisation (Pollard & Weeds, 1984). Actin polymerisation shall be discussed in more detail in section 1.2.3.

Until recently, G-actin was believed to act solely as the substrate for actin polymerisation. However, G-actin has also been implicated in nuclear signaling within the cell (Zheng, Han, Bernier, & Wen, 2009). Although this is an area of fascinating research, this thesis shall focus on the role of actin in the cytoskeleton.

1.2.2 Actin monomer binding proteins

Actin that has hydrolysed its ATP remains bound to the resulting ADP and inorganic phosphate with the later being released only after an extended period of time (Carlier & Pantaloni, 1986). Although ATP and ADP-bound G-actin are both capable of polymerisation, ATP-actin polymerises more readily (Pollard, 1986). The nucleotide status of depolymerised ADP-bound G-actin is regulated by actin monomer binding proteins. Profilins are actin monomer binding proteins that bind G-actin and promote the release of ADP in exchange for ATP (Goldschmidt-Clermont et al., 1992). Therefore they act to maintain a pool of ATP-bound actin to fuel polymerisation. Furthermore, many regulators of actin polymerisation bind profilin, which has been proposed to concentrate ATP-bound actin at sites of polymerisation (Machesky, Atkinson, Ampe, Vandekerckhove, & Pollard, 1994, Suetsugu, Miki, & Takenawa, 1998, Miki, Suetsugu, & Takenawa, 1998).

Animals (although not *Dictyostelium*) possess thymosin β4, which binds ADP bound actin and prevents its conversion to ATP-bound actin, thus blocking repolymerisation (Goldschmidt-Clermont et al., 1992). It was proposed that thymosin β4 acts to prevent the polymerisation of ADP-bound G-actin and competes with profilin to regulate the availability of ATP-bound actin in animal cells.

1.2.3 Actin polymerisation

As introduced in the previous two sections, the principal role of G-actin is to polymerise to form filamentous (F) actin. Pure actin monomers are capable of self-assembling without the aid of other proteins. Actin polymerisation has been exhaustively studied *in vitro*, as shall be briefly discussed in this section. The actin filament is composed of two helical ribbons of actin, with all the monomers orientated in one direction (Holmes et al., 1990). Historically, one end is termed the barbed end and the other is termed the pointed end due to the appearance of the filament when decorated with the myosin head group or S1 fragment (Huxley, 1963, Begg, Rodewald, & Rebhun, 1978).

An actin filament elongates as long as the concentration of available G-actin is above the dissociation constant, a threshold that is known as the critical concentration (Kasai, Asakura, & Oosawa, 1962). F-actin depolymerises below the critical concentration, which raises G-actin levels until conditions for polymerisation are reached again. At the critical concentration, a steady state is reached wherein an actin filament grows as fast as it depolymerises. At high concentration of G-actin, an actin filament will grow at both the barbed and the pointed ends. However, the critical concentration is lower for the barbed end than the pointed end (Pollard & Mooseker, 1981). This difference results in the elongation of F-actin at the barbed end and depolymerisation at the pointed end. Furthermore, as discussed in the previous section, ATP-bound actin also has a lower critical concentration than ADP-bound actin, which favours the addition of ATP-bound actin at the barbed end of F-actin (Pollard, 1986). Polymerisation induces the newly added actin monomer to irreversibly hydrolyse its ATP (Carlier et al., 1988). ATP hydrolysis is not required for the addition of subsequent actin monomers (Pollard & Weeds, 1984). Nor does ATP hydrolysis initiate monomer dissociation. Following, hydrolysis, actin remains

bound to the resulting ADP and inorganic phosphate (Pi) and even the eventual release of the Pi does not automatically initiate disassembly. Instead ATP hydrolysis confers filament polarity whereby freshly added ATP-bound actin is enriched at the barbed end and ADP-bound actin is depolymerised from the pointed end. In what is commonly known as actin treadmilling, the combination of all these properties allows the dynamic growth of an actin filament in a single direction whilst the turnover of the filament at the other end maintains a steady state (Wegner, 1976). Actin treadmilling is summarised in the diagram shown in figure 1.1a.

1.2.4 The Arp2/3 complex and other actin nucleators

Actin trimers rapidly elongate, but actin dimers are unstable and therefore initiation or 'nucleation' of the actin trimer is the limiting step in actin polymerisation (Frieden, 1983). Many different actin nucleators that act to form a stable actin dimer to induce polymerisation have been discovered (Campellone & Welch, 2010). One of the major actin nucleators within the cell is the highly conserved Arp2/3 complex. This complex is composed of seven subunits including two Arps (Arp2 and Arp3), which share sequence similarities with conventional actin (Machesky et al., 1994). Rather than nucleating actin filaments *de novo*, the Arp2/3 complex initiates the polymerisation of a new barbed-end growing off of the body of an existing filament at a 70° angle (Mullins, Heuser, & Pollard, 1998). The Arp2 and Arp3 subunits are proposed to mimic an actin dimer to nucleate a new actin filament (Kelleher, Atkinson, & Pollard, 1995, Rouiller et al., 2008). Branches form the substrate for more Arp2/3 complex induced branches and very quickly the Arp2/3 complex can generate a very dense meshwork of cross-linked F-actin (Svitkina & Borisy, 1999). The role of the Arp2/3 complex in actin nucleation is highlighted in figure 1.1b.

In contrast to the Arp2/3 complex, the formins nucleate actin filaments *de novo* and generate linear, unbranched filaments (Pruyne et al., 2002). All formins possess two C-terminal formin homology (FH) domains and it is the FH2 domain that is sufficient to induce actin nucleation (Castrillon & Wasserman, 1994, Pruyne et al., 2002). Formins act as dimers and remain associated with the barbed end of a growing filament during elongation (Moseley et al., 2004, Xu et al., 2004). The diaphanous-related formins (DRFs) are a subset of formins, which possess an additional FH3

domain that is required for DRF subcellular localisation (Petersen, Nielsen, Egel, & Hagan, 1998). DRFs also possess a N-terminal GTPase binding domain (GBD), which interacts with a Dia-autoregulatory domain (DAD) in the C-terminus and acts to hold the DRF in an inactive conformation (Alberts, 2001). The binding of a member of the Rho GTPase family to the Cdc42/Rac interactive binding (CRIB) motif within the GBD, releases the DAD and frees the FH2 domain to nucleate actin. The *Dictyostelium* genome encodes 10 identifiable formins of which two are DRFs (Schirenbeck, Bretschneider, Arasada, Schleicher, & Faix, 2005).

Other proteins that have been found to nucleate F-actin include Spire and Cordon-bleu (Cobl). Spire is present in *Drosophila* and vertebrates whereas Cobl exists only in vertebrates. These two proteins possess tandem repeats of WASP homology 2 (WH2) domains and create a new growing barbed-end by bringing together actin monomers through these G-actin binding domains (Qualmann & Kessels, 2009, although debated by Renault, Bugyi, & Carlier, 2008).

1.2.5 F-actin capping, bundling and severing proteins

Once nucleated, F-actin interacts with a host of different actin binding proteins, which act to limit elongation, cross-link multiple filaments into different arrays or promote filament turnover (Winder & Ayscough, 2005).

Many proteins bind actin filament ends and in doing so, prevent further elongation at the capped site. Capping of the barbed end in general promotes filament depolymerisation as barbed end growth is inhibited leading to net monomer loss from the pointed end. Examples of proteins that cap barbed ends included capping protein and gelsolin (Casella, Maack, & Lin, 1986, Wang & Bryan, 1981). Formins also cap barbed ends, although they also simultaneously promote barbed end elongation (Moseley et al., 2004). *Dictyostelium* possesses capping protein and gelsolin-related proteins, as well as formins as described in the previous section. Capping of the pointed end is associated with filament stabilisation as barbed end elongation is maintained whilst monomer loss from the pointed end is prevented. Proteins that cap the pointed end of filaments include tropomodulin and the Arp2/3 complex (Weber, Pennise, Babcock, & Fowler, 1994, Mullins et al., 1998). *Dictyostelium* possesses the Arp2/3 complex but not tropomodulin. Capping protein in particular has been shown

to have an important role in limiting the exponential increase in barbed ends created by the activity of the Arp2/3 complex (Pantaloni, Boujemaa, Didry, Gounon, & Carlier, 2000).

Other ABPs act to cross-link assembled actin filaments into different arrays to form F-actin superstructures. Fascin and espin are examples of ABPs that cross-link actin filaments into parallel bundles that are often found in long-thin cellular projections (Cant, Knowles, Mooseker, & Cooley, 1994, Edwards, Herrera-Sosa, Otto, & Bryan, 1995, Bartles, Zheng, Li, Wierda, & Chen, 1998). In contrast, filamin acts to cross-link actin filaments into orthogonal networks (Nakamura, Osborn, Hartemink, Hartwig, & Stossel, 2007). Both α-actinin and fimbrin, along with myosin II, are capable of cross-linking anti-parallel actin filaments (Laporte, Ojkic, Vavylonis, & Wu, 2012). The activity of these F-actin cross-linkers underlies the formation of a wide range of different cellular structures (Bartles, 2000, Stevenson, Veltman, & Machesky, 2012).

Finally, F-actin severing proteins such as the ADF/cofilin family help breakdown actin networks by promoting actin filament disassembly. ADF/cofilin increases the rate of F-actin turnover, which is otherwise too slow to maintain the level of actin treadmilling observed *in vivo* (Carlier et al., 1997). ADF/cofilin has also been shown to have a role in debranching Arp2/3 complex generated actin meshworks, which again acts to promote actin depolymerisation and maintain a sufficient pool of G-actin for further polymerisation (Chan, Beltzner, & Pollard, 2009).

1.2.6 Actomyosin contractility

Myosins are molecular motors that couple ATP hydrolysis to movement along F-actin. Myosin-II is historically known as the conventional myosin due to its specialised role in vertebrate muscle, however it also underlies eukaryotic cell contractility. Many unconventional myosins have also been discovered, which have diverse roles throughout the cell (Hartman & Spudich, 2012). However, here the focus shall be on non-muscle myosin-II and its role in actomyosin contractility. Myosin-II is composed of a pair of intertwined heavy chains, each paired with an essential and a regulatory light chain. The myosin heavy chain (MHC) consists of a C-terminal tail, through which it dimerises, a flexible neck region and a N-terminal

head domain, which is responsible for the force production required for movement (Hynes, Block, White, & Spudich, 1987, Toyoshima et al., 1987). The head domain possesses both the ATP and actin binding sites (Rayment et al., 1993). The binding of ATP has been shown to promote the head domain to detach from the F-actin, freeing it to move or 'step' forward before ATP hydrolysis induces reattachment (Lymn & Taylor, 1971, De La Cruz & Ostap, 2004). Actomyosin contractility is dependent on the polymerisation of myosin-II dimers to form bipolar filaments, which in *Dictyostelium* is regulated by the dephosphorylation of the myosin heavy chain (Egelhoff, Lee, & Spudich, 1993). Phosphorylation of the myosin essential light chain (MLC$_E$) has also been shown to be required for myosin-II ATPase activity and therefore motor function in *Dictyostelium* (Griffith, Downs, & Spudich, 1987). However, regulation of myosin-II by phosphorylation in mammals appears very different and is less well understood (Redowicz, 2001).

Dictyostelium possesses a single MHC encoded from the *mhc*A gene, making it a good model for studying non-muscle myosin-II activity (DeLozanne, Lewis, Spudich, & Leinwand, 1985). Surprisingly, a viable *mhc*A knock out was generated and although it exhibited a severe defect in cytokinesis when cultured in suspension, it was able to divide independently of myosin-II when grown on Petri dishes (De Lozanne & Spudich, 1987). The ability of the *mhc*A null to divide in the absence of actomyosin contractility demonstrated the robust mechanisms underlying *Dictyostelium* cytokinesis as discussed in section 1.1.3. The *mhc*A null was shown to have no defect in pseudopod extension, however myosin-II was needed for maintaining cortical integrity during migration under mechanically restrictive conditions (Laevsky & Knecht, 2003). Interestingly myosin-II contractility was not required and instead it appeared that the actin cross-linking ability of myosin-II in the absence of the MLC$_E$ was sufficient to support cell motility under restrictive conditions. In summary, actomyosin contractility underlies a diverse range of cellular behaviours.

1.2.7 Models of actin dynamics

Many pathogenic bacteria, such as *Listeria monocytogenes and Shigella flexneri*, can hijack a host cell's nucleation machinery to induce actin-based motility (Loisel,

Boujemaa, Pantaloni, & Carlier, 1999). This motility has been reconstituted *in vitro*, which demonstrated that only five components were essential for bacterial propulsion (Loisel et al., 1999). These include actin, the Arp2/3 complex, an activator of the Arp2/3 complex (as will be discussed in subsequent sections), capping protein and ADF/cofilin. The motility of the bacteria was aided by the inclusion of profilin and α-actinin. The role of these proteins in promoting actin nucleation and maintaining actin treadmilling is summarised in figure 1.1c. How these factors and many others interact to yield a functional cytoskeleton within a eukaryotic cell has yet to be fully understood.

By far the most widely accepted model and the one that is advocated here is the dendritic model of actin nucleation (Mullins et al., 1998, Svitkina & Borisy, 1999). In this model, dense branched F-actin meshworks are generated by the activity of the Arp2/3 complex. Capping protein acts to limit the elongation of any given filament and the pool of available G-actin is maintained by the debranching and depolymerisation of older sections of the network. Recently however, other models have emerged that claim the branched actin networks observed by Svitkina & Borisy, 1999 are a sample preparation artifact and do not exist *in vivo*. Urban, Jacob, Nemethova, Resch, & Small (2010) have proposed that the Arp2/3 complex does not cross-link actin filaments and instead forms unbranched F-actin networks. In their paper the authors asserted that crisscrossing of linear actin filaments, rather than cross-linking, was responsible for the branched appearance of actin networks. Although independent re-analysis of the data from this study has disputed this (Yang & Svitkina, 2011), it is likely that branching by the Arp2/3 complex has been over estimated. However, this model has yet to address the substantial *in vitro* evidence that demonstrates that the Arp2/3 complex is an F-actin cross-linker and initiates actin branching (Mullins et al., 1998, Amann & Pollard, 2001). Others have suggested that Arp2/3 complex-mediated branching is limited to the barbed ends of filaments, restricting actin nucleation to a very confined area (Pantaloni et al., 2000).

Although other models of actin dynamics remain possible, this thesis shall focus on the regulation of the Arp2/3 complex within the context of a dendritic nucleation model.
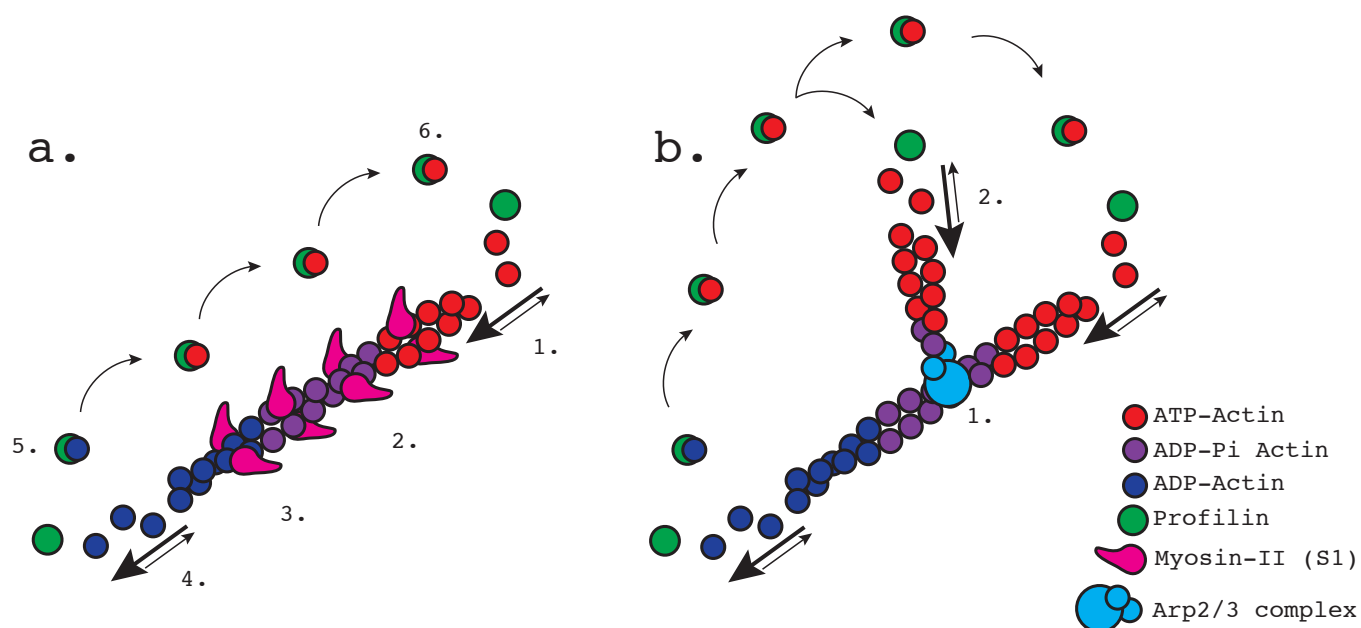
Figure 1.1, Key concepts and regulators underlying actin polymerisation: a) During actin treadmilling, actin polymerises at the barbed end and depolymerises at the pointed end. (1) ATP-bound actin monomers are added at the barbed end of a growing filament. The polarity of a filament can be determined through the use of myosin-II S1 fragments, which decorate actin filaments with a distinct orientaion. (2) Once polymerised, actin hydrolyses its ATP, however it remains bound to the resulting ADP and inorganic phosphate (Pi). ATP hydrolysis is not required for polymerisation, nor does it trigger depolymerisation. (3) Eventually, the Pi is released, but the actin remains bound to the ADP. (4) The critical concentration is higher at the pointed end than the barbed end, resulting in net lose of actin at this end of the filament. (5) Profilin binds disassembled actin monomers and promotes exchange of ADP for ATP. (6) Profilin-bound ATP-actin is recycled back to the barbed end, ready for repolymerisation. **b) The Arp2/3 complex induces actin filament branching.** (1) The Arp2/3 complex binds the side of an existing actin filament and nucleates a new actin filament, at 70° angle to the original actin filament. (2) The Arp2/3 complex initiates the formation of new growing barbed ends, which in turn can be used by the Arp2/3 complex to generate more branches. In this way the Arp2/3 complex can very quickly generate a thick meshwork of actin filaments.
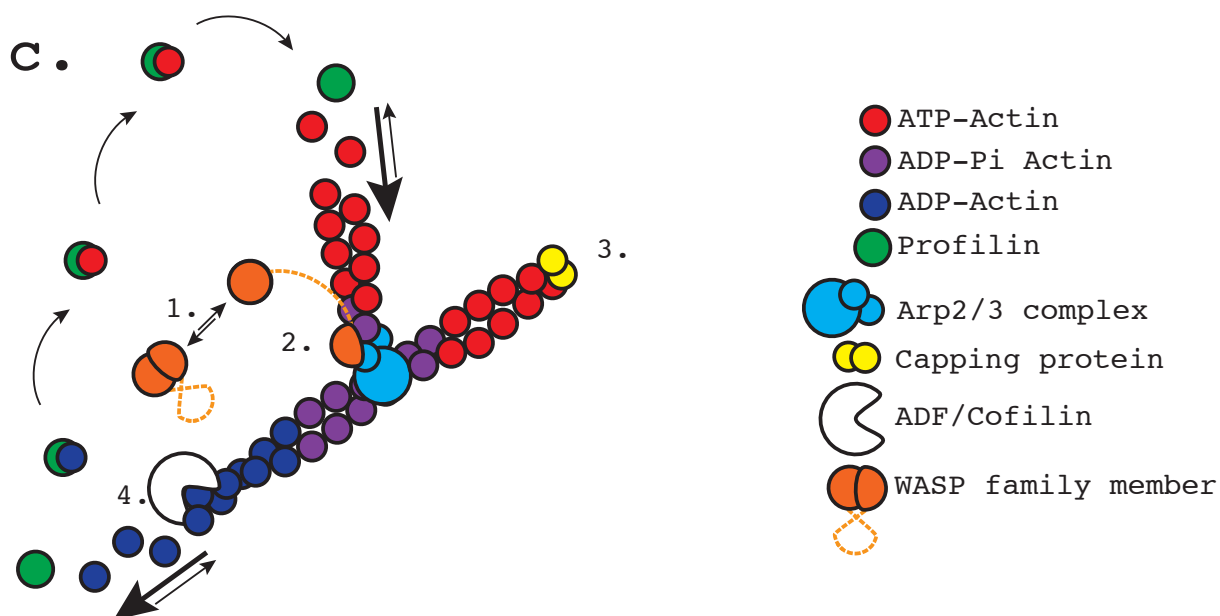
Figure 1.1, Key concepts and regulators underlying actin polymerisation (continued): c) Sustained actin treadmilling requires many different proteins. (1) The Arp2/3 complex alone is a poor nucleator and requires an activated WASP family member to promote efficient filament branching. Therefore, the control of WASP family members is key to the regulation of Arp2/3 complex nucleation. (2) Activated WASP family members interact with the Arp2/3 complex and stimulate it to nucleate a new barbed end. (3) Left unchecked, Arp2/3 complex activation would result in the exponential increase in barbed end number, leading to the rapid depletion of G-actin. Capping protein acts to counteract the Arp2/3 complex by capping barbed ends and preventing their further elongation. (4) The ADF/cofilin family of proteins promote filament dissasembly at the pointed ends of actin filaments in order to maintain a pool of G-actin for further polymerisation.

1.3 The WASP family

1.3.1 Introduction to the WASP family

The Arp2/3 complex alone has a low basal level of actin nucleation (Mullins et al., 1998). As illustrated in figure 1.2c, it has been found that activation of the Arp2/3 complex requires a nucleation promoting factor (NPF), such as a member of the Wiskott-Aldrich syndrome protein (WASP) family (Machesky et al., 1999). Members of this family include WASP, SCAR (also commonly known as WAVE in mammals) and WASH (Machesky & Insall, 1998, Miki et al., 1998, Linardopoulou et al., 2007). Vertebrates also possess specialist members such as WHAMM and JMY (Campellone, Webb, Znameroski, & Welch, 2008, Zuchero, Coutts, Quinlan, Thangue, & Mullins, 2009). Furthermore, many WASP family-like proteins have also been identified (Kollmar, Lbik, & Enge, 2012).

As well as WASP (the haemopoietic-specific founding member of the family, which is mutated in Wiskott Aldrich syndrome), humans possess the ubiquitously expressed N-WASP (Derry, Ochs, & Francke, 1994, Miki, Miura, & Takenawa, 1996). For the sake of clarity, human WASP shall be henceforth referred to as haemopoietic WASP. Human cells also express three SCAR proteins, multiple WASH proteins, WHAMM and JMY (Veltman & Insall, 2010, *T. Zech personal communication*). In contrast, *Dictyostelium discoideum* possesses single, well-conserved homologues of SCAR, N-WASP (WASP A) and WASH. It also possesses two unique WASP-like proteins, which both lack the WASP homology 1 (WH$_1$) domain and have been designated WASP B and WASP C (Veltman & Insall, 2010).

1.3.2 Arp2/3 complex activation by the WASP family

As illustrated in figure 1.2, WASP family proteins interact with the Arp2/3 complex via their C-terminal VCA. All WASP family members possess a VCA, which consists of one or more of the actin monomer binding WASP homology 2 (WH$_2$) domain, a Central (C) linker and the Arp2/3 complex binding Acidic (A) region (Machesky & Insall, 1998). It was proposed that the WH$_2$ domain supplies the first actin monomer, which, along with the two Arp subunits of the activated Arp2/3 complex, nucleates a

new actin filament. Alternatively, it has been suggested that WASP family proteins use the WH_2 domain to remain in contact with the growing barbed ends of actin filaments (Co, Wong, Gierke, Chang, & Taunton, 2007). It has also been found that the Arp2/3 complex possesses two VCA binding sites, consistent with the proposed role of multimerisation in SCAR complex activity (Ti, Jurgenson, Nolen, & Pollard, 2011, Padrick, Doolittle, Brautigam, King, & Rosen, 2011, Lebensohn & Kirschner, 2009).

The N-termini of WASP family proteins are more varied and comprise the regulatory regions that connect the Arp2/3 activating C-termini to intracellular signaling (Pollitt & Insall, 2009). The WASP family is the focus of intense research due to their ability to couple the activity of the Arp2/3 complex to intracellular signaling events.

1.3.3 Subcellular localisation of the WASP family

The distinct subcellular localisation of the individual WASP family members is responsible for the differing spatial and temporal dynamics of the Arp2/3 complex observed within the cell (Pollitt & Insall, 2009). Therefore, the WASP family members are involved in the formation of many different actin-based structures, which in turn underlie a wide range of cellular processes.

Both WASPs and SCARs have been localised to forefront of migrating *Dictyostelium* and mammalian cell lines (Myers, Han, Lee, Firtel, & Chung, 2005, Veltman, King, Machesky, & Insall, 2012, Lorenz, Yamaguchi, Wang, Singer, & Condeelis, 2004, Hahne, Sechi, Benesch, & Small, 2001). WASPs have also been implicated in clathrin-mediated endocytosis in yeast, *Dictyostelium* and murine cell lines (Naqvi, Zahn, Mitchell, Stevenson, & Munn, 1998, Veltman et al., 2012, Merrifield, Qualmann, Kessels, & Almers, 2004). In mammals, N-WASP has been co-opted to drive podosome and invadapod formation (Schachtner et al., 2013, Lorenz et al., 2004). WASH has been shown to be involved in endocytic trafficking in *Dictyostelium* and mammalian cell lines (Carnell et al., 2011, Derivery et al., 2009). Mammalian WHAMM localises to the Golgi and JMY is found in the nucleus, although whether it functions there as a NPF or elsewhere remains uncertain (Campellone et al., 2008, Zuchero et al., 2009).

How the WASP family members are differentially regulated to control where and when the Arp2/3 complex is active remains the focus of ongoing research.

1.3.4 Regulation of the WASP family

WASP family members are regulated by Rho-family GTPases. Members of this subfamily of the Ras family of the GTPases include Cdc42, Rac and Rho, each of which has been implicated in a distinct pattern of actin organisation within the cell (Allen, Jones, Pollard, & Ridley, 1997). Of the WASP family members, the regulation of human haemopoietic WASP by Cdc42 is perhaps best understood and is similar to the regulation of DRFs discussed in the previous section. As shown in figure 1.2a, the VCA of haemopoietic WASP is held in an inactive state by its interaction with a GBD in the N-terminus of the protein (Kim, Kakalis, Abdul-Manan, Liu, & Rosen, 2000). The GBD of haemopoietic WASP contains a CRIB motif and the competitive binding of Cdc42 releases the VCA to interact with the Arp2/3 complex. All WASPs contain an N-terminal GBD and therefore are all believed to be regulated in a highly analogous manner. Although *Dictyostelium* does not possess Cdc42, RacC has been proposed to be the activator or WASP A (Han, Leeper, Rivero, & Chung, 2006). Both haemopoietic WASP and N-WASP have been shown to interact with <u>W</u>ASP-<u>i</u>nteracting <u>p</u>rotein (WIP) through their N-terminal WH_1 domains (Ramesh, Anton, Hartwig, & Geha, 1997, Volkman, Prehoda, Scott, Peterson, & Lim, 2002). *Dictyostelium* also possesses a WIP homologue, which has been shown to interact with WASP A and regulate its activity (Myers, Leeper, & Chung, 2006).

The Rho-GTPase that activates SCAR is known to be Rac (Steffen et al., 2004, Lebensohn & Kirschner, 2009). However, as illustrated in figure 1.2b, SCAR does not contain a GBD or CRIB motif and is constitutively active *in vitro* (Machesky et al., 1999). However, *in vivo* its activity is known to be regulated by its inclusion within a large pentameric complex consisting of PIR121, Nap1, Abi, HSPC300 and SCAR itself (Eden, Rohatgi, Podtelejnikov, Mann, & Kirschner, 2002, figure 1.2c). Originally it was proposed that activation caused SCAR to disassociate from the complex, however that has since been demonstrated not to be true (Ismail, Padrick, Chen, Umetani, & Rosen, 2009). The five members of the SCAR complex are highly conserved across eukaryotes to the extent that SCAR is rarely found in the absence of

the full complex (Veltman & Insall, 2010). In contrast to higher eukaryotes, a single, well-conserved homologue of each member of the SCAR complex exists within *Dictyostelium* (Caracino, 2007). Members of the SCAR complex are dependent on one another for stability and consequently the loss of any one member generally results in a complete loss of SCAR protein (Ibarra, 2006, Kunda, Craig, Dominguez, & Baum, 2003). The same was found to be true of the WASH complex, suggesting that complex-dependent stabilisation is a general feature of both SCAR and WASH (Park et al., 2013, Derivery et al., 2009). Furthermore, the SCAR and WASH complexes share many other similarities and have been proposed to function in a highly analogous manner (Jia et al., 2010). The inherent instability of the SCAR complex (and the WASH complex) has confounded efforts to address the contribution of the individual complex members to the activity of the complex as a whole. Within its complex, SCAR activity is inhibited until activation by a combination of Rac and negatively charged phospholipids (Ismail et al., 2009, Lebensohn & Kirschner, 2009). Multiple phosphorylation sites have also been identified and implicated in the regulation of the SCAR complex (Lebensohn & Kirschner, 2009, Ura et al., 2012). Furthermore, positive feedback loops have also been implicated in the control of SCAR complex activity (Weiner, O D, Rentel, M C, Ott, A, Brown, G E, Jedrychowski, M, Yaffe, M & Gygi, 2006). However, the exact mechanisms that lead to SCAR activation are not yet fully understood.
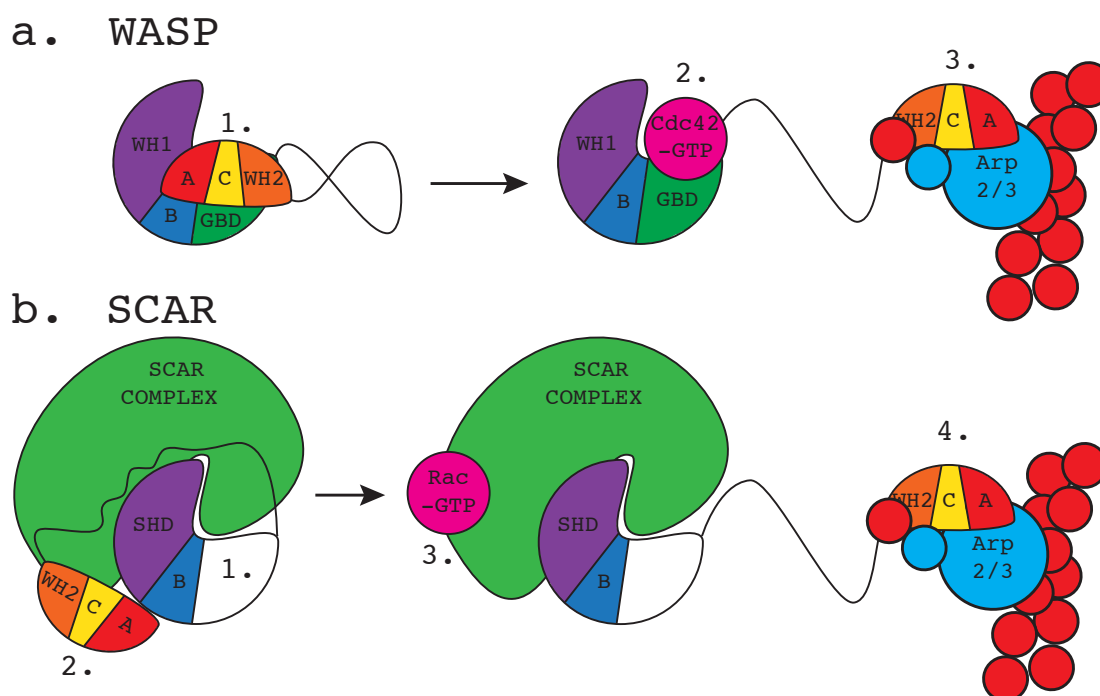
Figure 1.2, The domain structure and regulation of WASPs and SCARs: a) haemopoietic WASP is regulated by autoinhibition until activated by Cdc42. All WASP family members possess a C-terminal VCA consisting of one or more <u>W</u>ASP <u>h</u>omology <u>2</u> (WH_2) domains, a central (C) linker and an acidic (A) region. WASPs also possess an N-terminal WH_1 domain, a basic (B) region and a GTPase-bind domain (GBD). (1) The VCA of WASPs bind the GBD, which holds the protein in an inactive conformation. (2) The competitive binding of active (GTP-bound) Cdc42 to the GBD releases the VCA. (3) This frees the VCA to interact with the Arp2/3 complex and promote actin nucleation. **b) SCARs are regulated by their inclusion in a large, multi-protein complex.** The domain structure of SCARs is similar to that of WASPs. Instead of a WH_1 domain, they possess an N-terminal <u>SCAR</u> <u>h</u>omology <u>d</u>omain (SHD), which is followed by a basic (B) region as found in WASPs. (1) SCARs do not have a GBD and are not regulated by autoinhibition. Instead, SCAR activity is controlled by its inclusion within the SCAR complex. (2) The VCA of SCARs is sequestered within the complex, where it is held in an inactive state. (3) Active (GTP-bound) Rac interacts with the SCAR complex and dislodges the VCA. (4) As with WASPs, this allows the VCA to bind and activate the Arp2/3 complex.

c. The SCAR complex
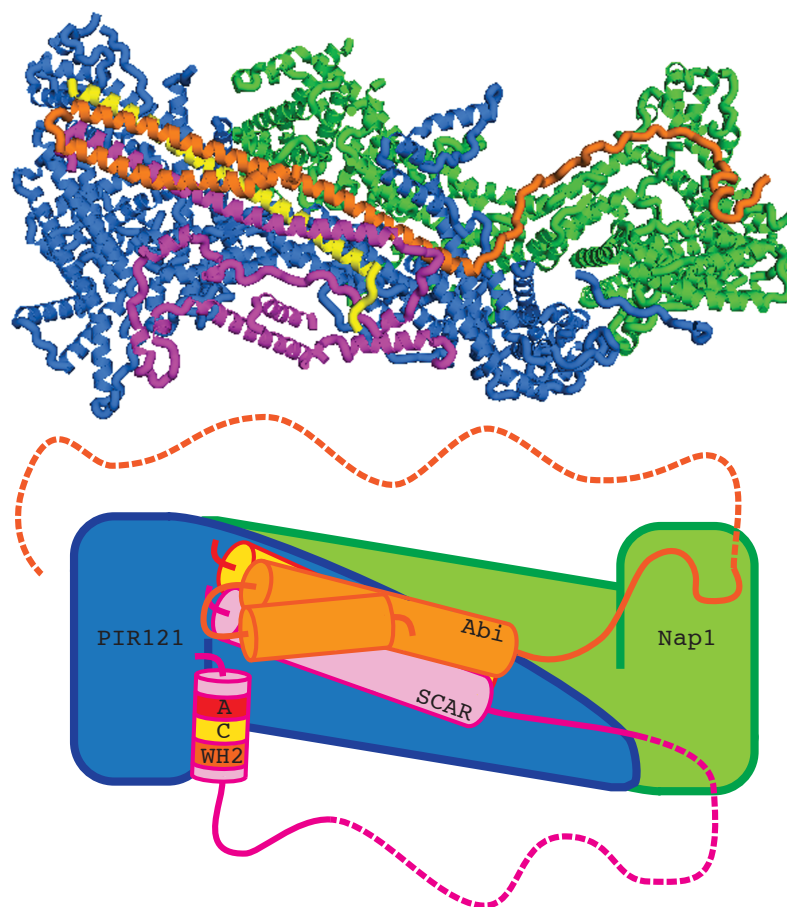
Figure 1.2, The domain structure and regulation of WASPs and SCARs (continued): c) The architecture of the SCAR complex. The crystal structure of the human SCAR complex (PDB: 3P8C) is shown with the subunits and prominent features highlighted in the cartoon beneath. The largest subunits, PIR121 and Nap1 form a platform on top of which rests a bundle of helices formed from HSPC300 and the N-termini of Abi and SCAR (HSPC300 is the yellow coloured subunit, buried in the middle of the complex). Both SCAR and Abi possess large poly-proline regions, which are not present in the crystal structure and are represented in the cartoon by dashed lines (not to scale). In the inactive state, the C-terminal VCA of SCAR is sequestered in an alcove within PIR121. Active Rac binds PIR121 and causes a conformational change that dislodges the VCA (not shown.)

1.3.5 The structure of the SCAR complex

Recently, the crystal structure of the human SCAR/WAVE1 complex has been solved revealing the complex architecture (Chen et al., 2010). The architecture of the SCAR complex is illustrated in figure 1.2c. PIR121 and Nap1 form a large platform, one side of which possesses many positively charged residues. It was proposed that these mediated the interaction with negatively charged phospholipids in the plasma membrane and act to correctly orientate the complex. Upon the other side of this PIR121/Nap1 platform, nestles a trimer composed of the other three complex members. Abi is situated at the entrance to the PIR121/Nap1 cradle where it rests on top of HSPC300 and the N-terminus of SCAR. It was previously shown that Abi interacted strongly with Nap1 (Gautreau et al., 2004, Innocenti et al., 2004). Now that the crystal structure is available, it is notable that of the Abi/SCAR/HSPC300 trimer, Abi is the only one to make any substantial contact with Nap1. The long C-terminal proline rich regions of both SCAR and Abi had to be removed to aid crystallisation, presumably because of their intrinsic disorder. However it is probable that following activation, they protrude out from the main body of the complex where they are free to interact with other factors and each other in the cytosol (Davidson & Insall, 2011). The C-terminal VCA of SCAR is sequestered within a recess in the interface between PIR121 and SCAR, suggesting a means by which it is inhibited. PIR121 had previously been shown to interact with Rac and targeted mutagenesis was used to map the binding site on to the crystal structure (Kobayashi et al., 1998, Chen et al., 2010). From this work, a model emerged where by the binding of Rac to PIR121 results in a conformational change that dislodges the VCA of SCAR leading to activation. Many other factors have been proposed to bind to and regulate the SCAR complex via interactions with the different complex members (Weiner, O D, Rentel, M C, Ott, A, Brown, G E, Jedrychowski, M, Yaffe, M & Gygi, 2006, Innocenti et al., 2003). However, due to the inherent instability of the SCAR complex, the role of the other complex members and how they contribute to overall SCAR activity remains poorly understood.

1.3.6 Abi and the SCAR complex

Abi has long been considered a key component of the SCAR complex. It has been reported that Abi directly recruits the SCAR complex to signaling complexes containing its established activator, Rac (Innocenti et al., 2003). Numerous phosphorylation sites have also been identified in Abi, some of which have been found to be responsive to stimuli such as EGF treatment or serum starvation in mammalian cells (Lebensohn & Kirschner, 2009). Also, it has been suggested that Abi localises and activates the complex through its interaction with ABL kinases, from which it originally derived its name (Leng et al., 2005). Overall, the literature describes Abi as a fundamental regulator of the SCAR complex.

Previously, our lab reported the phenotype of *Dictyostelium* lacking Abi (Pollitt & Insall, 2008). Unlike knockouts in any of the other complex members, in which SCAR is no longer stable and barely detectable by Western blot, *Dictyostelium abi*A nulls still retain appreciable levels of SCAR protein. It was also demonstrated that cells lacking Abi possess a cytokinesis defect unique to it amongst the nulls of the SCAR complex members. Since cells devoid of Abi and SCAR (double *abi*A/*scr*A nulls) have a phenotype equivalent to that of the *scr*A null, this defect has been attributed to the residual SCAR that is still present in the *abi*A null and its possible mislocalisation or inappropriate activity during cytokinesis.

All of the above strongly imply that Abi is a crucial component of the SCAR complex responsible for its localisation and subsequent activation during chemotaxis and cytokinesis.

1.4 Actin-driven cellular processes

1.4.1 Actin-based protrusions and cell migration

Actin plays a critical role in all cell motility. Co-ordinated cycles of actin polymerisation and depolymerisation induce the changes in cell shape that drive cell migration. Cells are capable of generating a wide range of different types of actin-based protrusions and cell motility is derived in part from persistently extending such

protrusions in one direction. The different kinds of protrusions include pseudopodia, lamellipodia, filopodia and blebs. These protrusions can be divided into those that are exclusively generated by the Arp2/3 complex, such as pseudopodia and lamellipodia (Suraneni et al., 2012, Wu et al., 2012), and those that are not, such as filopodia and blebs (Steffen et al., 2006, Langridge & Kay, 2006, Charras, Hu, Coughlin, & Mitchison, 2006). Pseudopodia and lamellipodia are very similar structures and essentially only differ in morphology. For instance, a lamellipod can be considered one large, sustained pseudopod. They are both large protrusions that are supported by dense actin meshworks formed by the activity of the Arp2/3 complex (Svitkina & Borisy, 1999). In contrast, filopodia are long, thin cellular spikes that consist of bundles of parallel actin filaments and are associated with the activity of formins (Schirenbeck et al., 2005). Blebs are a very different type of protrusion and are supported by actin polymerisation rather than directly promoted by it. During bleb formation, actomyosin contractility raises intracellular pressure until the plasma membrane ruptures free of the underlying actin cortex and bulges outwards (Paluch, Piel, Prost, Bornens, & Sykes, 2005, Charras, Yarrow, Horton, Mahadevan, & Mitchison, 2005). The cortex quickly reforms itself resulting in a small cortical bubble or bleb. No recruitment of the Arp2/3 complex is required for bleb formation and the involvement of any other actin nucleator is yet to be established (Charras et al., 2006).

Dictyostelium motility appears to be supported by a mix of both pseudopodia and blebs (Yoshida & Soldati, 2006). Therefore, *Dictyostelium* offers an opportunity to study the formation of these different types of protrusions and how they both contribute to cell migration.

1.4.2 The role of WASP family members in cell motility

SCAR localises to the leading edge of cells where it recruits the Arp2/3 complex to drive pseudopod extension. Consistent with this, the loss of SCAR impairs pseudopod formation and cell migration in *Dictyostelium*, fruit flies and human cell lines (Veltman et al., 2012, Evans, Ghai, Urbancic, Tan, & Wood, 2013, Hahne et al., 2001). However, it has also been published that WASP A localises to and is essential for pseudopodia in *Dictyostelium* (Myers et al., 2005). In stark contrast to this work, our lab recently demonstrated that WASP A is not found in the pseudopodia of wild-

type *Dictyostelium* and instead predominantly localises to sites of CME (Veltman et al., 2012). Further complicating the issue, WASP A was found to assume the role of SCAR in the *scr*A null and appeared to be responsible for the residual pseudopodia in these cells. The roles or SCAR and WASP A in chemotaxing *Dictyostelium* are summarised diagrammatically in figure 1.3. In short, the presence of WASP A in the pseudopodia of *Dictyostelium* remains controversial. Although *Dictyostelium scr*A nulls are capable of extending morphologically normal pseudopodia, their reduced rate of pseudopod formation appears to be supplemented with increased bleb formation during cell migration (Ura et al., 2012, Veltman et al., 2012). Therefore it appears that *scr*A nulls maintain motility through the use of both WASP A driven pseudopodia and Arp2/3 complex independent blebs (figure 1.3). Whether other proteins (WASP family members or otherwise) can promote pseudopod formation, how WASP A is able to assume the role of SCAR and how cells are able to switch between different modes of migration remain unanswered questions.

1.4.3 Actin and clathrin-mediated endocytosis

The cell uses clathrin-mediated endocytosis (CME) to internalise and turnover its membrane and trans membrane proteins. During CME, adaptor proteins (AP) cluster transmembrane proteins and recruit clathrin monomers to form a lattice (Reider & Wendland, 2011). As depicted in figure 1.4, this drives budding of the membrane until a clathrin-coated pit (CCP) is formed on the membrane. Internalisation is complete once sufficient membrane invagination has occurred to allow dynamin-mediated scission (Mettlen, Pucadyil, Ramachandran, & Schmid, 2009). A burst of actin polymerisation is observed at CCPs, coinciding with internalisation (Merrifield, Feldman, Wan, & Almers, 2002).
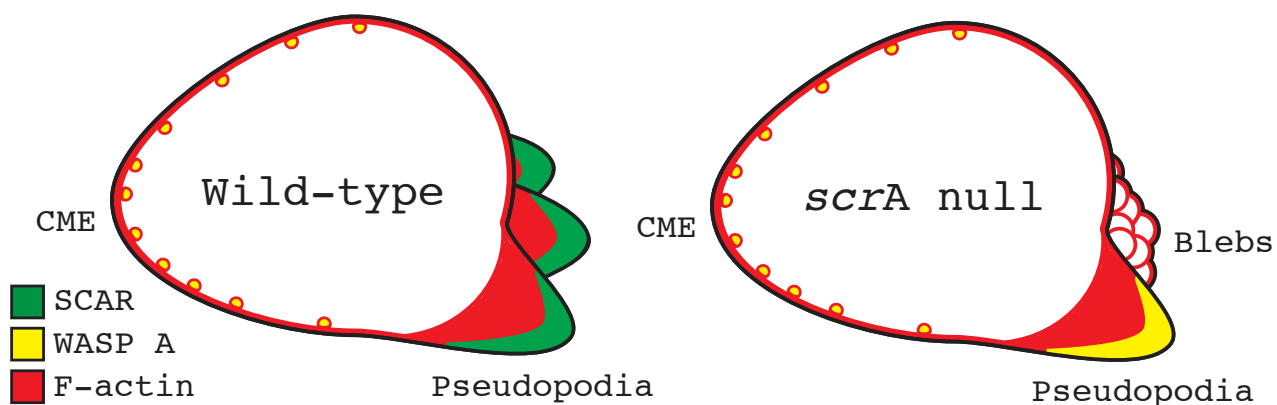
Figure 1.3, The localisation of SCAR and WASP A in motile *Dictyostelium*: During cell migration, SCAR and WASP A normally localise to distinct actin-based structures. SCAR is found promoting the sustained actin polymerisation that underlies pseudopod extension. In contrast, WASP A is seen at the short busts of actin polymerisation that aid vesicle internalisation during clathrin-mediated endocytosis (CME). The *Dictyostelium scr*A null has a suppressed rate of pseudopod formation, which it compensates for with an increased rate of bleb production. Neither WASP family members or the Arp2/3 complex have been observed at sites of blebbing. Although reduced in frequency, the *scr*A null is still capable of extending morphologically normal pseudopodia between the bursts of blebs. Surprisingly, it appears that WASP A can assume the role of SCAR and is responsible for the residual pseudopodia of the *scr*A null.

Whether actin plays a supportive or an essential role in CME has been disputed, although recent developments have went someway to resolve the debate. It has always been clear that actin polymerisation is required for yeast endocytosis (Ayscough et al., 1997). Actin polymerisation also appears necessary for CME in *Dictyostelium* (Brady, Damer, Heuser, & O'Halloran, 2010). However, whether actin is similarly essential for mammalian CME is less clear. Although a burst of Arp2/3 complex mediated actin polymerisation strongly coincides with CME, neither the Arp2/3 complex or actin polymerisation appeared to be required for successful vesicle internalisation in mammalian cell lines (Merrifield et al., 2004, Benesch et al., 2005). The issue is further complicated by the finding that actin polymerisation appeared to be needed to drive CME on the apical but not the basal surface of mammalian cells (Gottlieb, Ivanov, Adesnik, & Sabatini, 1993).

Aghamohammadzadeh & Ayscough, (2009) demonstrated that yeast CME could be restored when actin polymerisation was inhibited by relieving membrane tension. It has subsequently been shown that mammalian CME also requires actin polymerisation when membrane tension is increased (Boulant, Kural, Zeeh, Ubelmann, & Kirchhausen, 2011). For instance, the promotion of microvilli formation was sufficient to increase membrane tension to the point where CME became dependent on actin polymerisation. This possibly explains why in some cells actin is required for apical (where the microvilli are) and not basolateral CME as discussed above (Gottlieb et al., 1993). A role for actin polymerisation in providing the force to overcome membrane tension during CME is consistent with the detailed electron microscopy-based examination of CCPs carried out by Collins, Warrington, Taylor, & Svitkina (2011). Here it was shown that a concentrated patch of branched actin was often associated with the neck of CCP. Actin comet tails were also frequently observed at highly invaginated CCPs, where membrane tension would be at its highest. When under low tension, the membrane presumably retains enough flexibility to support CME without actin polymerisation. However, it is clear that yeast, *Dictyostelium* and mammalian cells possess a well-conserved mechanism to utilise the force generated by actin polymerisation to maintain CME under conditions of high membrane tension.

1.4.4 The role of WASP family members in clathrin-mediated endocytosis

In the previous section, the role of actin polymerisation in supporting membrane invagination during CME was described and the role of WASPs and actin polymerisation in CME is summarised in figure 1.4. As already discussed in section 1.2.2, WASPs and the Arp2/3 complex have been colocalised at CCP during vesicle internalisation (Merrifield et al., 2004). Murine N-WASP knockout fibroblasts have been shown to only have a mild defect in CME (Benesch et al., 2005). This result can be partially explained by the inessential role of actin under conditions of low membrane tension as discussed in the previous section. Consistent with this, it has been established that the yeast homologue of WASP, Las17p, is required for CME in this organism (Naqvi et al., 1998). However, residual recruitment of the Arp2/3 complex to CCPs was still observed in N-WASP knock out cells, implying that N-WASP has a redundant role in mammalian CME. Both haemopoietic WASP and SCAR were excluded as possible compensators and the source of this redundancy remains a mystery.

In *Dictyostelium*, WASP A has also been shown to colocalise with CCPs (Veltman et al., 2012). Furthermore, both the WASP-like proteins WASP B and WASP C were shown to be present at CCPs during internalisation (Veltman & Insall, 2010). Although WASP B and WASP C are unique to *Dictyosteium*, they possibly represent another example of the redundancy that exists within the WASP family. However, such redundancy and CME in general has yet to be examined in a *Dictyostelium* devoid of WASP A.

CME has been shown to be required for adhesion turnover during cell migration and cytokinesis in mammalian cell lines (Ezratty, Bertaux, Marcantonio, & Gundersen, 2009, Pellinen et al., 2008). Independent of CME, clathrin has also been implicated in SCAR complex membrane recruitment and stabilisation of the mitotic spindle (Gautier et al., 2011, Royle, Bright, & Lagnado, 2005).
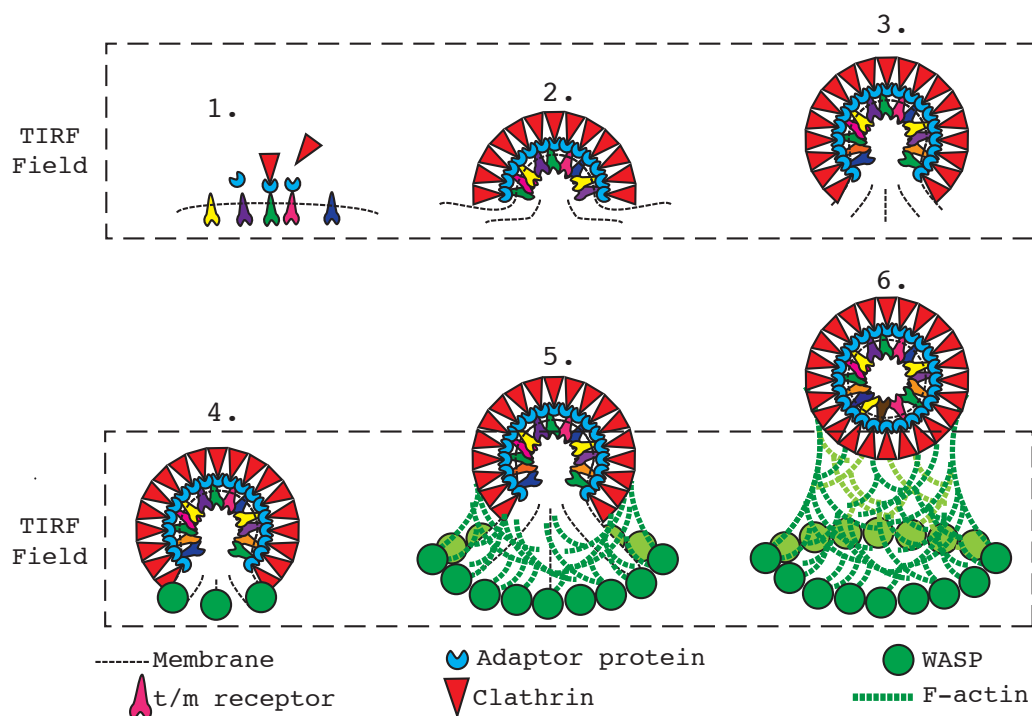
Figure 1.4, WASPs support vesicle internalisation during CME: CME is the means by which a cell internalises and recycles its transmembrane (t/m) receptors. (1) CME begins when adaptor proteins are recruited to t/m receptors, which they cluster in preparation for internalisation. The adaptor proteins also recruit clathrin monomers to build the CCP. (2) The clathrin monomers polymerise to form a lattice and the nascent CCP. (3) Under conditions of low membrane tension, the above can be sufficient to deform the membrane enough to allow vesicle completion and internalisation. (4) Alternatively, WASP localises to the base of the CCP and recruits the Arp2/3 complex to induce actin polymerisation. (5) A burst of actin polymerisation is sufficient to to counteract membrane tension and drive membrane invagination. The force provided by actin polymerisation drives narrowing of the vesicle neck, which allows scission by dynamin (not shown). (6) Once internalised, actin polymerisation may also help push the vesicle up into the cytosol. CME can be easily visualised by TIRF microscopy, as internalisation results in the loss of the CCP from the TIRF field of view (dashed box) as the vesicle moves up and into the cell.

Since motility and cytokinesis are cellular processes that can be better studied in amoebae than budding yeast, the gentetically tractable *Dictyostelium* offers a unique opportunity to investigate the contribution of CME to cellular behaviour that is highly analogous to that found in higher eukaryotes.

1.5 Aims of thesis

1.5.1 Determining the role of individual SCAR complex members

SCAR functions as part of large complex consisting of PIR121, Nap1, HSPC300, Abi and SCAR itself (Eden et al., 2002). The role of SCAR is to recruit and activate the Arp2/3 complex, which promotes actin nucleation. However, the role of the remainder of this high molecular weight complex remains poorly understood. The SCAR complex is known to hold SCAR in an inactive conformation until it is activated (Eden et al., 2002, Ismail et al., 2009). One of the best-established activators, Rac, has been shown to activate the complex through an interaction with PIR121 (Kobayashi et al., 1998, Chen et al., 2010). However, the individual contributes of the other complex members to SCAR complex function are not known. This is primarily due to the dependence of the complex members on one another for stability. Consequently disruption of any one complex member results in a *scr*A null phenotype, which has confounded genetic dissection of the SCAR complex.

It was reasoned that if the SCAR complex could be stabilised in one of the complex member nulls, it would be possible to investigate the individual role of the repective complex member. For this project, Abi presented itself as the obvious candidate, due to the presence of residual SCAR protein within the *Dictyostelium abi*A null (Pollitt & Insall, 2008). This implied that, of all the complex members, it contributed the least to SCAR complex stability. Our objective was to generate a deletion series of *Dictyostelium* Abi and identify minimal fragments that stabilised the SCAR complex in the *abi*A null. Such fragments would then be used to determine if they also restored every aspect of SCAR complex activity. Any phenotypes identified would aid us in assigning functions to specific domains of Abi.

1.5.2 Resolving the role of WASP A in *Dictyostelium*

Dictyostelium is ideally suited for use as a simple model to study the WASP family members. However, the conflicting data surrounding the role of WASP A in *Dictyostelium* diminishes the effectiveness with which it can be used as a model for studying actin dynamics (Myers et al., 2005, Veltman et al., 2012). Our lab has consistently observed WASP A colocalisation with clathrin, coinciding with actin-driven vesicle internalisation (Veltman et al., 2012). Its localisation is in stark contrast to that of SCAR, which is found at the tips of growing pseudopodia during cell migration (Ura et al., 2012, Veltman et al., 2012). However, in the absence of a *was*A null, it has not been possible to exclude the possibility that WASP A does have a role in pseudopod formation. A *Dictyostelium was*A knockout has long eluded both our lab and the *Dictyostelium* research community at large, leading to the assumption that WASP A is essential for *Dictyostelium* viability. The only group to claim success took an inducible approach and subsequently asserted that WASP A was essential for the actin polymerisation underlying pseudopod extension and chemotaxis in general (Myers et al., 2005). Further complicating the issue is our labs finding that although WASP A is never observed localised to the pseudopodia of wild-type cells, WASP A is able to substitute for SCAR in the *Dictyostelium scr*A null and appears to be responsible for the residual pseudopodia in these cells (Veltman et al., 2012). Here we aimed to resolve the controversial role of WASP A in *Dictyostelium* by generating our own inducible *was*A knockout. The strategy adopted was to introduce *was*A under the control of the doxycycline inducible promoter into the genome of *Dictyostelium* and then disrupt the endogenous *was*A gene by homologous recombination. An inducible approach would allow growth to be maintained if *was*A did prove essential for cell viability. If *was*A was found not to be necessary for cell growth, *was*A would be then disrupted in an otherwise wild-type background. Once obtained, a *was*A null would be used to establish the role of WASP A in pseudopod formation, cell motility and clathrin-mediated endocytosis.

1.5.3 The interplay between WASP family members and their contribution to different modes of migration

Our lab has consistently found that WASP A predominantly localises to sites of clathrin-mediated endocytosis in wild-type *Dictyostelium*. However, recently it was found that in the *Dictyostelium scr*A null, WASP A localised both to clathrin-coated pits and to the residual pseudopodia formed by this mutant (Veltman et al., 2012). It was proposed that WASP A was able to assume the role of SCAR in the *scr*A null in order to maintain pseudopod-based motility in these cells. Despite the ability of WASP A to substitute for SCAR, the *scr*A null still has a suppressed rate of pseudopod formation. Interspersed amongst its diminished number of pseudopodia, the *scr*A null extends many more blebs, which do not require the recruitment of the Arp2/3 complex for their formation (Ura et al., 2012, Veltman et al., 2012). Therefore, it appears that the WASP A driven pseudopodia and increased blebbing work together to maintain the motility in the *scr*A null.

We sought to establish whether WASP A was indeed responsible for the residual pseudopodia in the *scr*A null and if these two WASP family members were the only proteins capable of promoting pseudopod extension. Furthermore we wanted to understand the interplay between these two proteins and how it was possible that they could both induce pseudopod formation under different circumstances. Finally, we wanted to investigate how the different types of protrusions and the molecular pathways that underlie their formation cooperate and interact to maintain robust cell motility. In order to achieve this we aimed to generate a double *scr*A/*was*A null. It was predicted that all pseudopod formation would be abolished in these cells leaving their motility entirely dependent on blebs. By comparing wild-type, *scr*A null, *was*A null and double null cell migration, it was hoped that the role of WASP family members in Arp2/3 complex dependent and independent protrusion formation could be elucidated.

45

Chapter 2

Materials and Methods

2.1 Molecular Cloning

2.1.2 Plasmid Digestions and Ligations

Restriction digests of DNA were carried out using restriction enzymes and buffers from NEB. Digested DNA was separated by molecular weight through agarose gel electrophoresis and extracted through the use of a Zymoclean™ Gel DNA recovery kit (Zymo research). When required, the termini of digested DNA were dephosphorylated with shrimp alkaline phosphatase (Fermentas) or blunt-ended through the use of DNA Polymerase I, large (Klenow) fragment (NEB) as per the manufactures' protocols. DNA ligations were performed using Fermentas rapid DNA ligation kits as according to the manufactures' instructions.

2.1.2 Bacterial Transformations and Plasmid purification

Ligated or purified plasmids were transformed into chemically competent DH5α *E. coli* by heat shock. 5 µL of ligation or diluted plasmid were mixed with 50 µL competent cells and cooled on ice for 25 minutes before heat shock at 42°C for 30 seconds. Cells were then incubated shaking with 0.5 mL LB or SOC for 1 hr at 37°C, following which all of the inoculum was plated on LB agar containing either 100 µg/ml ampicillin or 50 µg/ml kanamycin. The plates were incubated over night at 37°C to yield clonal colonies. For minipreps, individual colonies were selected and used to inoculate 5 mL of LB, which were then cultured shaking (200 rpm) overnight at 37°C. The bacteria were then pelleted from these cultures by centrifugation at 3,000 xg for 10 minutes, following which the supernatant was discarded. Purified plasmids were extracted from bacterial pellets through the use of a QIAprep spin miniprep kit (Qiagen) or robotically by a Qiagen 8000 Bio-Robot. All plasmids were confirmed by restriction enzyme digest and/or sequencing.

2.1.3 Polymerase chain reaction

PCR was conducted using Phusion® High-Fidelity DNA polymerase (Thermoscientific) with the accompanying reagents. The template used for PCR amplification was either diluted plasmid or purified wild-type *Dictyostelium* (Ax3) genomic DNA (extracted using DNAzol® reagent, Life technologies). A list of primers used in this work is shown in section 2.7. PCR products were purified using a DNA clean and concentrator^{TM} kit (Zymo research) as according to the manufacture's protocol. PCR products were then blunt-end ligated into the cloning vector pDM368 and fully sequenced before being sub-cloned into other expression vectors etc.

2.2 DNA constructs

2.2.1 Construction of the Abi deletion series

The Abi deletion series was generated based on the human SCAR/WAVE complex crystal structure ((Chen et al., 2010)). Primers 24F, 80F, 25R, 28R, 29R were designed and used in different combinations during PCR to create the Abi deletion series flanked by BglII and SpeI restriction sites. The full cDNA of *abi*A contained within pDM364 was used as a template for these reactions. The products were blunt-end ligated into pDM368 and then confirmed by sequencing. The *abi*A fragments were excised by BglII/SpeI digest, gel purified and then cloned into BglII/SpeI digested pDM304-HSPC300-GFP and pDM448 expression vectors to create the untagged and GFP-tagged Abi deletion series respectively.

2.2.2 Fluorescent tag expression constructs

All single and dual expression vectors were constructed using the pDM modular vector system (Veltman, Akar, Bosgraaf, & Van Haastert, 2009). For example, an inducible GFP-WASP A expression vector (pAD52) was obtained by cloning the full *was*A cDNA from pDM551 into the Tet-on GFP- expression vector, pDM371 via the BglII/SpeI restriction sites shared by both plasmids (Veltman, Keizer-Gunnink, &

Haastert, 2009). Dual fluorescent vectors were created by first N-terminally/C-terminally tagging constructs with RFP by cloning them into pDM602/pDM603 shuttle vectors. An expression cassette possessing the RFP-tagged construct was then excised with NgoMIV and ligated into an NgoMIV digested GFP- expression vector. The HSPC300-GFP vector (pDM304-HSPC300-GFP) into which the Abi deletion series was cloned was obtained from S. Ura (Ura et al., 2012). GFP-WASP A with or without CLC-mRFP (pDM656/pDM482 respectively), GFP-ArpC4 with Lifeact-mRFP (pDM641) and SCAR-TagRFP with GFP-WASP A (pDM981), as well as many others, were acquired from D. Veltman (Veltman et al., 2012). The GFP-MHC expression vector (pBIG GFP-MYO, Moores, Sabry, & Spudich, 1996) was obtained from the *Dictostelium* stock centre (www.dictybase.org). A full list of all the plasmids used in this work and their source can be found in section 2.6.

2.2.3 Creation of the REMI construct

The inducible GFP-WASP A expression vector (pAD52) described above was adapted for REMI. (Kuspa & Loomis, 1992, King et al., 2010). Sequence essential for the extrachromosomal maintenance was excised from pAD52 by NarI/CspcI digestion. The linearised vector was then blunt-ended with Klenow polymerase and recircularised by ligation yielding the REMI vector named pAD65. This construct was then lineraised by XhoI digestion prior to REMI.

2.2.4 Creation of the *was*A knockout construct

To create the *was*A knock out construct, approximately 1 kb of genomic sequence either side of the *was*A locus were amplified by PCR with BglII/Spe I restriction sites introduced to the 5' and 3' ends of the products via the forward (98F/100F) and reverse (99R/101R) primers respectively. All but the first and last few basebairs of the *was*A coding region were excluded from the knock out construct so as to eliminate the possibility that a truncated WASP A fragment remained expressed after homologous recombination. This also ensured that only the endogenous *was*A locus was targeted

for deletion rather than the inducible GFP-WASP A construct in the WIKO parent when creating the inducible *was*A null.

These sequences were then individually cloned into pDM368 and confirmed by sequencing, following which they were excised by BglII/SpeI digestion. The first of these sequences was then ligated into the BglII/XbaI restriction sites, 5' of the blasticidin resistance (BsR) cassette in pAD70. The other sequence was ligated into the BamHI/SpeI sites 3' of the BsR cassette to yield pAD94. The whole *was*A knock out construct was then excised from pAD94 by BglII/SpeI digestion prior to electroporation.

2.3 Cell biology

2.3.1 Transfection of *Dictyostelium*

Dictyostelium cells were cultured axenically in HL5 medium (Formedium), at 22°C in Petri dishes. Transformation of *Dictyostelium* cells with extrachromosomal plasmids was achieved by electroporation. Cells were harvested, pelleted by centrifugation (3 minutes at 380 xg) and resuspended at approximately 1 x 10^{7} cells/mL in 0.4 mL chilled E-buffer. The cells were then immediately added to electroporation cuvettes (2 mm gap Electroporation Cuvettes Plus$^{\text{TM}}$) along with 1-20 ng of plasmid. The cells were then quickly electroporated at 500 V using an ECM 399 Electroporation System (BTX Harvard Apparatus) and immediately added to 10 cm Petri dishes containing 10 mL HL5 media. Selection was achieved by adding either 50 µg/mL hygromycin or 10 µg/ml G418 to the media approximately 24 hours after transfection. Transformants were maintained under selection thereafter.

2.3.2 REMI

Linearised pAD65 was introduced into the genome of Ax3 cells by REMI to yield the WIKO parent strain (IR202) in which GFP-WASP A expression was induced by addition of doxycycline. 15 µg of XhoI digested pAD65 was electroporated into cells as described in the previous section except cells were electroporated in the presence

of 100 units of XhoI at 1.2 kV. A no enzyme control was also performed. Approximately 24 hours after electroporation, cells were harvested, diluted in HL5 and replated into 96 well dishes in the presence of 50 µg/mL hygromycin. Several weeks later, individual colonies were identified and transferred to 10 cm Petri dishes. The successful integration of the GFP-WASP A construct was confirmed by treating the transformants with 10 µg/mL doxycycline for 24 hours followed by Western blotting using an anti-body specific to WASP A. The inducibility of verified clones was then tested by confirming the loss of GFP-WASP A expression upon doxycycline deprivation. This yielded a strain where GFP-WASP A expression could be induced over and above the endogenous WASP A expression and was utilised as a parent strain for the generation of the WIKO cell line.

2.3.3 *was*A knockout generation

The endogenous *was*A locus was targeted for deletion by homologous in a number of different cell lines using the knock out construct excised from pAD94. Disruption of the *was*A gene in the inducible GFP-WASP A ' WIKO Parent' (IR202) described in the previous subsection was used to create the WIKO cell line (IR203). Alternatively, the deletion of *was*A in wild-type Ax3 cells yielded the *was*A null (IR204). A *was*A was also disrupted in a cell line that stably expressed the nuclear marker, GFP-PCNA (Muramoto & Chubb, 2008) yielding IR206. Finally, an inducible double *scr*A/*was*A mutant was generated (IR207) by disrupting the *was*A gene in the SIKO mutant (IR201, King et al., 2010). In all cases, 10 µg of digested and purified knock out construct was electroporated into cells as described in subsection 2.3.1. The following day, cells were diluted in HL5 and replated in 96 well plates along with 20 µg/mL blasticidin. Due to suspected viability problems, the WIKO and the inducible double mutant cell lines were cultured in the presence of 10 µg/mL doxycycline to maintain GFP-WASP A or SCAR expression respectively. The loss of endogenous WASP A expression in isolated clones was confirmed by Western blotting using an antibody specific to WASP A.

2.3.4 Growth measurements

The growth of various strains was tested under different conditions such as in the presence of a substratum on Petri dishes or in suspension in shaking flasks. In the case of the former, 5×10^4 cells were plated in 6-well Petri dishes with an individual well harvested and cell count performed every 12 hours. The growth of cells in Petri dishes was monitored in HL5 and SIH minimal medium. Alternatively, for growth in shaking culture, flasks filled with HL5 were inoculated with 5×10^4 cells/ml and a cell count was again performed every 12 hours. In both cases, cell counts were performed with a CASY® Cell Counter + Analyser system Model TT (Innovates AG). Doubling times were derived through the use of the following formula:

Doubling time = Time / $\log_2$(Final cell $N^{o.}$/Initial cell $N^{o.}$)

The average doubling times between different cell lines were compared through the use of unpaired student's t-tests, which yielded two-tailed p values.

2.3.5 SDS- and Native PAGE

For SDS-PAGE, equal numbers of cells were pelleted and were immediately lysed with boiling (70^oC) 1x LDS sample buffer containing 50 mM DTT reducing agent. After a further 10 minutes of incubation at 70^oC, the samples where centrifuged at >16,000 xg for 10 minutes at 4^oC in a tabletop centrifuge to remove any insoluble cell debris. The equivalent of 0.5-2 $x10^5$ cells were then pipetted into the wells of NuPAGE precast, Bis-Tris gels of varying percentage (Life technologies). SDS-PAGE was conducted in 1x NuPAGE MOPS SDS running buffer for approximately 1-2 hours at 150-200 V.

For the separation of intact protein complexes by Native PAGE, equal numbers of cells were pelleted and were lysed on ice with 0.1% DDM detergent plus HALT protease inhibitors. The samples were >16,000 xg for 10 minutes at 4^oC in a tabletop centrifuge to remove any insoluble cell debris. The equivalent of 7.5 $x10^4$ cells were

loaded into the wells of Novex Bis-Tris 4-16% gels (Life technologies) and the Native PAGE was conducted as according to the manufacture's instructions. The entire experiment was conducted in the cold room at 4°C.

2.3.6 Immunoblotting

Following both SDS-PAGE and Native PAGE, specific proteins of interest were detected by immunoblotting. After SDS-PAGE, proteins were transferred on to nitrocellulose membranes (Hybond-C-extra, Amersham Biosciences) in a BioRad transfer tank filled with 1x SDS-transfer buffer at 100 V for 1 hour. The membranes were then blocked with a solution containing 5% non-fat dried skimmed milk dissolved in TBS. The membranes were then probed with primary antibodies overnight at 4°C, followed by the use of fluorescence secondary antibodies that were subsequently detected using the Odyssey IR imaging system (LI-COR Biosciences). Quantification of SCAR levels was achieved by normalisation of the SCAR band intensity to the PIR121 band intensity for each sample over four blots. Unpaired student's t-tests were used to derive two-tailed p-values and determine statistical significance. Alternatively, following Native PAGE (and some SDS-PAGE gels), PVDF membranes (Hybond-P, Amersham) were used for blotting and were then blocked as described above. At this point, membranes derived from Native PAGE were treated with 50 mM DTT, 2% SDS and 1x TBS for 1 hour at room temperature in order to denature the protein and promote epitope exposure. The membranes were then probed with primary antibodies overnight at 4°C followed by detection through the use of HRP conjugated-secondary antibodies and chemiluminescence (Immobilon Western chemiluminescent HRP substrate, Millipore).

2.3.7 Cell fixation and staining

Cells were seeded at low density on glass coverslips and then cells were fixed for 5 minutes with a solution containing 6% Formaldehyde (w/v), 15% picric acid (v/v) and 10 mM PIPES, adjusted to pH 6.5. The cells were then washed with PBS before permeabilisation with 70% ethanol for 2 minutes. The fixed cells were washed

repeatedly with PBS and then stained for 30 minutes with either 33 nM Texas red phalloidin (Life technologies) for F-actin alone or in combination with 161 nM Alexa Fluor 488 DNaseI (Life technologies) for G-actin. Coverslips were washed again in PBS, then dH$_2$O and finally mounted on glass slides with antifade reagent containing DAPI (Prolong Gold, Life technologies). Image acquisition shall be described in detail in section 2.4.

For the quantification of multinuclearity, the number of nuclei per cell was counted for 100s of cells/cell line over multiple experiments. In the case of the Abi deletion series, the proportion of cells with 1, 2, 3, 4 or ≥5 nuclei/cell was calculated and then plotted. For statistical analyisis, the cells were grouped into those with either 1 or ≥2 nuclei due to the subtlety of the phenotype. A Chi-square test was then used to investigate the differences between observed frequencies of nuclei per cell, from which two-tailed p-values were derived (statistical analysis performed by Gabriela Kalna). When the expected counts fell below 5, the Yates' correction was applied. For the *was*A knock out cell lines, the mean number of nuclei/cell was calculated.

For the ratiometric F-/G-actin staining of control cells, *scr*A mutants, *was*A mutants and double mutants, cells were fixed and stained with phalloidin and DNaseI as described above. 75 cells/cell line over 3 independent experiments were outlined using imageJ software and the average intensity of both the F-actin and G-actin staining within the area of the cell was determined. A F-/G-actin ratio was calculated for each cell and all the values were the normalised to the mean F-/G-actin ratio of the wild-type control. As a control, wild-type cells were also sub-maximally treated with 5 μM Latrunculin A (5 minute compared to normal 10-15 minute treatment) to artificially decrease F-actin levels prior to fixation. Statistical comparison of the mean F-actin levels between different cell lines was achieved through the use of unpaired Student's t-tests.

2.3.8 Cortical FRAP

Vegetative cells expressing GFP-actin (pDM478) were incubated in LoFlo for 4 hours to reduce intracellular autofluorescence. Cells were then harvested and plated in 30 mm glass bottom dishes (MatTek). Compression under agarose was not performed as this was found to stimulate random motility in otherwise immobile vegetative cells. A

region of the actin cortex within the middle of the cell was photobleached and fluorescence recovery was monitored within the bleached region and a close by non-bleached region (the microscope set up is described in full detail in section 2.4.3). For analysis, a kymograph of each region was created. Slight movement of the cortex was corrected for by realignment of the fluorescent 'streak' that corresponded to the cortex over time. The fluorescence intensity along this streak was measured using the plot profile tool in imageJ and the values were normalised to the average fluorescence of the cortex pre-bleach (first two frames).

2.3.9 Motility assays

Dictyostelium cell motility was induced and studied in a number of different ways. Firstly, pseudopod formation was studied in randomly migrating developed NC4A2 cells. Developed cells become sensitive to cAMP, but are also inherently more motile even in the absence of this chemoattractant. The HL5 media from confluent Petri dishes of cells was aspirated and replaced with nutrient free developmental buffer (DB). The cells were then left undisturbed until early signs of development were shown (~7 hours). The Petri dishes were then harvested and cells were seeded in 30 mm glass bottom dishes (Iwaki) in fresh DB and slightly compressed under 0.4% agarose (SeaKem GTG) slabs. The agarose slab helped confine the cells to the one plane of focus and aided imaging. Alternatively, pseudopod formation and chemotaxis was studied through the use of an under-agarose folate chemotaxis assay (Laevsky & Knecht, 2001). Agarose (SeaKem GTG) was melted in SIH to yield a 0.4% gel, 5 mL of which was cast in a 50 mm glass bottomed dish (MatTek) that had been pretreated with 10 mg/mL BSA. Once the agarose had set, two 5 mm x 20 mm wells were cut 5 mm apart in the centre of the gel using a scalpel. This left a central 'bridge', which was gently wriggled loose. Vegetative cell were harvested, pelleted by centrifugation (3 minutes at 380 xg) and resuspended in SIH at 0.5-1 x10^6 cells/mL. One well of the assay was filled with this cell suspension, whilst the other was filled with 0.01 mM folic acid diluted in SIH. A coverslip was then carefully lowered on top of the agarose to cover the majority of the wells and prevent evaporation. The chemotaxis of the vegetative cells under the agarose bridge was monitored and wild-type cells were

found to reach migratory speeds of >10 μm/min. These conditions were found to strongly favour pseudopod as opposed to bleb formation in wild-type cells.

In order to promote migration through blebs rather than through pseudopodia, the conditions of the under-agarose chemotaxis assay were modified. The percentage agarose was increased to 1.5%, cooled to 40°C and was then cast in untreated glass bottomed dishes. This increased the resistance encountered by the cells when they migrated under the agarose causing severe cellular compression. These conditions strongly suppressed pseudopod formation and induced a switch to bleb-based migration. These two different assay set-ups were defined as pseudopod-promoting conditions and bleb-promoting conditions.

Finally, the severe compression of cells was performed as described by King, Veltman, & Insall, (2011). In brief, cells were washed in SIH and plated in 30 mm glass bottomed dishes (MatTek). The cells were then compressed under a slab of 1% agarose gel (SeaKem GTG) using an array of metal discs.

2.3.10 Actomyosin contractility assay

Myosin-II function was tested in different cell lines by treating them with sodium azide, as has been performed in *Dictyostelium* before (Pasternak, Spudich, & Elson, 1989, Patterson & Spudich, 1995, Xu et al., 2001). Cells were plated in HL5 at the maximum density supported by the well of a 6 well Petri dish (6 x10^{6} cells). The cells were allowed to settle and then the HL5 was aspirated and replaced with HL5 and 5 mM sodium azide. Cells were then incubated on a rocker for 15 minutes before a cell count was performed. The mean proportion of detached cells was calculated for each cell line over 4 independent experiments and differences were compared statistically using one-way ANOVA combined with a Tukey's multiple comparisons test to derive p-values.

2.4 Microscopy

2.4.1 Phase contrast, DIC and widefield fluorescence microscopy

Phase contrast and DIC images were acquired through the use of a Nikon ECLIPSE TE2000-E inverted microscope equipped with a monochrome Retiga Exi cooled CCD camera. Phase contrast microscopy was performed using either a 10x/0.3 NA or a 20x/0.45 NA objective. DIC microscopy was performed using either a 60x/1.4 NA or a 100x 1.4 NA objective.

Images of fixed and stained cells were acquired through the use of an inverted widefield microscope (IX81; Olympus) with a 60× 1.42 NA objective. This microscope was equipped with a Photometrics Coolsnap HQ camera.

2.4.2 TIRF microscopy

TIRF microscopy was adopted for the imaging of the basal surface of cells and was advantageous for visualising SCAR recruitment and/or CCP dynamics in live cells. Dual colour TIRF and DIC microscopy was performed simultaneously on a modified Nikon Eclipse TE 2000-U microscope in conjunction with a 100×/1.45 NA Nikon TIRF objective, a photometrics Evolve 512 camera and a DualView DV2 emission splitter. Images were recorded every 1-2 seconds. The angle of laser illumination could be altered for one laser to allow simultaneous TIRF and epi fluorescence imaging.

2.4.3 Confocal microscopy

Spinning disc confocal microscopy was performed with an Andor Revolution XD spinning disc system (Nikon Ti-E inverted microscope with a Yokogawa CSU-X spinning disc confocal unit and a High resolution Andor Neo sCMOS camera). This system was used in combination with a 60x/1.4 NA or a 100x/1.4 NA objective. Images were acquired every 2 seconds. FRAP was performed using an Andor mosaic FRAPPA unit. Images were acquired every 0.5 seconds for 30 seconds, with two images captured prior to a one second photobleach.

Occasionally, scanning confocal microscopy was performed using a Nikon A1R confocal microscope with a 60×/1.4 NA objective.

2.4.4 Image processing and analysis

All images acquired by microscopy were exported as TIFFs and imported into imageJ (National Institutes of Health). The representative images presented in this thesis were minimally processed. Noise was reduced in these images through the use of the despeckle tool in imageJ. Otherwise the images were cropped, resized and their contrast/brightness was altered.

Image analysis was always performed on the raw, unprocessed TIFFs. Often, cells or regions of interest were outlined and the average fluorescence intensity was measured within such defined areas. Kymographs were constructed through the reslice tool in imageJ. The vast majority of data were generated by analysing image stacks frame-by-frame for the appearance of different cellular structures (e.g. cellular protrusions).

2.5 Antibodies

The antibodies used throughout this work are listed below:

1° Antibodies:	Dilution:	Source/Reference:
Rabbit anti-SCAR	1:1,000	Ibarra, 2006
Sheep anti-PIR121	1:5,000	Ibarra, 2006
Rabbit anti-Abi	1:1,000	Pollitt & Insall, 2008
Mouse anti-GFP	1:500	Cell signaling technology
Rabbit anti-WASP A	1:1,000	Soldati lab
2° Antibodies	Dilution	Source/Reference:
anti-Rabbit/Goat/Mouse-HRP	1:10,000	Sigma
anti-Rabbit/Goat/Mouse-DyLight/Alexa Fluor-680/800	1:10,000	Thermoscientific /Life technologies

2.6 List of IR strains

The following list provides information on all the IR strains used or generated during the course of this work:

IR46 (*scr*A null)   JH8, *scr*A:*pyr*5-6

IR60 (*abi*A null)   NC4A2, *abi*A::*bsr*^{R}

IR201 (SIKO)   JH8, *scr*A:*pyr*5-6, $^{tet-on}$*scr*A; *neo*^{R}

IR202 (WIKO Parent)   Ax3, $^{tet-on}$*gfp*-*was*A; *hygro*^{R}

IR203 (WIKO)   Ax3, $^{tet-on}$*gfp*-*was*A; *hygro*^{R}, *was*A::*bsr*^{R}

IR204 (*was*A null)   Ax3, *was*A::*bsr*^{R}

IR206   Ax3 (JC1), *gfp*-*pcna*; *neo*^{R}, *was*A::*bsr*^{R}

IR207 (double mutant)   JH8, *scr*A:*pyr*5-6, $^{tet-on}$*scr*A; *neo*^{R}, *was*A::*bsr*^{R}

2.7 List of plasmids

pDM304-*hspc*300-GFP   Expression vector expressing HSPC300-GFP

pBIG GFP-Myo   Expression vector expressing GFP-MHC

pAD42   Dual expression vector expressing ΔCt_2 Abi and HSPC300-GFP

pAD43   Dual expression vector expressing ΔCt_1 Abi and HSPC300-GFP

pAD50   Dual expression vector expressing Abi and HSPC300-GFP

pAD53   Tet-ON expression vector expressing GFP-WASP A

pAD65   Tet-on expression REMI vector expressing GFP-WASP A

pAD70   Knock out construction vector containing BsR cassette

pAD81   Dual expression vector expressing $\Delta Abi\Delta$ and HSPC300-GFP

pAD85   Expression vector expressing GFP-ΔCt_2 Abi

pAD86   Expression vector expressing GFP-ΔCt_1 Abi

pAD87   Expression vector expressing GFP-$\Delta Abi\Delta$

pAD88	Expression vector expressing GFP-Abi
pAD89	Expression vector expressing GFP-ΔNt Abi
pAD90	Dual expression vector expressing ΔNt Abi and HSPC300-GFP
pAD94	*was*A knock out vector
pAD131	Expression vector expressing CLC-mRFP
pAD145	Dual expression vector expressing CLC-mRFP and HSPC300-GFP
pAD146	Dual expression vector expressing CLC-mRFP and PAX-GFP
pAD148	Dual expression vector expressing CLC-mRFP and PAK B (GBD)-GFP
pDM364	Cloning vector containing *abi*A cDNA
pDM368	Blunt-ended cloning and sequencing vector
pDM448	Expression vector for N-terminally tagging proteins with GFP-
pDM471	Expression vector expressing GFP-WASP B
pDM473	Expression vector expressing GFP-WASP C
pDM478	Expression vector expressing GFP-Actin
pDM482	Expression vector expressing GFP-WASP A
pDM602	Shuttle vector for N-terminally tagging proteins with RFP-
pDM603	Shuttle vector for C-terminally tagging proteins with -RFP
pDM641	Dual expression vector expressing Lifeact-mRFP and GFP-ArpC4
pDM656	Dual expression vector expressing CLC-mRFP and GFP-WASP A
pDM945	Dual expression vector expressing PAKB(GBD)-mRFP and HSPC300-GFP
pDM981	Dual expression vector expressing SCAR-TagRFP and GFP-WASP A

2.8 List of primers

24F	GCGAGATCTAAAATGAGTGAATCAATCGATATTAACG
25R	GCGACTAGTTTACATTGGTGGAGGTGGTG
28R	GCGACTAGTTTATGCCTTTGTTGCTTCTGTATC
29R	GCGACTAGTTTAAATATCAGATGCACTAATACCATAAG
80F	GAGATCTAAAATGGCAGCTCAAGCATATGAACAAACTC
98F	GACTAGTTCAGGAGGTGGTGGTGCC
99R	GAGATCTTACTAATGGTGTTGATTCATCTGTCAC
100F	GACTAGTGTACGTTGGGTAAATACAATGTC
101R	GAGATCTTCACTAATAGTTGGACTACCTAT

2.9 Buffer recipes

Coomassie Stain:

- 45% Methanol

- 45% dH$_2$O

- 10% Acetic acid

- 1g/L Brillant Blue G

(destaining buffer as above except minus Brillant Blue G)

Developmental buffer:

-5 mM KH$_2$PO$_4$

-5 mM Na$_2$HPO$_4$

-2 mM MgCl$_2$

-1 mM CaCl$_2$

=pH 6.5

DNA Gel loading buffer (6x):

- 40% (w/v) sucrose

- 0.25% (w/v) bromophenol blue

- 0.25% (w/v) xylene cyanol FF

E-buffer:

- 10 mM KK$_2$

- 50 mM sucrose

=pH 6.5

<u>Picric acid fixative solution:</u>

- 6% Formaldehyde (w/v)

- 15% saturated picric acid (v/v)

- 10 mM PIPES,

adjusted to pH 6.5 with 1-5 M NaOH

<u>HL5 medium (Formedium):</u>

- 14 g/L Peptone

- 7 g/L Yeast extract

- 0.5 g/L KH_2PO_4

- 0.5 g/L Na_2HPO_4

<u>LB:</u>

-1% Bacto-tryptone (Difco)

-0.5% Bacto-yeast extract (Difco)

-17 mM NaCl

=pH 7.0

(LB agar -1.5% Bacto-agar (Difco))

<u>LoFlo medium (Formedium):</u>

- 11 g/L glucose

- 0.68 g/L KH_2PO_4

- 5 g/L Casein peptone

- 26.8 mg/L NH_4Cl

- 37.1 mg/L $MgCl_2$

- 1.1 mg/L $CaCl_2$

- 8.11 mg/L $FeCl_3$

- 4.84 mg/L Na_2-EDTA.$2H_2O$

- 2.3 mg/L $ZnSO_4$

-1.11 mg/L H_3BO_4

-0.51 mg/L $MnCl_2.4H_2O$

-0.17 mg/L $CoCl_2$

-0.15 mg/L $CuSO_4.5H_2O$

-0.1 mg/L $(NH_4)_6Mo_7O_{24}.4H_2O$

=pH 6.5

PBS

-137 mM NaCl

-2.68 mM KCl

-7.98 mM Na_2HPO_4

- 1.47 mM KH_2PO_4

= pH 7.2

SDS-transfer buffer:

-48 mM Tris-Cl (pH 6.8)

-96 mM glycine

-20% v/v methanol

SIH (Formedium):

Amino acids:

- 700 mg/L Arg
- 300 mg/L Asp
- 150 mg/L Asp A
- 300 mg/L Cys
- 545 mg/L Glu A
- 900 mg/L Gly
- 300 mg/L His
- 600 mg/L Ile
- 900 mg/L Leu
- 1,250 mg/L Lys
- 250 mg/L Met
- 350 mg/L Phe
- 800 mg/L Pro
- 500 mg/L Thr
- 350 mg/L Trp
- 700 mg/L Val

- 0.2 mg/L Folic Acid
- 0.4 mg/L Lipoic Acid
- 0.5 mg/L Riboflavin
- 0.6 mg/L Thiamine

Minerals:

- 53.5 mg/L NH4Cl
- 2.94 mg/L CaCl2.2H2O
- 16.2 mg/L FeCl3
- 81.32 mg/L MgCl2.6H2O
- 870 mg/L KH2PO4

Micro Elements:

- 4.84 mg/L Na2EDTA.2H2O
- 2.3 mg/L ZnSO4
- 1.11 mg/L H3BO3
- 0.51 mg/L MnCl2.4H2O
- 0.17 mg/L CoCl2.6H2O
- 0.15 mg/L CuSO4.5H2O
- 0.1 mg/L (NH4)6Mo7O24.4H2O

Vitamins:

- 0.02 mg/L Biotin
- 0.01 mg/L Cyanocobalamin

Carbohydrate:

- 10 g/L Glucose

Chapter 3

Abi is required for SCAR complex stability, but not localisation

3.1 The design and implementation of the Abi deletion series

The SCAR complex consists of SCAR, PIR121, Nap1, HSPC300 and Abi. The recent resolution of the human SCAR complex architecture has greatly advanced our understanding of how the individual complex members interact with one another (Chen et al., 2010). This work also offered new insight into how SCAR was inhibited within the complex and even offered a possible mechanism for how it was activated. However, the function of the majority of the complex remains a mystery, one that is all the more puzzling since our lab's finding that in *Dictyostelium,* WASP A substitutes for SCAR without the need for the rest of the complex (Veltman et al., 2012).

Our lab has long sought to determine the contribution of the individual SCAR complex members to the function of the whole. However, due to the inherent fragility of these proteins, the individual nulls reveal little as the entire complex is compromised in these cells (Kunda et al., 2003). Uniquely, the *Dictyostelium abi*A null (IR60) still retains residual SCAR protein. The *abi*A null also possesses a slight defect in cytokinesis B (i.e. it has a tendency to become multinucleate even in the presence of a substratum), which is not observed in any of the other SCAR complex member nulls. This defect was previously attributed to the misregulation of the remaining SCAR in the *abi*A null during cell division and suggested that Abi had a role in regulating the SCAR complex. However, due to the reduced SCAR complex integrity in these cells, it has been difficult to separate the regulatory role of Abi from its contribution to complex stability. It was reasoned that if minimal fragments of Abi that were still incorporated into the complex could be identified, the function(s) of Abi could be separated from its overriding requirement for complex stability. The human SCAR complex crystal structure (PDB ID: 3P8C) was utilised to identify domain boundaries, which was in turn used to design a targeted deletion series of *Dictyostelium* Abi. As shown in figure 3.1a it is apparent that Abi2 is incorporated into the human SCAR/WAVE1 complex through the second of its two N-terminal alpha helices ("α2"). This domain and others were identified in *Dictyostelium* Abi by protein alignment as depicted in figure 3.1b. Other conserved domains/features that were identified in the *Dictyostelium* Abi included the first N-terminal alpha helix ("α1") and an interesting loop formed from the most distal C-terminal Abi2 sequence for which there was crystal structure data available. We designated this the 'conserved

loop (CL)'. The C-terminal poly-proline tail, which comes after the CL, was absent from the crystal structure, presumably due to its intrinsic disorder. Although the human and *Dictyostelium* Abi C-termini do not align well, both are clearly identifiable due to the sheer number of prolines present.

Based on the crystal structure, it was reasoned that the α2 helix alone would be sufficient to fully stabilise the complex in the *Dictyostelium abi*A null and therefore the sequence peripheral to the α2 helix was incrementally deleted. The implemented deletion series is shown diagrammatically in figure 3.1c and included N-terminally deleted ΔNt Abi (minus the α1 helix), C-terminally deleted ΔCt_1 (minus the polyproline tail) and ΔCt_2 Abi (minus the poly-proline tail and the CL). Finally, ΔAbiΔ was a combination of both the ΔNt and the ΔCt_2 truncations and consisted of little more than the α2 helix.

3.2 Abi fragments stabilise both SCAR and the SCAR complex

As described in the previous section, our lab has previously generated and characterised the *Dictyostelium abi*A null (Pollitt & Insall, 2008). Despite the absence of a complete complex, these cells still retain some residual SCAR. It was first determined if any of the generated fragments were capable of fully stabilising SCAR. The various Abi fragments were expressed in the *abi*A null along with the established SCAR complex marker, HSPC300-GFP (Veltman et al., 2012). Co-expression of the Abi deletion series with HSPC300-GFP allowed localisation of the complex as discussed in subsequent sections.

Western blotting was used to verify the expression of the truncated Abi fragments and initially utilised SCAR protein level as a read out of complex integrity. It has been previously shown by our lab that SCAR complex member PIR121 is stable in *abi*A and *scr*A nulls and so we adopted it as a loading control (Pollitt & Insall, 2008). The stability of PIR121 appears to depend solely on the presence of Nap1 (Ibarra, 2006).

a.
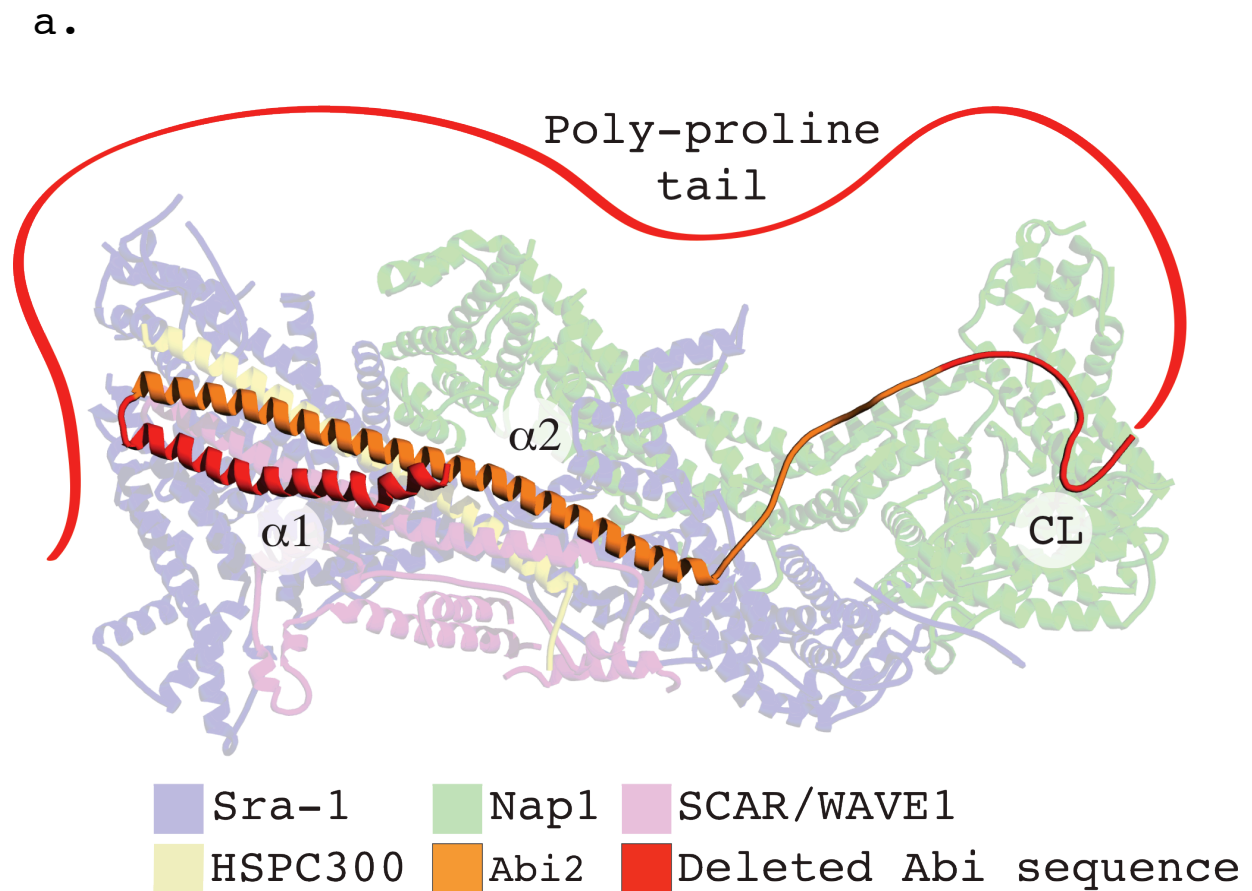
Figure 3.1, Design and implementation of the Abi deletion series: a) Different structural features of Abi were targeted for deletion based on the human Abi2 structure. An illustration of Abi2 within the human SCAR/WAVE1 complex derived from the recently resolved crystal structure (PBD ID: 3P8C). The labels designate different structural features of Abi2: α1= 1st alpha-helix, α2= 2nd alpha-helix. CL=conserved loop. The sequence corresponding to that subsequently targeted for deletion in the *Dictyostelium* Abi is highlighted in red. The red "ribbon" represents the Abi2 poly-proline region that is absent from crystal structure (not to scale).

c.

Poly-Proline tail

CL

α2

α1

WT Abi

ΔNt Abi

ΔCt₁ Abi

ΔCt₂ Abi

ΔAbiΔ

b.

α1

α2

CL

```
Hs. ---MAELQMLLEEEIPGGRRALFDSYTNLERVADYCENNYIQSADKQRALEETKAYTTQSLASVAYLINTLANNVLQMLDIQASQLRMESSINHISQTVDI
Dd. MSESIDINVYSQTTIPNAMAELMDNHNKMEQISAYCKSLYAN-GDAAQAYEQTQYAKNALLNVAYHIQTVGTHITSLLQLQTNEMEKLNIEIQTLTQRVRM
```

```
Hs. HKEKVARREIGILTNK--NTSRTHKIIAPANLERPVRYIRKPIDYTILDDIGHGVKVSTQNMKMGGLPRTTPPTQKPPSPPMSGKGTLGRHSPYRTLEPVR
Dd. IHDSTGTNVFSNQDAAKPYKSSLKNRKVDTEATKAPVKVVHKPISY----------GISASDINQNGVP---PPLNHSNS------
```

```
Hs. PPVVPNDYVPSPTRNMAPSQQSPVRTASVNQRNRTYSSSGSSGGSHPSSRSSSRENSGSGSVGVPIAVPTPSPPSVFPGHPVQFYSMNRPASRHTPPTIGGS
Dd. ---SANLTSSSGHLAASSTSNSSTPSYQSPSYSSQQPTISSGTPPPIQKQPPR--VGNAPPPSLSVPAAPPPPVMNVPPP------PPTSQRPSSVNNN
```

```
Hs. LPYRRPPSITSQTSLQNQMNGGPFYSQNPVSLAPPPPSILQVTPQLPLMGFVARVQENISDTPPPPPVEEPVFDESPPPPPPPEDYEEEEAAVVEYSDPYA
Dd. APSNDFPPPPPPSSSS---SGGDLPPPPSFGLPPPP-------------TLGDDFPPPPPPVGSYDFPPPPARPQSQFYDH------NDFP
```

```
Hs. EEDPPWAPRSYL
Dd. PPPPPM------
```

Figure 3.1, Design and implementation of the Abi deletion series (continued): b) Structural features of Abi2 were identified in the *Dictyostelium* Abi by alignment. Protein alignment between human (Hs.) Abi2, represented in (a), and *Dictyostelium* (Dd.) Abi with identical colour scheme and labelling to (a). The sequence corresponding to the C-terminal SH3 domain of Human Abi2 was removed to aid alignment as *Dictyostelium* Abi does not possess this domain. Asterisks highlight amino acid identities. **c) Diagrammatic representation of *Dictyostelium* Abi domain structure and the subsequent deletion series undertaken.** Based on (a) and (b), the following constructs were generated: Full length Abi (WT Abi), N-terminally truncated Abi (ΔNt Abi), C-terminally truncated Abi fragments (ΔCt₁ and ΔCt₂ Abi) and an Abi truncated at both termini (ΔAbiΔ).

Unfortunately, as shown in figure 3.2a, deletion of the N-terminus of Abi resulted in the loss of the anti-Abi epitope, which confounded detection of all the fragments. We were reluctant to directly tag Abi in case this interfered with its normal activity, especially since the final position of the tag within the whole complex would differ between the different constructs. However, for the sole purpose of confirming the expression of all the Abi fragments, we additionally N-terminally fused our deletion series to GFP allowing it to be detected with an anti-GFP antibody. Between the anti-Abi and anti-GFP blots shown in figure 3.2a and b, it was clear that the Abi all fragments were expressed and there were no gross differences in expression level.

As shown in figure 3.2a, ΔNt Abi, ΔCt$_1$ and ΔCt$_2$ Abi were sufficient to restore SCAR protein levels in the *abi*A null to the same extent as full length (WT) Abi. The Abi constructs tagged with GFP also restored SCAR levels in the *abi*A null to a comparable extent (figure 3.2b). Further truncation of the C-terminus of Abi yielded fragments that were expressed but did not contribute to SCAR stability (data not shown). Finally, ΔAbiΔ also restored SCAR protein levels in the *abi*A null, if only partially. The levels of SCAR in each of the transformants was quantified by normalising the SCAR level of SCAR to the amount of PIR121 over 4 independent blots. As demonstrated by figure 3.2c, it was found that ΔAbiΔ restored SCAR significantly less than WT Abi (unpaired Student's t-test, $p<0.05$) but significantly more than the basal level found in the null expressing HSPC300-GFP alone (unpaired Student's t-test, $p <0.001$). The stabilisation of the complex as a whole by the Abi fragments was confirmed by native PAGE. During native PAGE proteins are not denatured, which allows the separation of intact protein complexes by electrophoresis and their subsequent detection by conventional Western blotting. As demonstrated in figure 3.2d, *Dictyostelium* SCAR was found in the one, high molecular weight complex, the presence of which depended on Abi. Residual SCAR complex was undetectable in the *abi*A null expressing HSPC300-GFP alone. However, this was perhaps not surprising given the instability of the complex and the low level of SCAR present in the *abi*A null. Also of note was the appearance of a prominent bandshift in the complexes containing C-terminally truncated Abi. Since Abi does not contribute a large amount to the total mass of the SCAR complex, it is more likely that truncation of the disordered poly-proline tail allows more efficient passage of the complex through the gel during electrophoresis.
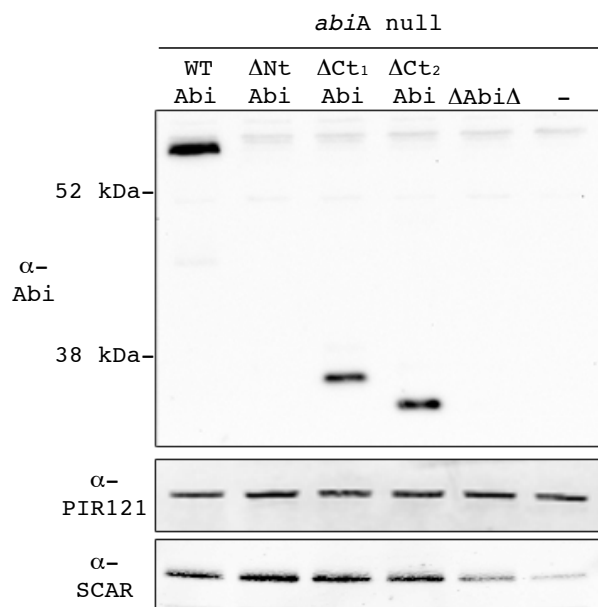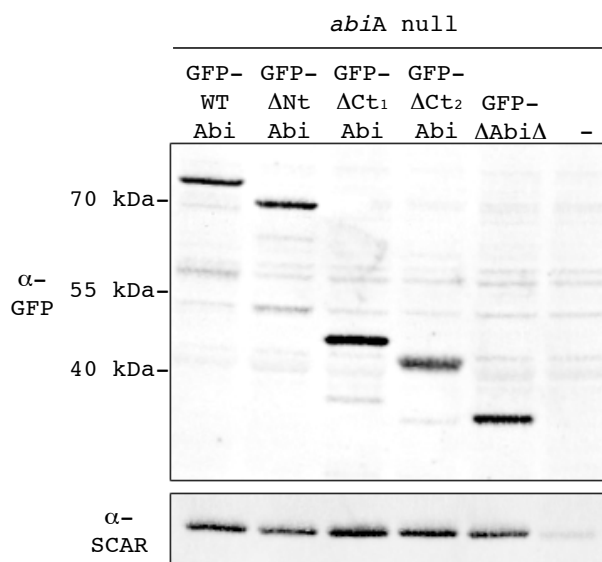
Figure 3.2, Identification of a minimal Abi fragment that stabilises SCAR: a) Western blots demonstrating stabilisation of SCAR by the untagged Abi deletion series transformed into the *abi*A null. Top panel: The expression of untagged Abi deletion series in the *abi*A null was demonstrated. The loss of the N-terminal anti- (a-) Abi epitope confounded detection of this Abi fragment as well as ΔAbiΔ. Middle panel: PIR121, a stable member of the complex, was used to confirm even loading. Bottom panel: The stabilisation of SCAR by the different Abi fragments was revealed. ΔNt Abi, ΔCt$_1$ and ΔCt$_2$ all appeared to restore SCAR protein in the *abi*A null to the same extent as WT Abi. ΔAbiΔ also appeared to stabilise SCAR, if only partially. '-' = *abi*A null transformed with vector containing HSPC300-GFP only. **b) Western blots demonstrating expression of GFP-tagged Abi deletion in the *abi*A null**. Top panel: The expression of the full Abi deletion series was confirmed by GFP-labeling the Abi fragments allowing their detection through the use of an anti- (a-) GFP antibody. No gross difference in expression between the different constructs was observed. Bottom Panel: The GFP-Abi tagged Abi deletion series was found to stabilise SCAR in the *abi*A null to the same extent as the untagged Abi deletion series. '-' = *abi*A null transformed with an empty vector.

c.

d.
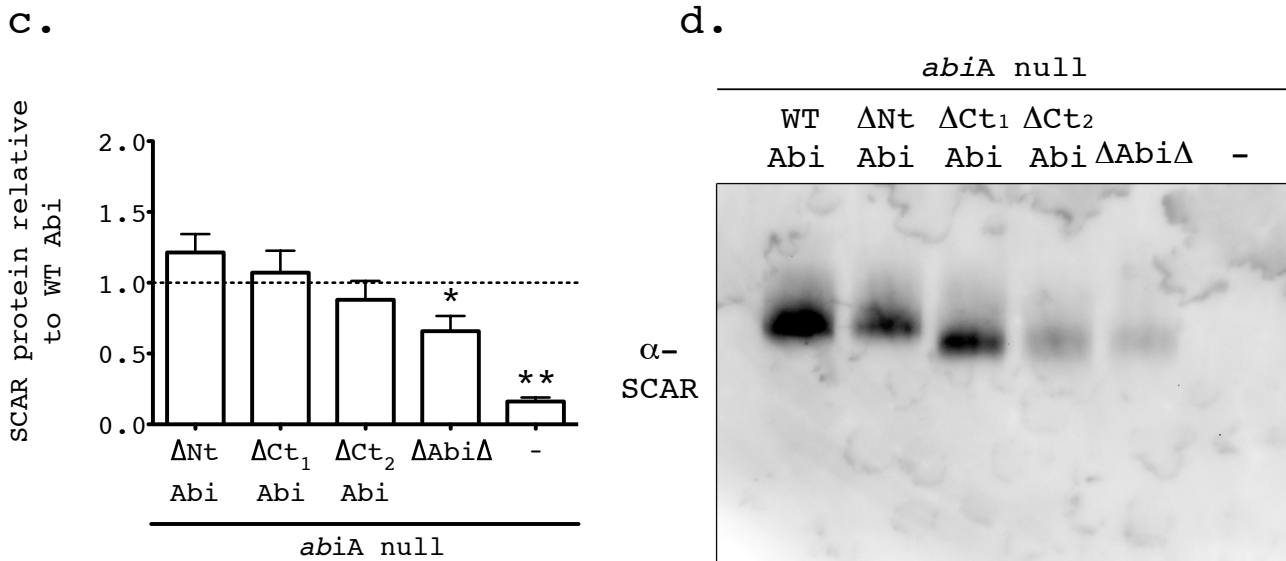
Figure 3.2, Identification of a minimal Abi fragment that stabilises SCAR (continued): c) Neither the N-terminal α1-helix nor the C-terminal poly-proline tail of Abi are required for the stabilisation of SCAR. Quantification of SCAR stabilisation by the untagged Abi deletion series was achieved by normalising the SCAR band intensity to the PIR121 band intensity for each transformant over four blots. *=significantly different from WT Abi (unpaired student's t-test, $p<0.05$). **=significantly different from WT Abi and ΔAbiΔ SCAR levels (unpaired stundent's t-tests, $p<0.0001$ in both cases). The error bars indicate SEM. '-' = *abi*A null transformed with vector containing HSPC300-GFP only. **d) Abi fragments stabilise the entire SCAR complex.** Intact protein complexes were separated by native PAGE and probed with an anti- (a-) SCAR antibody following Western blot. SCAR was found in only one high molecular weight complex in all cases. These data demonstrated that neither the N-terminal α1-helix nor the C-terminal poly-proline tail of Abi was required for SCAR complex stability. '-' = *abi*A null transformed with vector containing HSPC300-GFP only.

In summary, a total of 239 of the 332 amino acids comprising *Dictyostelium* Abi were successfully deleted, yielding a number of fragments that still stabilised the SCAR complex.

3.3 Abi fragments rescue the growth of the *abi*A null

Through the various truncated constructs we had generated, we had deleted the majority of Abi, leaving only those residues that were essential for SCAR complex stability. For the first time, we were in a position to interrogate the contribution of an individual complex member to the activity of the whole. With this in mind, we sought to determine if our Abi constructs restored every aspect of the wild-type SCAR complex in an *abi*A null with the aim of identifying functions that could be specifically attributed to Abi.

Our lab has previously demonstrated that both the NC4A2 *abi*A null and *scr*A null have growth defects. SCAR has previously been implicated in macropinocytosis and a defect in this process would undoubtedly impair growth in liquid medium (Seastone et al., 2001). However, the different lab strains of *Dictyostelium* appear to vary in their requirement for SCAR to support growth. SCAR is not required for normal growth of Ax3 cells as will be discussed in chapter 5. This discrepancy likely reflects the differences in axenic growth between these two backgrounds. For instance, the axenic laboratory strains such as Ax3 were heavily mutagenised and selected to acquire optimal growth in liquid culture (Watts & Ashworth, 1970, Loomis, 1971). This is in contrast to the NC4A2 strains, which were supposedly derived by less harsh means and have poorer growth in liquid culture to begin with (Shelden & Knecht, 1995). Because the growth of NC4A2 is dependent on SCAR, the ability of the different Abi fragments constructs to rescue the growth impairment of *abi*A null was tested. As can be seen in figure 3.3a, ΔNt Abi, ΔCt$_1$ Abi and ΔCt$_2$ Abi all restored growth on substrate to a comparable rate to that of *abi*A nulls rescued with full length WT Abi. ΔAbiΔ did not significantly improve the growth of *abi*A nulls in Petri dishes.
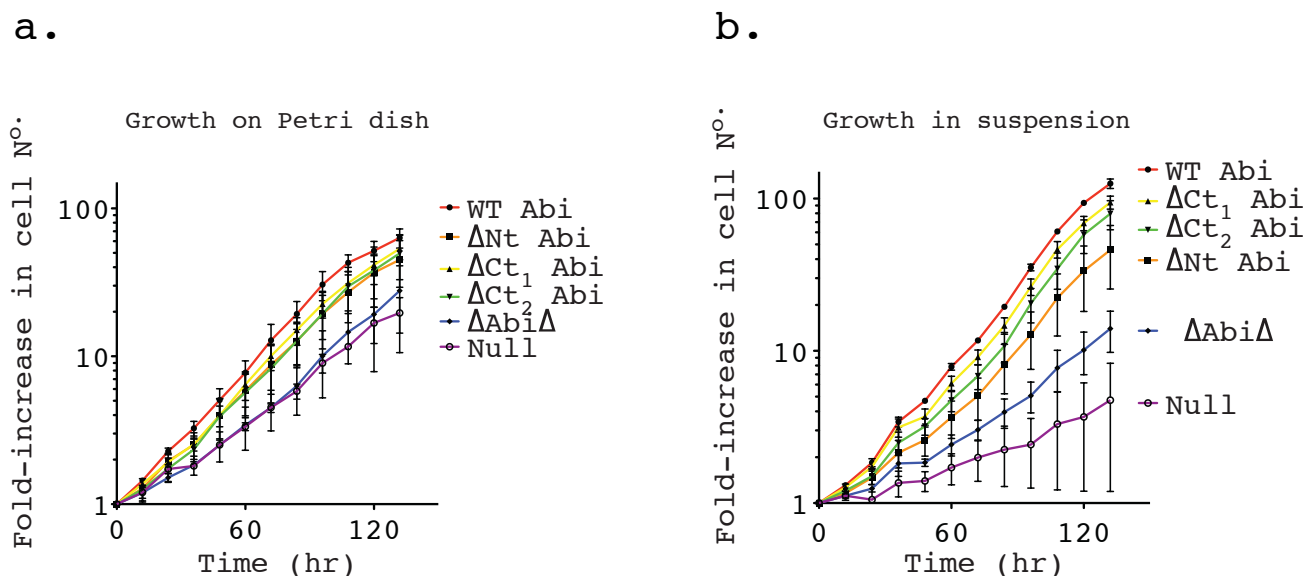
Figure 3.3, Abi fragments rescue the growth defect of the *abi*A null: a) Abi fragments rescued growth of *abi*A null when cultured on Petri dishes. Cells were plated on Petri dishes and a cell count was performed every 12 hours over 6 days. The mean fold-increase was calculated from 3 independent experiments and was plotted as shown. ΔNt Abi, ΔCt_1 and ΔCt_2 all rescued the growth of the *abi*A null to the same extent as WT Abi. Error bars indicate SEM. **b) Abi fragments rescued growth of *abi*A null when cultured in suspension.** Cells were introduced to shaking culture and a cell count was performed every 12 hours over 6 days. The mean fold-increase was calculated from 3 independent experiments and was plotted as shown. ΔNt Abi, ΔCt_1 and ΔCt_2 all rescued the growth of the *abi*A null to the same extent as WT Abi. Shaking culture demonstrated intermediate phenotype of *abi*A nulls expressing ΔAbiΔ. Error bars indicate SEM.

However, partial rescue was difficult to observe under these conditions as the defect is relatively small. As shown in figure 3.3b, growth in suspension exacerbated the growth defect of the *abi*A null and revealed an intermediate phenotype of cells rescued with ΔAbiΔ. Under these conditions, ΔAbiΔ-rescued cells doubled significantly slower than cells rescued with WT Abi (by 13.9 ± 3.9 hours, unpaired Student's t-test, p<0.05). The severe growth defect of the *abi*A null in suspension led to uneven growth and made it impractical to calculate a doubling time and perform statistical comparisons. However, it is clear that transformation with ΔAbiΔ consistently improved the growth of the *abi*A null in suspension. It was therefore concluded that loss of either terminus of Abi individually has no detrimental effect on cell growth. Furthermore, since ΔAbiΔ partially restored SCAR levels and partially restored growth, the extent to which the growth defect of the *abi*A null was rescued appeared to simply correlate with the SCAR protein levels in these cells. It was inferred that Abi contributes little to cell growth beyond stabilisation of the SCAR complex. This result implies that even when lacking a large proportion of Abi sequence, the SCAR complex still retains sufficient functionality to support optimal growth and so argues against a central role for Abi in complex recruitment and activation.

3.4 SCAR complex containing truncated Abi localises normally in migrating cells

Abi has been proposed to have a central role in the recruitment and activation of the SCAR complex during pseudopod formation and cell migration (Innocenti et al., 2004, Leng et al., 2005). In previous sections it was demonstrated that neither terminus of Abi alone was required for SCAR complex stability. We next wished to determine whether either terminus of Abi was required for normal SCAR complex localisation and if the Abi fragments could restore the suppressed rate of pseudopod formation observed in the *abi*A null. Co-expression of GFP-tagged complex member HSPC300 alongside the Abi fragments identified above in an *abi*A null background
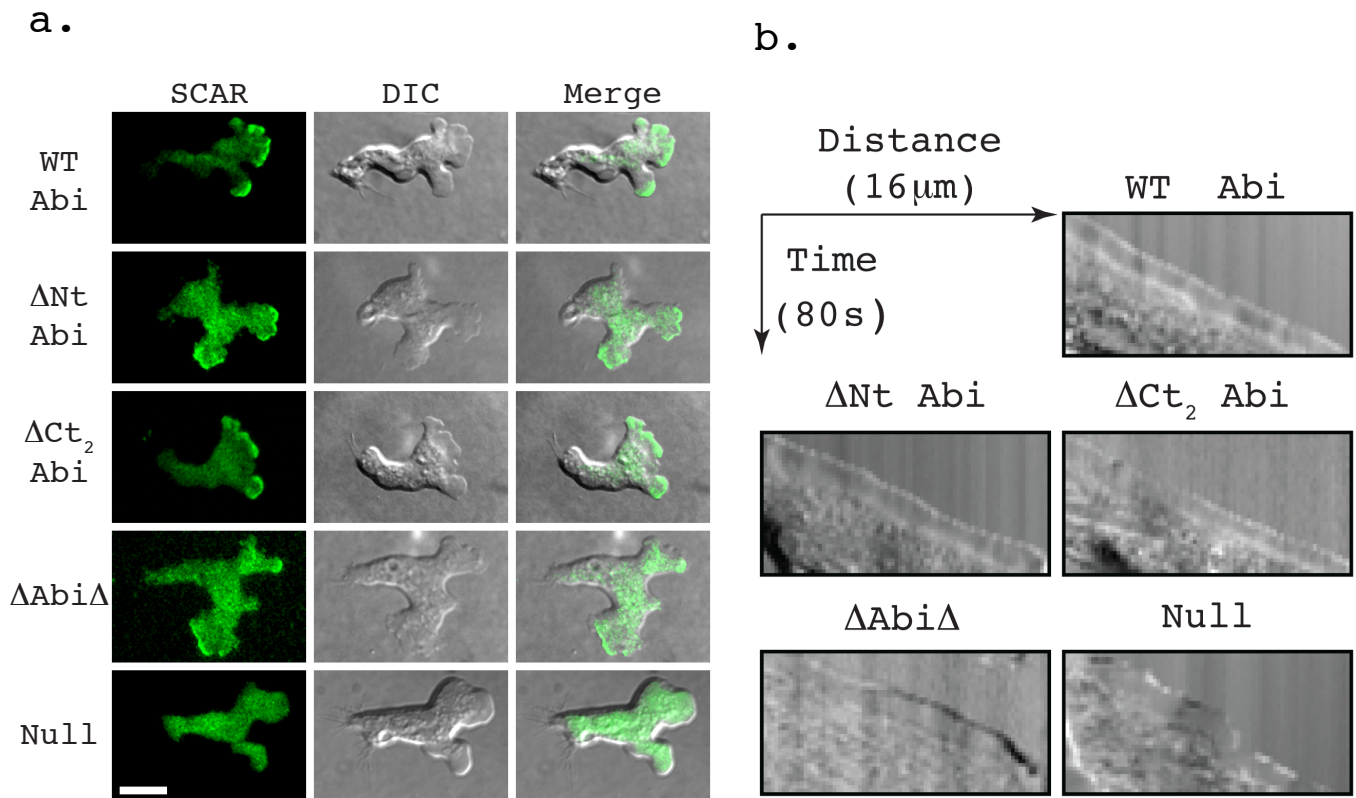
Figure 3.4, Abi fragments support normal SCAR complex dynamics: a) SCAR complexes containing truncated Abi proteins localised normally in motile cells. Representative TIRF and DIC images of motile *abi*A nulls co-expressing Abi truncated constructs and HSPC300-GFP (SCAR). All the Abi fragments tested restored the recruitment of the SCAR complex to the pseudopodia. The scale bar represents 10 μm. **b) Abi fragments restored smooth pseudopod extension of the *abi*A null.** Representative kymographs highlighting smooth progression of advancing pseudopodia in cells expressing Abi deletion series. In contrast, the *abi*A null presented with a 'ragged' slope indicative of blebbing. Each kymograph represents a total of 16 μm in distance (X-axis) and 80 seconds in time (Y-axis).

c.
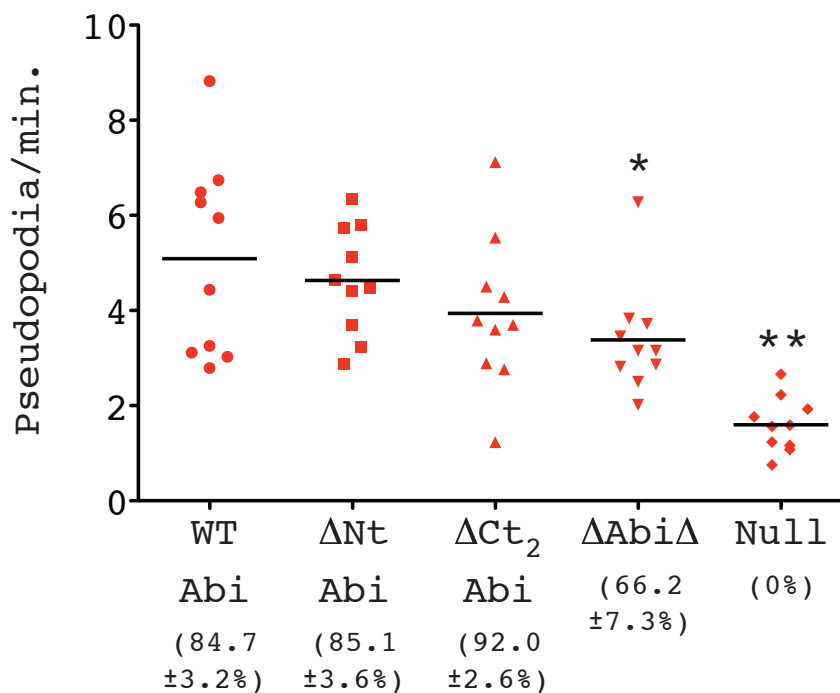
Figure 3.4, Abi fragments support normal SCAR complex dynamics (continued): c)
All truncated Abi proteins rescue suppressed rate of pseudopod formation in the
***abi*A null**. Pseudopod formation in motile *abi*A nulls rescued with Abi deletion series
was observed by TIRF and DIC microscopy. Rates of pseudopod extension were
calculated and plotted in the above graph (10 cells/transformant over two independent
experiments). The black horizontal bars represent the mean rate of pseudopod
formation. HSPC300-GFP recruitment to the pseudopodia was also determined
(percentages in brackets indicate proportion of pseudopodia with robust HSPC300-GFP
localisation ±SEM). *=significantly reduced rate of pseudopod formation compared to
WT Abi rescued cells (unpaired student's t-test, $p < 0.05$). **=significantly reduced rate
of pseudopod formation compared to WT Abi and ΔAbiΔ rescued cells (unpaired
student's t-test, $p < 0.001$ in both cases).

allowed the localisation of the respective mutant complexes to be determined. When visualised by TIRF microscopy, which illuminates only the bottom hundred nanometres of a cell, HSPC300-GFP is seen to localise strongly to the leading edge of migrating wild-type cells, correlating with pseudopd extension (Veltman et al., 2012). As shown in figure 3.4a, no obvious differences in SCAR complex dynamics were observed between any of the Abi fragments or full length Abi, which all showed robust concentration of the complex at the leading edge of randomly migrating cells. This was accompanied by the smooth extension of cellular protrusions as illustrated by the kymographs in figure 3.4b. The HSPC300-GFP recruitment was weaker in *abi*A nulls expressing ΔAbiΔ, and they were also more prone to outbreaks of blebbing. Both observations are consistent with there being reduced levels of SCAR in these cells (Ura et al., 2012, Veltman et al., 2012). As shown in figure 3.4c and in Movie 1, SCAR complex driven pseudopodia were clearly formed by the cells transformed with ΔAbiΔ, although the rate of pseudopod extension was significantly decreased compared to WT Abi rescued cells (unpaired Student's t-test, p<0.05). HSPC300-GFP was essentially completely delocalised in *abi*A null transformed with HSPC300-GFP alone and the motility of these cells was driven more by blebs than by pseudopodia (figure 3.4a). This was reflected in a significant reduction in protrusion rate of ~30% compared to WT Abi rescued cells (figure 3.4c, unpaired Student's t-test, p<0.001). The few pseudopodia that were generated were devoid of concentrated HSPC300-GFP (figure 3.4c) and were likely driven by WASP A as our lab has previously shown in SCAR complex deficient cells, including the *abi*A null (Veltman et al., 2012). All of this implies that not only is the majority of Abi sequence unnecessary for SCAR complex stabilisation, but neither is it essential for normal complex localisation. Furthermore, since N-terminally or C-terminally truncated Abi fully restored the suppressed rate of pseudopod formation in the *abi*A null, it would appear that neither termini of Abi is required for SCAR complex activation or function either.

3.5 Loss of 1st alpha helix of Abi exacerbates the cytokinesis defect of *abi*A null

Our lab has previously shown that the *Dictyostelium abi*A null has a tendency to become multinucleate due to impaired cytokinesis (Pollitt & Insall, 2008). Many *Dictyostelium* mutants accumulate multinucleate cells during growth in shaking culture but can resolve such cells when introduced to a substratum by myosin-II independent cytokinesis B or by the mitosis independent cytokinesis C (Nagasaki et al., 2002). However, even in the presence of a substratum, *abi*A nulls became multinucleate, implying a defect that disturbed all three of these modes or aspects of cytokinesis. The *abi*A constructs generated here were tested to determine which deletions rescued this phenotype. Doubling times were derived from the growth curves shown in figure 3.3a and cells were plated at a low density on glass coverslips and cultured for the time taken for ten divisions. Following this the cells were then fixed and stained with DAPI to visualise the nuclei and fluorescently labeled phalloidin so as to stain the F-actin cortex and clearly define the cell boundaries. Although WT Abi and ΔCt₂ Abi appeared to rescue the cytokinesis defect of the *abi*A null, multinuclear cells were still evident in *abi*A nulls expressing ΔNt Abi and ΔAbiΔ. Examples of fixed and stained multinucleate cells are shown in figure 3.5a. The number of nuclei per cell was counted and the proportion of multinucleate cells for each of the transformants is shown in figure 3.5b. Cells with ≥2 nuclei were rarely seen in *abi*A nulls rescued with full-length Abi or Abi lacking the C-terminal poly-proline tail. The majority of these cells were mononucleate, with only a small population of cells with ≥2 nuclei (12 and 7% of total respectively). As has been previously documented, the *abi*A nulls expressing only HSPC300-GFP accumulated multinucleate cells with a significant increase in the number of cells with ≥2 nuclei compared to the WT Abi controls (26%, chi-square test yielded p<0.0001). Furthermore, there were also more severely multinucleate cells present, including some with as many as ten nuclei per cell. Surprisingly, deletion of the N-terminal α1 helix resulted in a significant increase in the number of cells with ≥2 nuclei (42%)
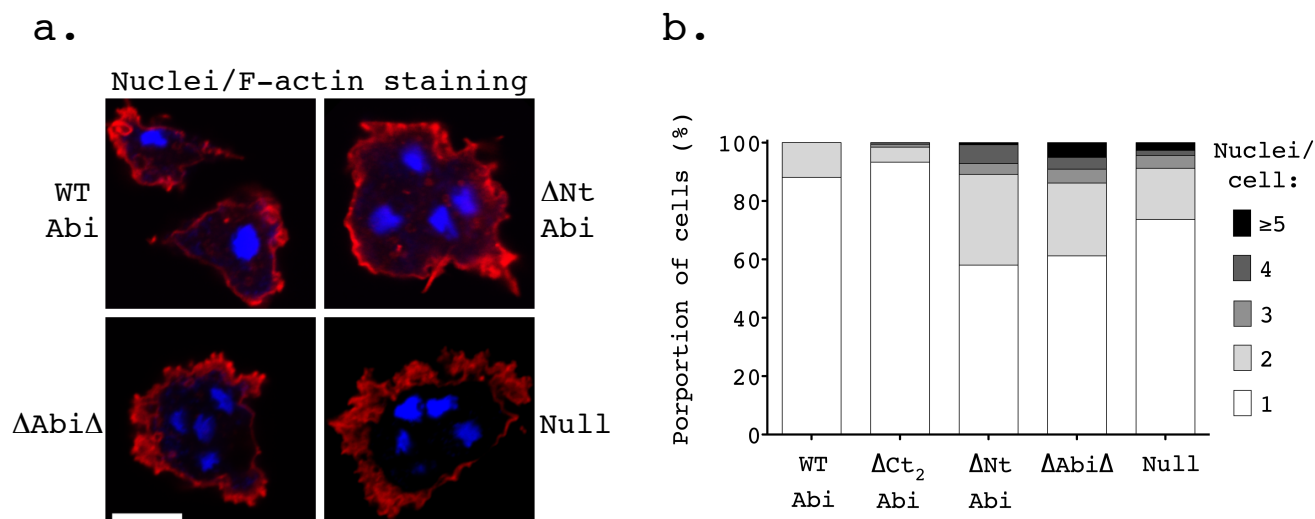
Figure 3.5, The N-terminus of Abi regulates the SCAR complex during cytokinesis: a) Examples of normal and multinucleate cells found in *abi*A nulls expressing WT Abi, ΔNt Abi, ΔAbiΔ and the *abi*A null. Cells were cultured for time taken for 10 divisions on glass cover slips before fixation and staining with DAPI (nuclei, blue) and fluorescently-labelled phalloidin (F-actin, red). Representative images of normal and multinuclear cells found in *abi*A nulls expressing WT Abi, ΔNt Abi, ΔAbiΔ or an empty vector (Null). WT Abi rescued the cytokinesis defect of the *abi*A null, however multinuclear cells were still evident in *abi*A nulls expressing ΔNt Abi and ΔAbiΔ. The scale bar represents 10 μm. **b) Deletion of 1st alpha-helix is sufficient to reproduce and to exacerbate the cytokinesis defect of the *abi*A null.** A graph illustrating the percentage of cells with 1, 2, 3, 4 or ≥5 nuclei cells rescued with the different Abi constructs (~100 cells/experiment, ≥2 independent experiments). Whereas the C-terminal poly-proline tail of Abi was not required to rescue the cytokinesis defect of the *abi*A null, loss of the N-terminus was sufficient to replicate and exacerbate the defect of the *abi*A null.

even when compared to the *abi*A null (chi-square test, p<0.0001). This was also true of ΔAbiΔ expressing cells (39% of cells with ≥2 nuclei). Again this proved a significant increase compared to both the WT Abi controls and the null (chi-square test, p<0.0001 and <0.01 respectively) although there was no statistical difference when compared to the ΔNt Abi expressing cells. The differing severity in the phenotype observed between the null, ΔAbiΔ and ΔNt Abi expressing cells correlated with increasing SCAR in these cells (figure 3.2) and therefore presumably an increasing amount of deregulated SCAR complex.

These data are consistent with our lab's previous conclusion that it is the remaining SCAR in the *abi*A null that is responsible for the cytokinesis defect in these cells. The data presented here identify the α1 helix of Abi as being important for the regulation of the SCAR complex during cytokinesis.

As to exactly how the α1 helix of Abi is regulating SCAR complex activity and what it is interacting with remains to be answered. Nevertheless, this work has identified one functional domain on what still remains a mostly impenetrable complex.

3.6 Chapter 3 summary

In this chapter, the role of SCAR complex member Abi was explored. Establishing the individual contributions of the different complex members has been impeded by the inter-dependence of the complex members on one another for stability. Here, an Abi deletion series was generated and fragments that stabilised the SCAR complex were identified. Loss of either the N-terminal α1 helix or the C-terminal poly-proline tail alone did not impair SCAR protein of complex stability. A minimal fragment was created that was truncated at both termini and it was found that this construct could also stabilise SCAR, if only partially. The ability of these constructs to rescue the phenotype of the *abi*A null was then investigated. It was firstly found that neither terminus alone was required to restore SCAR dependent growth of the NC4A2 *abi*A null, which suggested that Abi does not regulate the SCAR complex during macropinocytosis. Next investigated was SCAR complex localisation during cell migration and again it was found that neither terminus of Abi was required for complex recruitment to the leading edge during pseudopod extension. It was also found that neither terminus of Abi was required to restore the suppressed rate of pseudopod formation in the *abi*A null. From these data we inferred that Abi was not

required for normal complex localisation or activation during cell migration, despite what has previously been published.

Finally, the cytokinesis defect of the *abi*A null was exacerbated by the expression of Abi fragments that lacked the N-terminal α1 helix. The cytokinesis defect of the *abi*A null has been attributed to the misregulation of the residual SCAR in these cells during cell division ((Pollitt & Insall, 2008)). Given that Abi fragments lacking the α1 helix stabilise the SCAR complex, it was reasoned that this aggravated the cytokinesis defect by increasing the amount of misregulated SCAR present during cell division. Finally, it was tentatively concluded that Abi is not required for SCAR complex recruitment or activation, but instead acts as a modulator of SCAR activity during such events as cytokinesis.

Chapter 4

WASP is not required for pseudopod formation but instead confines Rac activity to the leading edge

4.1 Creation of a *Dictyostelium was*A inducible knockout

Work from our lab has established that SCAR and not WASP A is the major promoter of Arp2/3 complex-mediated actin polymerisation that underlies pseudopod extension and cell movement in *Dictyostelium*. In our hands, GFP-WASP A is predominantly found at sites of CME and its localisation is clearly distinct from that of SCAR in wild-type cells (Veltman et al., 2012). It is also observed at sites of macropinocytosis, as shall be discussed in more detail in the next chapter. A *Dictyostelium was*A null had always eluded both our lab and other labs and the community has long considered *was*A to be an essential gene. One group has claimed to have created an inducible *Dictyostelium was*A null and asserted that WASP A is vital for chemotaxis (Myers et al., 2005). Complicating the issue, we have recently found that although SCAR and not WASP A promotes pseudopod formation in wild-type cells, WASP A is capable of assuming the role of SCAR in a *scr*A null (Veltman et al., 2012). Whilst WASP A is by no means capable of fully compensating for SCAR, the residual pseudopodia that a *scr*A null does form contain WASP A localising where it normally would not. However, without a *was*A null of our own we have been unable to exclude the possibility that WASP A does somehow contribute to normal pseudopod formation. To help clarify the exact role of WASP A within the cell, another attempt at creating a *was*A knockout was undertaken. Because WASP A was perceived to be essential for cell viability, an inducible approach was adopted as is outlined in figure 4.1a. To create the WASP A inducible knockout (WIKO), first the full coding sequence of *was*A was N-terminally fused with GFP and cloned into an inducible expression vector whereby the expression of GFP-WASP A could be controlled by the addition of doxycycline (Veltman et al., 2009). Following the removal of sequence required for extrachromosomal maintenance, the linearised vector was introduced into the genome of wild-type (Ax3) *Dictyostelium* by Restriction Enzyme Mediated Integration (REMI), which is a well-characterised means of insertional mutagenesis for use with *Dictyostelium* (Kuspa & Loomis, 1992). The inducibility of GFP-WASP A expression was confirmed by probing lysates from cells treated with or without
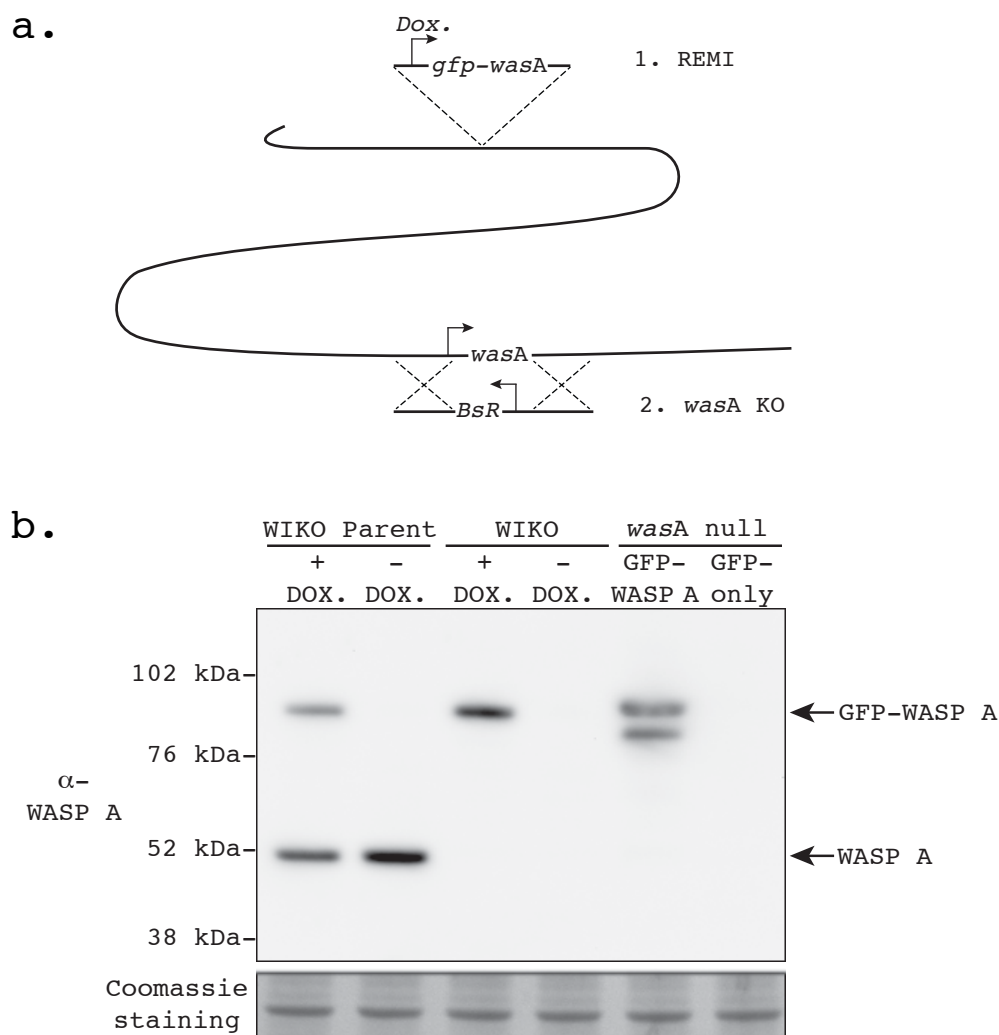
Figure 4.1, Generation of *was*A knock out cell lines: a) Diagrammatic representation of *was*A knockout strategy. GFP-WASP A under the control of a doxycycline (*Dox.*) inducible promoter was introduced into the genome of Ax3 cells by REMI to create the WIKO Parent cell line (1). The endogenous *was*A locus was then targeted for deletion by homologous recombination to create WIKO (2). Alternatively, *was*A was targeted for deletion in the Ax3 cells to create the *was*A null.**b) Validation of the various *was*A knockout cell lines by Western blotting.** Upper Panel: Lysates prepared from the WIKO Parent / WIKO ±doxycycline (DOX.) and the *was*A null ±GFP-WASP A were probed with an anti- (α-) WASP A antibody. The lower band corresponding to endogenous WASP A has clearly been lost in the WIKO and the *was*A null cell lines. A double band was always present when GFP-WASP A was expressed extrachromosomally and was presumed to be a degradation product resulting from excessive expression. Lower Panel: Subsequent Coomassie staining of the membrane was used to demonstrate equal loading.

doxycycline and with an antibody specific to WASP A following Western blotting. This yielded a strain where GFP-WASP A expression could be induced or suppressed in an otherwise wild-type background and this cell line was designated the 'WIKO Parent (IR202)'. Validation of this cell line is shown in figure 4.1b.

A *was*A knockout vector was then created with minimal overlap with the *was*A coding region itself. The purpose of excluding almost the entire *was*A coding sequence from the knockout construct was to ensure targeting of the endogenous *was*A locus rather than the integrated inducible GFP-WASP A and to prevent the possibility of a truncated *was*A fragment remaining. Using this knockout vector the endogenous *was*A locus was targeted for deletion by homologous recombination in the WIKO Parent cell line to generate the WIKO (IR203). Clones were then isolated in the presence of doxycycline to maintain GFP-WASP A expression. The complete loss of endogenous untagged WASP A expression was then confirmed by Western blot using the anti-WASP A antibody (figure 4.1b). Having successfully generated and validated the WIKO strain, these cells were then deprived of doxycycline and to our great surprise there was no obvious sign of cell death.

4.2 Generation of a *Dictyostelium was*A null

Having generated an inducible *was*A knockout, we were surprised to find that WASP A did not appear to be required for cell viability as had been published before (Myers et al., 2005). To verify that this was not due to residual, undetectable expression of GFP-WASP A in the absence of doxycycline, the endogenous *was*A locus was targeted for deletion by homologous recombination in a wild-type (Ax3) background using the same knockout construct (figure 4.1a). Clones were isolated and verified by Western blot. As shown in figure 4.1b, a *was*A null cell line (IR204) was successful generated and this cell line could be rescued by transformation with an extrachromosomal plasmid expressing GFP-WASP A. Of note from the Western blot shown in figure 4.1b was the apparent inability to increase WASP A expression above the endogenous level. The overexpression of GFP-WASP A through the use of an extrachromosomal plasmid consistently
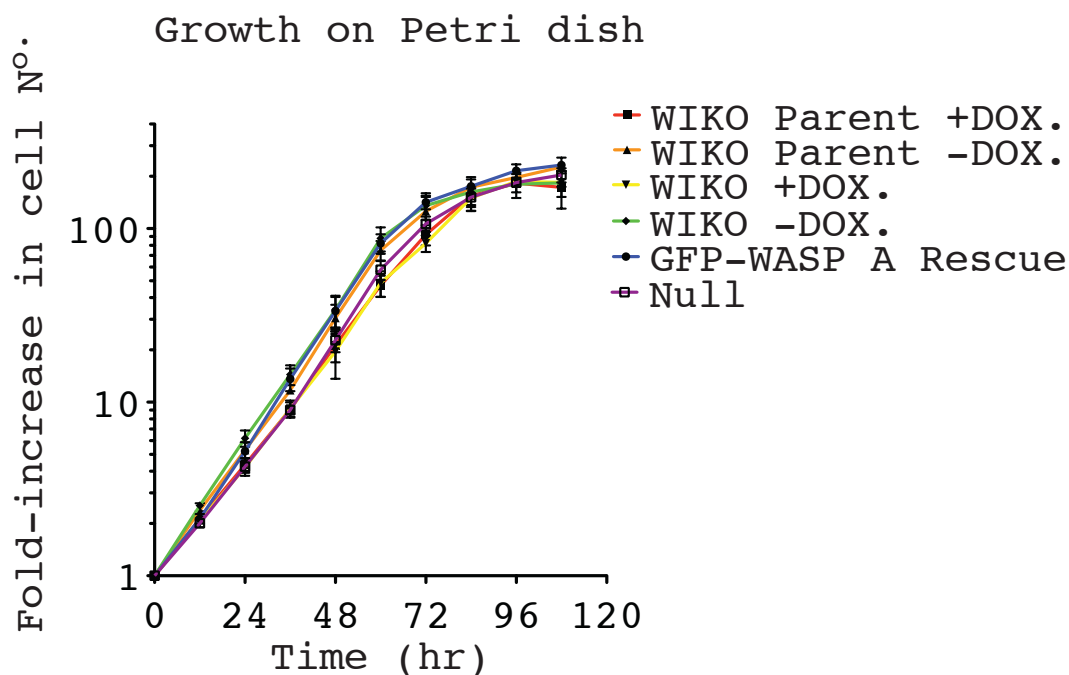
Figure 4.2, WASP A is not required for *Dictyostelium* viability: Growth curves demonstrating that *was*A deficient cell lines have no defect in growth when cultured on Petri dishes. The WIKO Parent/WIKO ±doxycycline (DOX.) and the *was*A null ±GFP-WASP A were plated on Petri dishes and a cell count was performed every 12 hours over a period of 5 days. The mean fold-increase in cell number was calculated from a number of independent experiments (Parent/WIKO ±DOX. n=2, *was*A null ±GFP-WASP A n=3) and plotted in the graph shown above. Error bars indicate SEM.

resulted in the appearance of a lower molecular weight band that presumably corresponded to degraded GFP-WASP A. Consistent with our earlier observation, there was again no indication of a growth defect in the *was*A null. To confirm this, first the WIKO Parent and WIKO cells were treated with or deprived of doxycycline for 48 hours in order to ensure GFP-WASP A expression was fully induced or suppressed prior to monitoring growth. The *was*A null was transformed with either a GFP-WASP A expressing plasmid or an empty vector. The cells were plated in Petri dishes and a cell count was performed every 12 hours over the course of 5 days.

As can be seen from figure 4.2, the growth of both *was*A deficient cell lines was identical to the controls (WIKO Parent/WIKO ±DOX. n=2, *was*A null ±GFP-WASP A n=3). Importantly, it was also clear from these data that GFP-WASP A expression had no detrimental effect on growth in the WIKO Parent cell line that still retained endogenous *was*A.

Having generated two independent WASP A deficient cell lines, we next set about characterising the phenotype of the *was*A knockout.

4.3 The *was*A null has a cytokinesis defect

Although WASP A was not required for the normal growth of *Dictyostelium* when cultured on Petri dishes, it was found that WASP A was required for efficient growth in suspension as shown in figure 4.3a (WIKO Parent/WIKO ±DOX. n=2, *was*A null ±GFP-WASP A n=5). The inability to grow in suspension immediately suggested that the *was*A deficient cells had a defect in cytokinesis as has been previously demonstrated in the myosin-II heavy chain null (De Lozanne & Spudich, 1987) and, of particular interest, the clathrin heavy chain null (Niswonger & O'Halloran, 1997). Both these mutants have defects in furrowing that can only be overcome in the presence of a substratum. To test whether WASP A is required for cytokinesis in suspension, the WIKO ± doxycycline and the *was*A null ±GFP-WASP A cells were cultured in a shaking flask and a sample of cells was removed at regular time points over the course of 5 days.

a.

Figure 4.3, The *was*A null has a defect in cytokinesis a) The *was*A null became severely multinucleate when cultured in suspension. Growth curves demonstrating that *was*A deficient cells exhibit impaired growth when cultured in suspension. The WIKO Parent/WIKO ±doxycycline (DOX.) and the *was*A null ±GFP-WASP A were introduced to shaking culture and a cell count was performed every 12 hours over 5 days. The mean fold-increase in cell number was calculated for each cell line over a number of independent experiments (Parent/WIKO ±DOX. n=2, *was*A null ±GFP-WASP A n=4) and plotted in the graph shown above. Error bars indicate SEM.
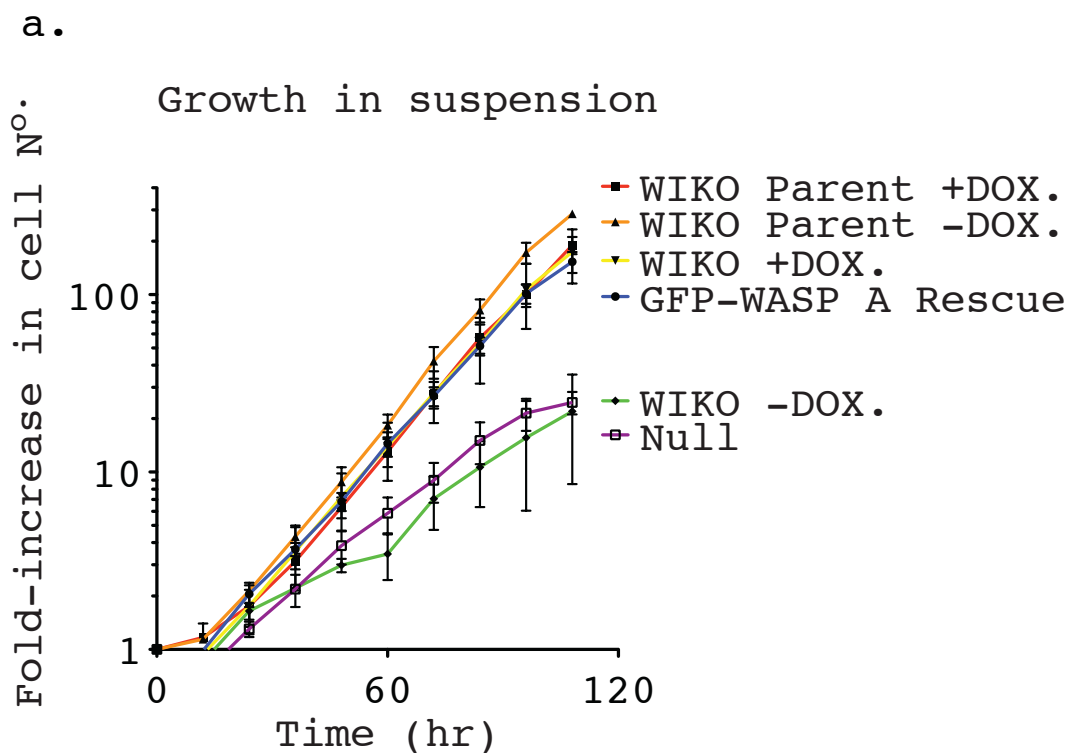
b.

c.
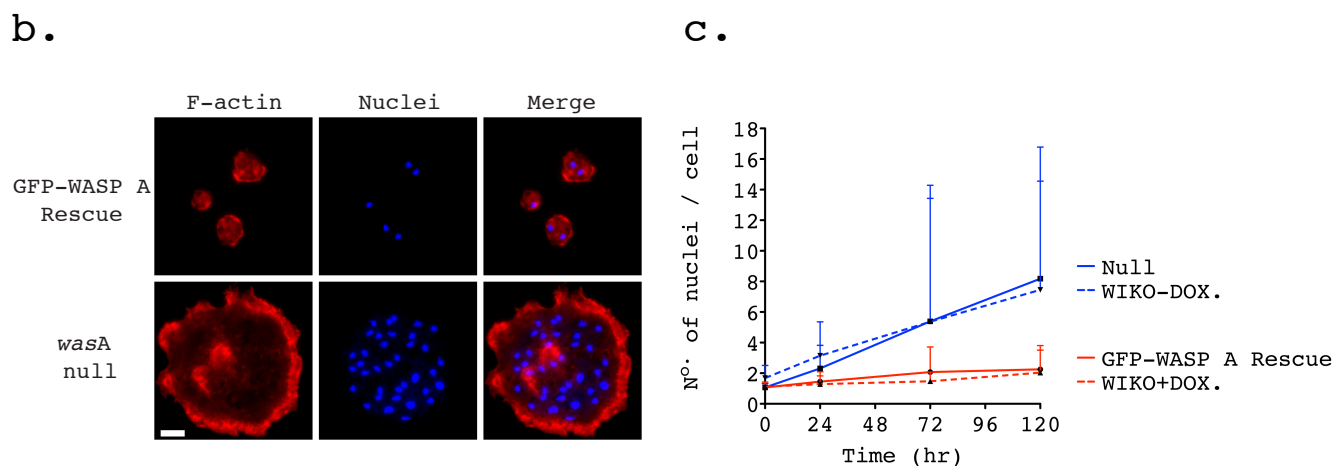
Figure 4.3, The *was*A null has a defect in cytokinesis (continued): b and c) The *was*A null becomes severely multinucleate when cultured in suspension. WIKO ±doxycycline (DOX.) and the *was*A null ±GFP-WASP A were introduced to shaking culture. A sample of cells for each cell line were taken at selected time points and were fixed and stained with fluorescently labeled phalloidin (F-actin) and DAPI (Nuclei). **b)** an extreme example of a multinucleate *was*A null cell obtained through shaking culture. The scale bar represents 10 μm. **c)** The number of nuclei per cell was counted at the indicated time points and the mean was plotted to demonstrate that *was*A deficient cells rapidly become multinucleate when cultured in suspension (*was*A null ±GFP-WASP A n≈200 cells/cell line over 2 independent experiment, WIKO±DOX. n≈100 cells/cell line for 1 experiment). Error bars represent standard deviation (only upper bars shown for clarity).

d.
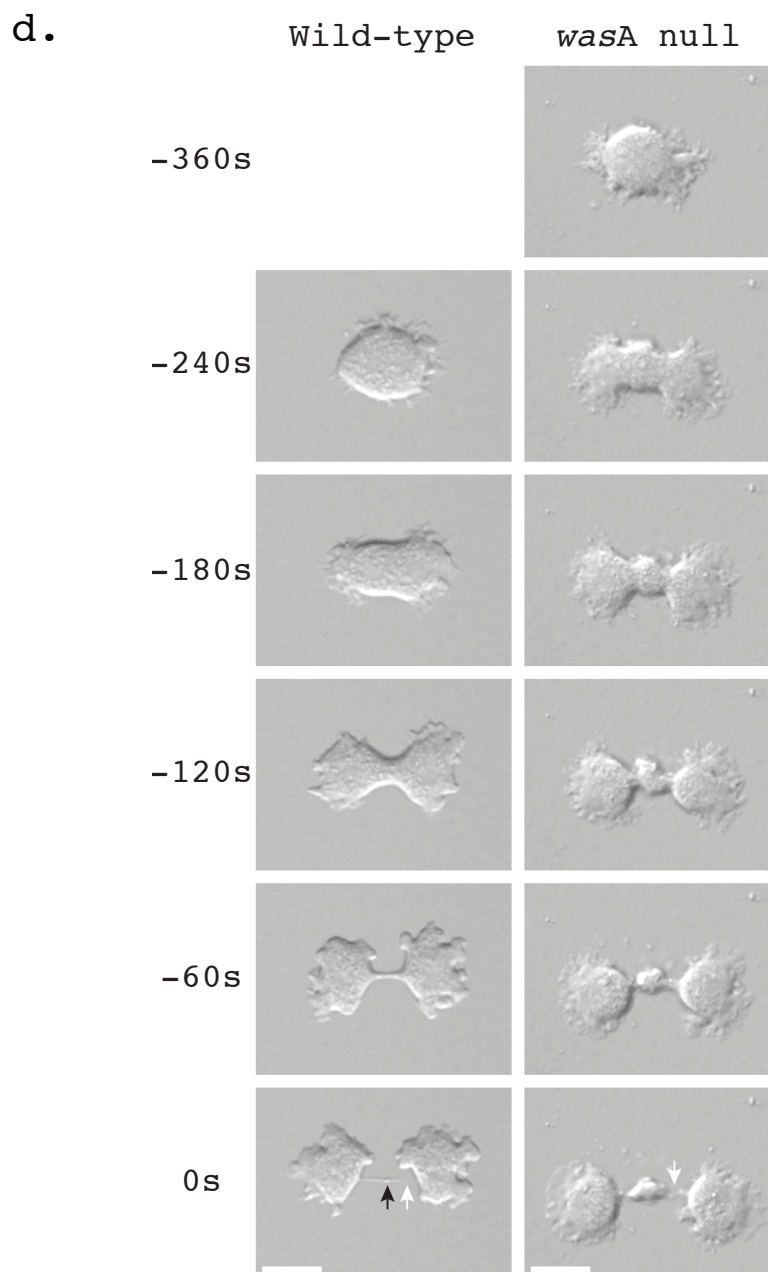
Figure 4.3, The *was*A null has a defect in cytokinesis (continued): d) The *was*A null exhibits abnormal bulging in its cleavage furrow during ingression. Individual DIC images of representative dividing wild-type and *was*A null cells. Images separated by indicated time (in seconds) prior to abscission (=0 seconds). The *was*A null takes longer to complete cytokinesis and frequently exhibits bulging within its cleavage furrow. The black arrow indicates the midbody in the wild-type cell, which is obscured in the *was*A null and the white arrows indicate the point of abscission. The scale bars represent 10 μm.

The cells were then fixed and stained with DAPI and Texas Red conjugated phalloidin to highlight the nuclei and actin cortex respectively. It was immediately apparent that *was*A knockout cells had a defect in cytokinesis when deprived of a substratum and an extreme example of a multinucleate *was*A null cell is depicted in figure 4.3b. The number of nuclei per cell was quantified and is shown in figure 4.3c (WIKO ± DOX. n=1, *was*A null ±GFP-WASP A n=2). All the cells, regardless of WASP A status, were essentially mononucleate when harvested from a Petri dish and introduced to shaking culture at the start of the experiment (0 hour). However, the mean number of nuclei per cell very quickly increased in the *was*A deficient cell lines with increasing time in suspension. By 120 hours, the average *was*A null had 8.2 nuclei, although as suggested by the image shown in figure 4.3b and the large standard deviation (±8.6 nuclei/cell), the average masks how extremely multinucleate some of the cells had become. This was compared to the *was*A null rescued with the GFP-WASP A expressing plasmid which after 120 hours of growth in suspension had on average 2.3 nuclei per cell with a standard deviation of 1.6 nuclei. The *was*A null had on average become significantly more multinucleate than the GFP-WASP A rescued cells by the first 24 hours of growth in shaking culture (unpaired Student's t-test, $p<0.0001$).

Even when cultured on a surface where they can divide successfully, the *mhc*A null and the *chc*A null exhibit obvious cleavage furrow defects during cytokinesis (Zang et al., 1997, Gerald, Damer, O'Halloran, & De Lozanne, 2001). To address whether the *was*A null had a defect in furrowing during cytokinesis, wild-type and *was*A null cells were plated on glass bottom dishes, allowed to adhere and compressed slightly under an agarose slab. High magnification DIC was used to identify round, mitotic cells, which were then followed over the course of cytokinesis. As can be seen from the representative cells shown in figure 4.3d, the *was*A null had clear difficulties in forming a stable cleavage furrow during cytokinesis. In contrast to wild-type cells, the cleavage furrow of the dividing *was*A null was prone to bulging, which in turn impaired ingression and final abscission. This bulge did not appear to be a grossly enlarged mid-body, with mid-bodies only evident in wild-type cells just prior to abscission. Instead these bulges were observed from almost the outset of furrowing and appeared to be composed of excessive material that was trapped between the contractile rings of the two forming daughter cells. Although not formally quantified, the cytokinesis of the *was*A null was consistently seen to take longer and usually

ended with the cells failing to complete abscission and instead tearing themselves apart by cytokinesis B. In summary, the *was*A null has impaired furrow formation, rendering it deficient in myosin-II dependent cytokinesis A and unable to grow in the absence of a substrate in a manner that was very reminiscent of the *chc*A null (Gerald et al., 2001).

4.4 Other phenotypes of the *was*A null

Despite the normal growth of the *was*A null on Petri dishes (figure 4.2), a number of other phenotypes were clearly evident. Although the *was*A null had no growth defect when cultured in Petri dishes in conventional, undefined, 'full' HL5 medium, it struggled to grow in the defined, 'minimal' SIH medium, which is still capable of supporting robust wild-type cell growth (figure 4.4a, n=2). When cultured on bacterial lawns, it was also noted that the *was*A null failed to form fruiting bodies once it had consumed all the available bacteria (data not shown). The absence of fruiting bodies in the colonies of the *was*A null grown on bacterial lawns suggested a developmental defect. To verify the developmental defect, WIKO ± doxycycline and the *was*A null ±GFP-WASP A cells were harvested and washed with nutrient-free developmental buffer. They were plated at equal cell density to yield a confluent layer of cells. Following slight compression under agarose, the cells were left to develop over a 24-hour period with their progress monitored by low magnification phase contrast microscopy. As demonstrated by figure 4.4b, the WASP A positive controls began to aggregate after 7-12 hours of starvation, however, the *was*A deficient cells failed to show any signs of entering development (repeated over three independent experiments). Identical results were observed when the control and *was*A deficient cells were plated and starved on top of moist agar, when fully submerged in developmental buffer or when applied to moist filter pads as well as when cultured on bacterial lawns as reported above (data not shown).

a.
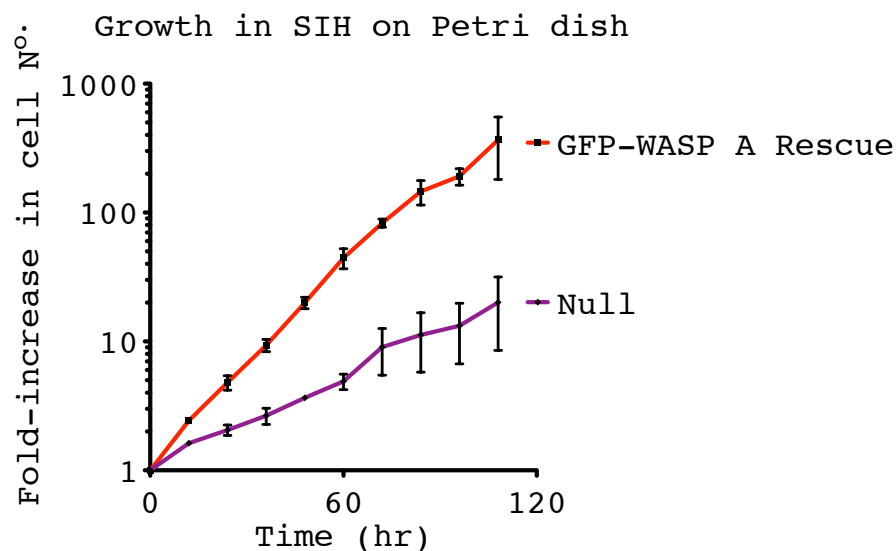
b.
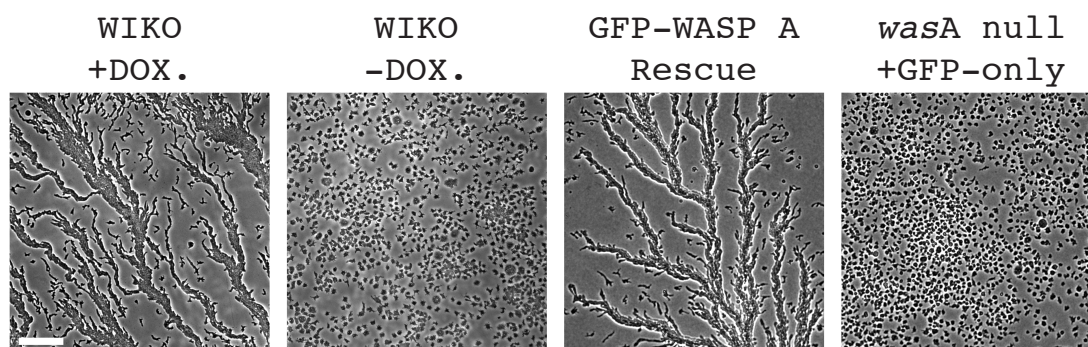
Figure 4.4, Other notable phenotypes of the *was*A null: a) Growth curve demonstrating that *was*A deficient cells have impaired in growth in minimal medium. The *was*A null ±GFP-WASP A was plated in Petri dishes in minimal (SIH) medium and a cell count was performed every 12 hours over a period of 5 days. The mean fold-increase in cell number for each time point was calculated from two independent experiments and plotted in the above graph. Error bars indicate SEM. **b) The *was*A null has a complete block in development.** WIKO ±doxycycline (DOX.) / the *was*A null ±GFP-WASP A were washed free of nutrients, plated at an equal cell density and left to develop over a 24 hour period. Representative phase contrast images are shown demonstrating that *was*A deficient cells are unable to aggregate to initiate development. The scale bar represents 100 μm.

To summarise our preliminary phenotypic characterisation of the *was*A knockout, we have demonstrated that it has impaired furrowing during cytokinesis and has an inability to divide when cultured in suspension. We have also shown that the *was*A null has an impaired ability to grow in minimal media and has a complete block in development.

4.5 WASP A is not required for pseudopod formation

Previously, our lab has shown that in wild-type cells, it is SCAR that localises to the tips of growing pseudopodia and not WASP A, which instead predominantly localises to sites of CME (Veltman et al., 2012). These findings are also consistent with what has been demonstrated in human cell lines (Weiner, et al., 2006, Merrifield et al., 2004). However, such observations remain in direct contradiction to the work of Myers et al., (2005), who generated an inducible *was*A null and found that WASP A was essential for actin driven chemotaxis. Having created an independent *was*A null, we found ourselves in a position to resolve the controversy surrounding the role of WASP A in *Dictyostelium* motility. From this point forward we chose to perform all experiments using the *was*A null rather than WIKO.

Unstimulated, vegetative axenic cells move very little, possibly due to their constitutive macropinocytosis (*D. Veltman, personal communication*). One of the standard means of testing *Dictyostelium* motility is to starve the cells and induce sensitisation towards cAMP. The highly chemotactic nature of developed cells towards a source of cAMP can then be utilised to compile data on speed, directionality or pseudopod formation rate. However, as has been shown, the *Dictyostelium was*A null has a complete block in development and so motility could not be assessed in this way. As an alternative, we adopted the under-agarose folate chemotaxis assay devised by Laevsky & Knecht, (2001). This assay tests the chemotaxis of vegetative cells by utilising folic acid as a chemoattractant and circumvents the requirement for development. The slight compression induced by the agarose
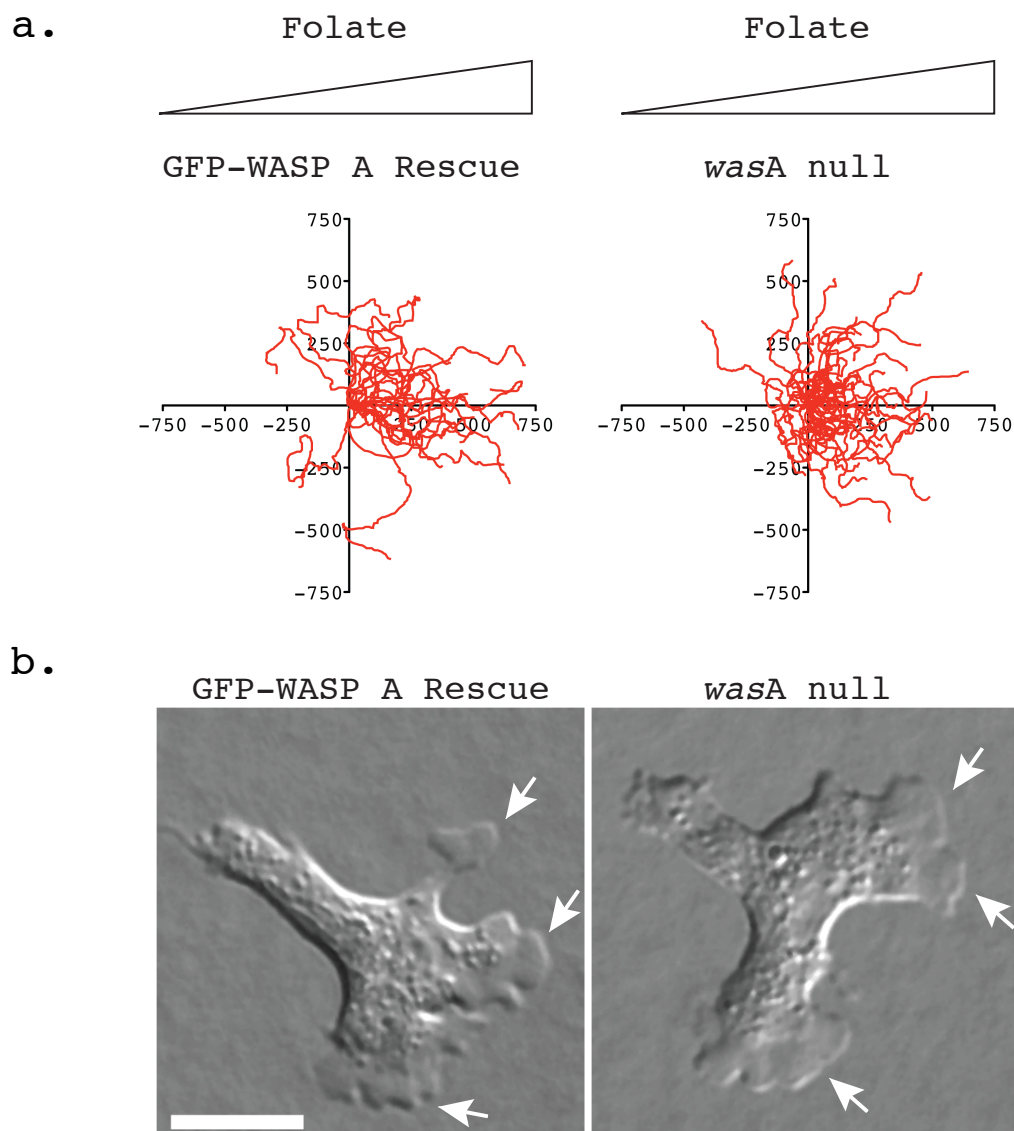
Figure 4.5, WASP A is not required for chemotaxis or pseudopod formation: a) The wasA null is capable of robust chemotaxis. The motility of the wasA null ±GFP-WASP A was investigated through the use of the under agarose folate chemotaxis assay. Cell tracks representing 30 minutes of GFP-WASP A rescue and wasA null cell migration (>20 cells/cell line from 3 independent assays) show equivalent, strong bias in the direction of the chemoattractant (from left to right, with triangles representing the folate gradient) The scale of both axes is in μm. **b) Pseudopod formation in the wasA null appears normal.** Representative DIC images demonstrating that the wasA null extends pseudopodia that are identical to those formed by the GFP-WASP A rescue. White arrows highlight prominent pseudopodia. The scale bar represents 10 μm.

c.

Pseudopodia/min.

GFP-WASP A Rescue   wasA null

d.

F-actin   Arp2/3 complex   Merge

Wild-type
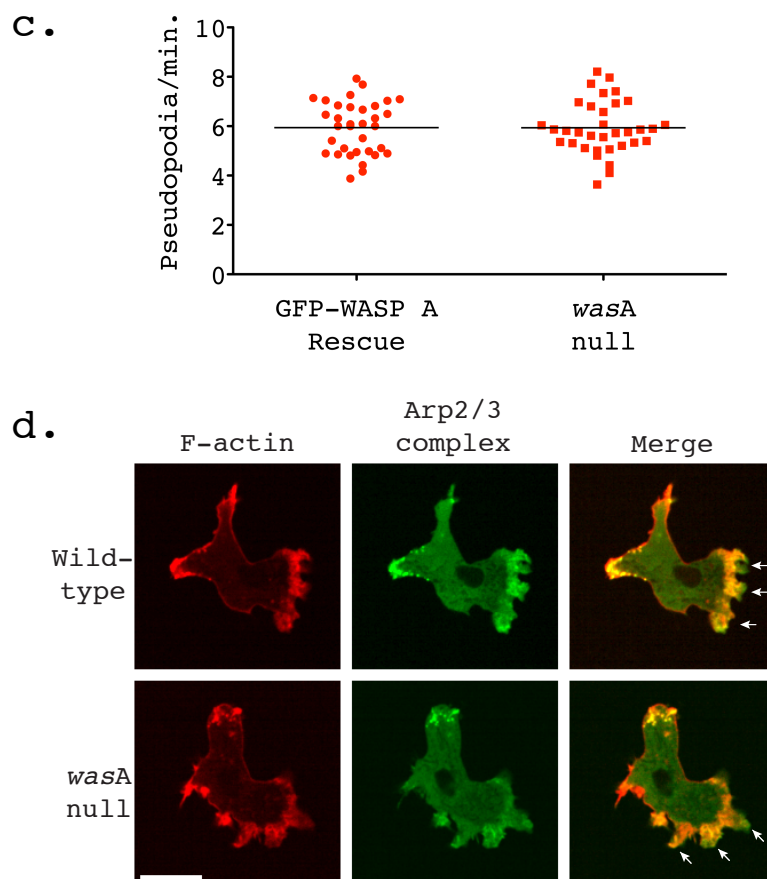
wasA null

Figure 4.5, WASP A is not required for chemotaxis or pseudopod formation (continued): c) The *was*A null has a normal rate of pseudopod formation during chemotaxis. Pseudopod formation in chemotaxing GFP-WASP A rescue and *was*A null cells was observed by DIC. Rates of pseudopod extension were calculated and plotted in the above graph (34 cells/cell line over two independent chemotaxis assays). The black horizontal bars represent the mean rate of pseudopod formation for the GFP-WASP A rescue and the *was*A null, which were found to be nearly identical (5.94 versuses 5.93 pseudopodia/min. respectively). An unpaired student's t-test confirmed that there was no significant difference in the mean rate of pseudopod formation between the two cell lines. **d) The chemotaxis of the *was*A null is driven by pseudopod formation.** RFP-Lifeact (F-actin) and a GFP-ArpC4 (Arp2/3 complex) were co-expressed in wild-type and *was*A null cells and visualised in chemotaxing cells by spinning disc confocal microscopy. The representative images shown demonstrate that the *was*A null is capable of recruiting the Arp2/3 complex to the leading edge to drive actin-based pseudopod extension. The scale bar represents 10 μm.

confines the chemotaxing cells to one plane, which benefits optical visualisation. Conditions that strongly favoured pseudopod- as opposed to bleb-based migration were obtained by varying factors such as the percentage agarose used in the assay.

Having established suitable conditions for observing pseudopod-driven cell migration, vegetative *was*A nulls were submitted to this assay and chemotaxis was first visualised by low magnification phase contrast microscopy. As demonstrated by the cell tracks in figure 4.5a and contrary to what has been previously published by Myers et al., (2005), the *was*A null was capable of robust chemotaxis (>35 cells tracked over 3 independent experiments). The tracks were visually indistinguishable from those generated by *was*A null cells rescued with a GFP-WASP A expressing plasmid. High magnification DIC was used to study the morphology of the chemotaxing *was*A null. As can be seen form the examples shown in figure 4.5b, normal pseudopod formation supported the motility of the *was*A null. To confirm that the *was*A had no defect in pseudopod formation, we made short time lapses of migrating GFP-WASP A rescue and *was*A null cells using DIC microscopy and counted the number of pseudopodia extended. As demonstrated in figure 4.5c, the *was*A null had an identical rate of pseudopod formation when compared to the GFP-WASP A rescue (>30 cells over 2 independent experiments). On average, the *was*A null extended 5.94 pseudopodia per minute, with a SEM of ±0.18 compared to the GFP-WASP A rescue that had a mean rate of 5.93 pseudopodia per minute with a SEM of ±0.18. The normal rate of pseudopod formation observed in the *was*A null was also confirmed in an independent mutant, which shall be discussed in subsequent chapters. Finally, we co-expressed Lifeact-mRFP as a marker for F-actin and GFP-ArpC4 as an Arp2/3 complex marker in both wild-type and *was*A nulls and submitted them to the under-agarose folate chemotaxis assay. Live cell spinning disc confocal microscopy revealed enrichment of the Arp2/3 complex and F-actin at the leading edge of both wild-type and *was*A null cells, examples of which are shown in figure 4.5d and Movie 2. In summary, it was quite clear that the *was*A null had no defect in pseudopod formation despite what has been previously published.

4.6 WASP A does contribute to cell motility

We have shown that WASP A is not required for actin-driven pseudopod formation or for chemotaxis. However, during analysis of the *was*A null cell tracks (figure 4.5a), it was noted that it had a small, but consistent decrease in migratory speed. As shown in figure 4.6a, the *was*A null has a statistically significant ~30% decrease in speed during folate chemotaxis when compared to the GFP-WASP A rescue (>30 cells over 3 independent experiments, unpaired Student's t-test, p<0.0001). Again, this was also verified with an independent *was*A mutant as shall be discussed in later chapters. The reduced migratory speed of the *scr*A null can be directly explained by its suppressed rate of pseudopod formation (Veltman et al., 2012). However, it has been shown here that the *was*A null has no such defect. Instead, it was reasoned that the WASP A must have an indirect role in cell motility and so we studied its migration for clues as to what it could be. It was noted that the *was*A null frequently exhibited an enlarged, bulbous uropod during persistent cell migration, with high magnification examples shown in figure 4.6b. Quantification of this phenotype based on morphology alone proved difficult, despite it being visually very obvious. The uropod defect was better defined through the use of several fluorescent probes, which will be discussed in later sections. A similar phenotype has also been described for the *Dictyostelium mhc*A null and its impaired ability to retract its rear during cell migration has been shown to account for its reduced cellular speed (Laevsky & Knecht, 2003, Jay, Pham, Wong, & Elson, 1995). Rather than possessing a defect in actin-driven pseudopod formation, it was proposed that the *was*A null had an impaired ability to retract its uropod during cell migration, which caused drag and in turn slowed the cell.

a.

b.
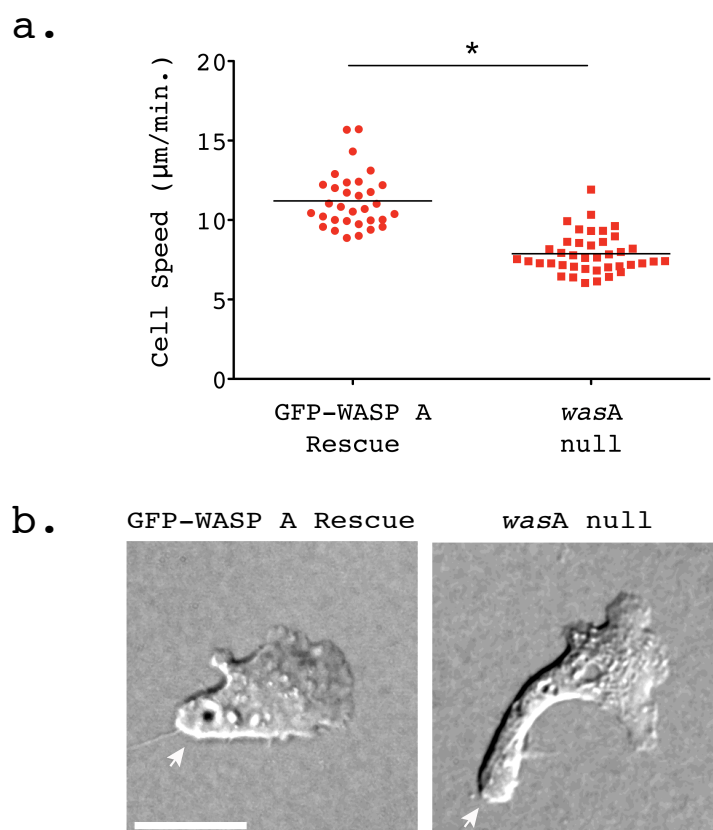
Figure 4.6, The motility of the *was*A null is impaired by its enlarged uropod: a) The migratory speed of the *was*A null is significantly slower than that of the GFP-WASP A rescue control. The speed of chemotaxing GFP-WASP rescue and *was*A null cells was derived from the cell tracks generated for figure 4.5a and are plotted in the graph shown above (>30 cell tracks/cell line, over 3 independent assays). This revealed a slight, but consistent decrease in mean cell speed (black horizontal bars) in the chemotaxing *was*A null (7.88 ±0.20 (±SEM) μm/min.) compared to the GFP-WASP A rescue (11.20 ±0.31 (±SEM) μm/min.). This difference was proved significant through the use of an unpaired student's t-test (p<0.0001). **b) The *was*A null has a defect in uropod retraction during persistent cell migration.** The morphology of the GFP-WASP A rescue and the *was*A nulls chemotaxing under agarose was visualised by DIC microscopy. The representative cells shown above highlight the uropod retraction defect present in the *was*A null. The white arrows indicate the uropod in both cells and the scale bar represents 10 μm.

4.7 The *was*A null has functional but disorganised myosin-II within the uropod

Combined with the cytokinesis defect demonstrated in section 4.3, these data strongly suggested that the *was*A null had impaired myosin-II function. Therefore we proceeded to test myosin-II contractility in our *was*A null cells. In *Dictyostelium,* the established method for assaying myosin-II function in cells is to treat them with the poison sodium azide and observe how they react (Pasternak et al., 1989, Patterson & Spudich, 1995). Wild-type cells respond to azide by violently contracting and deadhering from the substratum. This response was originally likened to 'rigor' by Pasternak et al., (1989), although is more likely to be an immediate survival response induced to try and escape poisons such as azide (*D. Knecht, personal communication)*. As demonstrated by Xu et al., (2001), both the *mhc*A null (which lack all myosin-II) and the *mlc*E null (which lack contractile myosin-II) do not exhibit this immediate reaction to azide. Instead they remain adherent until the azide presumably kills them and they detach en masse. We tested the immediate response of the *was*A null to sodium azide and as shown in figure 4.7a, there was no statistically significant difference in cell detachment when compared to the GFP-WASP A rescue (repeated over 4 independnet experiments). In both cases, an average of >70% of cells rapidly deadhered after treatment with 5 mM sodium azide This was in contrast to the *mlc*E null and the *mhc*A null, both of which showed prolonged resistance to the sodium azide. This result implied that the *was*A null did possess functional myosin-II that it could use to drive robust cellular contraction. GFP-myosin-II localises to the rear of migrating cells, consistent with its role in inducing uropod retraction (Laevsky & Knecht, 2003). In order to visualise myosin-II dynamics in motile cells, GFP-myosin-II was expressed in wild-type and *was*A null cells, which were then submitted to the under-agarose folate chemotaxis assay. As shown in figure 4.7b, the *was*A null was capable of recruiting GFP-myosin-II to the uropod during chemotaxis. However, whereas GFP-myosin-II was strictly confined to the cortex of the uropod in wild-type cells, there were clear indications of myosin-II disorganisation within the enlarged uropod of the *was*A null.

a.

b.
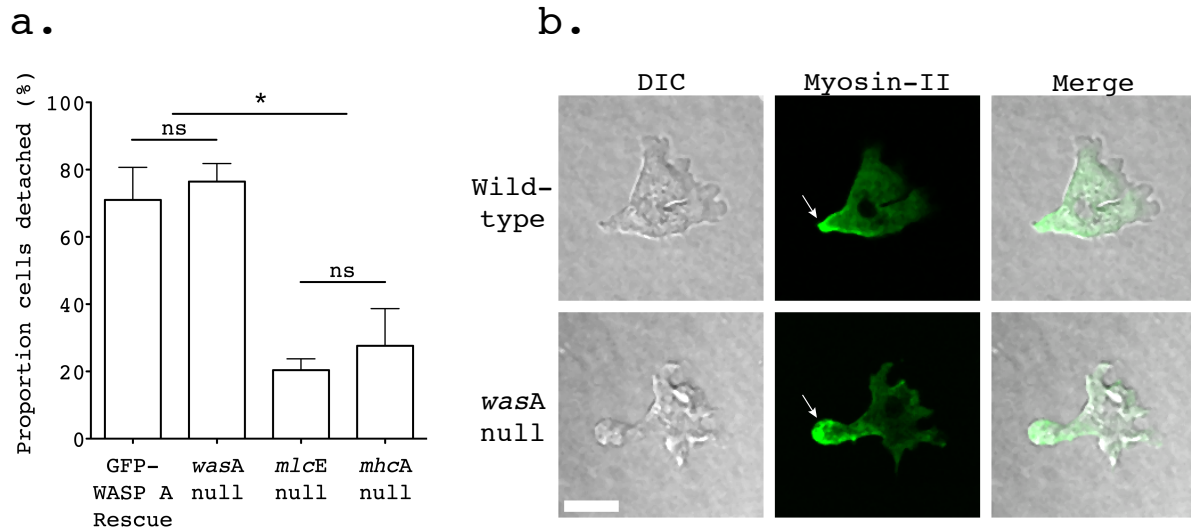
Figure 4.7, The *was*A null possesses functional but disorganised myosin-II: a) The *was*A retains robust actomyosin contractility. The *was*A null ±GFP-WASP A as well as *mlc*E and *mhc*A nulls were seeded at a high density on Petri dishes and were treated with 5 mM sodium azide. The immediate azide-induced detachment of cells is dependent on robust myosin-II contractility. The mean proportion (%) of cells that immediately detached in response to the sodium azide was plotted in the above graph (represents four independent experiments/cell line). No significant difference in response was observed between the GFP-WASP A rescue and the *was*A null in contrast to the myosin-II mutant controls, which were resistant to the early effects of the azide. * indicates that the proportion of the GFP-WASP A rescue and the *was*A null that detached significantly differed from the myosin-II mutant controls (one-way ANOVA) and ns denotes non-significance. The error bars represent the SEM. **b) Myosin-II is aberrantly distributed within the uropod of the *was*A null.** GFP-MHC (Myosin-II) was expressed in wild-type and *was*A nulls, which were then subjected to an under-agarose folate chemotaxis assay. Chemotaxing cells were then visualised by DIC and scanning confocal microscopy and representative cells are shown above. GFP-MHC was robustly recruited to the rear of wild-type and *was*A null during cell migration (white arrows). However, in contrast to the wild-type cells, GFP-MHC often appeared disorganised within the bulbous uropod of the *was*A null. The scale bar represents 10 μm.

The localisation of GFP-myosin-II often appeared 'patchy' within the uropod of the *was*A null, rather than the smooth layering of myosin-II seen at the rear of motile wild-type cells. It was concluded that the disorganisation of myosin at the rear of chemotaxing *was*A nulls was locally impairing actomyosin contractility resulting in defective uropod retraction. This in turn increased drag during migration, which was likely exacerbated in the under-agarose chemotaxis assay where the cells were slightly compressed. Ultimately drag would have counteracted the action of the actin-driven pseudopodia at the front of the cell and so reduced migratory speed.

4.8 The *was*A null has a severe defect in CME

Clathrin-mediated endocytosis is the means by which cells internalise their membrane and transmembrane proteins. A burst of actin polymerisation occurs at clathrin-coated pits prior to and during vesicle internalisation and has been shown to provide the force to overcome membrane tension (Merrifield et al., 2002, Boulant et al., 2011). WASP mediated recruitment of the Arp2/3 complex to CCPs also coincides with internalisation in yeast and human cells and is responsible for the spatial and temporal control of actin polymerisation at CCPs (Naqvi et al., 1998, Merrifield et al., 2004). Our lab has previously demonstrated colocalisation between WASP A and CCPs in *Dictyostelium* ((Veltman et al., 2012)) and it has been shown in section 4.3 that the cytokinesis defect of the *was*A null is reminiscent of that observed in the *Dictyostelium chc*A null (Gerald et al., 2001). To determine the requirement for WASP A in *Dictyostelium* CME we either co-expressed GFP-WASP A and clathrin light chain (CLC)-mRFP or CLC-mRFP alone in the *was*A null and visualised CCP internalisation on the basal plasma membrane by TIRF microscopy (figure 4.8a). When viewed by TIRF microscopy, CME appears first as a small punctum of clathrin, persisting for tens of seconds on the basal surface of the cell. Following the recruitment of WASP A, the clathrin punctum is internalised and, as it moves up and into the cell, it is lost from the TIRF field of view (Merrifield et al., 2004).
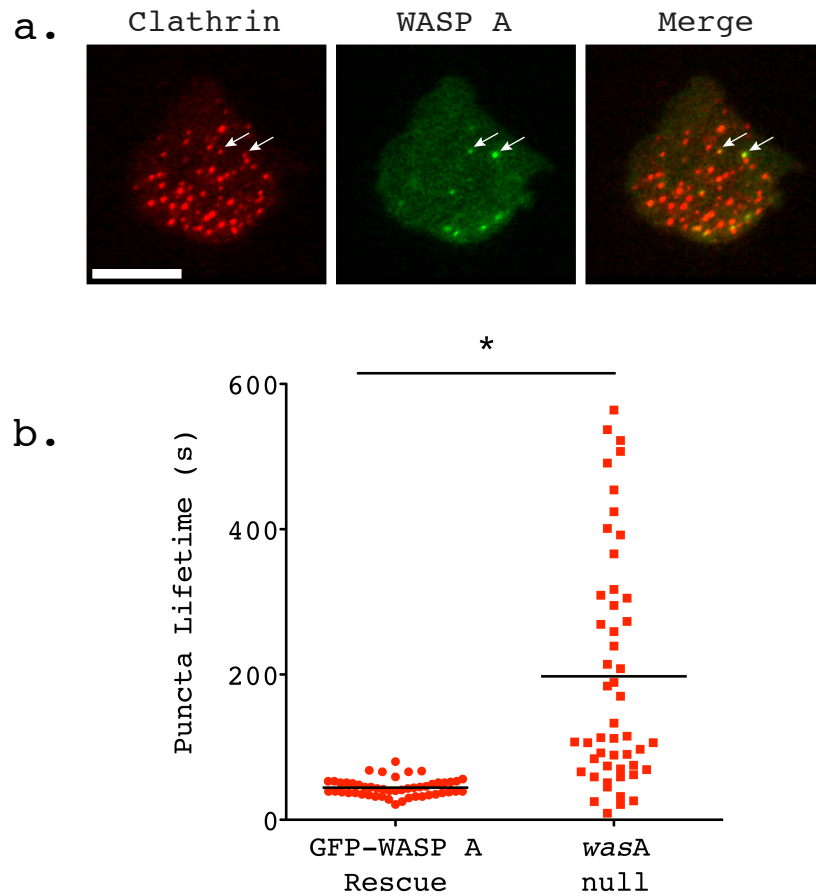
Figure 4.8, The *was*A null has a severe defect in CME: a) WASP A transiently colocalises with CCPs during prior to internalisation. CLC-mRFP (clathrin) and GFP-WASP A were co-expressed in *was*A null cells and CME was visualised by TIRF microscopy. A representative image demonstrates that WASP A colocalises with a subset of CCPs at any one time (white arrows highlight two examples). The scale bar represents 10 μm. **b) The *was*A null has a defect in CCP internalisation.** CLC-mRFP or CLC-mRFP and GFP-WASP A were expressed in *was*A null cells and CME was visualised by TIRF microscopy. CCP lifetime (time taken to disappear from TIRF field of view) was measured and plotted in the graph shown above (50 CCPs/cell line over two independent experiments). The black horizontal bars indicate the average CCP lifetime for the GFP-WASP rescue (44.2 ±1.7 (±SEM) seconds) and the *was*A null (197.5 ±22.8 (±SEM) seconds). The mean CCP lifetime was significantly increased in the *was*A null as established through the use of an unpaired Student's t-test (p<0.0001).
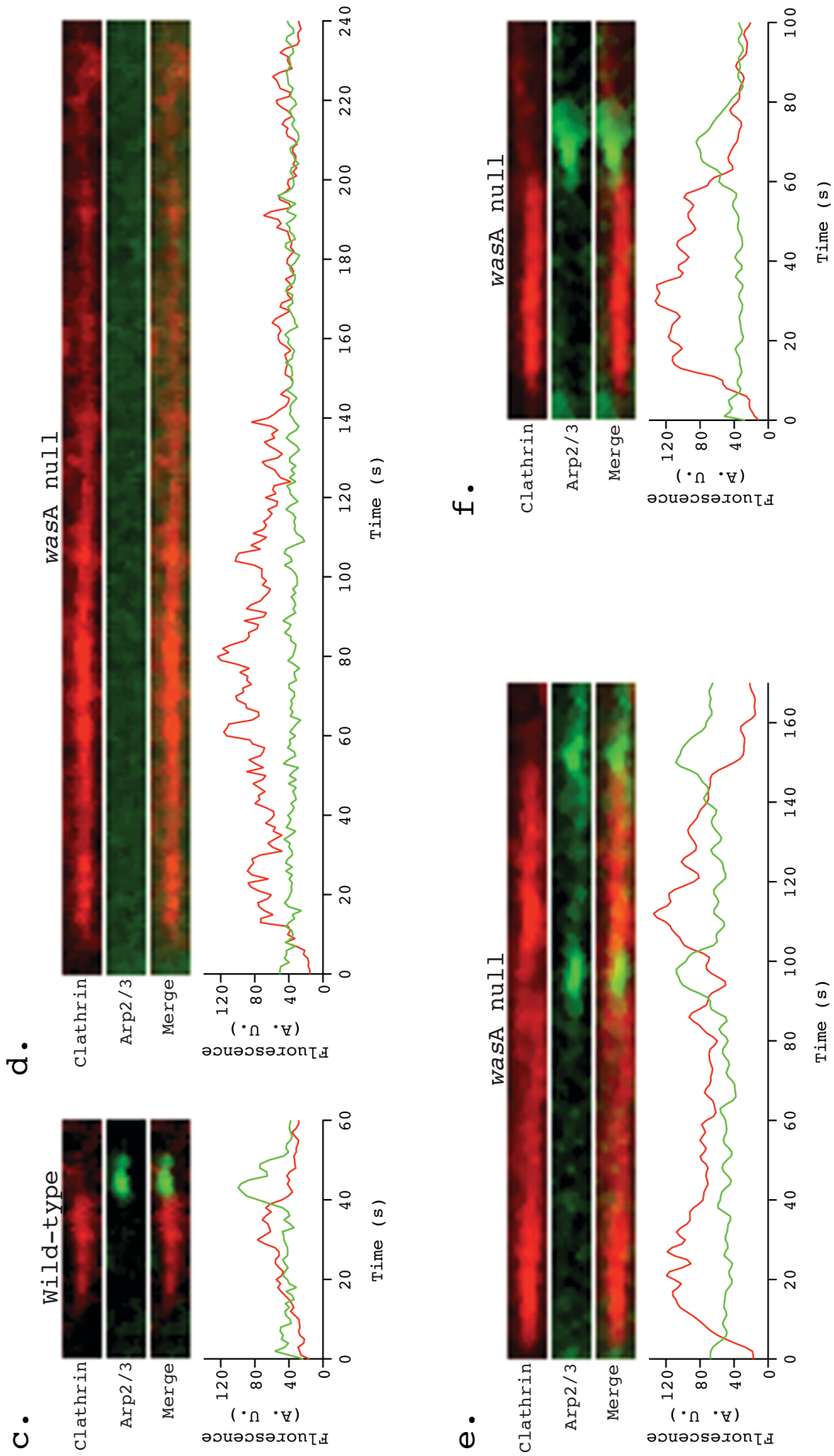
Figure 4.8, The *wasA* null has a severe defect in CME (continued): c-f) The *wasA* null has an impaired ability to recruit the Arp2/3 complex to CCPs to drive CME.

Figure 4.8, The *was*A null has a severe defect in CME (continued): c-f) The *was*A null has an impaired ability to recruit the Arp2/3 complex to CCPs to drive CME. CLC-mRFP (clathrin) and GFP-ArpC4 (Arp2/3 complex) were co-expressed in wild-type and *was*A null cells. CME was visualised in these cells by TIRF microscopy and the recruitment of the Arp2/3 complex to individual CCPs was observed. Representative kymographs and accompanying fluorescence intensity plots demonstrate the dynamic localisation of clathrin and the Arp2/3 complex at CCPs in wild-type and *was*A nulls. **c)** Recruitment of the Arp2/3 complex to CCPs in wild-type cells coincides with internalisation. **d)** In the *was*A null, many CCPs fail to recruit the Arp2/3 complex and persist on the plasma membrane for 100s of seconds. However, *was*A null retains residual ability to recruit the Arp2/3 complex to CCPs **(e-f)**. Even in the event of Arp2/3 complex recruitment, internalisation was still usually impaired, often requiring multiple bouts of Arp2/3 complex recruitment to drive internalisation **(e)**. Despite the majority of CCPs showing no or aberrant Arp2/3 complex recruitment, a few cases of normal CME were documented **(f).**

Individual CCPs were followed over the course of their lifetime as they appeared and disappeared from the TIRF field of view. As shown in figure 4.8b, the *was*A null had a severe defect in CCP internalisation during CME (50 puncta over two independent experiments). Statistical significance was confirmed through the use of an unpaired Student's t-test, yielding a p-value of <0.0001. Whereas interalisation was a short and regular event in the GFP-WASP A rescue, lasting on average 44 seconds (SD = ±11.9 seconds), the mean lifetime of a CCP in the *was*A null was 197.5 seconds and internalisation was also highly variable (SD = ±161.0 seconds). This data also undoubtedly under-represents the *was*A mean coated pit lifetime as only puncta where the full event, from initiation to internalisation, were included in this analysis, excluding many puncta that persisted on the plasma membrane for the entire length of the recorded timelapses. However, it remained clear that the *was*A null had a defect in CME. We next sought to determine whether the *was*A null had completely lost the ability to recruit the Arp2/3 complex to sites of CME by co-expressing a GFP-Arp2/3 complex marker and CLC-mRFP in wild-type and *was*A null cells. When viewed by TIRF microscopy, it was evident that in the *was*A null the majority of the CCPs were unable to recruit the Arp2/3 complex to drive internalisation. This is shown in figure 4.8c-f, where kymographs and their respective intensity plots represent the temporal recruitment of the Arp2/3 complex to individual CCPs and their subsequent internalisation. Consistent with the lifetime data shown in figure 4.8a, in wild-type cells clathrin accumulates over tens of seconds before a burst of Arp2/3 complex recruitment promotes internalisation (figure 4.8c). In the *was*A null, many clathrin-coated pits persisted on the plasma membrane for hundreds of seconds with no detectable colocalistation with the Arp2/3 complex (figure 4.8d). However, the ability to recruit the Arp2/3 complex to sites of CME had not been completely lost in the *was*A null. As can be seen in figures 4.8e-f, the Arp2/3 complex was occasionally found at CCPs in the *was*A null, although in many of these cases, internalisation required multiple bouts of Arp2/3 complex recruitment (figure 4.8c). However, there were a few internalisation events that looked almost normal in the *was*A null, one of which is shown in figure 4.3.1f. In summary, we have demonstrated that the *was*A null has defective vesicle internalisation during CME. Underlying this defect is a severely impaired ability to recruit the Arp2/3 complex to CCPs to promote actin polymerisation in order to drive internalisation.

4.9 WASP family members account for the residual recruitment of the Arp2/3 complex to clathrin-coated pits in *was*A nulls

In section 4.8, we showed that the *was*A retains some residual ability to recruit the Arp2/3 complex to sites of CME. Our lab has previously demonstrated that WASP A substitutes for a loss of SCAR in the remaining pseudopodia of the *Dictyostelium scr*A null. We wondered whether redundancy was a general feature of the WASP family and asked whether SCAR accounted for the residual recruitment of the Arp2/3 complex to CCPs in the *was*A null. To do this, we co-expressed CLC-mRFP and the SCAR complex marker HSPC300-GFP in wild-type and *was*A nulls and visualised CME on the basal plasma membrane by TIRF microscopy. We found no colocalisation between CCPs and the SCAR complex in either wild-type or *was*A null cells as shown in the representative images in figure 4.9a. It was also noted that the CCPs in the *was*A nulls had a tendancy to aggregate in more motile cells. Having, excluded SCAR, our attention was turned to the other two WASPs found in *Dictyostelium*, which have previously been shown at sites of CME (Veltman & Insall, 2010). It was found that the exogenous expression of both GFP-WASP B and GFP-WASP C was sufficient to rescue different aspects of the *was*A null phenotype. As shown in figure 4.9b, GFP-WASP B and GFP-WASP C expression were both capable of restoring the growth defect of the *was*A null in shaking culture (n=3) and in minimal medium (n=2) to the same extent as GFP-WASP A. GFP-WASP B and, to a lesser extent, GFP-WASP C were also capable of rescuing the developmental defect of the *was*A null (data not shown).

Based on our previous finding that WASP B and WASP C colocalise with CCPs and the data presented here, it is proposed that WASP B and WASP C
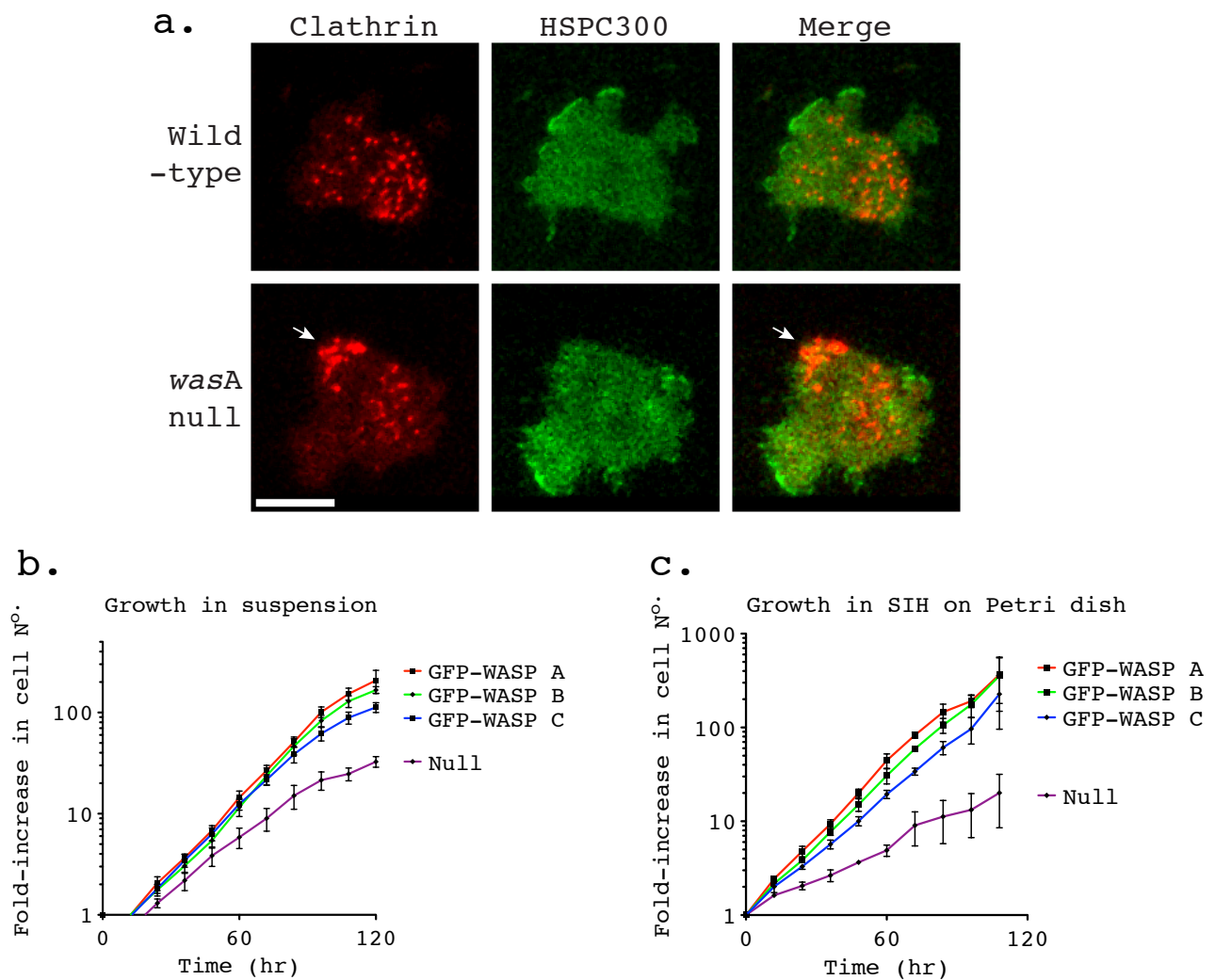
Figure 4.9, WASP B and C, but not SCAR accounted for residual CME in *was*A null: a) **the SCAR complex did not localise to CCPs in wild-type or *was*A null cells.** CLC-mRFP (clathrin) and HSPC300-GFP were co-expressed in wild-type and *was*A null cells. CCPs were visualised by TIRF microscopy and no colocalisation with the SCAR complex was observed in either cell line as shown in representative images shown above. The white arrow highlights an aggregate of CCPs, which was a common occurrence in motile *was*A null cells. The scale bar represents 10 μm. **Overexpression of GFP-WASP A, B or C rescued the growth of the** ***was*A null in shaking culture (b) and in minimal (SIH) medium (c).** Cells were introduced to shaking culture or were plated on Petri dishes in SIH and a cell count was performed every 12 hours over a period of 5 days. The mean fold-increase in cell number was calculated from a number of independent experiments and plotted in the above graph ((b) represents ≥3 independent growth curves, (c) represents 2 independent growth curves). The error bars represent the SEM.

account for the residual recruitment of the Arp2/3 complex to sites of CME in the *was*A null. Since endogenous WASP B and WASP C levels were evidently insufficient to compensate for the loss of WASP A, it is possible that either WASP B and WASP C are very weakly expressed, or their normal function is distinct from WASP A, with overexpression bolstering a low affinity for CCPs.

4.10 The accumulation of CCPs in the cleavage furrow of the dividing *was*A null disrupts cytokinesis

The *was*A null appears to have a very similar cytokinesis defect to that found in the *Dictyostelium chc*A null (Gerald et al., 2001). It has been previously shown that there is no enrichment of clathrin in the cleavage furrow of dividing *Dictyostelium* ((Damer & O'Halloran, 2000)). In order to confirm this and to visualise WASP A dynamics during cytokinesis, GFP-WASP A and CLC- mRFP were co-expressed in the *was*A null. It was found that the cleavage furrow of a dividing *Dictyostelium* had a tendency to lift up and out of the TIRF field of view, obscuring the final few moments before abscission. To combat this, we compressed the cells under a slab of agarose, which helped restrict the cleavage furrow to the TIRF field for more of cytokinesis. As demonstrated in figure 4.10a and Movie 3, WASP A driven CME occurs throughout the cell, throughout the duration of cytokinesis, including within the cleavage furrow right up to just prior to abscission. However, consistent with previous studies, there was no evidence of clathrin enrichment in the cleavage furrow that would suggest that CME is playing a direct role in ingression. In order to aid the identification of mitotic cells, *was*A was disrupted in an Ax3 cell line that stably expressed GFP-PCNA (IR206). GFP-PCNA is a nuclear marker that briefly dissipates during nuclear envelope breakdown just prior to cytokinesis (Muramoto & Chubb, 2008). We then expressed CLC-mRFP in both the WASP A positive GFP-PCNA expressing parent and the GFP-PCNA expressing *was*A null. Nuclear GFP-PCNA was observed with epifluorescence and clathrin dynamics was visualised simultaneously with TIRF microscopy.
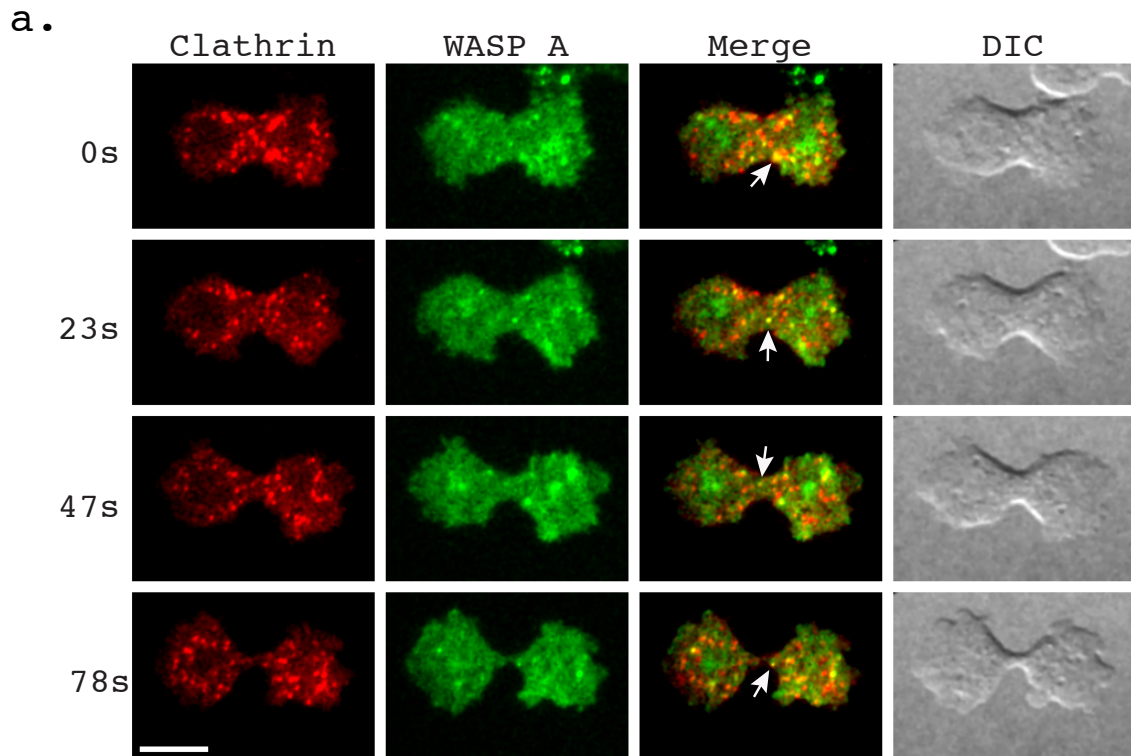
Figure 4.10, CCPs aggregate within the cleavage furrow of dividing *was*A nulls and impair cytokinesis: a) WASP A driven CME continued within the cleavage furrow during the whole of cytokinesis. CLC-mRFP (clathrin) and GFP-WASP A were co-expressed in the *was*A null. CME was visualised during cytokinesis by TIRF microscopy and selected images of a representative dividing cell are shown (time in seconds). CME occurred throughout the whole cell during the whole of cytokinesis and no prolonged enrichment of CCPs was observed prior to or during furrow formation in GFP-WASP A rescued cells. The white arrows highlight a few examples of CCP and WASP A colocalisation within the cleavage furrow at various stages of cytokinesis. The scale bar represents 10 μm.

b.
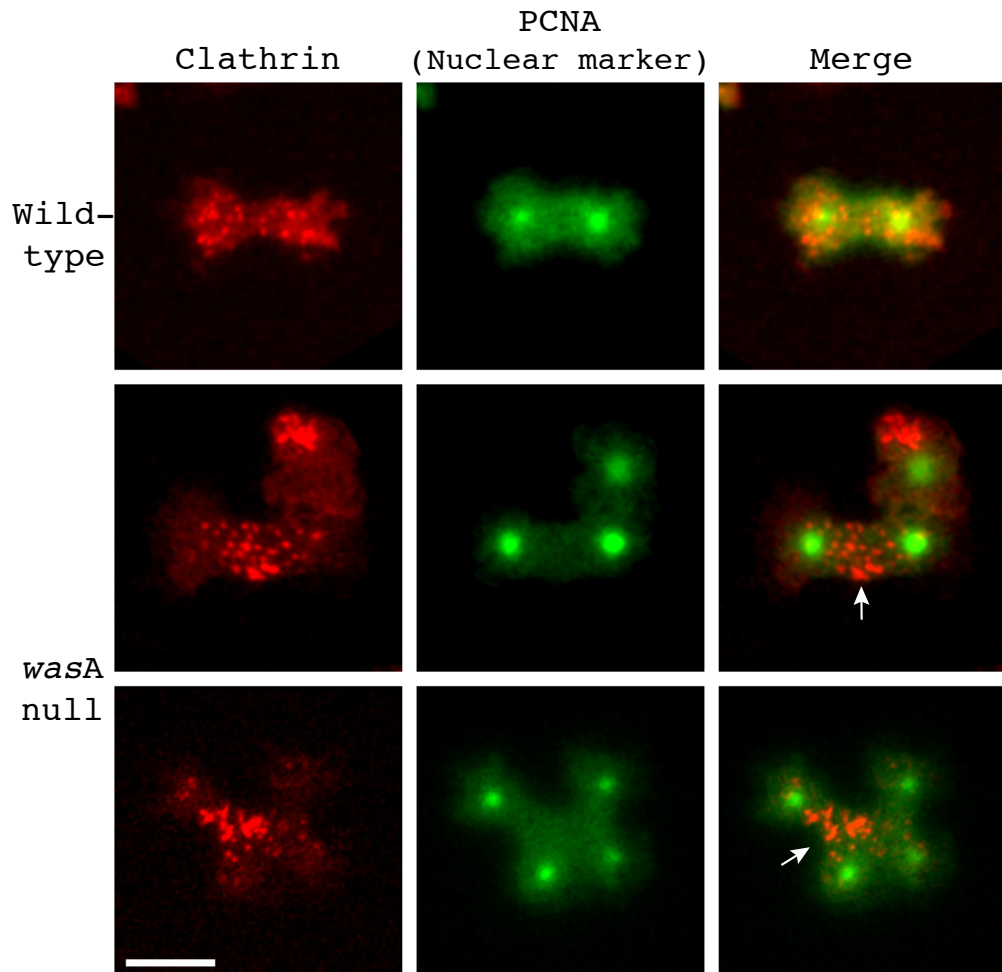
Figure 4.10 (continued), CCPs aggregate within the cleavage furrow of dividing *was*A nulls: b) CCPs accumulated in the cleavage furrow of dividing *was*A null cells. CLC-mRFP (clathrin) and GFP-PCNA (nuclei) were co-expressed in wild-type and *was*A null cells. Mitotic cells were identified by the brief dissipation of the nuclear PCNA marker prior to cytokinesis. CCP dynamics were then visualised during cytokinesis by TIRF microscopy. The upper panel shows a wild-type cell undergoing cytokinesis with no accumulation of CCPs observed. The lower two panels show CCP accumulation in the cleavage furrow of dividing *was*A null cells (white arrows). The bottom panel shows a multinucleate *was*A null attempting to resolve a four-way cleavage furrow. In both *was*A null cells, CCPs were swept into the cleavage furrow and appeared to impede ingression and final abscission (Movie 4). The scale bar represents 10 μm.

As can be seen in the examples shown in figure 4.10b and movie 4, the CCPs clearly accumulate in the cleavage furrow of the dividing *was*A null. In the dividing *was*A null, the CCPs that were presumably trapped on the plasma membrane awaiting internalisation appear to be swept into the cleavage furrow. Unfortunately, the cleavage furrow lifts out of the TIRF field of view before abscission but once the two daughter cells have torn themselves apart, the remainder of the characteristic bulge forms a ball filled with CCPs that bounces in and out of the TIRF field, trailing behind one of the daughter cells. In the other example shown in figure 4.10b and Movie 4, this time of a multinucleate *was*A null cell, again all the CCPs accumulate in the four-way cleavage furrow. As before the cleavage furrow lifts out of view, but this time when the tightly packed ball full of CCPs emerges it is slowly retracted back into the cell as two of the daughter cells snap back together resulting in a binucleate cell. The CCP filled ball was eventually reabsorbed back into the cell and the individual clathrin puncta can be seen spilling back out on to the plasma membrane of the cell. Based on many timelapses such as those shown in movie 4.10b (n=10), we concluded that the accumulation of CCPs in the cleavage furrow of the dividing *was*A null was interfering with normal ingression. The sheer bulk of CCPs in the confined and rapidly diminishing space that forms the cleavage furrow appears to be responsible for the bulging of the furrow during ingression. This in turn could prevent the furrow narrowing sufficiently to form the thin cytoplasmic bridge that is cut during abscission. When adhered to a surface, *was*A null cells can usually overcome this defect by physically tearing itself in two by cytokinesis B. However, in suspension where a cell is entirely dependent on its ability to divide by furrowing, the *was*A null would have a complete block in cytokinesis and become highly multinucleate as has been shown in section 4.3.

4.11 The accumulation of CCPs in the rear of the chemotaxing *was*A null impairs uropod retraction

In the previous sections, it has been demonstrated that *was*A null cells have impaired CCP internalisation during CME. It has also been shown that the
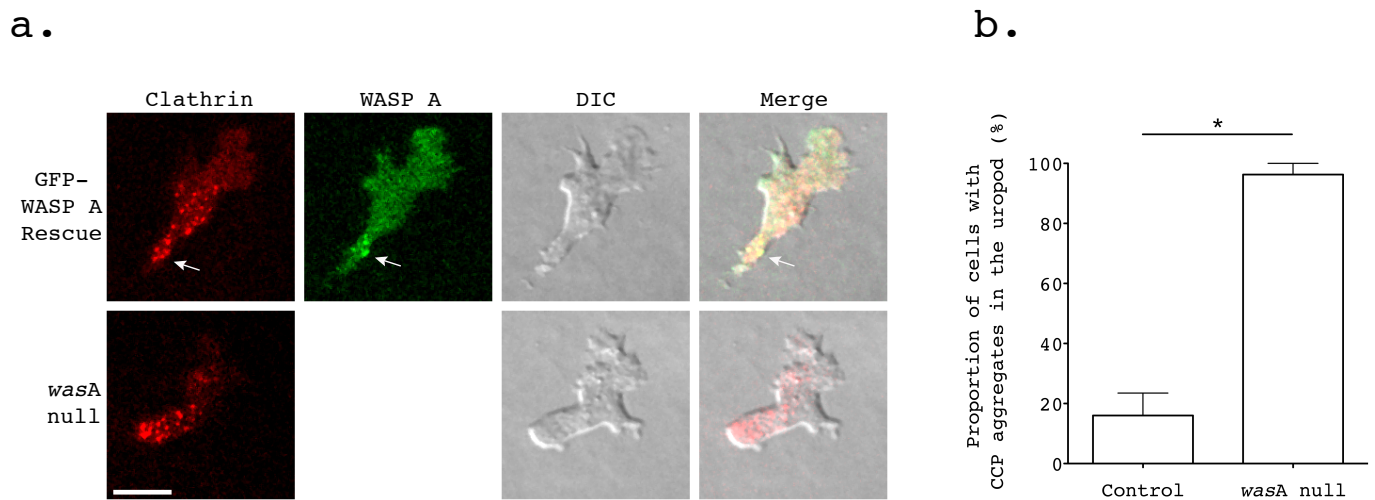
Figure 4.11, CCPs accumulate within the uropod of the chemotaxing *was*A null a) WASP A driven internalisation prevents accumulation of CCPs at rear of migrating cells. CLC-mRFP (clathrin) or CLC-mRFP and GFP-WASP A were co-expressed in the *was*A null and CME was visualised in chemotaxing cells by TIRF microscopy. As shown in the representative images shown in (a), WASP A recruitment prevents the aggregation of CCPs at the rear of chemotaxing cells (white arrows). In contrast, CCPs were found to accumulate in in the enlarged uropod of the *was*A null. The scale bar represents 10 μm. **b) Aggregates of CCPs were consistently found in the enlarged uropods of chemotaxing *was*A null.** The number of chemotaxing wild-type/GFP-WASP A rescue controls and *was*A nulls that possessed prominent CCP aggregates within the uropod was quantified over 3 independent assays. On average, 16.0% of controls exhibited prominent CCP accumulation at the rear of the cell at any point during their chemotaxis. In contrast, 96.3% of migrating *was*A null cells possessed uropods that contained CCP aggregates and this proved significantly different from the controls ($p < 0.0001$, unpaired Student's t-test). The error bars represent the SEM.

accumulation of CCPs in the cleavage furrows of dividing *was*A nulls appears to disrupt normal cytokinesis. We next considered whether CCP accumulation could also underlie the uropod retraction defect observed in chemotaxing *was*A null cells. In support of this, clathrin has been previously shown to transiently associate at the rear of the cell during migration and the *chc*A null has been reported to have uropod defects (Damer & O'Halloran, 2000, Wessels et al., 2000)). GFP-WASP A and CLC-mRFP or CLC-mRFP alone were expressed in the *was*A null and clathrin dynamics were visualised in motile cells in the under-agarose folate chemotaxis assay using TIRF microscopy. As can be seen in the examples shown in figure 4.11a, CME appeared to be excluded from the pseudopodia of both the chemotaxing GFP-WASP A rescue and the *was*A null. Although CCPs were transiently found in the uropods of the GFP-WASP A rescue, WASP A driven internalisation was always observed. In contrast, CCPs appeared to accumulate in the enlarged, persistent uropods of the motile *was*A null. In order to quantify this, we counted the number of cells that exhibited an enlarged CCP filled uropod at any point during their time in the field of view. Even with this very low threshold, there was large, statistically significant difference between the GFP-WASP A rescue and the *was*A null (16.0% vs. 96.3%, n≥25, over 3 independent experiments, unpaired Student's t-test, p<0.0001).   From these findings it was concluded that the accumulation of CCPs at the rear of the chemotaxing *was*A null was contributing to its impaired ability to retract its uropod.

4.12 The *was*A null has no defect in adhesion turnover during chemotaxis

It has been shown in previous sections that CCPs accumulated in the cleavage furrow of dividing *was*A nulls and in their uropods during chemotaxis. Since both these defects share obvious similarities, further study was focused on the CCP accumulation in the uropod of the *was*A null due to the technical challenges faced when trying to image dividing *Dictyostelium*. We wished to ascertain whether the accumulated CCPs triggered a specific

| Clathrin | Paxilin | DIC | Merge |
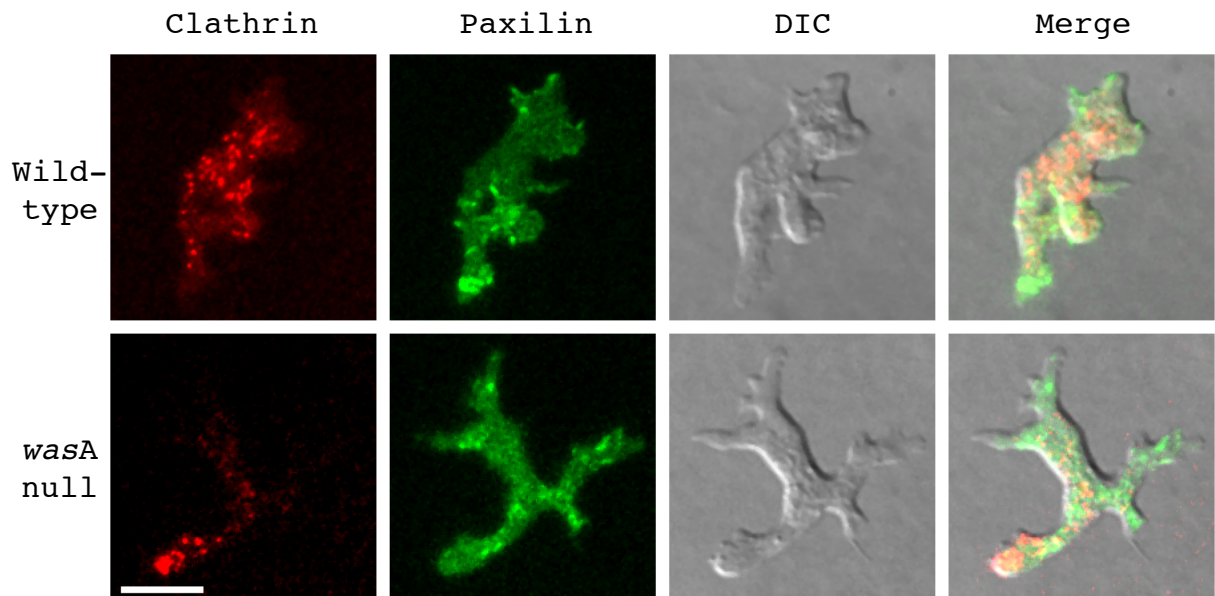
Figure 4.12, Adhesions do not accumulate in the uropod of the *was*A null: CLC-mRFP (clathrin) and GFP-Paxilin (an adhesion marker) were co-expressed in wild-type and *was*A null cells. CME and adhesions were visualised in chemotaxing cells by TIRF microscopy. As demonstrated in the representative images shown above, there was no colocalisation between adhesions and CCPs in chemotaxing wild-type or *was*A null cells. Importantly, there was no accumulation of adhesions observed in the enlarged uropod of the *was*A null. The scale bar represents 10 μm.

mechanism that was responsible for this defect or if the defect was a general consequence of bulk protein accumulation. For instance, CME has been previously shown by Ezratty et al., (2009) to be important in the turnover of focal adhesions in human cell lines. When CME was inhibited in these cells, the impaired recycling of adhesions caused a problem with uropod detachment during cell migration, resulting in the cells exhibiting enlarged, 'stretched' uropods. The turnover of adhesions (or other proteins and structures) could also underlie the uropod defect in the *Dictyostelium was*A null. Alternatively, the accumulated CCPs could merely be causing a 'dead weight', which the cells would be forced to drag behind them during migration.

To determine whether CME was important for the turnover for adhesions during *Dictyostelium* cell migration, CLC-mRFP and GFP-Paxillin (an established marker of adhesions as used by Bukharova et al., (2005)) were co-expressed in wild-type and *was*A null cells. Chemotaxing cells in the under-agarose folate chemotaxis assay were visualised by TIRF microscopy. As demonstrated in figure 4.12, there was no co-localisation between adhesions and CCPs in either wild-type or *was*A null cells, consistent with the previously observed lack of co-localisation between paxillin and F-actin puncta (Bukharova et al., 2005). Importantly, there was no accumulation of adhesions with the CCPs in the uropod of the *was*A null. These data implied that a defect in adhesion turnover did not underlie the enlarged, CCP-filled uropod of the *was*A null.

4.13 Rac is inappropriately activated in the uropod of the *was*A null

Having shown that adhesions have no role in the uropod retraction defect of the *was*A null, other possible alternatives were investigated. Serendipitously, it was discovered that Rac was aberrantly activated in the uropod of the *was*A null. To detect Rac activation within the cell we made use of a fluorescently tagged one-component probe consisting of the GBD domain of PakB, which specifically binds GTP bound Rac, fused to GFP or mRFP. A related probe has been shown to localise to the pseudopodia of migrating cells (Filic, Marinovic, Faix, & Weber, 2012, Veltman et al., 2012). As a one-component probe, it is not suitable for measuring absolute levels of Rac activation but is sufficient to determine the spatial distribution of active Rac within the cell. The PakB-GFP probe was co-expressed along with CLC-mRFP in wild-type and *was*A null cells and chemotaxing cells were imaged in the under-agarose folate chemotaxis assay using TIRF microscopy. As shown in figure 4.13a and Movie 5, Rac activity is confined to a broad area within the pseudopodia in the wild-type cells. There was also no detectable Rac activity at the CCPs, consistent with its role in regulating actin pseudopodia and not CME. In the *was*A nulls, Rac activity in the pseudopodia appeared normal. However, prolonged aberrant Rac activity within the enlarged uropod of the *was*A null along with the accumulated CCPs was also observed. Again, Rac was not detectably active at any other CCPs outside of those that had aggregated in the uropod. To quantify this, we counted the number of frames a given cell exhibited any Rac activity in its rear. Filic et al., (2012) originally observed some transient Rac activity in the retracting rear of motile wild-type cells. Although we also observed some Rac activity at the rear of wild-type cells, it was found this was mostly associated with retracting pseudopodia that had found themselves at the back of cell. This residual activity was also extinguished very quickly. As shown in figure 4.13b, the *was*A null exhibited Rac activity in its rear 88.19% of the time compared to 8.85% of the time seen in wild-type cells (n>10 cells over 3 independent experiments). This difference proved statistically significant when subjected to an unpaired Student's t-test ($p < 0.0001$). In summary, inappropriate, sustained Rac signaling was observed in the persistent uropod of the *was*A null.

a.
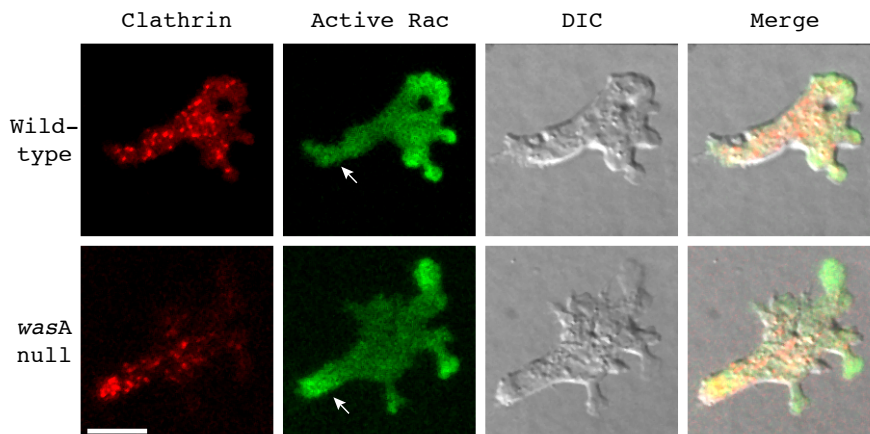
b.
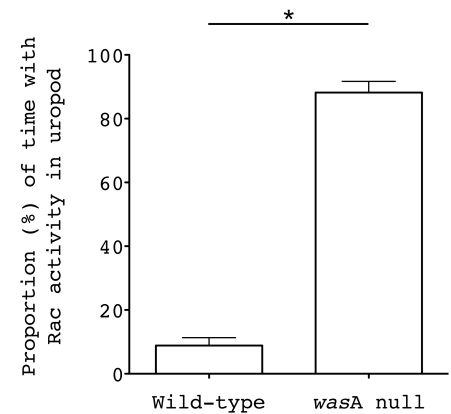
Figure 4.13, Rac is aberrantly activated in the uropod of the *was*A null: a) The aggregated CCPs in the uropod of the chemotaxing *was*A null was found to induce inappropriate Rac activation. CLC-mRFP (clathrin) and PakB-GFP (active Rac probe) were co-expressed in wild-type and *was*A null cells and CCPs were visualised in chemotaxing cells by TIRF microscopy. As shown in the representative images shown above, Rac activity was confined to the pseudopodia in wild-type cells but was also observed in the persistent uropod of the *was*A null (white arrows indicate uropods). Rac activity only colocalised with the CCPs in the uropod of the *was*A null and was not seen at sites of CME elsewhere in the cell. The scale bar represents 10 μm. **b) Rac activity was consistently observed in the persistent uropod of the *was*A null.** The number of frames with Rac activity observed at the rear of the chemotaxing cell as a proportion (%) of the total was quantified over 3 independent assays. Rac activation was rarely observed in the rear of chemotaxing wild-type cells (8.9% of the time). In contrast, Rac activity was observed in the persistent uropod of the *was*A null 88.2% of the time and this proved a significant increase when compared to wild-type cells (p<0.0001, unpaired Student's t-test). The error bars represent the SEM.

4.14 Aberrant Rac activity induces SCAR-promoted actin polymerisation within the uropod of the *was*A null

In the previous section, it was demonstrated that Rac is inappropriately activated in the uropod of the *was*A null. Since Rac is an established activator of the SCAR complex (Steffen et al., 2004, Lebensohn & Kirschner, 2009), we sought to determine if SCAR was being recruited to uropod to induce abnormal actin polymerisation. An mRFP- tagged version of the active Rac probe was co-expressed with the SCAR complex marker HSPC300-GFP in wild-type and *was*A null cells. Rac activity and SCAR dynamics were then visualised in chemotaxing cells in the under agarose folate chemotaxis assay using TIRF microscopy. As demonstrated in figure 4.13a, SCAR was recruited to the active Rac patch in the uropod of the *was*A null. Unlike the localisation observed in the pseudopodia, SCAR was confined to small, transient puncta in the uropod of the *was*A null. Since the role of SCAR is to recruit and activate the Arp2/3 complex, we revisited the data generated to study F-actin and Arp2/3 complex dynamics in *was*A null cells. As discussed earlier in the chapter in section 4.2, F-actin and the Arp2/3 complex were visualised by the co-expression of Lifeact-mRFP and GFP-ArpC4. Chemotaxing cells were in the under-agarose folate chemotaxis assay using spinning disc microscopy. As can be seen from figure 4.13b and Movie 2, the enlarged uropod of the *was*A null was full of Arp2/3 complex and F-actin positive puncta. Because spinning disc confocal was utilised rather than TIRF microscopy, we had been able to look deeper into the cell. With the examples shown in figure 4.13b, the middle of the cell had been imaged rather than the basal surface. These actin puncta were unlikely to be accounted for by the residual CME in the *was*A null based on their sheer abundance and their presence within the cytosol as opposed to being limited to the plasma membrane. In contrast, Arp2/3 complex and F-actin positive puncta were strictly confined to the cortex in the rear of the chemotaxing wild-type cells as would be expected of CME.

a.
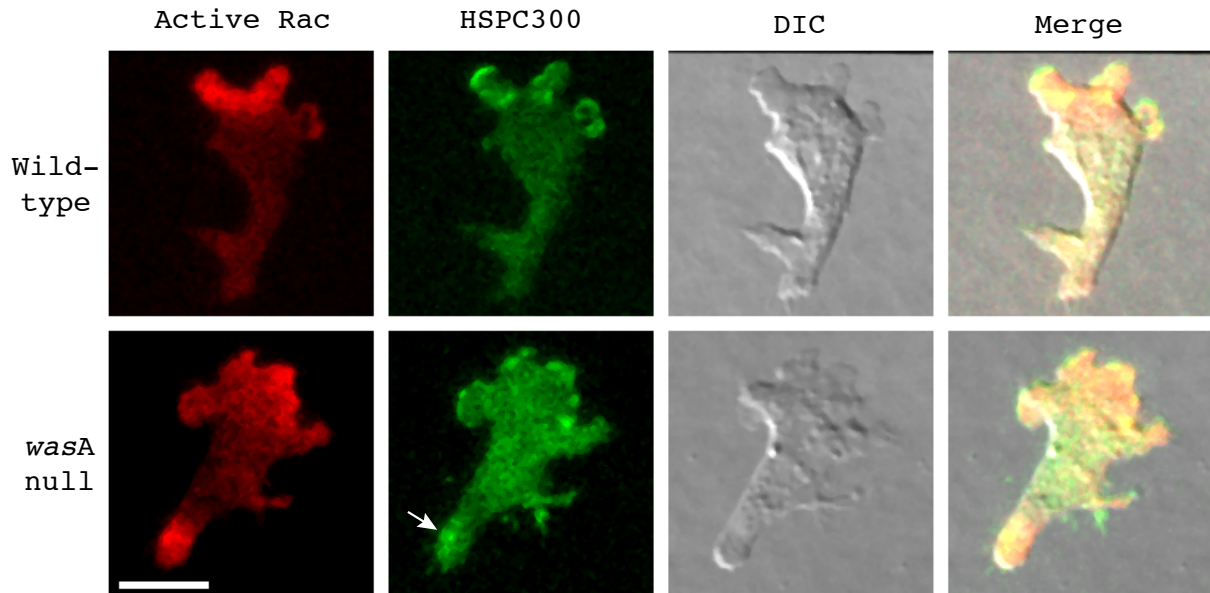
Figure 4.14, SCAR promoted actin polymerisation occurs within the uropod of the _was_A null: a) Rac recruits SCAR to the uropod of the _was_A null. PakB(GBD)-mRFP (active Rac probe) and HSPC300-GFP were co-expressed in wild-type and _was_A null cells, which were visualised by TIRF microscopy in chemotaxing cells. As shown in the representative images above, Rac activation within the uropod of the _was_A null induced aberrant SCAR complex recruitment (white arrow), which otherwise localises exclusively to the pseudopodia. The scale bar represents 10 μm.

b.
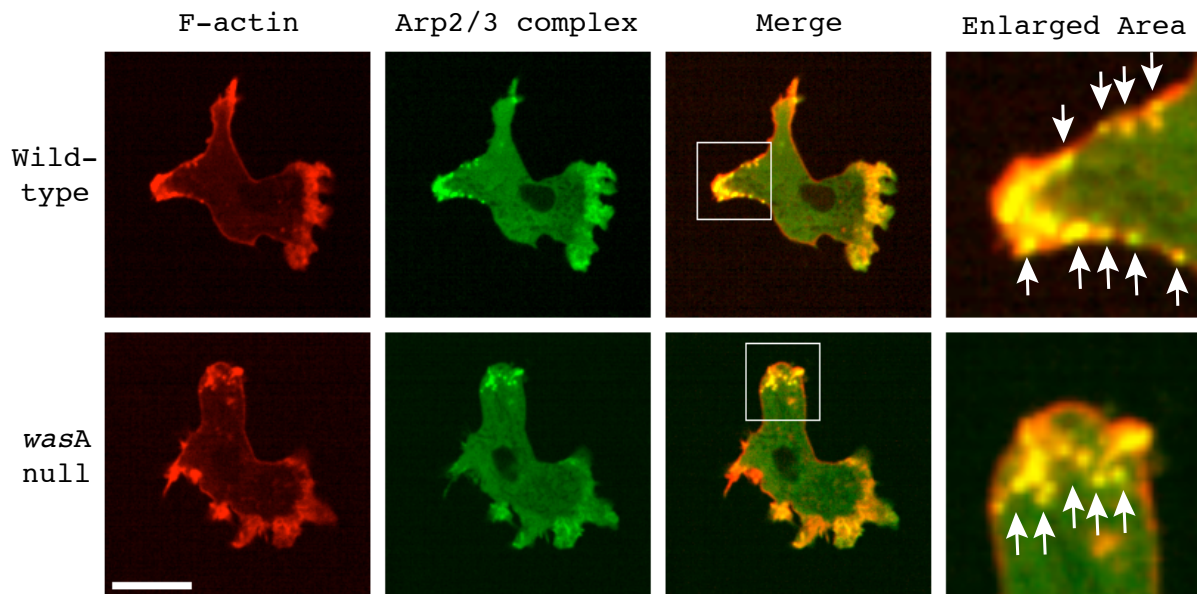
Figure 4.14, The aberrant Rac activity in the uropod of the *was*A null recruits SCAR and induces inappropriate actin polymerisation (continued): b) Excessive actin polymerisation is observed within the persistent uropod of the *was*A null. The spinning disc confocal images of chemotaxing wild-type and *was*A null cells expressing Lifeact-mRFP (F-actin) and GFP-ArpC4 (Arp2/3 complex) were revisited (as originally shown in figure 4.5). As shown in representative images above, inappropriate Arp2/3 complex activity was evident in the uropod of the *was*A null. Within the uropod of chemotaxing wild-type cells, Arp2/3 complex recruitment and actin polymerisation was confined to the cortex (white arrows), which was consistent with normal CME. In contrast, aberrant actin polymerisation was observed throughout the enlarged uropod of the *was*A null and was no longer confined to the cortex. White boxes designate enlarged area and the scale bar represents 10 µm.

Here it has been demonstrated that the uropod retraction defect of the *was*A null is not merely a passive consequence of CCP accumulation, but also possesses an active, signaling driven component that results in aberrant actin polymerisation. The inappropriate activation of Rac in the rear of the cell was shown to recruit SCAR, which in turn recruits and activates the Arp2/3 complex to induce aberrant actin polymerisation. It is possible that the activation of Rac and the resulting actin aggregates at the rear of the chemotaxing *was*A null could contest normal myosin-II recruitment. This could explain the poor myosin-II distribution throughout the uropod of the cell as we have shown in figure 4.7b. This in turn would result in inefficient actomyosin based contraction, which would impair retraction of the rear during cell translocation and ultimately yield the characteristic enlarged uropod observed in the motile *was*A null. Finally, the trailing uropod of the chemotaxing *was*A null would act to slow the cell during migration. Although this model fits all of our observations well, further study shall be required to confirm it.

4.15 Chapter 4 summary

In this chapter, the phenotype of the *Dictyostelium was*A null was investigated. Two independent *was*A knockout cell lines were generated and to our surprise, no detectable growth defect was observed when the cells were cultured on Petri dishes. However, the *was*A null was unable to grow in shaking culture due to a cytokinesis defect that it could only overcome on a surface by physically tearing itself apart. It was also shown that the *was*A null had impaired growth in minimal media and has a complete block in multicellular development.

Despite what has been previously published, it was demonstrated that the *was*A null had no defect in actin-driven pseudopod formation during chemotaxis. However, it was shown that the *was*A null consistently migrated with a reduced cell speed and it was concluded that this was due to an impaired ability to retract its uropod during cell translocation.

It was established that the *was*A null had a severe defect in vesicle internalisation during clathrin-mediated endocytosis. It was shown that the clathrin-coated pits were essentially trapped on the plasma membrane of the *was*A null and accumulated in the cleavage furrow during cytokinesis and in the uropod during cell migration. Focusing

on the uropod retraction defect, it was shown that Rac was inappropriately activated in the enlarged uropod of the *was*A null. This resulted in abnormal SCAR recruitment and aberrant actin polymerisation. It was proposed that these actin aggregates might interfere with proper myosin-II organisation at the rear of the chemotaxing cell and so impair uropod retraction.

Chapter 5

WASP family proteins are required for both Arp2/3 complex dependent and independent modes of migration

5.1 Creation of the double *scr*A/*was*A mutant

In the previous chapter, it was demonstrated that WASP A is not required for pseudopod formation in wild-type cells. Instead it was found that WASP A contributed indirectly to cell migration by maintaining efficient uropod retraction. However, our lab has recently shown that WASP A adopts a direct role in pseudopod formation in the *Dictyostelium scr*A null (Veltman et al., 2012). If pseudopod formation is dependent on SCAR and, in the absence of SCAR, WASP A, then the deletion of both SCAR and WASP A should result in the loss of all pseudopodia. Such a mutant would then be left entirely dependent on other types of protrusions (e.g. blebs) to support its motility. We wished to determine whether WASP A was alone in its ability to substitute for SCAR or if there were other proteins (WASP family members or otherwise) that could induce actin-driven pseudopod extension. We also sought to study the interplay between SCAR and WASP A and how both these proteins can promote pseudopod formation under different circumstances. Finally, we were also interested in understanding how the cell is able to switch between different modes of migration to maintain motility.

For the above reasons, an attempt to generate a double *scr*A/*was*A mutant was undertaken. However, all attempts to create a *was*A knock out in a *scr*A null background were met with failure. So instead an inducible approach was once again adopted as is outlined in figure 5.1a. Our lab has previously created a S̲CAR i̲nducible k̲nock o̲ut (SIKO, IR201) strain, where the expression of SCAR is promoted by the addition of doxycycline and suppressed in its absence (King et al., 2010). Using the SIKO as a parental strain, the endogenous *was*A locus was targeted for deletion by homologous recombination, utilising the same knock out vector used in chapter 4. Clones were cultured at all times in the presence of doxycycline and screened by Western blot. Having isolated *was*A knockout cells in the SIKO background, these cells were deprived of doxycycline to verify the inducibility of the double *scr*A/*was*A mutant. As shown by the Western blots in figure 5.1b, the SIKO parent in the presence of doxycycline remained a SCAR positive, WASP positive "control" cell. Deprived of doxycycline, the SIKO parent became a *scr*A mutant. As demonstrated by figure 5.b, WASP A expression had been successfully abolished in the double *scr*A/*was*A mutant (IR207). In the presence of doxycycline, SCAR expression was maintained, yielding a *was*A mutant. However, by depriving these cells of

doxycycline, SCAR expression was suppressed and a double *scr*A/*was*A mutant was obtained. Interestingly, the inducible double mutant consistently appeared to possess at least two-fold more SCAR protein than the SIKO parent. SCAR is entirely dependent on its inclusion within the SCAR complex and therefore normally cannot be expressed above the levels of the other complex members. However, this observation was not further investigated. It was determined that a minimum of 48 hours doxyclycline deprivation was required to maximally suppress SCAR expression in the double mutant (figure 5.1b). For the rest of this thesis, these different combinations shall be referred to as the "control", the "*scr*A mutant", the "*was*A mutant" and the "double mutant", however, it is important to remember that the double mutant is an inducible knockout. This had its disadvantages, such as the residual SCAR in the absence of doxyclyine, which was clearly visible by Western blotting as shown in figure 5.1b. However, the inducible nature of the double mutant also conferred some experimental advantages, which shall be discussed later in this chapter.

5.2 The double scrA/wasA mutant has a severe growth defect

Following doxycycline deprivation to suppress SCAR expression, it was immediately obvious that the double mutant had a severe growth defect. It was established in chapter 4 that *was*A deficient cells had an inability to grow in shaking culture and so, with this in mind, shaking culture was avoided. Control, *scr*A mutant, *was*A mutant and double mutant cells were plated on Petri dishes and a cell count was performed every 12 hours over 5 days.

a.
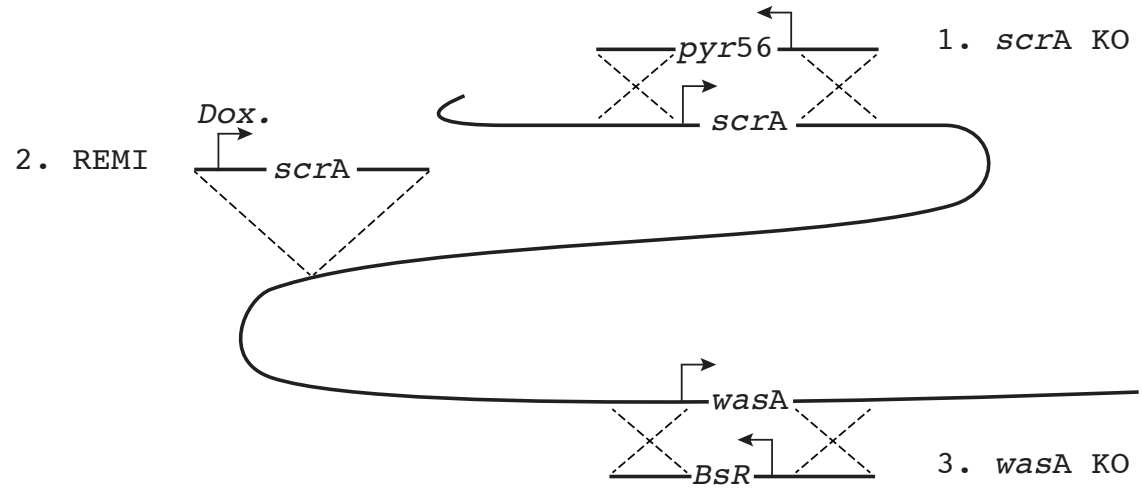
Figure 5.1, Creation of the inducible double *scr*A/*was*A mutant: a) Diagram outlining the strategy adopted to generate the inducible double *scr*A/*was*A mutant. Previously, the *scr*A null (IR46) was generated through deletion of the endogenous *scr*A locus by homologous recombination (1). To create SIKO, King *et al*., (2010) introduced *scr*A under the control of a doxycycline (*Dox.*) inducible promoter into the genome of Ax3 cells by REMI (2). Using SIKO as a parental cell line, the endogenous *was*A locus was then targeted for deletion by homologous recombination to create the inducible double *scr*A/*was*A mutant (3).

b.
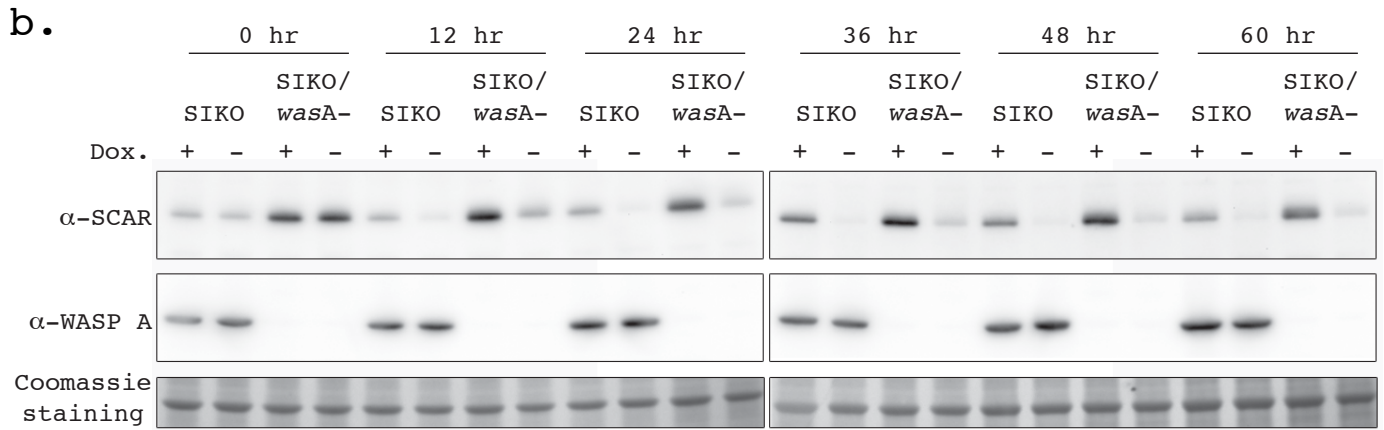
Figure 5.1, Creation of the inducible double *scr*A/*was*A mutant (continued): b) Western blots validating the inducible double *scr*A/*was*A mutant. Western blotting was used to confirm the loss of WASP A expression (middle panel) in the inducible double mutant (SIKO/*was*A-) as compared to the parental control (SIKO). SCAR expression was then suppressed in both the SIKO parent and the inducible double mutant by depriving the cells of doxycycline (DOX.). Lysates were prepared form these cells at 12 hour intervals and the loss of SCAR expression over time was demonstrated by Western blotting (top panel), thus confirming the successful creation of the inducible double mutant. SCAR levels consistently appeared higher in the inducible double mutant in the presence of doxycycline, which increased the time take for maximal SCAR suppression (48 hr). Bottom panel: Subsequent Coomassie staining of the membrane was used to demonstrate equal loading.

The cells were deprived of doxycycline at the start of the experiment (0 hour) and so the suppression of SCAR expression to yield the *scr*A mutant and the double mutant occurred during the course of the growth curve. As shown in figure 5.2a, the loss of either SCAR or WASP A alone had no consequence for growth compared to the growth of the control (represents 3 independent experiments). This was in contrast to the loss of SCAR in the NC4A2 background, which was discussed in chapter 3.

Figure 5.2a shows that control Ax3 cells require at least one of either SCAR or WASP A for optimal growth, as the loss of both causes all proliferation to cease. It was apparent that after 48-60 hours of doxycycline deprivation, the growth of the double mutant came to an immediate halt. This timing coincided with the maximal suppression of SCAR in the double mutant (figure 5.1b) and demonstrated the absolute requirement of either SCAR or WASP A for the maintenance of growth.

Of immediate concern was the possibility that the double mutant was inviable, however a number of observations reassured us that this was not the case. Firstly, the cell population was plateauing and not entering decline as would be expected of dying cells. Secondly, the double mutant remained adherent instead of rounding up and de-adhering (these being prominent signs of cell death in *Dictyostelium*). Thirdly, the double mutant was actively adherent, meaning if the cells were suspended, they would immediately re-adhere when re-introduced to a substratum. As shall be shown in subsequent sections, the double mutant was also capable of a diverse range of cellular processes, which implied cell viability despite the absence of growth. Unless otherwise stated, the double mutant was transformed and maintained in the presence of doxycycline until 48 hours prior to any given experiment.

a.

b.
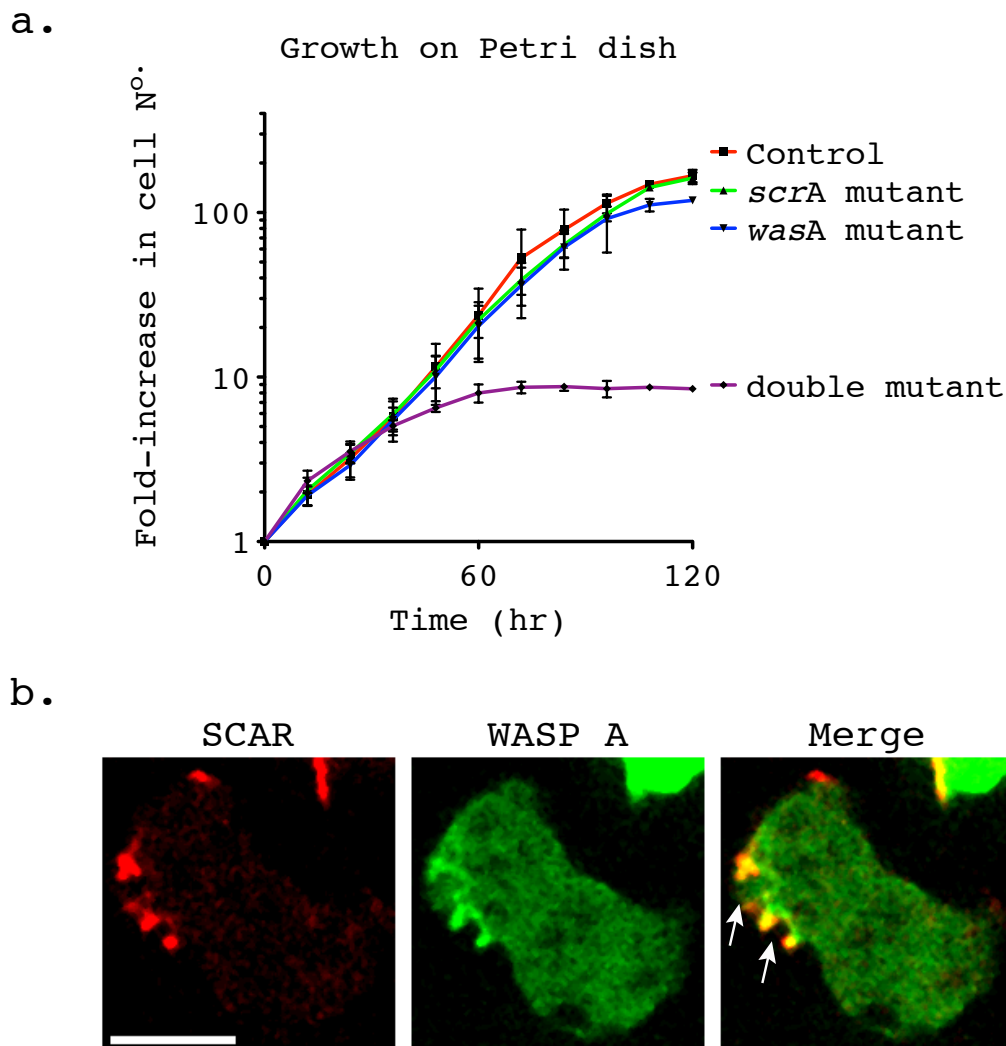
Figure 5.2, One of SCAR or WASP A is essential for axenic growth: a) Growth curves demonstrating that the double mutant has a severe growth defect. Cells were plated on Petri dishes and a cell count was performed every 12 hours over a period of 5 days. Cells were deprived of doxycycline at the time of plating (0 hr) meaning the suppression of SCAR expression to yield the *scr*A null and the double mutant occurred during the course of the experiment. The mean fold-increase in cell number was calculated from 3 independent experiments and was plotted in the graph shown above. The error bars indicate SEM. **b) SCAR and WASP A colocalise at sites of macropinocytosis.** SCAR-TagRFP and GFP-WASP A were co-expressed in wild-type cells and their localisation in unstimulated, vegetative *Dictyostelium* was visualised by spinning disc confocal microscopy. As demonstrated by the representative image shown above, SCAR and WASP A colocalise at macropinocytic cups. The scale bar represents 5 μm.

SCAR-TagRFP and GFP-WASP A were co-expressed in control cells and visualised in vegetative, non-motile cells by spinning disc confocal microscopy. As shown in figure 5.2b, SCAR and WASP A have partially overlapping localisation in the macropinocytic cups of *Dictyostelium*. It is proposed here that SCAR and WASP A act redundantly in Ax3 to drive macropinocytosis, the primary mode of nutrient uptake in liquid culture. When *Dictyostelium* are deprived of nutrients, they normally enter the developmental stage of their lifecycle. However, as was established in chapter 4, *was*A deficient cells have a complete block in development. In the double mutant we speculate that the cells are sensing they are no longer acquiring nutrients by macropinocytosis and as they are unable to develop, they are instead entering a quiescent state.

Here the creation and validation of an inducible double *scr*A/*was*A mutant has been described. It was shown that the double mutant has a severe growth defect possibly due to the requirement of either SCAR or WASP A for macropinocytosis.

5.3 WASP A alone is responsible for the residual pseudopod formation in the double *scr*A/*was*A mutant

Having generated and validated the double *scr*A/*was*A mutant, its motility was examined in comparison to the motility of the control, the *scr*A mutant and the *was*A mutant. As described in chapter 4, the *was*A null has a complete block in development and chemotaxis was again solely studied in vegetative cells. The cells were deprived of doxycycline for 48 hours to maximally suppress SCAR expression and, along-side the doxycycline treated controls, were subjected to the under-agarose folate chemotaxis assay (Laevsky & Knecht, 2001). Chemotaxis was first studied at low magnification using phase contrast microscopy. Cell tracking was then performed, which yielded the spider-plots shown in figure 5.3a (>35 cells/cell line tracked over 3 independent assays). The control, *scr*A mutant and *was*A mutant were all capable of robust migration towards the source of folate. However, it was immediately obvious that the double mutant had a severe defect in cell migration. Despite still orientating towards the chemoattractant, the tracks of the double mutant were extremely stunted. The poor motility of the double mutant was also evident from its reduced migratory speed, as demonstrated in figure 5.3b. Vegetative *scr*A mutant cells moved at a mean

speed of 6.5 ±0.16 (±SEM) μm/min., which was on average 36% slower than control cells (10.2 ±0.22 (±SEM) μm/min.). This difference proved statistically significant (p<0.0001, unpaired Student's t-test) and was consistent with what has been previously shown (Pollitt & Insall, 2008). Consistent with the findings presented in chapter 4, this independent *was*A mutant also exhibited reduced migratory speed. As shown in figure 5.3b, the *was*A mutant migrated with a mean speed of 7.7 ±0.17 (±SEM) μm/min., which was on average 25% slower than the control. The *was*A mutant was significantly slower than the controls but significantly faster than the *scr*A mutant (unpaired Student's t-tests, p<0.0001 in both cases). Finally, the average cell speed of the double mutant was only 1.2 ±0.10 (±SEM) μm/min., 88% slower than the controls. Its speed was significantly slower than the control, the *scr*A mutant and the *was*A mutant (unpaired Student's t-tests, p<0.0001 in all 3 cases).

High magnification DIC microscopy was utilised to study the morphology of the double mutant and to observe pseudopod formation. The double mutant had a very spiky, nonpolar cell shape, reminiscent of the morphology of the recently published mammalian Arp2/3 complex knock down/knock out cells (Wu et al., 2012, Suraneni et al., 2012). Again, the double mutant was seen to be barely motile and extended almost no pseudopodia. As described in chapter 3 and 4, we made short, DIC timelapses and counted the number of pseudopodia formed by chemotaxing control, *scr*A mutant, *was*A mutant and double mutant cells (n≥20 cells/cell line, over two independent assays). As shown in figure 5.3c and consistent with what has been previously published (Veltman et al., 2012), the *scr*A mutant had a significantly reduced rate of pseudopod extension compared to the control (unpaired Student's t-test, p<0.0001). On average, the *scr*A mutant was found to form 3.1 ±0.16 (±SEM) pseudopodia/min. compared to the control, which had a mean rate of 4.7 ±0.20 (±SEM) pseudopodia/min.
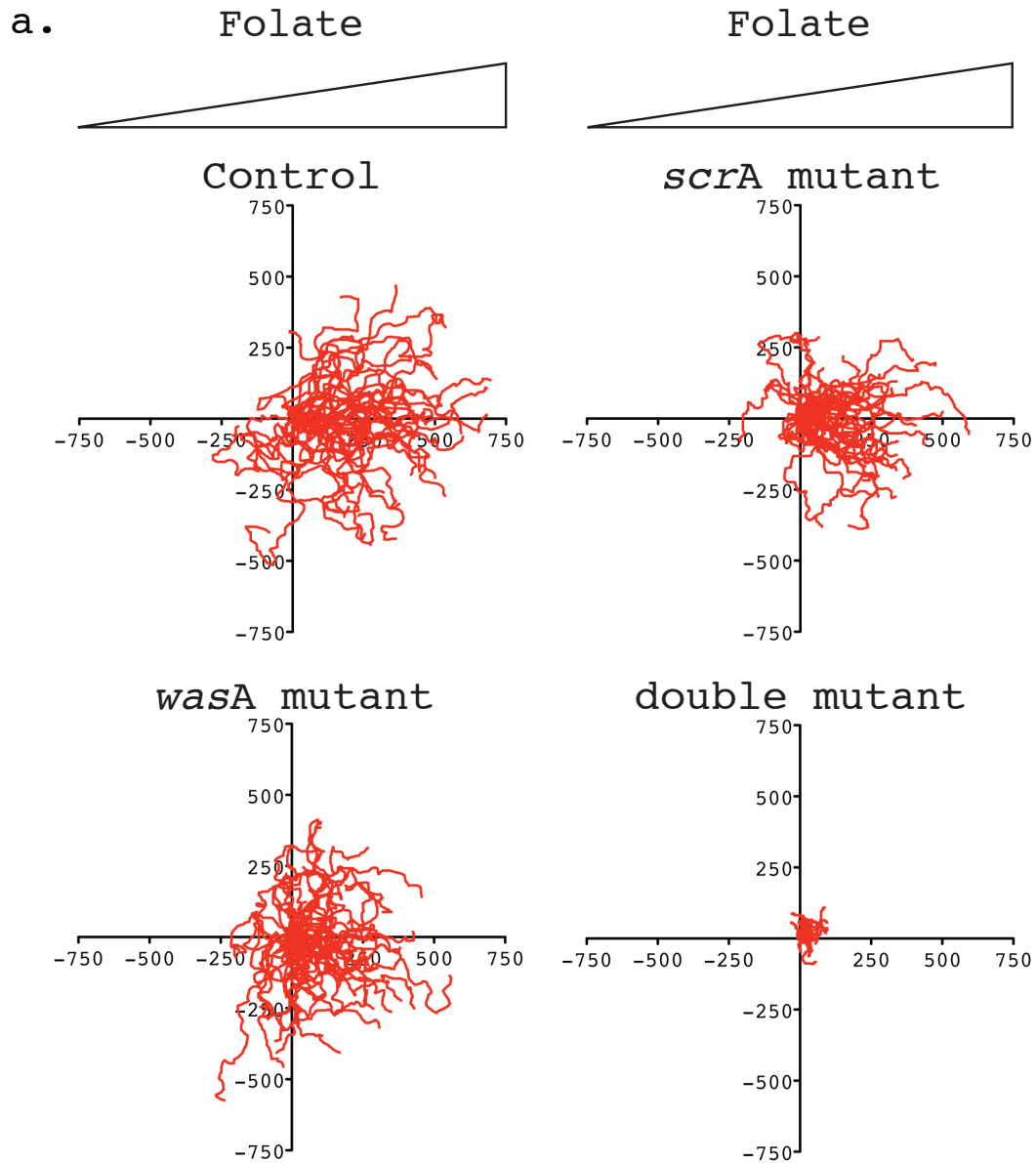
Figure 5.3, The double *scr*A/*was*A mutant has a severe motility defect: a) The double mutant has impaired chemotaxis. The motility of the double mutant was investigated through the use of the under agarose folate chemotaxis assay. Cell tracks represent 30 minutes of control, *scr*A mutant, *was*A mutant and double mutant chemotaxis (>35 cells tracked/cell line derived from three independent assays). The motility of all but the double mutant showed strong bias in the direction of the chemoattractant (from left to right with the triangles representing the folate gradient. The scale of both axes is in μm). It appeared that the double mutant had a severe defect in motility based on the stunted track lengths.

b.
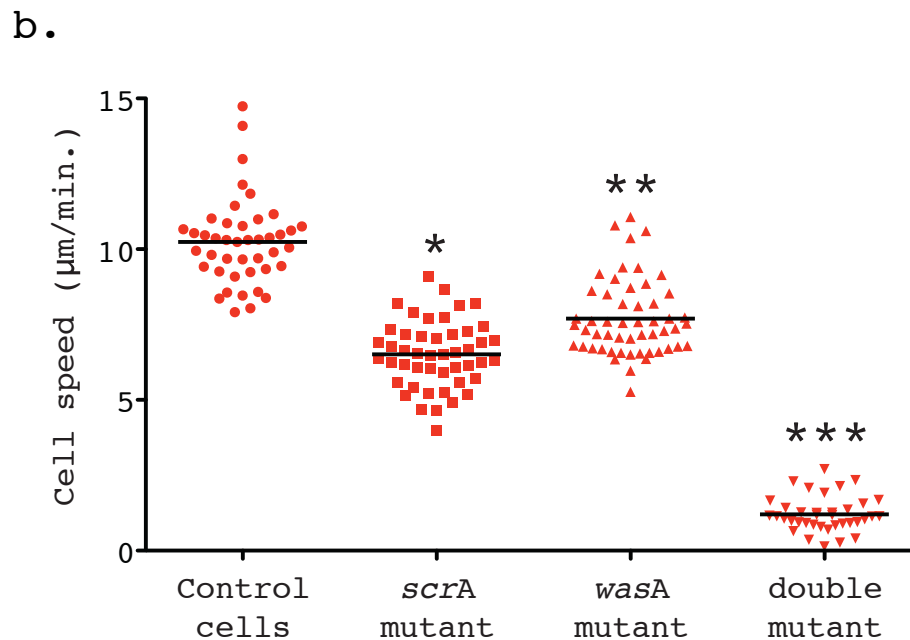
Figure 5.3, The double *scr*A/*was*A mutant has a severe motility defect (continued): b) The double mutant possesses only residual motility. The speed of chemotaxing control, *scr*A mutant, *was*A mutant and double mutant cells was derived from the cell tracks generated in (a) and were plotted in the graph shown above (>35 cell tracks/cell line analysed, over 3 independent assays). The black horizontal bars represent the mean cell speed for each of the cell lines. These data reconfirmed the decrease in migratory speed of the *scr*A mutant (6.51 ±0.16 (±SEM) μm/min.) and the *was*A mutant (7.70 ±0.17 (±SEM) μm/min.) as compared to the control (10.24 ±0.22 (±SEM) μm/min.). The double mutant has a severe defect in cell migration, with a mean cell speed of only 1.21 ±0.10 (±SEM) μm/min. *= significantly different from the control and the *was*A mutant ($p < 0.0001$), **=significantly different from the control and the *scr*A mutant ($p < 0.0001$) and ***=significantly different from the control, the *scr*A mutant and the *was*A mutant ($p < 0.0001$). Statistical significance was determined by use of unpaired Student's t-tests.

c.
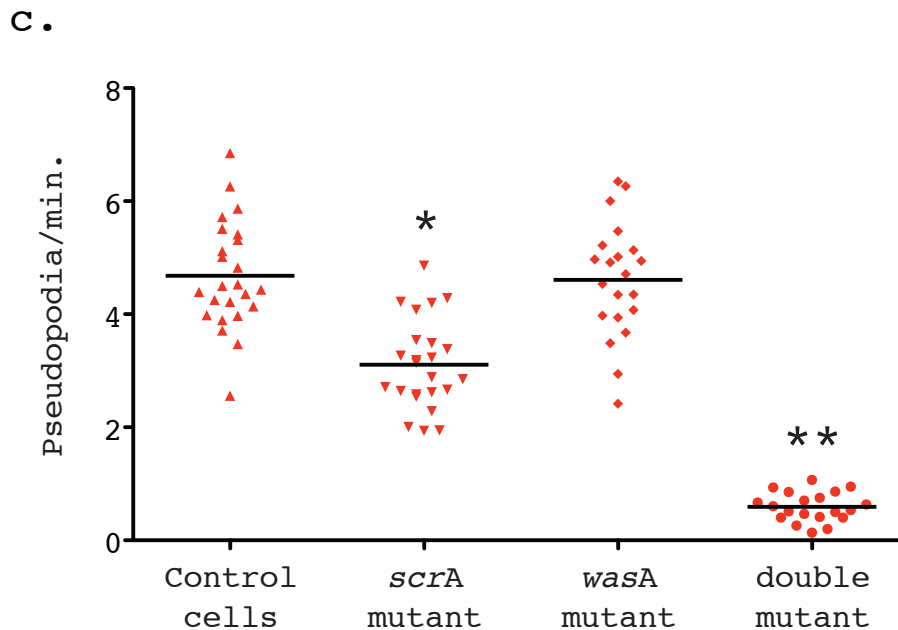
Figure 5.3, The double *scr*A/*was*A mutant has a severe motility defect (continued): c) The double mutant has a defect in pseudopod formation. Pseudopod formation in chemotaxing control, *scr*A mutant, *was*A mutant and double mutant cells was observed by DIC microscopy. Rates of pseudopod extension were calculated and plotted in the above graph (≥20 cells/cell line over two independent chemotaxis assays). The black horizontal bars represent the mean rate of pseudopod formation for each cell line. When compared to the control (4.68 ±0.20 (±SEM) pseudopodia/min.), these data reconfirmed the impaired pseudopod formation of the *scr*A mutant (3.11 ±0.16 (±SEM) pseudopodia/min.) and the normal rate of pseudopod formation in the *was*A mutant (4.61 ±0.22 (±SEM) pseudopodia/min). The double mutant was found to have a severe defect in pseudopod formation (0.59 ±0.06 (±SEM) pseudopodia/min.). *= significantly different from the control and the *was*A mutant (p<0.0001), **=significantly different from the control, the *scr*A mutant and the *was*A mutant (p<0.0001). Statistical significance was determined by use of unpaired Student's t-tests.

d.
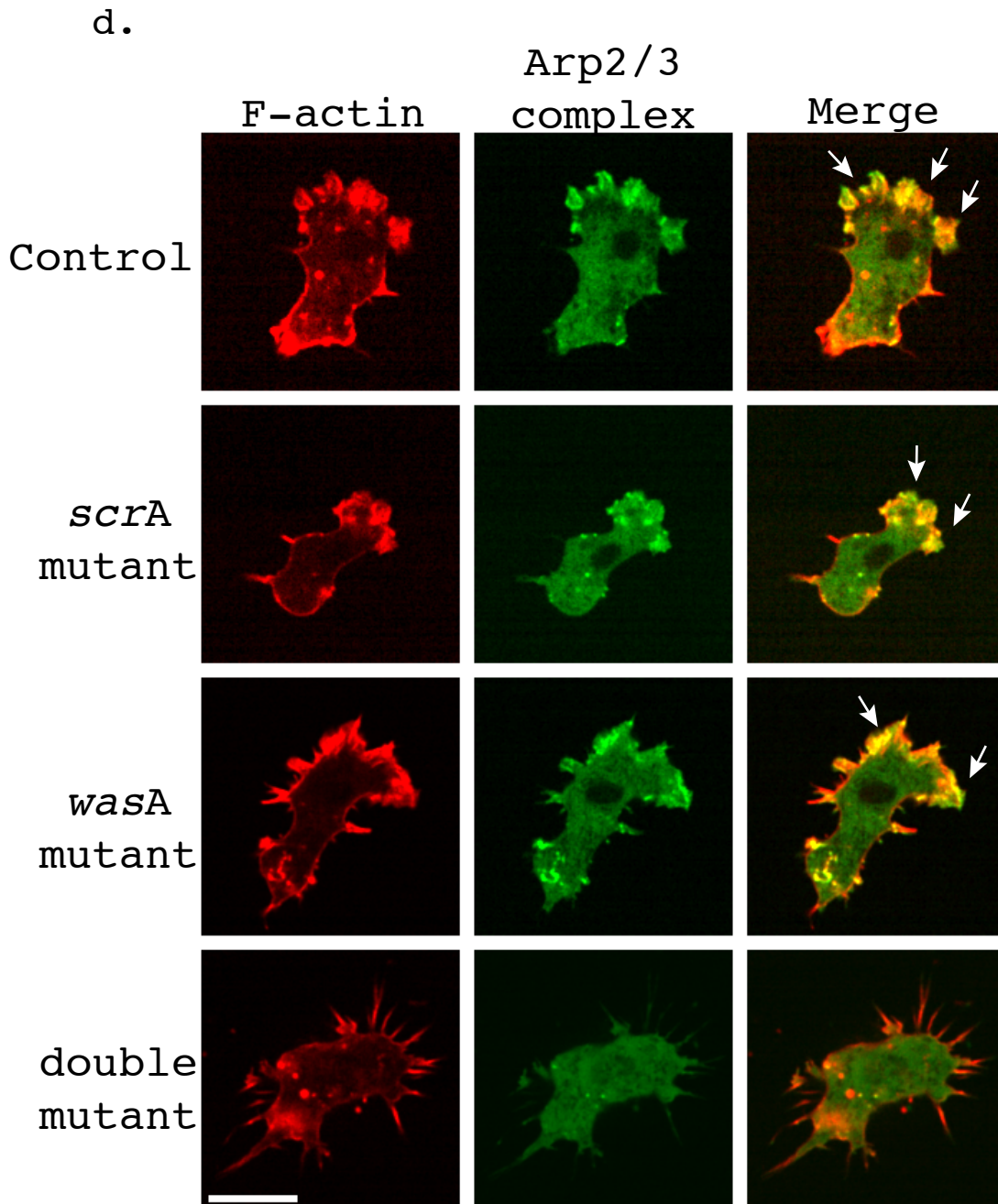
Figure 5.3, The double _scr_A/_was_A mutant has a severe motility defect (continued): d)
The double mutant cannot recruit the Arp2/3 complex to drive pseudopod
formation. Lifeact-mRFP (F-actin) and a GFP-ArpC4 (Arp2/3 complex) were co-
expressed in control, _scr_A mutant, _was_A mutant and double mutant cells and visualised in
chemotaxing cells by spinning disc confocal microscopy under conditions that favoured
pseudopod-based migration. The representative images shown demonstrate that the double
mutant was incapable of recruiting the Arp2/3 complex to the cortex to induce actin-
driven pseudopod extension as observed in the other cell lines (white arrows). Instead the
double mutant extended excessive, actin-rich filopodia. The scale bar represents 10 μm.

As was demonstrated in chapter 4, the *was*A mutant had a normal rate of pseudopod extension (4.6 ±0.22 (±SEM) pseudopodia/min., which was not significantly different from the wild-type). This was again consistent with the conclusions made in chapter 4, where the reduced speed of the *was*A null was not caused by a reduced rate of pseudopod formation but instead was explained by a defect in uropod retraction. Even when the very small, abnormal protrusions observed in the double mutant were included, it had an extremely low rate of pseudopod generation, extending on average 0.6 ±0.06 (±SEM) pseudopodia/min. This rate proved significantly different from the control, the *scr*A mutant and the *was*A mutant (unpaired Student's t-tests, $p < 0.0001$ in all 3 cases).

Finally, to determine if the double mutant had completely lost the ability to recruit the Arp2/3 complex to the cortex to induce actin polymerisation, Lifeact-mRFP and GFP-ArpC4 were co-expressed in the double mutant. The Arp2/3 complex and actin dynamics were visualised in chemotaxing cells using live cell spinning disc confocal microscopy. As shown in figure 5.3d and Movie 6, control, *scr*A mutant and *was*A mutant cells were all capable of recruiting the Arp2/3 complex to the front of the cell to promote actin polymerisation and drive pseudopod extension. This was in stark contrast to the double mutant, which was unable to recruit the Arp2/3 complex to the cell cortex to induce actin-driven pseudopod formation. Instead the double mutant possessed multiple, actin-rich spikes, which were devoid of the Arp2/3 complex and shall be referred to as filopodia. The double mutant also appeared to retain a robust actin cortex, despite the absence of the Arp2/3 complex.

From these data, it was concluded that no protein other than WASP A could substitute for SCAR to promote pseudopod formation. In the absence of both SCAR and WASP A, cells are unable to recruit the Arp2/3 complex to the cortex, which severely impaired motility.

5.4 The double *scr*A/*was*A mutant has a specific defect in cell motility

In the previous subsection, it was demonstrated that the double *scr*A/*was*A mutant was unable to recruit the Arp2/3 complex to promote pseudopod extension and support cell migration. However, due to the severe growth defect evident in the absence of both SCAR and WASP A (figure 5.2a), it remained possible that the double mutant had a compromised cytoskeleton in general, rather than a specific defect in pseudopod formation. With this in mind, we sought to establish whether the double mutant was capable of any other actin-dependent processes. As discussed earlier, the double mutant was still capable of cell spreading, which in *Dictyostelium* utilises SCAR (or, in the absence of SCAR, WASP A), the Arp2/3 complex and actin in an analogous process to pseudopod extension (Veltman et al., 2012). Cells co-expressing Lifeact-mRFP and GFP-ArpC4 were suspended at a high density and then dropped on to a glass-bottomed dish set up on a TIRF microscope, allowing observation of Arp2/3 complex and actin dynamics during cell spreading. As shown in figure 5.4, control, *scr*A mutant and *was*A mutant cells recruit the Arp2/3 complex to the cell cortex to promote actin-driven cell spreading. As was demonstrated in figure 5.3d, the double mutant lacks the ability to recruit the Arp2/3 complex to the cell cortex during cell migration and this was also true during cell spreading. However, the double mutant was still capable of mobilising its actin cytoskeleton to support cell spreading in an Arp2/3 complex independent manner, using a dense tangle of seemingly chaotically organised filopodia to adhere to the glass.

It was concluded that cells devoid of SCAR and WASP A were capable of actin-driven processes such as cell spreading, albeit in a highly abnormal manner. Instead, the double mutant was specifically incapable of utilising its cytoskeleton to mobilise itself to promote cell migration.

	F-actin	Arp2/3 complex	DIC	Merge
Control				
*scr*A mutant				
*was*A mutant				
double mutant				
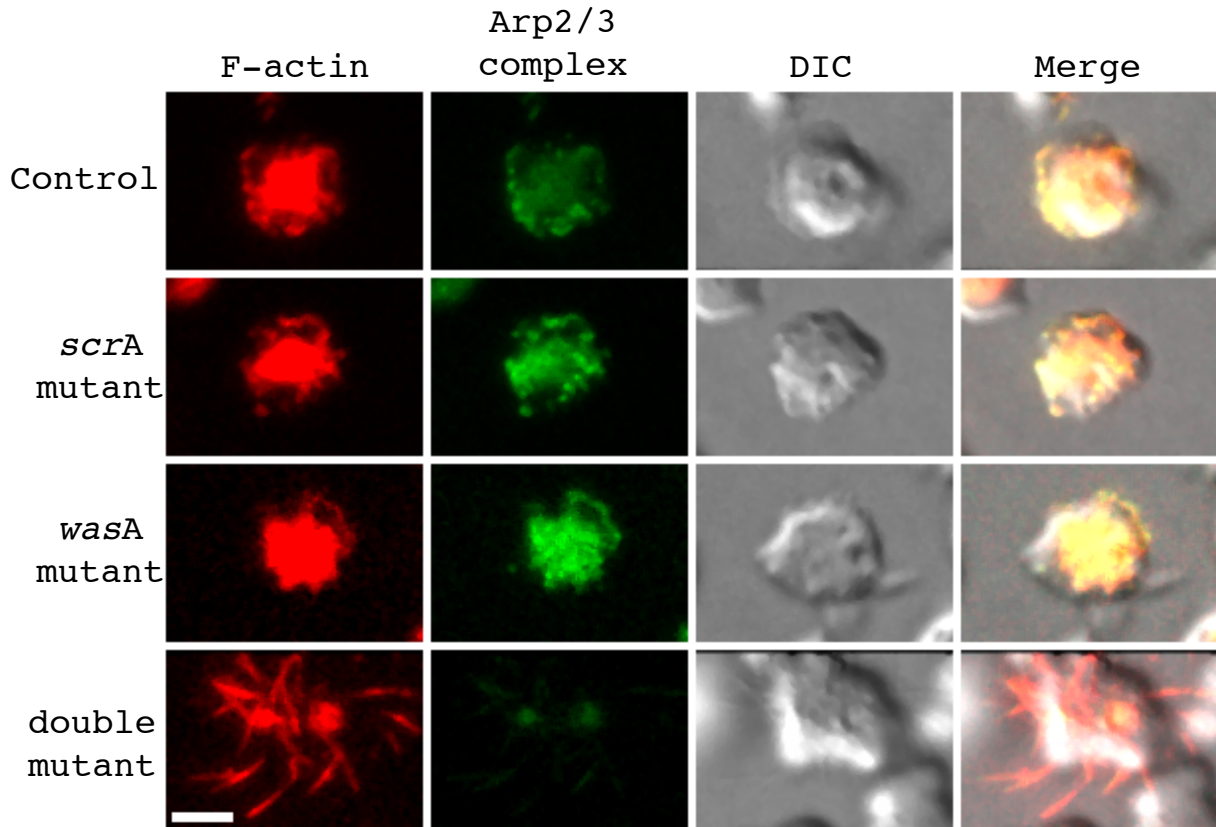
Figure 5.4, The double mutant can mobilise its actin cytoskeleton to drive cell spreading: Lifeact-mRFP (F-actin) and a GFP-ArpC4 (Arp2/3 complex) were co-expressed in control, *scr*A mutant, *was*A mutant and double mutant cells and cell spreading was visualised by TIRF and DIC microscopy. The representative images shown demonstrate that cell spreading is normally an Arp2/3 complex-driven process. The double mutant retained the ability to spread but instead utilised its Arp2/3 complex-independent filopodia. The scale bar represents 5 μm.

5.5 The double *scr*A/*was*A mutant has a defect in bleb-based migration

In section 5.3 it was demonstrated that the double *scr*A/*was*A mutant had a severe motility defect. However, herein lay a surprise. Although our lab has published that WASP A partially compensates for a loss of SCAR, the *scr*A null also clearly supplements its reduced rate of pseudopod formation with Arp2/3 complex independent blebs (Veltman et al., 2012, Ura et al., 2012). Therefore, although the double mutant had proved defective in pseudopod formation, it had been expected to maintain motility through the use of blebs. Bleb-based migration is a distinct mode of migration from pseudopod-based migration (Yoshida & Soldati, 2006). Both involve actin polymerisation. However, whereas pseudopodia are formed from large actin meshworks generated by the Arp2/3 complex, blebs are devoid of the Arp2/3 complex and possess considerably less F-actin (Langridge & Kay, 2006, Charras et al., 2006). Instead blebs depend on myosin-II based contractility to burst open the cortex. The reformation of the underlying actin cortex forms a cortical 'bubble' or bleb, which can be utilised by the cell as a type of small protrusion to support cell motility. Yoshida & Soldati, (2006) demonstrated in their paper that normal *Dictyostelium* migration consists of a mixture of both blebs and pseudopodia. However, here the under-agarose folate chemotaxis assay had been optimised to strongly favour pseudopod-based migration and so blebs were rarely seen during the migration of control cells. This was in contrast to the *scr*A mutant, in which blebbing was clearly evident. This suggested that the suppression of pseudopod formation in the *scr*A mutant lead to a compensatory upregulation of blebbing. These conditions were utilised to establish whether or not the double mutant was able to switch to bleb-based migration in the absence of pseudopodia. Blebs were visualised by spinning disc confocal in chemotaxing cells co-expressing Lifeact-mRFP and GFP-ArpC4 and were identified as actin-based protrusions that were devoid of the Arp2/3 complex. Bleb formation was quantified by counting the number of blebs the cells formed at the leading edge during their chemotaxis (n=≥12 cells, over 2 independent assays). As shown in figure 5.5a, control cells were
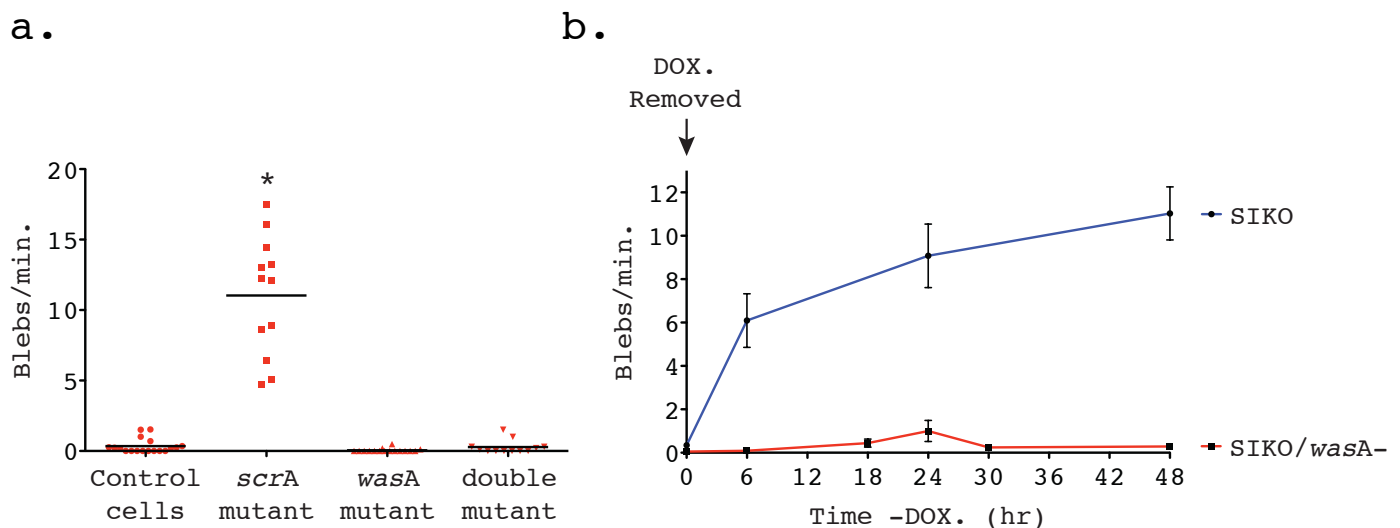
Figure 5.5, The double *scr*A/*was*A mutant has a defect in bleb-based motility: Lifeact-mRFP (F-actin) and a GFP-ArpC4 (Arp2/3 complex) were co-expressed in control, *scr*A mutant, *was*A mutant and double mutant cells and blebs were visualised in chemotaxing cells by spinning disc confocal microscopy. **a) The double mutant cannot utilise blebs to migrate in the absence of SCAR and WASP A.** Rates of bleb formation were calculated and plotted in the above graph (≥12 cells/cell line over two independent chemotaxis assays). The black horizontal bars represent the mean rate of bleb formation. The loss of SCAR alone induced a switch to bleb-based migration (11.03 ± 4.23 (±SEM) blebs/min.), however the double mutant was incapable of forming blebs to compensate for its loss of pseudopodia. *=significantly different from control, *was*A mutant and double mutant cells (unpaired student's t-tests, p<0.001). **b) Gradual suppression of SCAR expression in the inducible double mutant fails to induce a switch to bleb-based migration.** Due to the inducible nature of the double mutant, it was possible to control the expression of SCAR in a *was*A positive (SIKO) and *was*A negative (SIKO/*was*A-) background by depriving the cells of doxycycline (DOX.) for varying lengths of time prior to the assay. The number of blebs formed during chemotaxis was counted and the mean rate of bleb formation was plotted in the graph shown above (≥10 cells/time point over two independent assays). The suppression of SCAR in a *was*A positive background resulted in an immediate increase in bleb formation. However, the suppression of SCAR in a *was*A negative background failed to induce robust bleb-based. The error bars represent the SEM.

c.
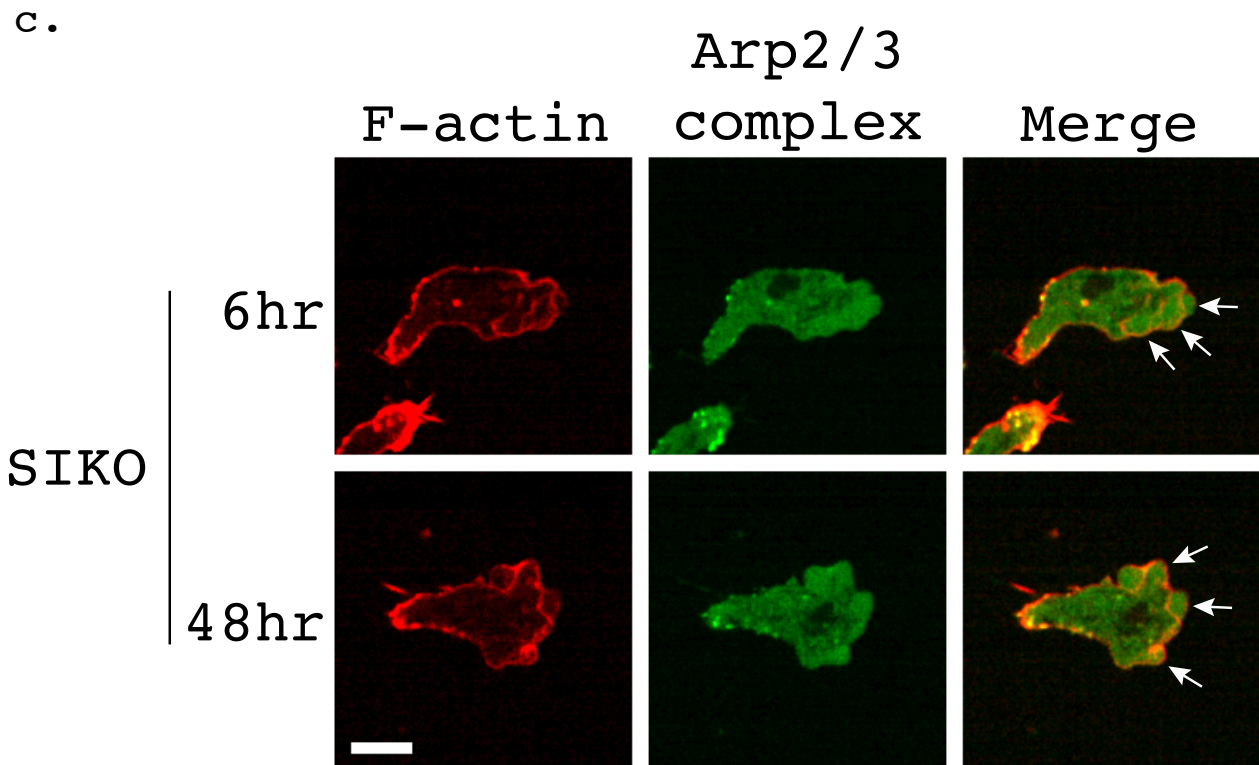
Figure 5.5, The double *scr*A/*was*A **mutant has a defect in bleb-based motility (continued): c) SIKO cells rapidly increases bleb formation during chemotaxis upon suppression of SCAR.** Lifeact-mRFP (F-actin) and a GFP-ArpC4 (Arp2/3 complex) were co-expressed in SIKO cells, which were then deprived of doxycycline for increasing amounts of time in order to vary SCAR expression. The cells were then applied to the under-agarose folate chemotaxis assay and actin-based protrusions were visualised in motile cells by spinning disc confocal microscopy. The representative images shown at two selected time points (6 hr and 48 hr post doxycycline deprivation) demonstrate that the SIKO supplements its decreasing rate of pseudopod formation with blebs. The white arrows highlight prominent blebs and the scale bar represents 10 μm.
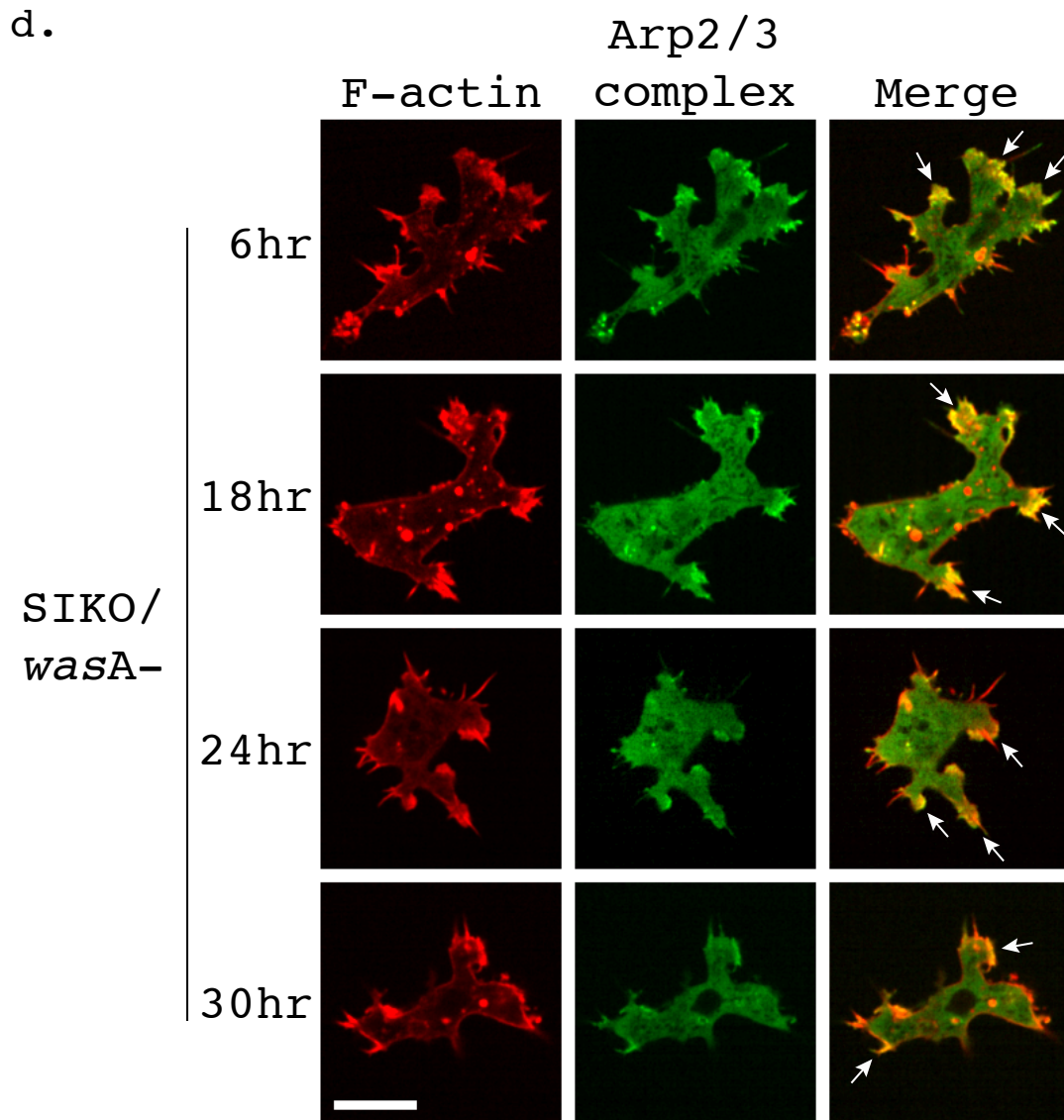
Figure 5.5, The double *scr*A/*was*A **mutant has a defect in bleb-based motility (continued): d) The inducible double mutant cannot switch to bleb-based migration upon the suppression of SCAR.** Lifeact-mRFP (F-actin) and a GFP-ArpC4 (Arp2/3 complex) were co-expressed in SIKO/*was*A null cells, which were then deprived of doxycycline for increasing amounts of time in order to vary SCAR expression in a *was*A null background. The cells were then applied to the under-agarose folate chemotaxis assay and actin-based protrusions were visualised in cells by spinning disc confocal microscopy. Representative images of cells at four selected time points (6-30 hr post-doxycycline deprivation) are shown. No blebs were observed at any time point despite the increasingly diminished pseudopodia evident (white arrows). By 24-30 hr post-doxycycline deprivation, the motility of the inducible double mutant was severely impaired. The scale bar represents 10 μm.

only averaging 0.35 ±0.12 (±SEM) blebs/min., consistent with these conditions favouring pseudopod-based migration. In contrast, the *scr*A mutant was clearly supplementing its motility with blebs, making on average 11.0 ±1.22 (±SEM) blebs/min. The difference in bleb rate between the control and the *scr*A mutant proved statistically significant (unpaired Student's t-test, p value <0.0001). As has been established in the previous chapter and in section 5.3, *was*A deficient cells have no defect in pseudopod formation and consequently formed very few blebs during its migration, averaging only 0.05 ±0.03 (±SEM) blebs/min. The low bleb rate of the double mutant (mean rate of 0.29 ±0.14 (±SEM) blebs/min) confirmed that this cell line had a defect in both pseudopod and bleb-based migration.

As the double mutant was in fact an inducible mutant, it was possibly to partially suppress SCAR expression in a *was*A positive (SIKO) and a *was*A negative (SIKO/*was*A null) background and observe how this affected the transition to bleb-based migration. This was achieved by depriving the double mutant of doxycycline in a staggered fashion before introducing them to the under-agarose folate chemotaxis assay. As demonstrated in figure 5.5b and 5.5c, *was*A positive cells switched to bleb-supplemented migration within only 6 hours of doxycycline deprivation (n=≥10 cells/time point, over 2 independent assays). However, the suppression of SCAR expression in the *was*A deficient cells induced a very weak, transient increase in bleb rate at best (n=≥10 cells/time point, over 2 independent assays). This occurred after 24 hours of doxycycline deprivation, where the bleb rate reached an average of 1.0 ±0.48 (±SEM) blebs/min and had dissipated by 30 hours doxycycline deprivation. As the time without doxycycline increased, the size and frequency of the pseudopodia extended by the double mutant visibly declined, as shown by the examples in figure 5.5d. However, instead of switching to bleb-based motility, the morphology of the double mutant became increasingly dominated by filopodia until all motility ceased.

5.6 Bleb-based motility does not depend on *was*A alone

Before it could be concluded that the defect in bleb-based migration was a consequence of losing the ability to recruit the Arp2/3 complex to the cell cortex, the possibility that the *was*A mutant had a specific defect in bleb-based migration had to be excluded. This remained a distinct possibility since bleb formation in *Dictyostelium* requires actomyosin-based and, as was discussed in chapter 4, myosin-II appeared aberrantly distributed within the uropod of the *was*A null. To confirm that the *was*A mutant was capable of bleb-based migration, conditions that favoured bleb formation during migration were optimised. It was found that by subjecting the cells to greater vertical compression in the under-agarose folate chemotaxis assay, it was possible to strongly inhibit pseudopod formation and instead promote bleb-based migration. These bleb-promoting conditions were primarily achieved by increasing the percentage agarose of the gel used in the assay. Again Lifeact-mRFP and GFP-ArpC4 were co-expressed in cells, which were imaged during chemotaxis using spinning disc microscopy. As can be seen from the examples shown in figure 5.6 and Movie 7, control cells, *scr*A mutants and importantly, *was*A mutants were all capable of supporting migration with blebs alone. Again, there was no recruitment of the Arp2/3 complex to the site of bleb formation observed. The severe conditions impaired the ability of even the control cells to migrate under the agarose, so it was not surprising that the double mutant failed to enter the assay. Finally, as shown in the example shown in figure 5.6, the high compression exaggerated the enlarged uropod of the *was*A mutant, providing a very good view of the actin aggregates accumulated in the rear of the cell, as was discussed in chapter 4. In summary, we have demonstrated that only WASP A can substitute for SCAR to promote the formation of pseudopodia in *Dictyostelium*. Unexpectedly, in the absence of both these proteins, cells had a severe defect in both pseudopod and bleb-based migration rendering them essentially immobile.
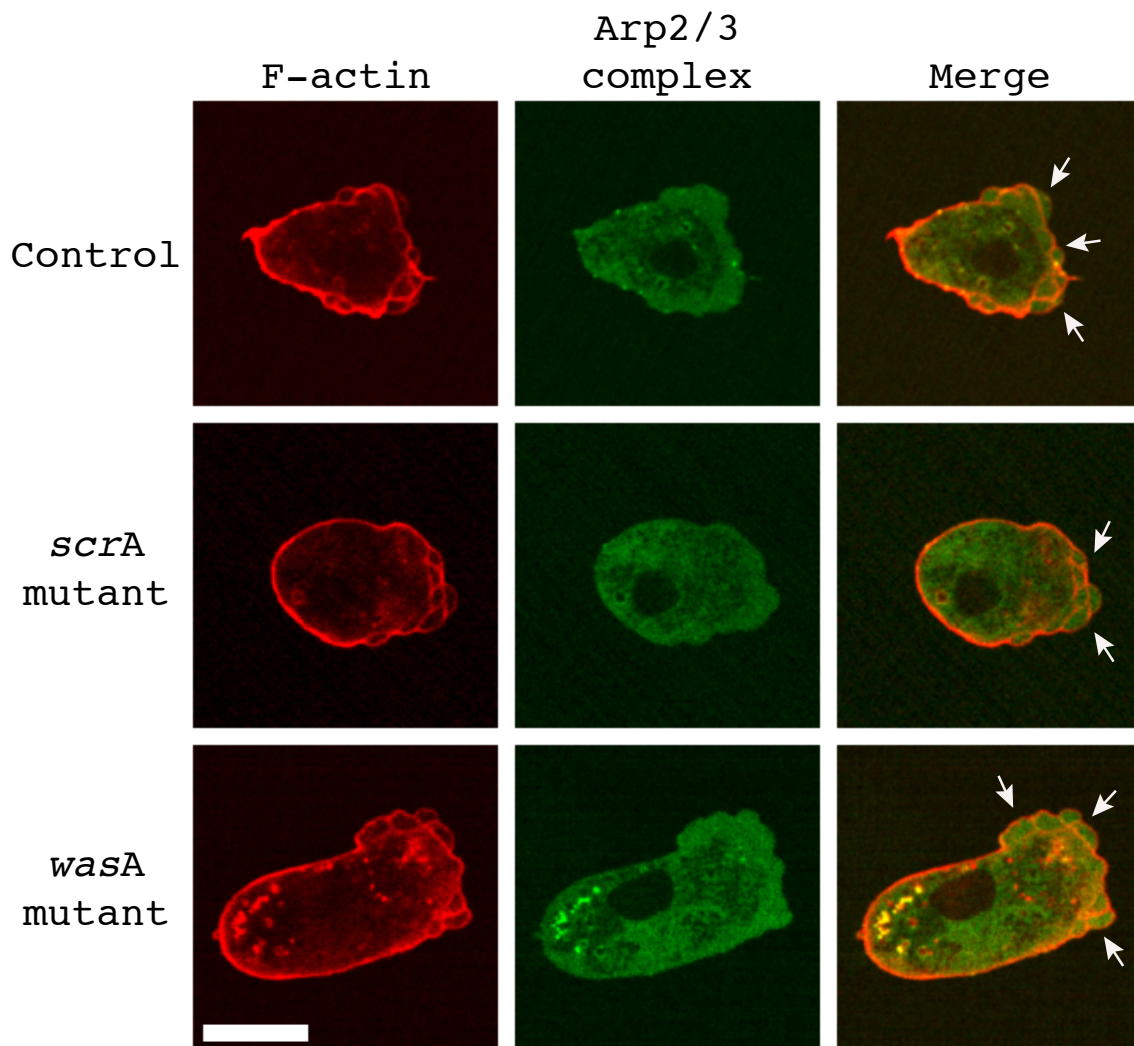
Figure 5.6, WASP A alone is not required for robust bleb-based motility: Lifeact-mRFP (F-actin) and a GFP-ArpC4 (Arp2/3 complex) were co-expressed in control, *scr*A mutant and *was*A mutant cells and visualised in chemotaxing cells by spinning disc confocal microscopy under conditions that favoured bleb-based migration. Under these conditions, Arp2/3 complex-driven pseudopodia were entirely absent. The representative images shown above demonstrate that control, *scr*A mutant and *was*A mutant cells were capable of robust migration through blebs alone. The white arrows indicate persistent, directional blebbing that was supporting chemotaxis in these cells. The double mutant failed to enter the assay under these conditions. The scale bar represents 10 μm.

5.7 The double *scr*A/*was*A mutant retains robust actomyosin contractility

In the previous section, it was established that the double mutant has a defect in bleb-based migration. However, the Arp2/3 complex is not recruited to the site of bleb formation so it remains an open question as to why WASP family members are essential for this type of protrusion. As discussed in the previous section, myosin-II based contractility is essential for bleb formation (Langridge & Kay, 2006, Yoshida & Soldati, 2006). Despite the aberrant localisation of myosin-II observed in the uropod of the *was*A mutant, these cells were still capable of migrating by blebs alone under severe compression (figure 5.6). However, it was possible that the double mutant had a more severe defect in actomyosin-based contractility. To test myosin-II function in the double mutant, cells were introduced to sodium azide as described in chapter 4. As can be seen from figure 5.7, the double mutant retained robust, myosin-II dependent cell detachment in response to treatment with 5 mM sodium azide (repeated over 4 independent experiments). The proportion of double mutant cells that detached in response to sodium azide was not significantly different from that found with control, *scr*A mutant or *was*A mutant cells (One-way analysis of variance), where in each case an average of >75% cells detached. This was in contrast to *mlc*E null (lacks functioning myosin-II) and *mhc*A null (lacks all myosin-II) cells, which lacked this immediate response to azide. Here we have demonstrated that the double mutant retains robust myosin-II function that is at least sufficient to drive the extreme contraction promoted by exposure to sodium azide. Therefore it presumably retains adequate myosin-II functionality to support bleb formation. Whether myosin-II is localised and organised in a manner that would allow bleb-based migration remains to be investigated.
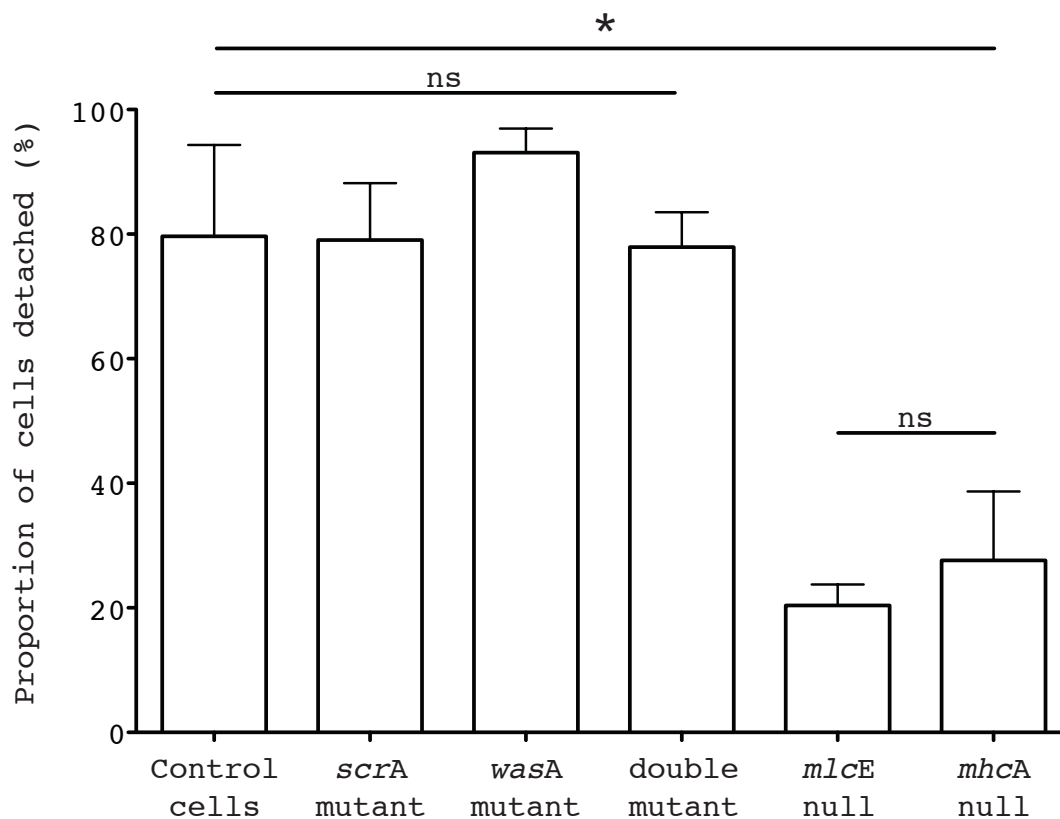
Figure 5.7, The double *scr*A/*was*A mutant retains actomyosin contractility: Control, *scr*A mutant, *was*A mutant and double mutant cells as well as *mlc*E and *mhc*A nulls were seeded at a high density on Petri dishes and were treated with 5 mM sodium azide. The immediate, azide-induced detachment of cells is dependent on robust myosin-II driven contractility. The mean proportion (%) of cells that immediately detached in response to sodium azide was plotted in the above graph (represents four independent experiments/cell line). No significant difference in response was observed between control, *scr*A mutant, *was*A mutant and double mutant cells compared to the myosin-II mutant controls. * indicates that the proportion of control, *scr*A mutant, *was*A mutant and double mutant cells that detached significantly differed from the myosin-II mutant controls (one-way ANOVA, $p < 0.05$ in all cases) and ns denotes non-significance. The error bars represent the SEM.

5.8 The double *scr*A/*was*A mutant possesses a robust actin cortex

In the previous section we had found that the double mutant retains global actomyosin-based contractility. The other major component of bleb formation involves cortical actin dynamics. Once the plasma membrane has ruptured away from the underlying cortex, Arp2/3 complex independent actin polymerisation is induced to reform the cortex, forming the distinctive actin bleb (Langridge & Kay, 2006, Charras et al., 2006). The expression of Lifeact-mRFP in the double mutant and subsequent fluorescence imaging, suggested that the double mutant still possessed an actin-rich cortex (figure 5.3d). However, having lost two major actin regulators, it was possibile that the double mutant had impaired cortical actin dynamics. Initially, the overall F-actin content of the double mutant was investigated. To quantify the amount of F-actin in the double mutant, a ratiometric staining approach was adopted. Here vegetative, unstimulated cells were fixed and stained with fluorescently labelled phalloidin (binds F-actin) and DNase I (binds G-actin). Images of the fixed and stained cells were then acquired by widefield fluorescence microscopy. An outline around the fixed cells was drawn and the average intensity of both the phalloidin and the DNaseI staining within the cell area was calculated using imageJ software. An example of both a stained control cell and a stained double mutant cell are shown in figure 5.8a. By dividing the average intensity of the phalloidin staining by the average intensity of the DNaseI staining for each individual cell and repeating this for many cells (n=75 cells/cell line, over 3 independent experiments), a mean F-/G- actin ratio was derived. This approach also had the advantage of revealing the morphology of the cytoskeleton in the cells. The representative example shown in figure 5.8a, confirmed the spiky, filopod-based morphology of the double mutant. Surprisingly, when the F-/G- actin ratios were compared between the control, *scr*A mutant, *was*A mutant and double mutant cells, there were no significant differences in F-actin content as demonstrated by figure 5.8b. As a comparison, control cells were briefly incubated with the actin poison latrunculin A before fixation.
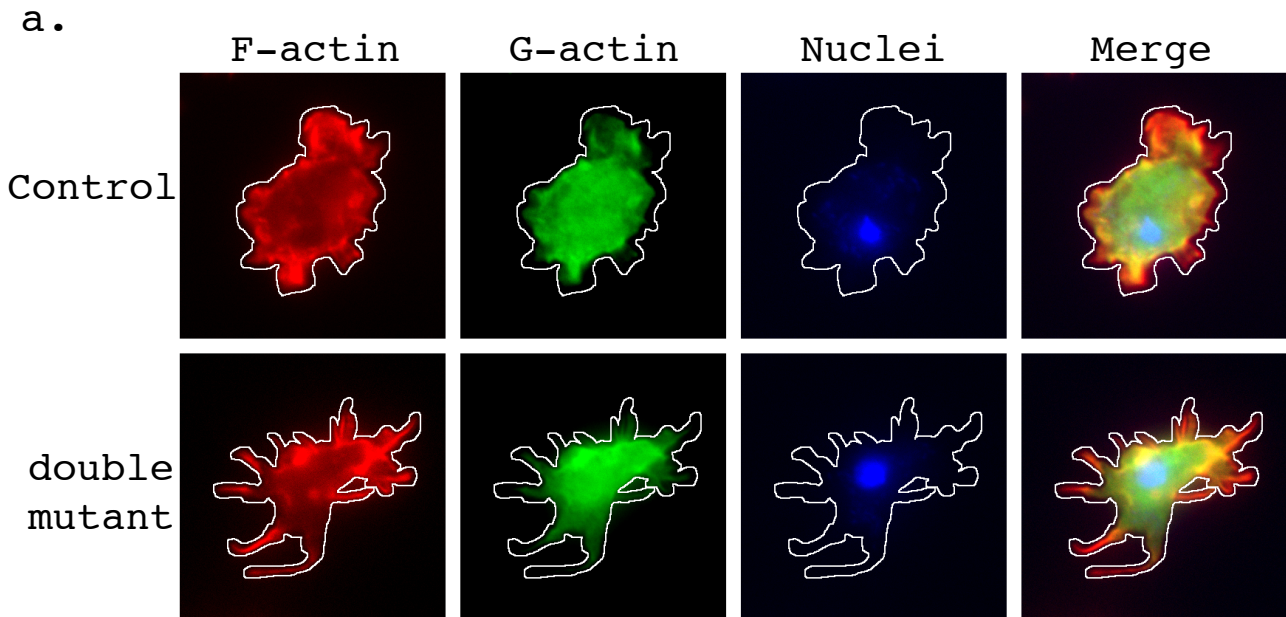
a.

Figure 5.8, The double mutant possesses normal levels of F-actin: a) The double mutant retains an actin-rich cortex. Unstimulated, vegetative control, *scr*A mutant, *was*A mutant and double mutant cells were fixed and stained with fluorescently labeled phalloidin (F-actin) and DNaseI (G-actin) as well as DAPI (Nuclei). The actin cytoskeleton was visusalised in these cells by widefield fluorescence microscopy. The representative images of fixed and stained control and double mutant cells shown above demonstrate that the double mutant retains an actin-rich cortex, which was dominated by filopodia in contrast to the other cell lines. Cell outlines are shown in white and the scale bar represents 10 μm.
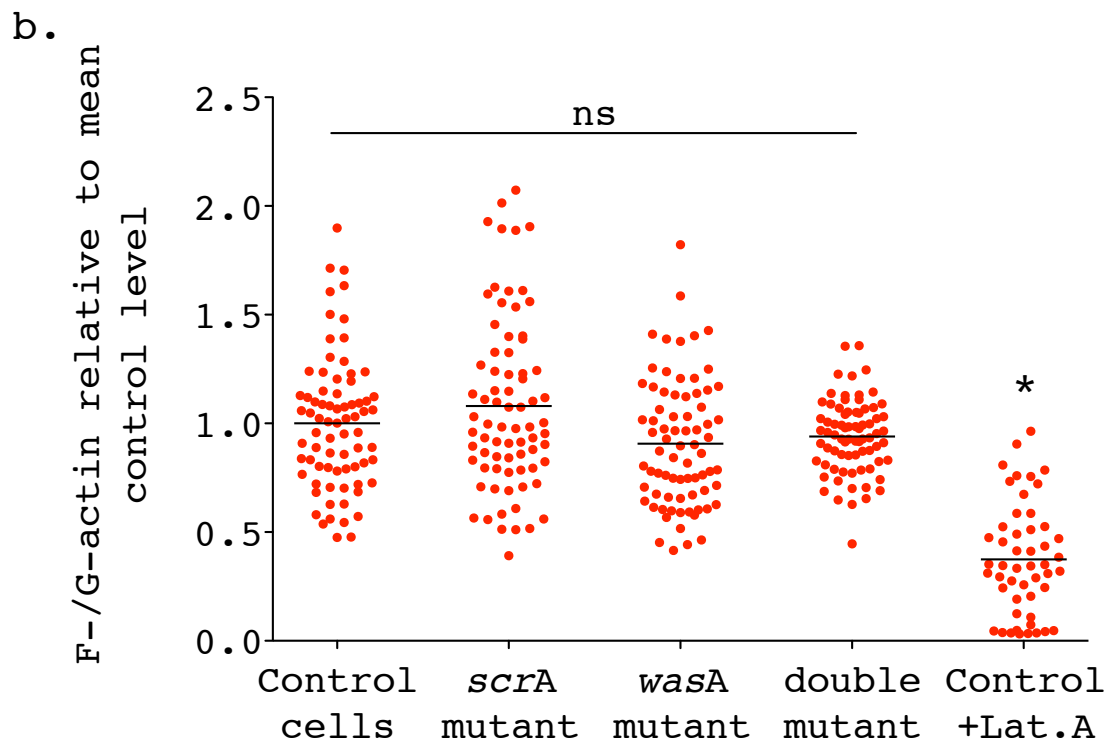
b.

Figure 5.8, The double mutant possesses normal levels of F-actin: a) The double mutant retains an actin-rich cortex (continued). b) The loss of *scr*A, *was*A or both *scr*A and *was*A does not alter cellular F-actin levels. Many control, *scr*A mutant, *was*A mutant and double mutant cells were fixed, stained and outlined as in (a). The average intensity of the F-actin staining within the cell outline was divided by that of the G-actin staining to yield a F-/G-actin ratio for each cell, which was then normalised to the mean control F-/G-actin ratio. These values were then plotted in the graph shown above (75 cells/cell line over three independent experiments). The black horizontal bars represent the mean normalised F-/G-actin ratio for each of the cell lines and no significant (ns) differences were observed between these values (one-way ANOVA, $p > 0.05$). This was in contrast to control cells sub-maximally treated with latrunculin A prior to fixation (5 minute incubation compared to 10-15 minutes), which did have significant reduced levels of F-actin compared to control, *scr*A mutant, *was*A mutant and double mutant cells (one-way ANOVA, $p < 0.05$ in all cases).

Latrunculin works by binding G-actin and trapping it in the monomeric form. As actin is constantly polymerising and depolymerising, latrunculin A very quickly sequesters all the actin, resulting in the collapse of the cytoskeleton. As shown in figure 5.8b, this was sufficient to reduce the F-actin content in cells to a level significantly different to the control, *scr*A mutant, *was*A mutant and double mutant cells (one-way ANOVA, $p < 0.05$ in all cases).

In summary, despite losing all ability to recruit the Arp2/3 complex to the cell cortex, the double mutant possesses a robust actin cytoskeleton with normal levels of F-actin.

5.9 The double *scr*A/*was*A mutant retains normal cortex turnover

Although the average F-actin content of the double mutant appeared to be equivalent to that found in the control cells, the variance of the data appeared suppressed (figure 5.8b). This was consistent with the Lifeact-mRFP fluorescence images previously generated, wherein it was found that the double mutant possessed an actin cortex but the whole cytoskeleton appeared very static. It was speculated that although the double mutant possessed an actin-rich cortex, the inability to recruit the Arp2/3 complex to the cortex might impair actin turnover in general. A stagnant cortex would in turn possibly lack sufficient dynamism to support bleb formation.

Latrunculin A treatment disrupts the actin cytoskeleton by inhibiting actin treadmilling through the sequestration of actin in the monomeric form. Therefore, it was reasoned that if the double mutant had defective cortical actin turnover, the cortex should show signs of resistance to latrunculin A. Focusing on control and double mutant cells only, the effect of latrunculin A treatment on unstimulated, vegetative cells was investigated. Cytoskeletal dynamics in the presence of latrunculin A was visualised in cells co-expressing Lifeact-mRFP and GFP-ArpC4 by spinning disc confocal microscopy. As can be seen from the examples shown in figure 5.9a and b, the cytoskeleton of the double mutant was no more resistant to latrunculin A treatment than control cells.
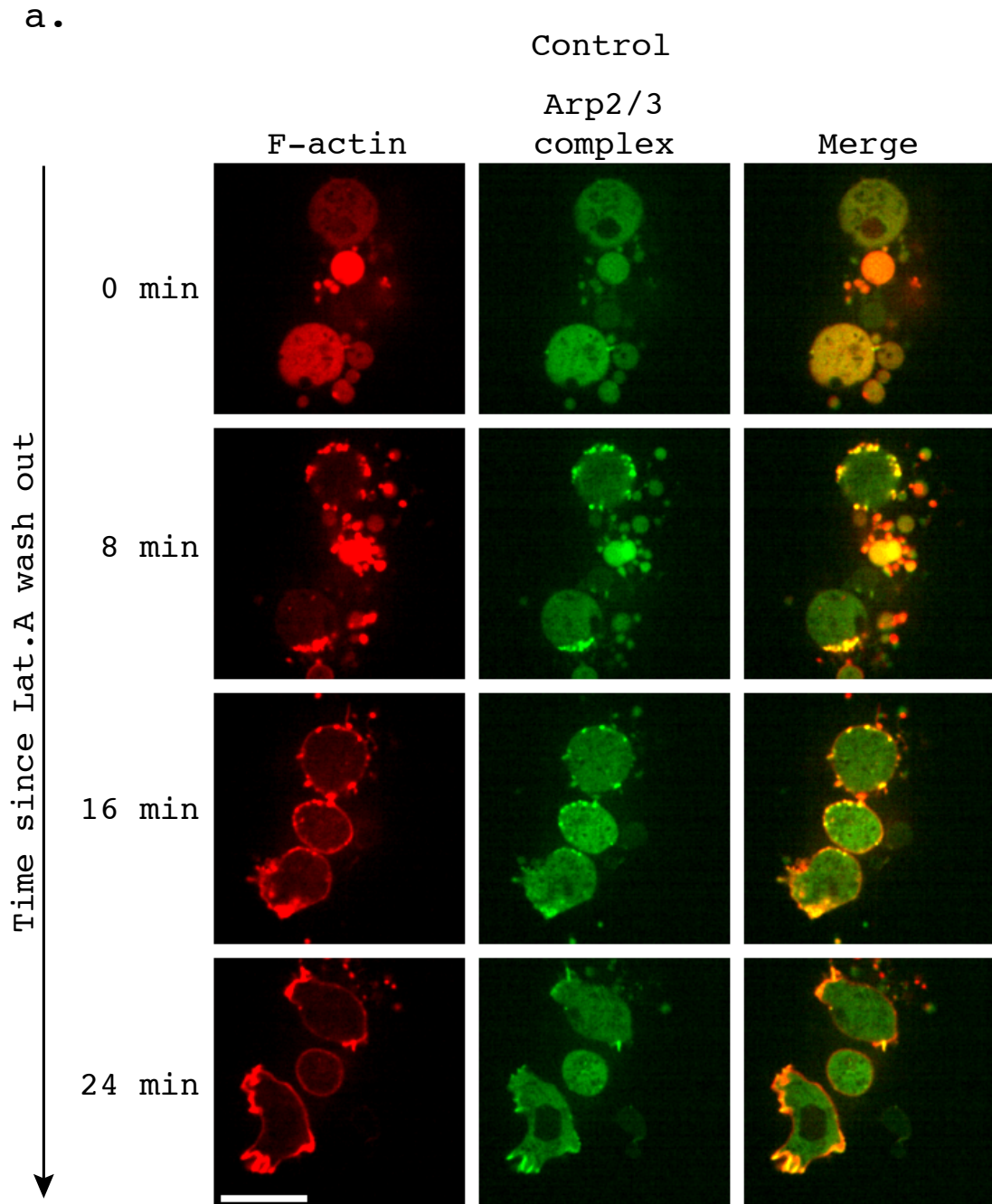
Figure 5.9, The double *scr*A/*was*A mutant possesses a dynamic actin cortex: a) The Arp2/3 complex was recruited to reconstitute the actin cortex following latrunculin A induced depolymerisation of the cytoskeleton. Lifeact-mRFP (F-actin) and a GFP-ArpC4 (Arp2/3 complex) were co-expressed in control cells and the reformation of the actin cortex following latrunculin A treatment was visualised by spinning disc confocal microscopy. The selected images shown demonstrate that control cells recruited the Arp2/3 complex to rebuild the actin cortex over a period of 20 minutes once the cells had been removed from latrunculin A. The scale bar represents 10 μm.
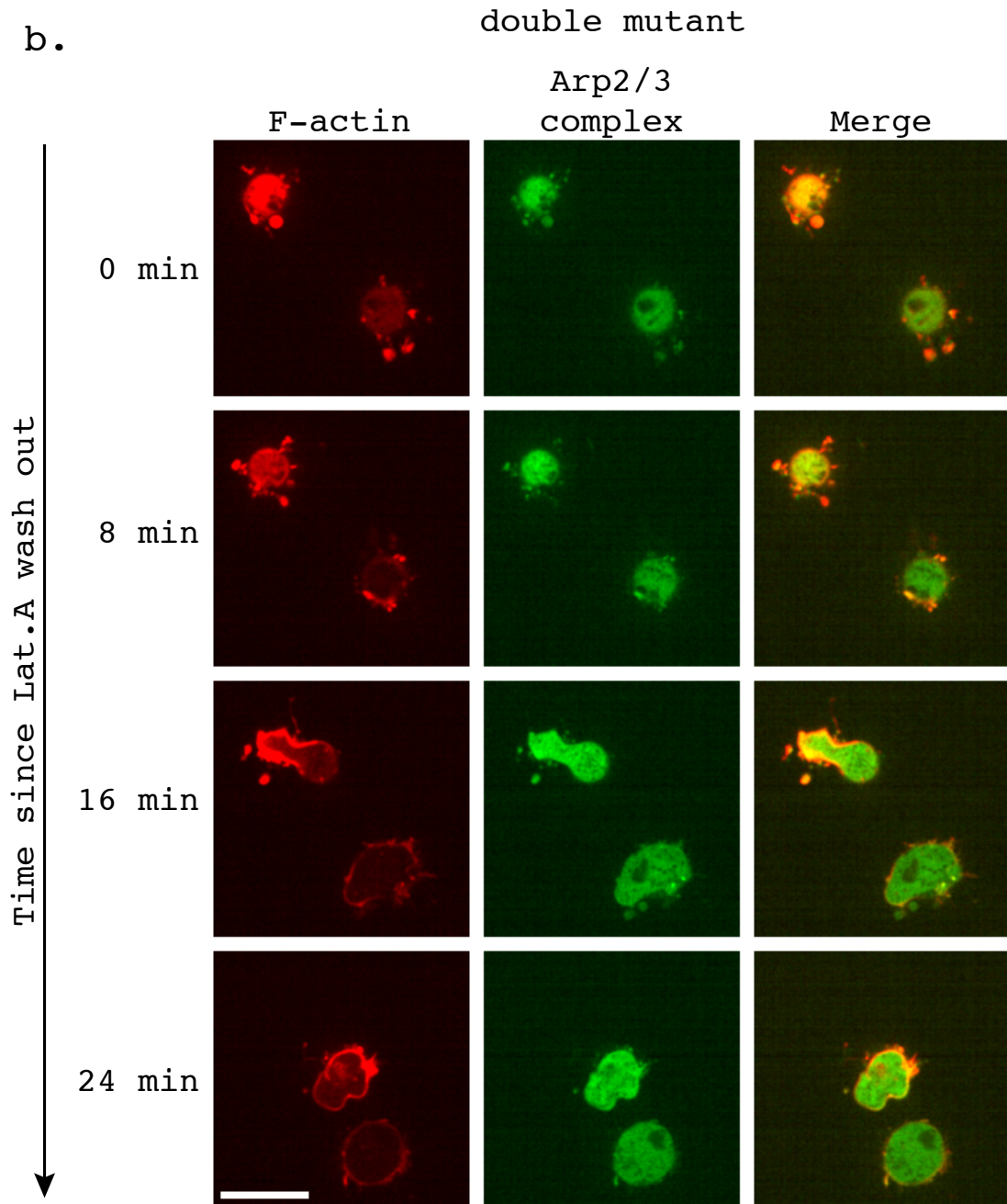
Figure 5.9, The double *scr*A/*was*A mutant possesses a dynamic actin cortex (continued): b) The double mutant retains the ability to reform the actin cortex following latrunculin A induced depolymerisation of the actin cytoskeleton. Lifeact-mRFP (F-actin) and a GFP-ArpC4 (Arp2/3 complex) were co-expressed in double mutant cells and the reformation of the actin cortex following latrunculin A treatment was visualised by spinning disc confocal microscopy. The selected images shown demonstrate that the double mutant was capable of reconstituting its actin cortex in the absence of the Arp2/3 complex once the cells had been removed from latrunculin A. The scale bar represents 10 μm.
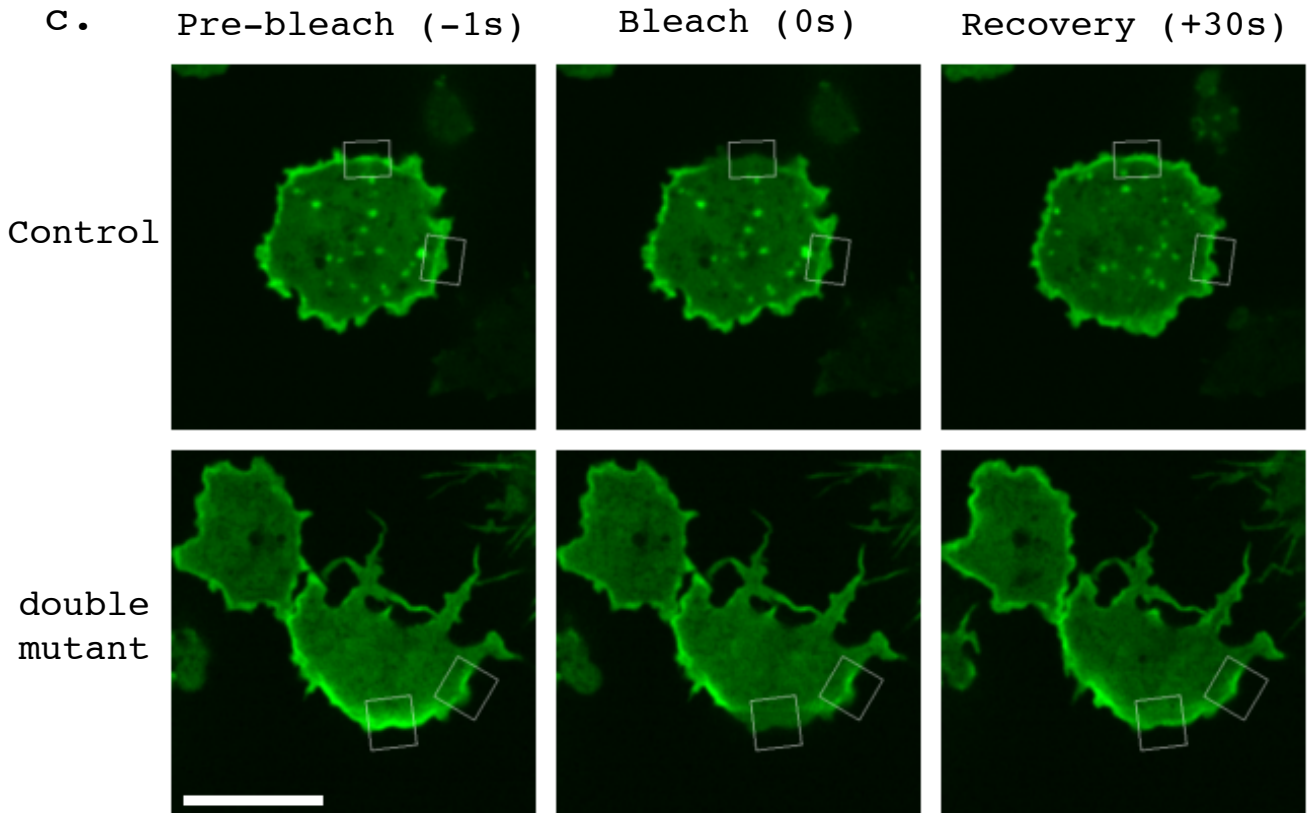
Figure 5.9, The double *scr*A/*was*A mutant possesses a dynamic actin cortex (continued): GFP-actin was expressed in control and double mutant cells and the turnover of the actin cortex was visualised by FRAP and spinning disc confocal microscopy. **c) The actin cortex of the double mutant appears to recover normally after photobleach of a region of cortical GFP-actin.** A sequence of images 1 second prior, during and 30 seconds after photobleach are shown for a control cell and a double mutant cell. The boxes highlight the photobleached region and an unbleached control region. Comparable recovery was observed in both cell lines after a period of 30 seconds. The scale bar represents 10 μm.

d.
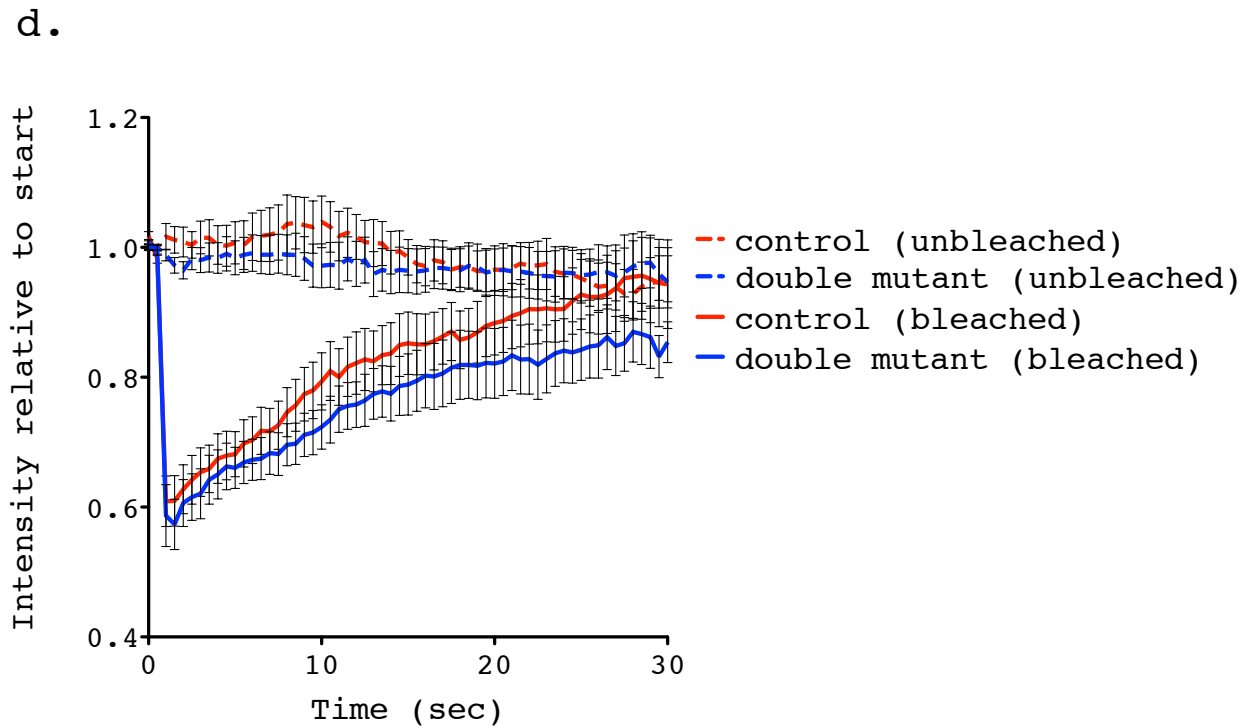
Figure 5.9, The double *scr*A/*was*A mutant possesses a dynamic actin cortex (continued): d) Quantification of FRAP data implies normal cortical actin turnover in the double mutant. FRAP was conducted on many control and double mutant cells and the average recovery was plotted as a proportion of the initial fluorescence compared to a non-bleached region (16 cells/cell line over three independent experiments). The mean cortical FRAP of the double mutant was found to be very similar to that observed in the control, implying normal cortical dynamics. The error bars represent the SEM.

Quite amazingly, latrunculin treated *Dictyostelium* can completely rebuild their cytoskeleton once the poison has been washed out (Gerisch et al., 2004). Following latrunculin A induced cytoskeleton depolymerisation, the drug was washed out and cortex reassembly was observed in control and double mutant cells. As demonstrated in figure 5.9a, control cells were able to completely reconstitute their entire actin cytoskeleton with ~20 min of latrunculin A wash out. The reformation of the cortex in the control appeared to involve the recruitment of the Arp2/3 complex to patches around the periphery of the cell. As we have shown in section 5.3, the double mutant lacks the ability to recruit the Arp2/3 complex to the cell cortex and yet it was still able to rebuild its actin cortex within ~20 min of latrunculin wash out (figure 5.9b). These results implied that not only did the double mutant possess a robust actin cortex, but it also possessed a dynamic cortex that was even capable of completely reconstituting itself following its dissolution by latrunculin A.

Although the actin cortex of the double mutant appeared to behave normally, even minuscule changes in the rate of cortical actin turnover could have severe implications for the whole cytoskeleton. To quantify the rate of cortical actin turnover, fluorescence recovery after photobleaching (FRAP) was performed on the cortex of the unstimulated, vegetative control and double mutant cells expressing GFP-actin. A similar approach was previously used to measure cortical actin turnover in *Dictyostelium,* except the actin cortex was indirectly visualised through the use of a fluorescently tagged actin-binding domain (Yumura et al., 2013). Due to the inherent motility of *Dictyostelium*, we were forced to target round, overtly spread, non-motile control cells. Indeed, the motility of the control cells was such that they often visibly flinched in response to the laser used during the photobleach. In contrast, the double mutant was far easier to perform FRAP on due to its extremely low motility. The cells were visualised by spinning disc confocal microscopy before, during and after a small region of the actin cortex was photobleached. The rate of fluorescence recovery of the cortex within this region and in an unbleached control region was measured. As seen in the examples shown in figure 5.9c and Movie 8, recovery of the actin cortex in the double mutant appeared normal when compared to the control. Figure 5.9d shows the average recovery after photobleaching compared to the unbleached regions for both the control and the double mutant (16 cells/cell line over 3 independent experiments). Although a small difference in recovery between the control and the double mutant was suggested by the graph shown in figure 5.9d, this was unlikely to

be significant as suggested by the overlapping error bars (SEM). Unfortunately, due to the large variation in recovery time and in the profile of the individual recovery curves, it has not yet been possible to obtain meaningful $t_{1/2}$ values. This is likely due to the inherent high motility of *Dictyostelium* and the fact that they were visibly responding to the laser during the photobleach. This complicated the interpretation of these data. However, it was evident from this experiment that the double mutant possessed a dynamic actin cortex that was at least visually indistinguishable from that of the contro cells. Combined with the quantitative phalloidin staining and the latrunculin A recovery experiments, it is evident that the double mutant retained a robust actin cortex, despite the loss of both SCAR and WASP A.

5.10 Blebbing can be induced in the double *scr*A/*was*A mutant

In the previous three sections, it has been demonstrated that the double mutant retains functional actomyosin-based contractility, has normal levels of F-actin and has a dynamic actin cortex. Therefore, why the double mutant was unable to form blebs to support cell migration remained an open question. As we have demonstrated in figure 5.6, high compression favours bleb formation during cell migration. As discussed in section 5.6, the double mutant was unable to enter the under-agarose folate chemotaxis assay when optimised to promote bleb-based migration. However, we have successfully been able to induce blebbing in the double mutant by compressing the cells under a slab of agarose. Using a technique our lab had previously established, severe compression (~1kPa) was achieved by placing a weight on top of the agarose slab (King et al., 2011). Co-expression of Lifeact-mRFP and GFP-ArpC4 in the double mutant allowed the response of the cytoskeleton to severe compression to be visualised using spinning disc confocal microscopy.
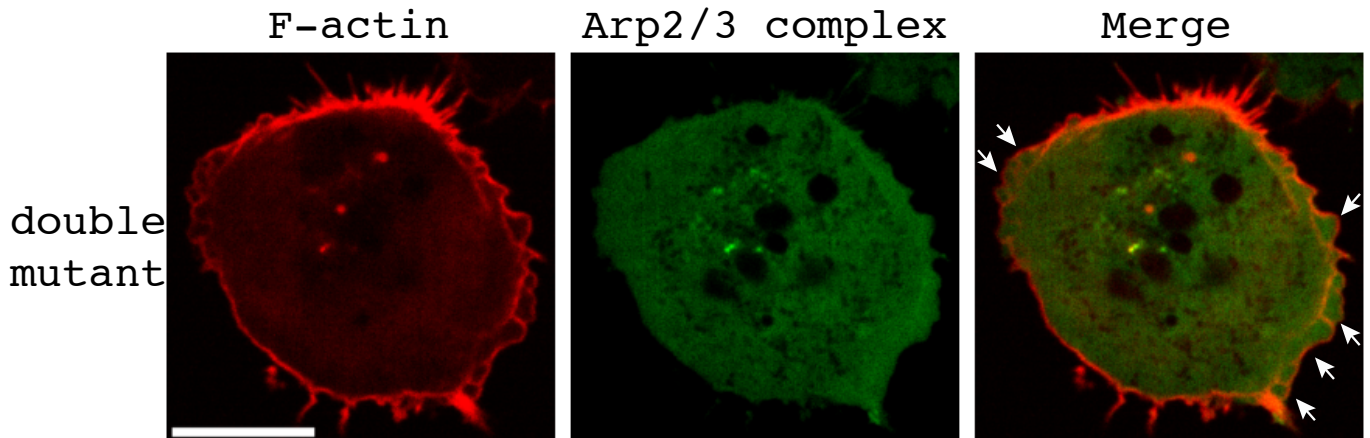
Figure 5.10, The double mutant is capable of bleb formation when severely compressed: Lifeact-RFP (F-actin) and a GFP-ArpC4 (Arp2/3 complex) were co-expressed in the double mutant. Robust bleb formation was observed by spinning disc confocal microscopy when the double mutant was severely compressed under agarose (~1 kPa). The arrows highlight prominent clusters of blebs. The scale bar represents 10 μm.

As the preliminary data shown in figure 5.10 and Movie 9 demonstrates, the double mutant was capable of forming normal looking blebs under conditions of severe compression (observed in 2 independent experiments). This observation awaits further verification and direct comparison with control, *scr*A mutant and *was*A mutant cells. However, when combined with the findings discussed in this section, it strongly suggests that the double mutant has no defect in physically forming blebs. Instead, in the absence of both SCAR and WASP A, the double mutant appears unable to induce and utilise blebbing to drive cell migration, rendering the double mutant essentially immobile in the absence of SCAR or WASP A driven pseudopodia.

5.11 Chapter 5 summary

In this chapter, the creation and characterisation of an inducible double *scr*A/*was*A mutant was described. SCAR and WASP A possibly function redundantly to support macropinocytosis, although this is yet to be confirmed. However, it was clear that the presence of at least one of SCAR or WASP A is vital for cell growth.

It was demonstrated that WASP A alone is responsible for the residual pseudopodia observed in the *scr*A null cells as the double mutant had severely impaired pseudopod formation. This defect was due to the inability of the double mutant to recruit the Arp2/3 complex to the cell cortex to promote the actin polymerisation that underlies pseudopod extension.

Unexpectedly, the double mutant also had a defect in Arp2/3 complex independent bleb formation. This left the double mutant with a near complete block in cell motility.

The possible underlying causes of this inability to migrate through the use of blebs were investigated and it was concluded that the double mutant possessed robust actomyosin contractility, normal F-actin levels and a dynamic cortex. Finally, it appeared that normal blebbing could be induced in the double mutant under conditions of severe compression. This implied the double mutant retained the ability to form blebs, but was not able to induce them to support bleb-based migration. Much work now remains to address why an inability to recruit the Arp2/3 complex to the cortex blocks all bleb- as well as pseudopod-based migration in *Dictyostelium*.

Chapter 6

Discussion

6.1 Abi is not required for pseudopod formation

Abi is considered a key component of the SCAR complex. It is thought to control complex activation by acting as a target for phosphorylation and through its interaction with various regulatory proteins such as receptor tyrosine kinases (Lebensohn & Kirschner, 2009, Leng et al., 2005). However, here we have deleted the majority of the Abi sequence, including all the conserved phosphorylation sites identified, and still observed robust localisation of the SCAR complex at the leading edge of migrating cells. The loss of Abi in its entirety results in a loss of complex integrity. Therefore, we were unable to exclude the possibility that the remaining alpha-helix that is essential for complex stability is also involved in SCAR complex activation. However, structural considerations suggest this is unlikely as the minimal Abi fragment that still stabilises the complex consists of little more than a single alpha-helix that incorporates Abi into the complex. Furthermore, based on the model that emerged from the resolution of the crystal structure, this helix would be oriented away from the plasma membrane where activation is presumed to take place. Most surprisingly, deletion of the entire C-terminal poly-proline tail of Abi, which accounts for almost half of the entire sequence, yielded no detectable phenotype.

Beyond its requirement for SCAR complex stability, it is proposed here that role of Abi is to modulate the activity of the SCAR complex and act as a signal integrator. Due to the subtlety of its influence, neither termini of Abi is required for pseudopod formation or cell migration. However, this does not imply that Abi has no role in cell motility.

There exists strong conservation between the *Dictyostelium* SCAR complex members and those found in higher eukaryotes, both in terms of sequence and function. However, in higher eukaryotes Abi is evidently more complicated, possessing a C-terminal SH3 domain and interactors not present in *Dictyostelium* (e.g. its namesake ABL). These presumably accommodate the increasingly complex layers of regulation required to control SCAR activity in multicellular organisms. As a modulator of SCAR complex activity, Abi would appear to be a natural target through which to exert these additional layers of regulation. It is proposed here that Abi is unlikely to directly mediate either SCAR complex recruitment to the membrane or activation in any cell types, including higher eukaryotes. Instead it most likely tunes the activity of the SCAR complex during or after activation.

6.2 Abi modulates SCAR complex activity during cytokinesis

Dictyostelium possesses multiple robust mechanisms to ensure successful cell division. These include the formation of a cleavage furrow to pinch the cell in two (cytokinesis A). This is coupled to adhesion dependent directed migration that acts to drive the newly forming daughter cells apart (cytokinesis B). These two modes of cytokinesis almost certainly work together in concert to ensure efficient cell division, however they are also sufficient to compensate in the absence of one or the other. As a final safeguard, multinucleate cells on a substratum can randomly tear themselves apart independently of mitosis by traction-mediated cytofission (cytokinesis C). Our lab has previously shown that these two adhesion-dependent means of cell division require the SCAR complex (King et al., 2010). The *scr*A null itself has a low level of multinuclearity as myosin-II is sufficient to drive efficient cell division through cytokinesis A. The fact that the *abi*A null becomes multinucleate has been attributed to a misregulation or mislocalisation of its residual SCAR protein with the resulting aberrant activity disrupting cell division even in the presence of a substratum. Despite restoring SCAR to wild-type levels, we only aggravated the cytokinesis defect in the absence of the N-terminal α1 helix of Abi. This supported our lab's previous conclusions that the aberrant regulation of the SCAR complex during cytokinesis in the absence of Abi that impairs normal cell division.

It is notable that the multinucleate phenotype documented here is not strong compared with other *Dictyostelium* mutants with defects in cytokinesis, such as the *was*A null. Given that the cells were cultured for ten divisions, the vast majority of even the most severely affected ΔNt Abi or ΔAbiΔ expressing cells were no more than binucleate. This is well below what the particularly robust *Dictyostelium* can tolerate and possibly explains why ΔNt Abi confers no significant adverse effect on growth despite its increased multinuclearity. By stabilising the SCAR complex with the N-terminally truncated Abi proteins, it was also likely that traction-mediated cytofission/cytokinesis C was restored, which would counteract any specific defect in cytokinesis.

It is possible that the N-terminus of Abi could have a direct role in modulating SCAR complex activity during cytokinesis. CDK1 mediated phosphorylation of mammalian

Abi1 has previously been associated with regulating the SCAR complex during mitosis (Zhuang et al., 2011). However, the conserved phosphorylation site identified lies within the C-terminal tail of Abi, which was deleted here and yielded no phenotype. Alternatively, the N-terminus could act to dampen the activity of the SCAR complex in general. During cytokinesis, the SCAR complex appears to be hyper-activated as part of its role in cytokinesis B (King et al., 2010). In such circumstances the small imbalance in activity conferred by the absence of the α1 helix of Abi would have greatest effect and could possibly accumulate to ultimately contest and disrupt normal cell division. As to how exactly the α1 helix of Abi regulates SCAR complex activity and what it is interacting with remains unknown. Nevertheless, this work has identified one regulatory role of Abi within what still remains a mostly impenetrable complex.

6.3 WASP A is not required for normal pseudopod formation

Until now, the only group to claim success in creating a *Dictyostelium was*A null had used it to show that WASP A was essential for viability and actin-driven cell migration (Myers et al., 2005). However, our lab has long maintained that it is SCAR and not WASP A that underlies *Dictyostelium* motility and recently demonstrated WASP A recruitment to CCPs rather than to the tips of growing pseudopodia in wild-type cells (Veltman et al., 2012). These data were consistent with what has been shown in yeast and human cell lines (Naqvi et al., 1998, Merrifield et al., 2004), however without a *was*A knockout, it was not possible to exclude the possibility that WASP A does somehow contribute to normal pseudopod-based migration.

Here a total of four independent, viable *was*A knock out cell lines have been generated (WIKO, *was*A null, *was*A null; GFP-PCNA and the inducible double mutant). These were used to demonstrate that WASP A is not required for normal pseudopod extension or robust chemotaxis in *Dictyostelium*. Importantly, it was confirmed that the *was*A null had an identical rate of pseudopod formation when compared to wild-type cells. Because these results fundamentally contradict the work of Myers et al., (2005), some time shall be devoted to exploring the possible reasons underlying this discrepancy. Firstly, the inducible *was*A knock out created by Myers *et al.* was generated in the Ax2 parental background compared to Ax3 background

used here. It is known that these strains possess distinct large genomic duplications and it is possible that genetic differences underlie the variation in phenotype observed between these different *was*A knockouts (Bloomfield et al., 2008). Furthermore, some Ax2 but not Ax3 strains have been shown to possess a large duplication that covers the *was*A locus on chromosome 6. Consistent with this, Myers *et al.* encountered a duplication of *was*A, which further complicated the genetics involved in the creation of their inducible knockout. They also did not have the anti-WASP A antibody at their disposal, meaning their knock out was verified by Northern blot. Although they demonstrated a reduction in mRNA when *was*A expression was suppressed in their inducible knockout, this did not conclusively prove that they had successful reduced WASP A protein level. In all, based on the data presented in their paper, we had genuine concerns about the validity of the *was*A knock out they had created.

Developmental defects were evident in the both the *was*A knockouts generated here and the mutant created by Myers *et al*. Therefore, chemotaxis was studied in vegetative rather than starved cells in contrast to Myers *et al*. Although Myers *et al.* observed a less severe developmental defect in their *was*A knock out than was documented here, it remains possible that impaired development rather than a specific problem in cell motility was responsible for the phenotype observed in their study.

Finally, the *was*A mutant created by Myers *et al.* was an inducible null, which would inevitably always possess some residual WASP A expression. We generated both an inducible *was*A knock out and several absolute knock outs where all WASP A expression was abolished. This allowed us to demonstrate conclusively that the WASP A is not required for pseudopod formation.

6.4 WASP A is required for clathrin-mediated endocytosis in *Dictyostelium*

Having established that WASP A was not required for pseudopod-based migration, the consequence of losing WASP A for CME was investigated. Whether or not WASP A promoted actin polymerisation is required for CME remains a matter of debate. It has been shown that the yeast homolog of WASP A, Las17p, is essential for its CME. Mammalian N-WASP also colocalises with CCPs in human cell lines and its arrival coincides with Arp2/3 complex recruitment and subsequent vesicle internalisation (Merrifield et al., 2004). However, N-WASP deficient fibroblasts

isolated from a N-WASP knock out mouse were found to have little defect in CME (Benesch et al., 2005). This was in part explained by some as yet unidentified redundancy, which recruited the Arp2/3 complex to CCPs in the absence of N-WASP. Nonetheless, CME in the absence of all discernable actin polymerisation was also clearly evident, calling into question the role of WASPs and actin in this process.

It was found here that the *Dictyostelium was*A null has a severe defect in CME due to the impaired recruitment of the Arp2/3 complex to CCPs. As observed in the mammalian N-WASP knock out cells, the *Dictyostelium was*A null has not completely lost the ability to recruit the Arp2/3 complex to CCPs in the absence of WASP A. Consistent with what was shown in the mammalian N-WASP knockout cells, this residual recruitment was not due to SCAR. Our lab has previously shown that the *Dictyostelium* specific WASP B and C also colocalise with CCPs (Veltman & Insall, 2010) and it was found that overexpression of WASP B and C could rescue different aspects of the *was*A null phenotype such as growth in shaking culture. Taken together, this suggested that WASP B and C accounted for the residual recruitment of the Arp2/3 complex to CCPs in the *was*A null. It was also another proof of the compensatory mechanisms that exists between the different WASP family members, such as has been shown between SCAR and WASP A in *Dictyostelium* pseudopod formation (Veltman & Insall, 2010). However, endogenous WASP B and C were evidently insufficient to fully compensate for WASP A. Even the few CCPs that were able to recruit the Arp2/3 complex exhibited aberrant endocytosis, sometimes requiring multiple bouts of Arp2/3 complex recruitment to eventually drive internalisation.

From these data it was concluded that WASP A and actin polymerisation are required for CME in *Dictyostelium*. This implies that, like yeast, the CME of *Dictyostelium* differs from that of mammalian cell lines, where it was found that actin has a supportive rather than an essential role. However, recent results suggest that N-WASP and actin may have a more important role to play in mammalian CME than first suggested. In an elegant study, Boulant et al., (2011) demonstrated that although actin was not required for CME in mammalian cell lines grown in standard tissue culture conditions, it became essential if the cells were introduced to conditions that increased membrane tension. It is speculated here that, compared to cells grown on a 2D surface during tissue culture, cells compacted into a 3D tissue would be under much higher membrane tension. Under such conditions, actin polymerisation would become vital

to provide the force to drive membrane deformation and promote vesicle internalisation.

Here, it was found that WASP A induced actin polymerisation during CME was essential for promoting vesicle internalisation. The robustness of the *was*A null and *Dictyostelium* in general granted us an opportunity to investigate the contribution of CME to cellular behaviours such as cytokinesis and cell migration.

6.5 WASP A is required for efficient cytokinesis

Although it was established that WASP A was not required for normal growth on Petri dishes, the *was*A null was found to have a cytokinesis defect that prevented its growth in shaking culture. The inability to divide specifically in suspension is a well-documented phenotype observed in many different *Dictyostelium* mutants, such as the *mhc*A null and the *chc*A null (De Lozanne & Spudich, 1987, Niswonger & O'Halloran, 1997). Such mutants have a defect in cleavage furrow ingression (or cytokinesis A), which can only be overcome in the presence of a substratum by allowing the daughter cells to physically pull themselves apart (cytokinesis B). Consistent with this, the cleavage furrow of the *was*A null often bulged during early ingression, ultimately impairing final abscission.

Having shown that the wasA null has a severe defect in CME, CCP dynamics were investigated in dividing wild-type and *was*A null cells. In contrast to what has been shown in mammalian cell lines, there was no pause in CME during wild-type *Dictyostelium* mitosis, nor was CME confined or enriched in any distinct region within the cell during cytokinesis (Fielding, Willox, Okeke, & Royle, 2012, Schweitzer, Burke, Goodson, & D'Souza-Schorey, 2005). As has been previously shown in *Dictyostelium*, clathrin puncta were found in the cleavage furrow during cytokinesis (Damer & O'Halloran, 2000). Here, CME was observed within the cleavage furrow until very late in cytokinesis. However, there was no indication that CME was coordinated with ingression and instead occurred randomly throughout the cell, throughout cytokinesis. Instead we found that CCPs accumulated in the cleavage furrow of the dividing *was*A null. As ingression progressed, the trapped CCPs were forced together into a smaller and smaller space until the cleavage furrow bulged outwards. At this point it was concluded that this aggregation of CCPs within the

cleavage furrow of the *was*A null impaired final abscission by physically clogging the cytoplasmic bridge between the dividing daughter cells.

Importantly, the *Dictyostelium chc*A null has an identical cleavage furrow defect to the *was*A null, despite not possessing any CCPs. Adaptor proteins, the role of which is to cluster transmembrane proteins and recruit clathrin to form CCPs, still form puncta in the *chc*A null (Macro, Jaiswal, & Simon, 2012). Therefore, we proposed that this defect was not specifically caused by the accumulation of clathrin, but instead was a result of general protein aggregation.

CME and vesicle trafficking has already been implicated in many aspects of mitosis and cytokinesis (Schweitzer et al., 2005, Pellinen et al., 2008). However, here we propose a new, general function for CME in supporting efficient cytokinesis. We concluded that the role of WASP A is to drive the continuous recycling of protein off of the plasma membrane through CME and, in its absence, protein aggregates accumulate and inhibit processes such as cell division.

6.6 WASP A contributes indirectly to cell migration

It has been demonstrated that the *was*A null has no defect in pseudopod formation. However, it was noted that the *was*A null had a small but consistent decrease in cell speed. The reduced cell speed of the *scr*A null can be directly explained by its decreased rate of pseudopod formation. In contrast, it was found the *was*A null had a uropod retraction defect, which was proposed to increase drag during cell migration.

We had established that the *was*A null had a severe defect CME and that CCPs accumulated in the cleavage furrow of the dividing *was*A nulls and impaired abscission. We were then able to demonstrate that CCPs also accumulated in the enlarged, persistent uropod of the motile *was*A null. Transient enrichment of CCPs at the rear of motile wild-type *Dictyostelium* has been previously shown (Damer & O'Halloran, 2000). However, rather than having an active role in uropod retraction, it is proposed here that CCPs accumulate at the rear by a more passive means. During persistent cell migration, CCPs were swept backwards in the opposite direction to cell movement. In wild-type cells, WASP A was recruited to drive vesicle internalisation, preventing the prolonged accumulation of CCPs at the rear of cell. However, in the absence of WASP A, CCPs aggregated in the uropod of the *was*A null, which in turn was engorged and was dragged behind the cell during persistent migration. A similar

phenomenon was observed during cytokinesis of the *was*A null, where the CCPs were swept from the forming daughter cells into the cleavage furrow during cell division and were enriched in the bulges that formed and impeded final abscission.

It was found that the persistent uropod of the *was*A null was not simply due to the passive accumulation of protein at the rear of the cell forming a mass that impaired retraction of the tail. Instead, these aggregates of CCPs appeared to be triggering aberrant Rac activity in the uropod of the *was*A. Importantly, active Rac was not observed at CCPs in wild-type cells or the CCPs that had yet to be swept into the uropod of the *was*A null. This implied that Rac does not have a role in normal CME, but instead was possibly being activated by the prolonged aggregation of the CCPs in the uropod. Consistent with the established role of Rac in the pseudopod, the active Rac patch present at the rear of the motile *was*A null was seen to recruit SCAR to induce Arp2/3 complex mediated actin polymerisation. The resulting actin puncta were found to be dispersed throughout the uropod and not confined to the plasma membrane as observed with normal CME. It was proposed that the inappropriate actin polymerisation in the uropod of the *was*A null was causing abnormal actin/myosin-II crosslinking yielding the observed abnormal myosin-II distribution. This in turn could be responsible for locally impairing actomyosin contractility resulting in defective uropod retraction during cell translocation. A similar mechanism could be occurring in the cleavage furrow, acting to impair myosin driven furrowing.

If it is assumed that the aggregated CCPs are responsible for the Rac activity in the rear of the *was*A null, why this is occurring remains an unanswered. It is possible that the Rac activity is in response to the enlarged uropod and is acting in an attempt to promote retraction. Alternatively, the aging CCPs in the uropod could be aborting and spilling their cargo back out onto the plasma membrane. This could include transmembrane receptors that normally function to activate Rac in the pseudopodia, which are normally recycled by CME in order to restrict their localisation to the front of the cell. The model that arised from these data is shown in figure 6.1.

We concluded that WASP A indirectly contributes to efficient cell migration by preventing the aggregation of CCPs at the rear of a motile cell and so maintaining efficient uropod retraction.
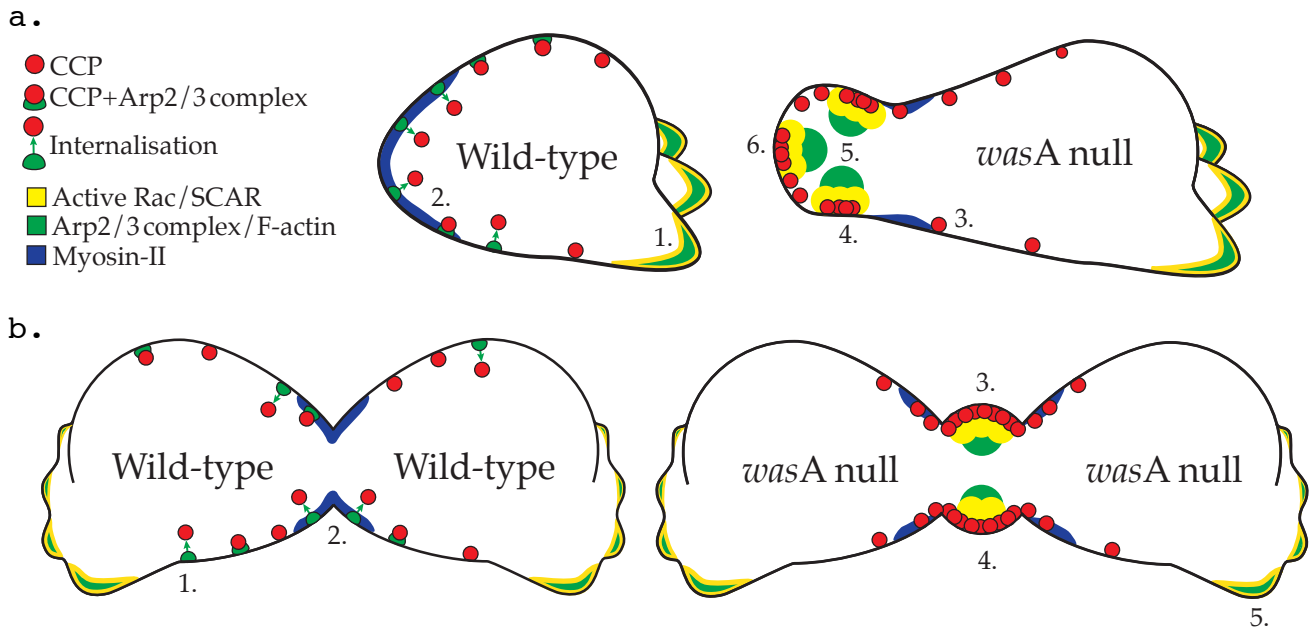
Figure 6.1, The role of WASP A in *Dictyostelium* uropod retraction and cytokinesis: a) Accumulation of CCPs in uropod of *was*A impairs actomyosin contractility. (1) In chemotaxing wild-type cells, SCAR and Rac activity are confined to the front of the cell in the pseudopodia. (2) Alternatively, WASP A is recruited to sites of CME where it promotes actin-driven vesicle internalisation. (3) However, in the *was*A null has a severe defect in CME. (4) During persistent migration, CCPs aggregate at the rear of the cell, which in turn somehow leads to the activation of Rac. (5) Active Rac recruits and activates the SCAR complex, which promotes the Arp2/3 complex to induce actin polymerisation within the uropod of the migrating cell. These actin aggregates cross-link with myosin-II, which disrupts normal actomyosin contractility and impairs coordinated retraction of the uropod during chemotaxis . (6) The enlarged, bulbous uropod of the *was*A null creates drag and impairs its migration, especially when compressed under agarose. **b) The cytokinesis defect of the *was*A null could also be caused by the disruption of actomyosin contractility during ingression.** Although not yet formally tested, it is proposed that a similar mechanism as to that described in (a) underlies the furrowing defect of the *was*A null. (1-2) WASP A supported CME prevents the aggregation of CCPs within the cleavage furrow of the *was*A null. (3-5) The aggregation of CCPs within the furrow triggers Rac activity and impairs actomyosin contractility as described in (a), causing the furrow to bulge. (6) The daughter cells are able to tear themselves apart through adhesion-dependent cytokinesis B.

6.7 SCAR and WASP A are essential for *Dictyostelium* growth

Although we had established that *was*A was not essential for *Dictyostelium* viability, it was found that at least one of SCAR or WASP A was required for growth. An inducible approach was adopted to allow growth of the mutant as a *was*A null since all growth immediately ceased upon suppression of SCAR expression to yield the double mutant. The lack of growth was of great concern, as it would have been inappropriate to study motility in dead or very sickly cells. Although all growth halted, the double mutant remained adherent for much longer than the 6 days over which growth was monitored.

Further evidence that these cells were still alive was to be found in their ability to spread when suspended and re-plated. As discussed earlier, SCAR and WASP A both contribute to different aspects of cell division. It was demonstrated in chapter 4 that WASP A is required for efficient furrowing/cytokinesis A. Our lab has previously shown that SCAR is important for driving the daughter cells apart through cytokinesis B and for tearing multinucleate cells apart during traction-mediated/cytofission cytokinesis C (chapter 3, King et al., 2010). In short, the double mutant undoubtedly possesses a cytokinesis defect and multinucleate cells would also complicate the study of motility in these cells. However, although not formally quantified, DAPI staining of the double mutant revealed low multinuclearity, at least after the 48 hours of SCAR suppression within which all experiments were conducted. This suggested that the double mutants had undergone cell cycle arrest.

SCAR and WASP A were colocalised at sites of macropinocytosis, which is the main means by which axenic *Dictyostelium* feed. Interestingly, the colocalisation of the two was only partial, with WASP A found to decorate the entire cup whereas SCAR was found only at the protruding tips. Although this is in need of further investigation, it is proposed here that SCAR and WASP A act redundantly to drive macropinocytosis and in the absence of both, the cells sense they are no longer acquiring nutrients and cease all growth. *Dictyostelium* normally enter development when deprived of nutrients, however, as shown in chapter 3, the *was*A mutation causes a complete block in development. Presumably, the double mutant persists through autophagy and perhaps low levels of macropinocytosis supported by WASP B and C.

Importantly, it was demonstrated that the double mutant retained a dynamic actin cytoskeleton that was capable of driving cell spreading and even completely

reforming itself after latrunculin A treatment. The latter in particular was considered strong proof that the double mutant was still alive. Furthermore, it was clear that the double mutant had a cytoskeleton that it could mobilise to drive various different cellular processes, which reassured us that the study of motility in these cells was valid.

6.8 WASP family members are essential for pseudopod formation

We had proven that WASP A was not required for pseudopod formation in wild-type *Dictyostelium*. However, it has been previously shown by our lab that WASP A assumes a direct role in pseudopod formation in the *scr*A null (Veltman et al., 2012). It was demonstrated here that WASP A was solely responsible for the residual pseudopodia in *scr*A null cells as the double mutant had a severe defect in pseudopod formation. It was evident that without SCAR and WASP A, cells were unable to recruit the Arp2/3 complex to the cortex to support pseudopod formation. These cells lacked the large actin meshworks that are generated by the Arp2/3 complex and underlie pseudopod extension. Instead, the double mutant possessed abundant actin-rich filopodia, which emanated from the cell in all directions. The morphology of the double mutant was strikingly reminiscent of the mammalian Arp2/3 complex knock down/knock out, which also lack pseudopodia and have excessive filopodia (Suraneni et al., 2012, Wu et al., 2012). This suggests that the inability to recruit the Arp2/3 complex to the cell cortex results in the predominance or upregulation of filopodia.

It is perhaps not surprising that WASP A can substitute for SCAR in *Dictyostelium* since, as a haploid amoeba, motility is central to its survival. However, the ability of WASP A to assume the role of SCAR and promote pseudopod formation is yet to be demonstrated in any other organism. In metastatic cancer cells, the loss of the SCAR complex enhances invasion through a 3D matrix (Tang et al., 2013). Although N-WASP was shown to be vital for this process, it is difficult to isolate the contribution of N-WASP to pseudopod formation from its important role in coordinating matrix degradation, both of which are required for invasion in a 3D environment (Yu et al., 2012).

Perhaps the most appropriate comparison is to be found in *Drosophila* macrophages, where the loss of SCAR resulted in a morphology that was strikingly similar to the *Dictyostelium* double *scr*A/*was*A mutant (Evans et al., 2013). Furthermore, the residual motility observed was found not to be dependent on WASP family members.

However, again the issue was complicated by the finding that the loss of SCAR resulted in the accumulation of engulfed apoptotic corpses in the macrophages, which impaired migration through some unknown mechanism. Motility was partially restored in these cells when apoptosis was inhibited and it is possible that this was due to WASP assuming the role of SCAR as has been demonstrated in *Dictyostelium*.

It remains to be seen whether the ability of WASP to substitute for SCAR is a general phenomenon or confined to *Dictyostelium*. However, the ability of WASP A to drive the formation of a morphologically normal pseudopod raises important questions about the role of the SCAR complex. Our lab has demonstrated that WASP A does not require any of the other SCAR complex members in order to assume the role of SCAR (Veltman et al., 2012). This finding suggests that SCAR is sufficient to promote pseudopod formation and does not require the other complex members other than for stability as was shown for SCAR complex member Abi in chapter 3. Instead, the SCAR complex likely acts to fine tune the activity of SCAR to promote optimal pseudopod formation, as implied by the reduced rate of pseudopod extension observed in the *scr*A null despite the compensatory action of WASP A.

In summary, we have demonstrated that WASP family members are essential for pseudopod-based migration.

6.9 WASP family members are required for bleb-based migration

We have established that SCAR and, in the absence of SCAR, WASP A are required for pseudopod-based migration. Surprisingly, it was found that the double mutant also had a complete defect in bleb-based migration and was therefore essentially immobile. Although WASP A compensates for the loss of SCAR, it is known that the *scr*A null supplements its motility with blebs (Ura et al., 2012, Veltman et al., 2012). Therefore, under conditions that normally favoured pseudopod-based motility, the *scr*A mutant moved through a mix of both pseudopodia and blebs. Of note was the speed with which a wild-type cell could switch from pseudopod-based migration alone to a mix of the two when SCAR expression was suppressed. This occurred after as little as 6 hours following the inhibition of SCAR expression, well before maximal SCAR suppression. This implies that the bleb-based motility was an inherent ability

of cells, consistent with the presence of blebs amongst pseudopodia during normal *Dictyostelium* chemotaxis (Yoshida & Soldati, 2006).

Based on these data, it was expected that in the absence of pseudopodia, the double mutant would have switched fully to bleb-based migration. However, the double mutant formed neither pseudopodia nor blebs, resulting in a complete loss of motility. Importantly, the inability of the double mutant to migrate through the use of blebs was not due to the loss of WASP A alone as the *was*A mutant was capable of robust bleb-based migration when pseudopodia were suppressed physically by increased compression.

Although the double mutant was capable of making abundant filopodia, it was unable to utilise this third kind of protrusion to drive cell migration. This was again reminiscent of what has been observed in the Arp2/3 complex knockdown/knockout mammalian cells (Wu et al., 2012, Suraneni et al., 2012). Despite the debate as to whether or not cells devoid of the Arp2/3 complex possess residual chemotaxis, both these studies demonstrated severely impaired motility. Although some blebs were shown to form between the numerous filopodia present in these cells, they were insufficient to promote robust cell migration.

Together, these data imply that the ability to recruit the Arp2/3 complex to the cell cortex by SCAR or WASP A is in some way required for bleb-based migration. However, when bleb-based migration was favoured by compression, no localisation of the Arp2/3 complex to the sites of bleb formation was observed. We concluded that although SCAR or WASP A are directly required for the recruitment of the Arp2/3 complex to drive pseudopod formation, they are indirectly required for bleb-based motility.

6.10 SCAR and WASP A are not required for bleb formation

WASP family members appear to be essential to induce bleb-based migration. Since the Arp2/3 complex was not recruited to the site of bleb formation, it was reasoned that the activity of the Arp2/3 complex was required at the cortex to indirectly support blebbing.

Bleb formation requires actomyosin contractility and a dynamic cortex, both of which require actin and therefore potentially the activity of Arp2/3 complex. Finally, in order to utilise blebs to drive persistent cell migration, cells must maintain contraction

at the rear in order to confine bleb formation in the one direction. Myosin-II based contractility, the actin cortex and polarity were investigated in the double mutant. It was firstly demonstrated that the double mutant possessed functional myosin and robust contractility. Surprisingly, *scr*A mutant, *was*A mutant and double mutant cells all possessed equivalent levels of F-actin to control cells. It remains possible that the ratiometric staining method adopted here to quantify F-actin levels was not sensitive enough to distinguish between the different mutants. As unstimulated, vegetative cells were used, it is also possible that differences would have been apparent if motility and pseudopod formation had been induced. However, the double mutant compensated for its lack of pseudopodia with abundant actin-rich filopodia and so normal F-actin levels are not implausible. Furthermore, the double mutant always possessed a robust actin cortex.

The cortex of the double mutant was importantly also able to completely rebuild itself following release from the actin poison, latrunculin A. This was despite the prominent recruitment of the Arp2/3 complex during the reconstitution of the cortex in control cells. It is speculated here that after latrunculin A treatment, a cell recruits every available actin regulatory protein to help reform the cortex and not specifically the Arp2/3 complex. This is consistent with the hyperactive actin dynamics previously observed in *Dictyostelium* recovering from latrunculin treatment (Gerisch et al., 2004). FRAP was also used to show that the actin cortex of the double mutant was turning over dynamically.

Finally, the double mutant was found to uniformly bleb in every direction when severely compressed. Together these data imply that the double mutant has no fundamental defect in the ability to form blebs. Instead, it appears unable to induce bleb-based migration in the absence of pseudopodia. The finding that compression rescued blebbing in the double mutant could indicate a defect in contractility, as both myosin-II and compression promote bleb formation by raising intra-cellular pressure. Since the double mutant possessed robust actomyosin contractility, it is instead possible that the double mutant has a defect in polarisation. Poor polarity would in turn prevent normal myosin-II localisation, resulting in uncoordinated contraction, and a failure to provide the unidirectional blebbing that underlies bleb-based migration. As to why the loss of SCAR and WASP A would impair polarisation, we can again only speculate. Arp2/3 complex driven pseudopod formation cannot simply be required to maintain polarity as control, *scr*A mutant and *was*A mutant cells were

all capable of supporting motility with blebs alone in conditions that strongly favoured bleb-based migration. However, even when pseudopodia were suppressed by compression, the Arp2/3 complex would still be expected to be present at the cortex through the few remaining pseudopodia and/or CME. Therefore, as illustrated in figure 6.2, it is proposed here that the activity of the Arp2/3 complex at actin cortex maintains cortical dynamism, without which the cytoskeleton stagnates. We suggest that this is at least in part due to the dominance of the filopodia in the absence of SCAR and WASP A. Since the double mutant is an inducible mutant, it was only ever induced to be a double mutant 48 hours before any given experiment. Therefore, we reason that the excessive filopodia cannot be a consequence of compensatory selection. Instead it is proposed here that the filopodia are normally held in check by the competition with the Arp2/3 complex at the cortex and in the absence of the latter, the filopodia dominate to the detriment of the cell. Support for the existence of such a contest can be found in the work from the Faix laboratory. Dumontier, Hocht, Mintert, & Faix, (2000) found that overexpression of wild-type or dominant negative Rac induced filopod formation. Alternatively, overexpression of constitutively active Rac suppressed filopodia and instead induced excessive macropinocytosis. Schirenbeck et al., (2005) demonstrated the *drf*2 (diaphanous-related formin, dDia2) null had reduced filopodia and increased motility. The opposite was found when GFP-dDia2 was overexpressed in cells, where filopodia were seen to be longer and more numerous. GFP-dDia2 overexpressing cells adopted a morphology that was similar to that observed in the double mutant and cell motility was found to be impaired. Again, excessive filopodia were observed in the Arp2/3 complex knock down/knock out mammalian cell lines,
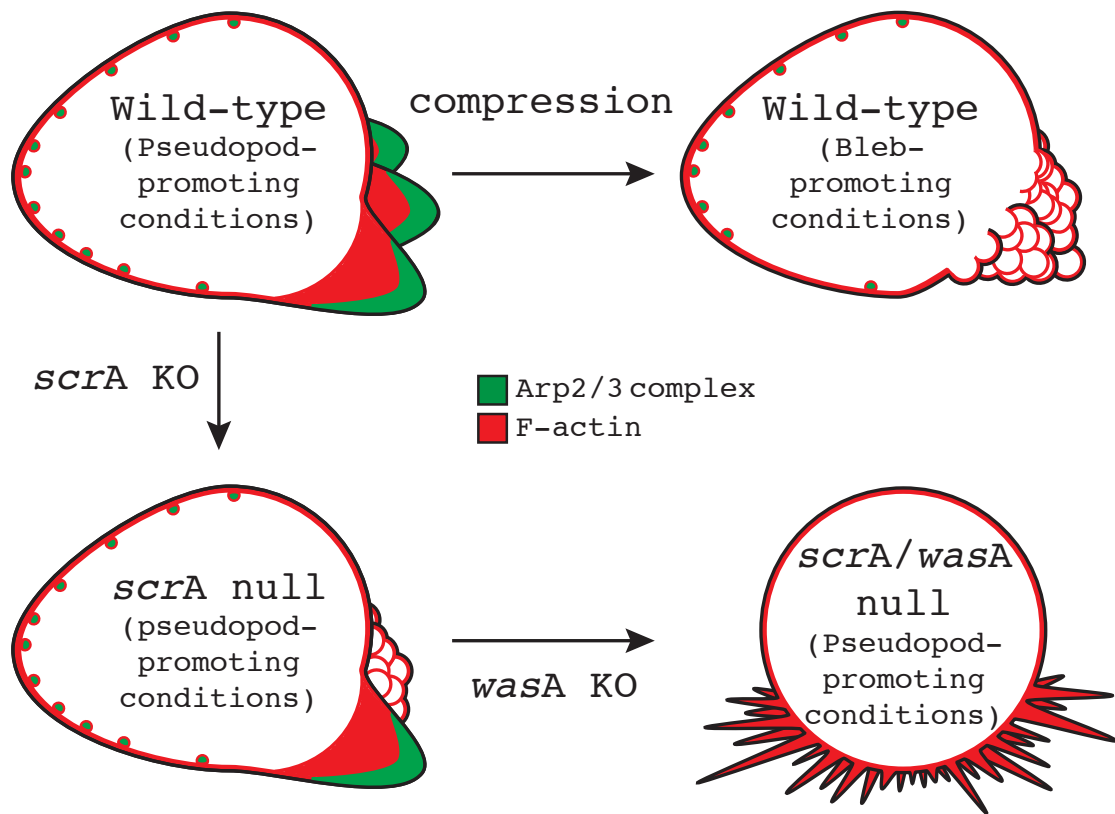
Figure 6.2, The proposed role of the Arp2/3 complex in bleb-based migration: Wild-type cells under pseudopod-promoting conditions utilise the Arp2/3 complex to generate and move through the use of pseudopodia. Cells can be promoted to move through the use of blebs either physically or genetically. Severe compression of cells suppresses pseudopod formation, resulting in a switch to bleb-based migration. Although recruitment of the Arp2/3 complex to the leading edge is suppressed under such conditions, it is also present at the cortext via CME. Alternatively, disruption of *scr*A leads to a reduced rate of pseudopod formation and a partial switch to bleb-based migration. Under such conditions, the Arp2/3 complex remains present at the cortex via CME and the residual, WASP A driven pseudopodia. However, in the double *scr*A/*was*A mutant, the Arp2/3 complex is no longer present at the cortex, resulting in the dominance of the formins and excessive filopod formation. This overwhelms the cortex, abolishes all polarity and suppresses bleb formation. The inability to induce either pseudopod or bleb formation results in the loss of all motility. Severe compression of the double mutant bursts the cortex and temporarily breaks the double mutant free from the dominance of the formins (not shown).

which had severely impaired cell motility (Wu et al., 2012, Suraneni et al., 2012). This also appears to be true of blebs, with increased blebbing observed when the activity of the Arp2/3 complex is partially inhibited through the expression of mutant Arp2/3 complex in *Dictyostelium*, following the loss of *scr*A or through cell compression (Langridge & Kay, 2006, Veltman et al., 2012). From these data, it appears that the distinct mechanisms underlying the formation of these different protrusions are primed such that if one is perturbed, the others immediately fill the void. This could be advantageous for motile cells in general by conferring them the ability to instantly switch between different modes of migration in the event one type of migration fails. For instance, it has been shown here that *Dictyostelium* are capable of switching to bleb-based migration under conditions of severe compression. In the case of the double *scr*A/*was*A mutant, we hypothesise that the Arp2/3 complex and formins such as dDia2 are in dynamic competition with one another and if the activity of one is inhibited, the other predominates. In the absence of SCAR and WASP A, unrestrained filopod formation possibly overburdens the cytoskeleton and traps it in an unpolarised state that inhibits bleb formation and cell migration in general.

6.11 Final summary

Here the role of WASP family members in different modes of migration was investigated. It was demonstrated that SCAR complex member Abi is required for complex stability, but not for recruitment or activation during pseudopod-based migration. Instead, it was concluded Abi acts as a modulator of SCAR activity during processes such as cytokinesis. The absence of a central role for Abi with the SCAR complex contradicts much of the current literature, but is consistent with our lab's recent finding that the SCAR complex is dispensable for pseudopod formation. This work showed that WASP A can assume the role of the entire SCAR complex and implies that the complex members have a subtler role in regulating SCAR activity.

Here a *Dictyostelium was*A null was generated and used to demonstrate that WASP A does not contribute to wild-type pseudopod formation in *Dictyostelium*, despite what has been previously published. However, it was found that the *was*A null had a defect in uropod retraction that slowed its migration. It was also found to have problems in cleavage furrow ingression, resulting in impaired cytokinesis. Consistent with what

has been shown in yeast and mammalian cell lines, we established that the *was*A null had a severe defect in clathrin-mediated endocytosis. Clathrin-coated pits were found to accumulate on the plasma membrane of the *was*A null and aggregated in the cleavage furrow and the uropod during cell migration. In the case of the latter, this was demonstrated to induce aberrant Rac activity in the rear of the cell, which in turn recruited SCAR to drive inappropriate actin polymerisation. It was proposed that this resulted in disorganised myosin-II distribution within the uropod and uncoorodinated retraction. Thus, in wild-type cells it was demonstrated that WASP A had an indirect role in supporting cell motility.

However, as discussed above, WASP A localises to pseudopodia in the *scr*A null and therefore appears to assume a direct role in cell migration. A double *scr*A/*was*A mutant was created and was used to confirm that WASP A alone was responsible for the residual pseudopodia in *scr*A null cells. We concluded that SCAR or, in the absence of SCAR, WASP A are essential for pseudopod-based migration.

Unexpectedly, it was found that one of SCAR or WASP A was also essential for bleb-based migration, leaving the double mutant essentially immobile. Since the Arp2/3 complex was not recruited to sites of bleb formation, it was at first hypothesised that the activity of the Arp2/3 complex was required to support conditions for blebbing. However, it was demonstrated that the double mutant possessed normal actomyosin contractility, robust cortical actin dynamics and appeared to be capable of blebbing under conditions of severe compression. Much work remains to determine the role of WASP family members in bleb-based migration. However, it was speculated that in the absence of the Arp2/3 complex at the cortex, filopodia dominate and trap the cell in an immobile state. If true, this would suggest that the different modes of migration are ultimately a product of competing actin regulatory pathways.

Biblography

Aghamohammadzadeh, S., & Ayscough, K. R. (2009). Differential requirements for actin during yeast and mammalian endocytosis. Nat Cell Biol*, 11(8), 1039-1042.*

Alberts, A. S. (2001). Identification of a carboxyl-terminal diaphanous-related formin homology protein autoregulatory domain. J Biol Chem*, 276(4), 2824-2830.*

Allen, W. E., Jones, G. E., Pollard, J. W., & Ridley, A. J. (1997). Rho, Rac and Cdc42 regulate actin organization and cell adhesion in macrophages. J Cell Sci*, 110(Pt 6), 707-720.*

Amann, K. J., & Pollard, T. D. (2001). Direct real-time observation of actin filament branching mediated by Arp2/3 complex using total internal reflection fluorescence microscopy. Proc Natl Acad Sci U S A*, 98(26), 15009-15013.*

Andrew, N., & Insall, R. H. (2007). Chemotaxis in shallow gradients is mediated independently of PtdIns 3-kinase by biased choices between random protrusions. Nat Cell Biol*, 9(2), 193-200.*

Ayscough, K. R., Stryker, J., Pokala, N., Sanders, M., Crews, P., & Drubin, D. G. (1997). High rates of actin filament turnover in budding yeast and roles for actin in establishment and maintenance of cell polarity revealed using the actin inhibitor latrunculin-A. J Cell Biol*, 137(2), 399-416.*

Barkley, D. S. (1969). Adenosine-3',5'-phosphate: identification as acrasin in a species of cellular slime mold. Science*, 165(3898), 1133-1134.*

Bartles, J. R. (2000). Parallel actin bundles and their multiple actin-bundling proteins. Curr Opin Cell Biol*, 12(1), 72-78.*

Bartles, J. R., Zheng, L., Li, A., Wierda, A., & Chen, B. (1998). Small espin: a third actin-bundling protein and potential forked protein ortholog in brush border microvilli. J Cell Biol*, 143(1), 107-119.*

Begg, D. A., Rodewald, R., & Rebhun, L. I. (1978). The visualization of actin filament polarity in thin sections. Evidence for the uniform polarity of membrane-associated filaments. J Cell Biol*, 79(3), 846-852.*

Benesch, S., Polo, S., Lai, F. P., Anderson, K. I., Stradal, T. E., Wehland, J. et al. (2005). N-WASP deficiency impairs EGF internalization and actin assembly at clathrin-coated pits. J Cell Sci, 118*(Pt 14), 3103-3115.*

Bloomfield, G., Skelton, J., Ivens, A., Tanaka, Y., & Kay, R. R. (2010). Sex determination in the social amoeba Dictyostelium discoideum. Science, 330*(6010), 1533-1536.*

Bloomfield, G., Tanaka, Y., Skelton, J., Ivens, A., & Kay, R. R. (2008). Widespread duplications in the genomes of laboratory stocks of Dictyostelium discoideum. Genome Biol, 9*(4), R75.*

Boulant, S., Kural, C., Zeeh, J. C., Ubelmann, F., & Kirchhausen, T. (2011). Actin dynamics counteract membrane tension during clathrin-mediated endocytosis. Nat Cell Biol, 13*(9), 1124-1131.*

Brady, R. J., Damer, C. K., Heuser, J. E., & O'Halloran, T. J. (2010). Regulation of Hip1r by epsin controls the temporal and spatial coupling of actin filaments to clathrin-coated pits. J Cell Sci, 123*(Pt 21), 3652-3661.*

Bukharova, T., Weijer, G., Bosgraaf, L., Dormann, D., van Haastert, P. J., & Weijer, C. J. (2005). Paxillin is required for cell-substrate adhesion, cell sorting and slug migration during Dictyostelium development. J Cell Sci, 118*(Pt 18), 4295-4310.*

Campellone, K. G., Webb, N. J., Znameroski, E. A., & Welch, M. D. (2008). WHAMM is an Arp2/3 complex activator that binds microtubules and functions in ER to Golgi transport. Cell, 134*(1), 148-161.*

Campellone, K. G., & Welch, M. D. (2010). A nucleator arms race: cellular control of actin assembly. Nat Rev Mol Cell Biol, 11*(4), 237-251.*

Cant, K., Knowles, B. A., Mooseker, M. S., & Cooley, L. (1994). Drosophila singed, a fascin homolog, is required for actin bundle formation during oogenesis and bristle extension. J Cell Biol, 125*(2), 369-380.*

Caracino, J., Compton & Saxe. (2007). 'The N-terminus of Dictyostelium Scar interacts with Abi and HSPC300 and is essential for proper regulation and function.'. Mol Biol Cell, 18, *1609-1620.*

Carlier, M. F., Laurent, V., Santolini, J., Melki, R., Didry, D., Xia, G. X. et al. (1997). Actin depolymerizing factor (ADF/cofilin) enhances the rate of filament turnover: implication in actin-based motility. J Cell Biol*, 136(6), 1307-1322.*

Carlier, M. F., & Pantaloni, D. (1986). Direct evidence for ADP-Pi-F-actin as the major intermediate in ATP-actin polymerization. Rate of dissociation of Pi from actin filaments. Biochemistry*, 25(24), 7789-7792.*

Carlier, M. F., Pantaloni, D., Evans, J. A., Lambooy, P. K., Korn, E. D., & Webb, M. R. (1988). The hydrolysis of ATP that accompanies actin polymerization is essentially irreversible. FEBS Lett*, 235(1-2), 211-214.*

Carnell, M., Zech, T., Calaminus, S. D., Ura, S., Hagedorn, M., Johnston, S. A. et al. (2011). Actin polymerization driven by WASH causes V-ATPase retrieval and vesicle neutralization before exocytosis. J Cell Biol*, 193(5), 831-839.*

Casella, J. F., Maack, D. J., & Lin, S. (1986). Purification and initial characterization of a protein from skeletal muscle that caps the barbed ends of actin filaments. J Biol Chem*, 261(23), 10915-10921.*

Castrillon, D. H., & Wasserman, S. A. (1994). Diaphanous is required for cytokinesis in Drosophila and shares domains of similarity with the products of the limb deformity gene. Development*, 120(12), 3367-3377.*

Chan, C., Beltzner, C. C., & Pollard, T. D. (2009). Cofilin dissociates Arp2/3 complex and branches from actin filaments. Curr Biol*, 19(7), 537-545.*

Charras, G. T., Hu, C. K., Coughlin, M., & Mitchison, T. J. (2006). Reassembly of contractile actin cortex in cell blebs. J Cell Biol*, 175(3), 477-490.*

Charras, G. T., Yarrow, J. C., Horton, M. A., Mahadevan, L., & Mitchison, T. J. (2005). Non-equilibration of hydrostatic pressure in blebbing cells. Nature*, 435(7040), 365-369.*

Chen, Z., Borek, D., Padrick, S. B., Gomez, T. S., Metlagel, Z., Ismail, A. M. et al. (2010). Structure and control of the actin regulatory WAVE complex. Nature*, 468(7323), 533-538.*

Co, C., Wong, D. T., Gierke, S., Chang, V., & Taunton, J. (2007). *Mechanism of actin network attachment to moving membranes: barbed end capture by N-WASP WH2 domains.* Cell, 128*(5), 901-913.*

Collins, A., Warrington, A., Taylor, K. A., & Svitkina, T. (2011). *Structural organization of the actin cytoskeleton at sites of clathrin-mediated endocytosis.* Curr Biol, 21*(14), 1167-1175.*

Cox, E. C., Vocke, C. D., Walter, S., Gregg, K. Y., & Bain, E. S. (1990). *Electrophoretic karyotype for Dictyostelium discoideum.* Proc Natl Acad Sci U S A, 87*(21), 8247-8251.*

Damer, C. K., & O'Halloran, T. J. (2000). *Spatially regulated recruitment of clathrin to the plasma membrane during capping and cell translocation.* Mol Biol Cell, 11*(6), 2151-2159.*

Davidson, A. J., & Insall, R. H. (2011). *Actin-based motility: WAVE regulatory complex structure reopens old SCARs.* Curr Biol, 21*(2), R66-8.*

De La Cruz, E. M., & Ostap, E. M. (2004). *Relating biochemistry and function in the myosin superfamily.* Curr Opin Cell Biol, 16*(1), 61-67.*

De Lozanne, A., & Spudich, J. A. (1987). *Disruption of the Dictyostelium myosin heavy chain gene by homologous recombination.* Science, 236*(4805), 1086-1091.*

DeLozanne, A., Lewis, M., Spudich, J. A., & Leinwand, L. A. (1985). *Cloning and characterization of a nonmuscle myosin heavy chain cDNA.* Proc Natl Acad Sci U S A, 82*(20), 6807-6810.*

Derivery, E., Sousa, C., Gautier, J. J., Lombard, B., Loew, D., & Gautreau, A. (2009). *The Arp2/3 activator WASH controls the fission of endosomes through a large multiprotein complex.* Dev Cell, 17*(5), 712-723.*

Derry, J. M., Ochs, H. D., & Francke, U. (1994). *Isolation of a novel gene mutated in Wiskott-Aldrich syndrome.* Cell, 79*(5), following 922.*

Devreotes, P. N., & Zigmond, S. H. (1988). *Chemotaxis in eukaryotic cells: a focus on leukocytes and Dictyostelium.* Annu Rev Cell Biol, 4*, 649-686.*

Dinauer, M. C., MacKay, S. A., & Devreotes, P. N. (1980). *Cyclic 3',5'-AMP relay in Dictyostelium discoideum III. The relationship of cAMP synthesis and secretion during the cAMP signaling response.* J Cell Biol, *86(2), 537-544.*

Dumontier, M., Hocht, P., Mintert, U., & Faix, J. (2000). *Rac1 GTPases control filopodia formation, cell motility, endocytosis, cytokinesis and development in Dictyostelium.* J Cell Sci, 113(*Pt 12), 2253-2265.*

Eden, S., Rohatgi, R., Podtelejnikov, A. V., Mann, M., & Kirschner, M. W. (2002). *Mechanism of regulation of WAVE1-induced actin nucleation by Rac1 and Nck.* Nature, 418*(6899), 790-793.*

Edwards, R. A., Herrera-Sosa, H., Otto, J., & Bryan, J. (1995). *Cloning and expression of a murine fascin homolog from mouse brain.* J Biol Chem, 270*(18), 10764-10770.*

Egelhoff, T. T., Lee, R. J., & Spudich, J. A. (1993). *Dictyostelium myosin heavy chain phosphorylation sites regulate myosin filament assembly and localization in vivo.* Cell, 75*(2), 363-371.*

Eichinger, L., Pachebat, J. A., Glockner, G., Rajandream, M. A., Sucgang, R., Berriman, M. et al. (2005). *The genome of the social amoeba Dictyostelium discoideum.* Nature, 435*(7038), 43-57.*

Evans, I. R., Ghai, P. A., Urbancic, V., Tan, K. L., & Wood, W. (2013). *SCAR/WAVE-mediated processing of engulfed apoptotic corpses is essential for effective macrophage migration in Drosophila.* Cell Death Differ, 20*(5), 709-720.*

Ezratty, E. J., Bertaux, C., Marcantonio, E. E., & Gundersen, G. G. (2009). *Clathrin mediates integrin endocytosis for focal adhesion disassembly in migrating cells.* J Cell Biol, 187*(5), 733-747.*

Fielding, A. B., Willox, A. K., Okeke, E., & Royle, S. J. (2012). *Clathrin-mediated endocytosis is inhibited during mitosis.* Proc Natl Acad Sci U S A, 109*(17), 6572-6577.*

Filic, V., Marinovic, M., Faix, J., & Weber, I. (2012). *A dual role for Rac1 GTPases in the regulation of cell motility.* J Cell Sci, 125*(Pt 2), 387-398.*

Frieden, C. (1983). Polymerization of actin: mechanism of the Mg2+-induced process at pH 8 and 20 degrees C. Proc Natl Acad Sci U S A, 80*(21), 6513-6517.*

Gautier, J. J., Lomakina, M. E., Bouslama-Oueghlani, L., Derivery, E., Beilinson, H., Faigle, W. et al. (2011). Clathrin is required for Scar/Wave-mediated lamellipodium formation. J Cell Sci, 124*(Pt 20), 3414-3427.*

Gautreau, A., Ho, H. Y., Li, J., Steen, H., Gygi, S. P., & Kirschner, M. W. (2004). Purification and architecture of the ubiquitous Wave complex. Proc Natl Acad Sci U S A, 101*(13), 4379-4383.*

Gerald, N. J., Damer, C. K., O'Halloran, T. J., & De Lozanne, A. (2001). Cytokinesis failure in clathrin-minus cells is caused by cleavage furrow instability. Cell Motil Cytoskeleton, 48*(3), 213-223.*

Gerisch, G., Bretschneider, T., Muller-Taubenberger, A., Simmeth, E., Ecke, M., Diez, S. et al. (2004). Mobile actin clusters and traveling waves in cells recovering from actin depolymerization. Biophys J, 87*(5), 3493-3503.*

Gerisch, G., & Wick, U. (1975). Intracellular oscillations and release of cyclic AMP from Dictyostelium cells. Biochem Biophys Res Commun, 65*(1), 364-370.*

Goldschmidt-Clermont, P. J., Furman, M. I., Wachsstock, D., Safer, D., Nachmias, V. T., & Pollard, T. D. (1992). The control of actin nucleotide exchange by thymosin beta 4 and profilin. A potential regulatory mechanism for actin polymerization in cells. Mol Biol Cell, 3*(9), 1015-1024.*

Gottlieb, T. A., Ivanov, I. E., Adesnik, M., & Sabatini, D. D. (1993). Actin microfilaments play a critical role in endocytosis at the apical but not the basolateral surface of polarized epithelial cells. J Cell Biol, 120*(3), 695-710.*

Griffith, L. M., Downs, S. M., & Spudich, J. A. (1987). Myosin light chain kinase and myosin light chain phosphatase from Dictyostelium: effects of reversible phosphorylation on myosin structure and function. J Cell Biol, 104*(5), 1309-1323.*

Hahne, P., Sechi, A., Benesch, S., & Small, J. V. (2001). Scar/WAVE is localised at the tips of protruding lamellipodia in living cells. FEBS Lett, 492*(3), 215-220.*

Han, J. W., Leeper, L., Rivero, F., & Chung, C. Y. (2006). Role of RacC for the regulation of WASP and phosphatidylinositol 3-kinase during chemotaxis of Dictyostelium. J Biol Chem, 281*(46), 35224-35234.*

Hartman, M. A., & Spudich, J. A. (2012). The myosin superfamily at a glance. J Cell Sci, 125*(Pt 7), 1627-1632.*

Holmes, K. C., Popp, D., Gebhard, W., & Kabsch, W. (1990). Atomic model of the actin filament. Nature, 347*(6288), 44-49.*

Huxley, H. E. (1963). ELECTRON MICROSCOPE STUDIES ON THE STRUCTURE OF NATURAL AND SYNTHETIC PROTEIN FILAMENTS FROM STRIATED MUSCLE. J Mol Biol, 7, *281-308.*

Hynes, T. R., Block, S. M., White, B. T., & Spudich, J. A. (1987). Movement of myosin fragments in vitro: domains involved in force production. Cell, 48*(6), 953-963.*

Ibarra, N., Blagg,S L, Vazquez, F & Insall, R H. (2006). 'Nap1 Regulates Dictyostelium Cell Motility and Adhesion through SCAR-Dependent and -Independent Pathways'. Current Biology, 16, *717-722.*

Innocenti, M., Frittoli, E., Ponzanelli, I., Falck, J. R., Brachmann, S. M., Di Fiore, P. P. et al. (2003). Phosphoinositide 3-kinase activates Rac by entering in a complex with Eps8, Abi1, and Sos-1. J Cell Biol, 160*(1), 17-23.*

Innocenti, M., Zucconi, A., Disanza, A., Frittoli, E., Areces, L. B., Steffen, A. et al. (2004). Abi1 is essential for the formation and activation of a WAVE2 signalling complex. Nat Cell Biol, 6*(4), 319-327.*

Ismail, A. M., Padrick, S. B., Chen, B., Umetani, J., & Rosen, M. K. (2009). The WAVE regulatory complex is inhibited. Nat Struct Mol Biol, 16*(5), 561-563.*

Jay, P. Y., Pham, P. A., Wong, S. A., & Elson, E. L. (1995). A mechanical function of myosin II in cell motility. J Cell Sci, 108(*Pt 1), 387-393.*

Jia, D., Gomez, T. S., Metlagel, Z., Umetani, J., Otwinowski, Z., Rosen, M. K. et al. (2010). WASH and WAVE actin regulators of the Wiskott-Aldrich syndrome protein (WASP) family are controlled by analogous structurally related complexes. Proc Natl Acad Sci U S A, 107*(23), 10442-10447.*

Joseph, J. M., Fey, P., Ramalingam, N., Liu, X. I., Rohlfs, M., Noegel, A. A. et al. (2008). The actinome of Dictyostelium discoideum in comparison to actins and actin-related proteins from other organisms. PLoS One*, 3(7), e2654.*

Kabsch, W., Mannherz, H. G., Suck, D., Pai, E. F., & Holmes, K. C. (1990). Atomic structure of the actin:DNase I complex. Nature*, 347(6288), 37-44.*

Kasai, M., Asakura, S., & Oosawa, F. (1962). The G-F equilibrium in actin solutions under various conditions. Biochim Biophys Acta*, 57, 13-21.*

Kelleher, J. F., Atkinson, S. J., & Pollard, T. D. (1995). Sequences, structural models, and cellular localization of the actin-related proteins Arp2 and Arp3 from Acanthamoeba. J Cell Biol*, 131(2), 385-397.*

Kim, A. S., Kakalis, L. T., Abdul-Manan, N., Liu, G. A., & Rosen, M. K. (2000). Autoinhibition and activation mechanisms of the Wiskott-Aldrich syndrome protein. Nature*, 404(6774), 151-158.*

King, J. S., Veltman, D. M., & Insall, R. H. (2011). The induction of autophagy by mechanical stress. autophagy*, 7(12), 1490-1499.*

King, J. S., Veltman, D. M., Georgiou, M., Baum, B., & Insall, R. H. (2010). SCAR/WAVE is activated at mitosis and drives myosin-independent cytokinesis. J Cell Sci*, 123(Pt 13), 2246-2255.*

Klein, P., Vaughan, R., Borleis, J., & Devreotes, P. (1987). The surface cyclic AMP receptor in Dictyostelium. Levels of ligand-induced phosphorylation, solubilization, identification of primary transcript, and developmental regulation of expression. J Biol Chem*, 262(1), 358-364.*

Kobayashi, K., Kuroda, S., Fukata, M., Nakamura, T., Nagase, T., Nomura, N. et al. (1998). p140Sra-1 (specifically Rac1-associated protein) is a novel specific target for Rac1 small GTPase. J Biol Chem*, 273(1), 291-295.*

Kollmar, M., Lbik, D., & Enge, S. (2012). Evolution of the eukaryotic ARP2/3 activators of the WASP family: WASP, WAVE, WASH, and WHAMM, and the proposed new family members WAWH and WAML. BMC Res Notes*, 5, 88.*

Konijn, T. M., Van De Meene, J. G., Bonner, J. T., & Barkley, D. S. (1967). *The acrasin activity of adenosine-3',5'-cyclic phosphate.* Proc Natl Acad Sci U S A, 58*(3), 1152-1154.*

Kudryashov, D. S., Sawaya, M. R., Adisetiyo, H., Norcross, T., Hegyi, G., Reisler, E. et al. (2005). *The crystal structure of a cross-linked actin dimer suggests a detailed molecular interface in F-actin.* Proc Natl Acad Sci U S A, 102*(37), 13105-13110.*

Kunda, P., Craig, G., Dominguez, V., & Baum, B. (2003). *Abi, Sra1, and Kette control the stability and localization of SCAR/WAVE to regulate the formation of actin-based protrusions.* Curr Biol, 13*(21), 1867-1875.*

Kuspa, A., & Loomis, W. F. (1992). *Tagging developmental genes in Dictyostelium by restriction enzyme-mediated integration of plasmid DNA.* Proc Natl Acad Sci U S A, 89*(18), 8803-8807.*

Laevsky, G., & Knecht, D. A. (2001). *Under-agarose folate chemotaxis of Dictyostelium discoideum amoebae in permissive and mechanically inhibited conditions.* Biotechniques, 31*(5), 1140-2, 1144, 1146-9.*

Laevsky, G., & Knecht, D. A. (2003). *Cross-linking of actin filaments by myosin II is a major contributor to cortical integrity and cell motility in restrictive environments.* J Cell Sci, 116*(Pt 18), 3761-3770.*

Langridge, P. D., & Kay, R. R. (2006). *Blebbing of Dictyostelium cells in response to chemoattractant.* Exp Cell Res, 312*(11), 2009-2017.*

Laporte, D., Ojkic, N., Vavylonis, D., & Wu, J. Q. (2012). *alpha-Actinin and fimbrin cooperate with myosin II to organize actomyosin bundles during contractile-ring assembly.* Mol Biol Cell, 23*(16), 3094-3110.*

Lebensohn, A. M., & Kirschner, M. W. (2009). *Activation of the WAVE complex by coincident signals controls actin assembly.* Mol Cell, 36*(3), 512-524.*

Leng, Y., Zhang, J., Badour, K., Arpaia, E., Freeman, S., Cheung, P. et al. (2005). *Abelson-interactor-1 promotes WAVE2 membrane translocation and Abelson-mediated tyrosine phosphorylation required for WAVE2 activation.* Proc Natl Acad Sci U S A, 102*(4), 1098-1103.*

Linardopoulou, E. V., Parghi, S. S., Friedman, C., Osborn, G. E., Parkhurst, S. M., & Trask, B. J. (2007). Human subtelomeric WASH genes encode a new subclass of the WASP family. PLoS Genet, 3*(12), e237.*

Loisel, T. P., Boujemaa, R., Pantaloni, D., & Carlier, M. F. (1999). Reconstitution of actin-based motility of Listeria and Shigella using pure proteins. Nature, 401*(6753), 613-616.*

Loomis, W. F. J. (1971). Sensitivity of Dictyostelium discoideum to nucleic acid analogues. Exp Cell Res, 64*(2), 484-486.*

Lorenz, M., Yamaguchi, H., Wang, Y., Singer, R. H., & Condeelis, J. (2004). Imaging sites of N-wasp activity in lamellipodia and invadopodia of carcinoma cells. Curr Biol, 14*(8), 697-703.*

Lymn, R. W., & Taylor, E. W. (1971). Mechanism of adenosine triphosphate hydrolysis by actomyosin. Biochemistry, 10*(25), 4617-4624.*

Machesky, L. M., Atkinson, S. J., Ampe, C., Vandekerckhove, J., & Pollard, T. D. (1994). Purification of a cortical complex containing two unconventional actins from Acanthamoeba by affinity chromatography on profilin-agarose. J Cell Biol, 127*(1), 107-115.*

Machesky, L. M., & Insall, R. H. (1998). Scar1 and the related Wiskott-Aldrich syndrome protein, WASP, regulate the actin cytoskeleton through the Arp2/3 complex. Curr Biol, 8*(25), 1347-1356.*

Machesky, L. M., Mullins, R. D., Higgs, H. N., Kaiser, D. A., Blanchoin, L., May, R. C. et al. (1999). Scar, a WASp-related protein, activates nucleation of actin filaments by the Arp2/3 complex. Proc Natl Acad Sci U S A, 96*(7), 3739-3744.*

Macro, L., Jaiswal, J. K., & Simon, S. M. (2012). Dynamics of clathrin-mediated endocytosis and its requirement for organelle biogenesis in Dictyostelium. J Cell Sci.

Merrifield, C. J., Feldman, M. E., Wan, L., & Almers, W. (2002). Imaging actin and dynamin recruitment during invagination of single clathrin-coated pits. Nat Cell Biol, 4*(9), 691-698.*

Merrifield, C. J., Qualmann, B., Kessels, M. M., & Almers, W. (2004). Neural Wiskott Aldrich Syndrome Protein (N-WASP) and the Arp2/3 complex are recruited to sites of clathrin-mediated endocytosis in cultured fibroblasts. Eur J Cell Biol, 83*(1), 13-18.*

Mettlen, M., Pucadyil, T., Ramachandran, R., & Schmid, S. L. (2009). Dissecting dynamin's role in clathrin-mediated endocytosis. Biochem Soc Trans, 37*(Pt 5), 1022-1026.*

Miki, H., Miura, K., & Takenawa, T. (1996). N-WASP, a novel actin-depolymerizing protein, regulates the cortical cytoskeletal rearrangement in a PIP2-dependent manner downstream of tyrosine kinases. EMBO J, 15*(19), 5326-5335.*

Miki, H., Suetsugu, S., & Takenawa, T. (1998). WAVE, a novel WASP-family protein involved in actin reorganization induced by Rac. EMBO J, 17*(23), 6932-6941.*

Moores, S. L., Sabry, J. H., & Spudich, J. A. (1996). Myosin dynamics in live Dictyostelium cells. Proc Natl Acad Sci U S A, 93*(1), 443-446.*

Morrison, A., & Harwood, A. (1992). A simple method of generating axenic derivatives of Dictyostelium strains. Exp Cell Res, 199*(2), 383-386.*

Moseley, J. B., Sagot, I., Manning, A. L., Xu, Y., Eck, M. J., Pellman, D. et al. (2004). A conserved mechanism for Bni1- and mDia1-induced actin assembly and dual regulation of Bni1 by Bud6 and profilin. Mol Biol Cell, 15*(2), 896-907.*

Mullins, R. D., Heuser, J. A., & Pollard, T. D. (1998). The interaction of Arp2/3 complex with actin: nucleation, high affinity pointed end capping, and formation of branching networks of filaments. Proc Natl Acad Sci U S A, 95*(11), 6181-6186.*

Muramoto, T., & Chubb, J. R. (2008). Live imaging of the Dictyostelium cell cycle reveals widespread S phase during development, a G2 bias in spore differentiation and a premitotic checkpoint. Development, 135*(9), 1647-1657.*

Myers, S. A., Han, J. W., Lee, Y., Firtel, R. A., & Chung, C. Y. (2005). A Dictyostelium homologue of WASP is required for polarized F-actin assembly during chemotaxis. Mol Biol Cell, 16*(5), 2191-2206.*

Myers, S. A., Leeper, L. R., & Chung, C. Y. (2006). WASP-interacting protein is important for actin filament elongation and prompt pseudopod formation in response to a dynamic chemoattractant gradient. Mol Biol Cell, 17*(10), 4564-4575.*

Nagasaki, A., de Hostos, E. L., & Uyeda, T. Q. (2002). Genetic and morphological evidence for two parallel pathways of cell-cycle-coupled cytokinesis in Dictyostelium. J Cell Sci, 115*(Pt 10), 2241-2251.*

Nakamura, F., Osborn, T. M., Hartemink, C. A., Hartwig, J. H., & Stossel, T. P. (2007). Structural basis of filamin A functions. J Cell Biol, 179*(5), 1011-1025.*

Naqvi, S. N., Zahn, R., Mitchell, D. A., Stevenson, B. J., & Munn, A. L. (1998). The WASp homologue Las17p functions with the WIP homologue End5p/verprolin and is essential for endocytosis in yeast. Curr Biol, 8*(17), 959-962.*

Neujahr, R., Heizer, C., & Gerisch, G. (1997). Myosin II-independent processes in mitotic cells of Dictyostelium discoideum: redistribution of the nuclei, re-arrangement of the actin system and formation of the cleavage furrow. J Cell Sci, 110(*Pt 2), 123-137.*

Niswonger, M. L., & O'Halloran, T. J. (1997). A novel role for clathrin in cytokinesis. Proc Natl Acad Sci U S A, 94*(16), 8575-8578.*

Padrick, S. B., Doolittle, L. K., Brautigam, C. A., King, D. S., & Rosen, M. K. (2011). Arp2/3 complex is bound and activated by two WASP proteins. Proc Natl Acad Sci U S A, 108*(33), E472-9.*

Paluch, E., Piel, M., Prost, J., Bornens, M., & Sykes, C. (2005). Cortical actomyosin breakage triggers shape oscillations in cells and cell fragments. Biophys J, 89*(1), 724-733.*

Pan, P., Hall, E. M., & Bonner, J. T. (1972). Folic acid as second chemotactic substance in the cellular slime moulds. Nat New Biol, 237*(75), 181-182.*

Pantaloni, D., Boujemaa, R., Didry, D., Gounon, P., & Carlier, M. F. (2000). The Arp2/3 complex branches filament barbed ends: functional antagonism with capping proteins. Nat Cell Biol, 2*(7), 385-391.*

Park, L., Thomason, P. A., Zech, T., King, J. S., Veltman, D. M., Carnell, M. et al. (2013). Cyclical action of the WASH complex: FAM21 and capping protein drive WASH recycling, not initial recruitment. Dev Cell, 24*(2), 169-181.*

Pasternak, C., Spudich, J. A., & Elson, E. L. (1989). Capping of surface receptors and concomitant cortical tension are generated by conventional myosin. Nature, 341*(6242), 549-551.*

Patterson, B., & Spudich, J. A. (1995). A novel positive selection for identifying cold-sensitive myosin II mutants in Dictyostelium. Genetics, 140*(2), 505-515.*

Pellinen, T., Tuomi, S., Arjonen, A., Wolf, M., Edgren, H., Meyer, H. et al. (2008). Integrin trafficking regulated by Rab21 is necessary for cytokinesis. Dev Cell, 15*(3), 371-385.*

Petersen, J., Nielsen, O., Egel, R., & Hagan, I. M. (1998). FH3, a domain found in formins, targets the fission yeast formin Fus1 to the projection tip during conjugation. J Cell Biol, 141*(5), 1217-1228.*

Pollard, T. D. (1986). Rate constants for the reactions of ATP- and ADP-actin with the ends of actin filaments. J Cell Biol, 103*(6 Pt 2), 2747-2754.*

Pollard, T. D., & Mooseker, M. S. (1981). Direct measurement of actin polymerization rate constants by electron microscopy of actin filaments nucleated by isolated microvillus cores. J Cell Biol, 88*(3), 654-659.*

Pollard, T. D., & Weeds, A. G. (1984). The rate constant for ATP hydrolysis by polymerized actin. FEBS Lett, 170*(1), 94-98.*

Pollitt, A. Y., Blagg, S. L., Ibarra, N., & Insall, R. H. (2006). Cell motility and SCAR localisation in axenically growing Dictyostelium cells. Eur J Cell Biol, 85*(9-10), 1091-1098.*

Pollitt, A. Y., & Insall, R. H. (2008). Abi mutants in Dictyostelium reveal specific roles for the SCAR/WAVE complex in cytokinesis. Curr Biol, 18*(3), 203-210.*

Pollitt, A. Y., & Insall, R. H. (2009). WASP and SCAR/WAVE proteins: the drivers of actin assembly. J Cell Sci, 122*(Pt 15), 2575-2578.*

Pruyne, D., Evangelista, M., Yang, C., Bi, E., Zigmond, S., Bretscher, A. et al. (2002). Role of formins in actin assembly: nucleation and barbed-end association. Science, *297(5581), 612-615.*

Qualmann, B., & Kessels, M. M. (2009). New players in actin polymerization--WH2-domain-containing actin nucleators. Trends Cell Biol, *19(6), 276-285.*

Ramesh, N., Anton, I. M., Hartwig, J. H., & Geha, R. S. (1997). WIP, a protein associated with wiskott-aldrich syndrome protein, induces actin polymerization and redistribution in lymphoid cells. Proc Natl Acad Sci U S A, *94(26), 14671-14676.*

Raper, K. B. (1935). DICTYOSTELIUM DISCOIDEUM, A NEW SPECIES OF SLIME MOLD FROM DECAYING FOREST LEAVES. Journal of Agricultural Research, *50(2), 135-147.*

Rayment, I., Rypniewski, W. R., Schmidt-Base, K., Smith, R., Tomchick, D. R., Benning, M. M. et al. (1993). Three-dimensional structure of myosin subfragment-1: a molecular motor. Science, *261(5117), 50-58.*

Redowicz, M. J. (2001). Regulation of nonmuscle myosins by heavy chain phosphorylation. J Muscle Res Cell Motil, *22(2), 163-173.*

Reider, A., & Wendland, B. (2011). Endocytic adaptors--social networking at the plasma membrane. J Cell Sci, *124(Pt 10), 1613-1622.*

Renault, L., Bugyi, B., & Carlier, M. F. (2008). Spire and Cordon-bleu: multifunctional regulators of actin dynamics. Trends Cell Biol, *18(10), 494-504.*

Rouiller, I., Xu, X. P., Amann, K. J., Egile, C., Nickell, S., Nicastro, D. et al. (2008). The structural basis of actin filament branching by the Arp2/3 complex. J Cell Biol, *180(5), 887-895.*

Royle, S. J., Bright, N. A., & Lagnado, L. (2005). Clathrin is required for the function of the mitotic spindle. Nature, *434(7037), 1152-1157.*

Saga, Y., & Yanagisawa, K. (1983). Macrocyst development in Dictyostelium discoideum. III. Cell-fusion inducing factor secreted by giant cells. J Cell Sci, *62, 237-248.*

Schachtner, H., Calaminus, S. D., Sinclair, A., Monypenny, J., Blundell, M. P., Leon, C. et al. (2013). *Megakaryocytes assemble podosomes that degrade matrix and protrude through basement membrane.* Blood, 121*(13), 2542-2552.*

Schirenbeck, A., Bretschneider, T., Arasada, R., Schleicher, M., & Faix, J. (2005). *The Diaphanous-related formin dDia2 is required for the formation and maintenance of filopodia.* Nat Cell Biol, 7*(6), 619-625.*

Schweitzer, J. K., Burke, E. E., Goodson, H. V., & D'Souza-Schorey, C. (2005). *Endocytosis resumes during late mitosis and is required for cytokinesis.* J Biol Chem, 280*(50), 41628-41635.*

Seastone, D. J., Harris, E., Temesvari, L. A., Bear, J. E., Saxe, C. L., & Cardelli, J. (2001). *The WASp-like protein scar regulates macropinocytosis, phagocytosis and endosomal membrane flow in Dictyostelium.* J Cell Sci, 114*(Pt 14), 2673-2683.*

Shelden, E., & Knecht, D. A. (1995). *Mutants lacking myosin II cannot resist forces generated during multicellular morphogenesis.* J Cell Sci, 108*(Pt 3), 1105-1115.*

Steffen, A., Faix, J., Resch, G. P., Linkner, J., Wehland, J., Small, J. V. et al. (2006). *Filopodia formation in the absence of functional WAVE- and Arp2/3-complexes.* Mol Biol Cell, 17*(6), 2581-2591.*

Steffen, A., Rottner, K., Ehinger, J., Innocenti, M., Scita, G., Wehland, J. et al. (2004). *Sra-1 and Nap1 link Rac to actin assembly driving lamellipodia formation.* EMBO J, 23*(4), 749-759.*

Stevenson, R. P., Veltman, D., & Machesky, L. M. (2012). *Actin-bundling proteins in cancer progression at a glance.* J Cell Sci, 125*(Pt 5), 1073-1079.*

Suetsugu, S., Miki, H., & Takenawa, T. (1998). *The essential role of profilin in the assembly of actin for microspike formation.* EMBO J, 17*(22), 6516-6526.*

Suraneni, P., Rubinstein, B., Unruh, J. R., Durnin, M., Hanein, D., & Li, R. (2012). *The Arp2/3 complex is required for lamellipodia extension and directional fibroblast cell migration.* J Cell Biol, 197*(2), 239-251.*

Sussman, R., & Sussman, M. (1967). *Cultivation of Dictyostelium discoideum in axenic medium.* Biochem Biophys Res Commun, 29*(1), 53-55.*

Svitkina, T. M., & Borisy, G. G. (1999). Arp2/3 complex and actin depolymerizing factor/cofilin in dendritic organization and treadmilling of actin filament array in lamellipodia. J Cell Biol*, 145(5), 1009-1026.*

Tang, H., Li, A., Bi, J., Veltman, D. M., Zech, T., Spence, H. J. et al. (2013). Loss of Scar/WAVE complex promotes N-WASP- and FAK-dependent invasion. Curr Biol*, 23(2), 107-117.*

Ti, S. C., Jurgenson, C. T., Nolen, B. J., & Pollard, T. D. (2011). Structural and biochemical characterization of two binding sites for nucleation-promoting factor WASp-VCA on Arp2/3 complex. Proc Natl Acad Sci U S A, 108(33), E463-71.*

Tomchik, K. J., & Devreotes, P. N. (1981). Adenosine 3',5'-monophosphate waves in Dictyostelium discoideum: a demonstration by isotope dilution--fluorography. Science, 212(4493), 443-446.*

Toyoshima, Y. Y., Kron, S. J., McNally, E. M., Niebling, K. R., Toyoshima, C., & Spudich, J. A. (1987). Myosin subfragment-1 is sufficient to move actin filaments in vitro. Nature*, 328(6130), 536-539.*

Ura, S., Pollitt, A. Y., Veltman, D. M., Morrice, N. A., Machesky, L. M., & Insall, R. H. (2012). Pseudopod growth and evolution during cell movement is controlled through SCAR/WAVE dephosphorylation. Curr Biol, 22(7), 553-561.*

Urban, E., Jacob, S., Nemethova, M., Resch, G. P., & Small, J. V. (2010). Electron tomography reveals unbranched networks of actin filaments in lamellipodia. Nat Cell Biol*, 12(5), 429-435.*

Vandekerckhove, J., & Weber, K. (1978). At least six different actins are expressed in a higher mammal: an analysis based on the amino acid sequence of the amino-terminal tryptic peptide. J Mol Biol*, 126(4), 783-802.*

Veltman, D. M., Akar, G., Bosgraaf, L., & Van Haastert, P. J. (2009). A new set of small, extrachromosomal expression vectors for Dictyostelium discoideum. Plasmid*, 61(2), 110-118.*

Veltman, D. M., & Insall, R. H. (2010). WASP family proteins: their evolution and its physiological implications. Mol Biol Cell*, 21(16), 2880-2893.*

Veltman, D. M., Keizer-Gunnink, I., & Haastert, P. J. (2009). An extrachromosomal, inducible expression system for Dictyostelium discoideum. Plasmid, 61*(2), 119-125.*

Veltman, D. M., King, J. S., Machesky, L. M., & Insall, R. H. (2012). SCAR knockouts in Dictyostelium: WASP assumes SCAR's position and upstream regulators in pseudopods. J Cell Biol, 198*(4), 501-508.*

Volkman, B. F., Prehoda, K. E., Scott, J. A., Peterson, F. C., & Lim, W. A. (2002). Structure of the N-WASP EVH1 domain-WIP complex: insight into the molecular basis of Wiskott-Aldrich Syndrome. Cell, 111*(4), 565-576.*

Wang, L. L., & Bryan, J. (1981). Isolation of calcium-dependent platelet proteins that interact with actin. Cell, 25*(3), 637-649.*

Watts, D. J., & Ashworth, J. M. (1970). Growth of myxameobae of the cellular slime mould Dictyostelium discoideum in axenic culture. Biochem J, 119*(2), 171-174.*

Weber, A., Pennise, C. R., Babcock, G. G., & Fowler, V. M. (1994). Tropomodulin caps the pointed ends of actin filaments. J Cell Biol, 127*(6 Pt 1), 1627-1635.*

Wegner, A. (1976). Head to tail polymerization of actin. J Mol Biol, 108*(1), 139-150.*

Weiner, O D, Rentel, M C, Ott, A, Brown, G E, Jedrychowski, M, Yaffe, M, & Gygi, S. P., Cantley, L C, Bourne, H R & Kirschner, M W. (2006). 'Hem-1 Complexes Are Essential for Rac Activation, Actin Polymerization, and Myosin Regulation during Neutrophil Chemotaxis'. PLoS Biology, 4*, 186-199.*

Weiner, O. D. (2002). Regulation of cell polarity during eukaryotic chemotaxis: the chemotactic compass. Curr Opin Cell Biol, 14*(2), 196-202.*

Wessels, D., Reynolds, J., Johnson, O., Voss, E., Burns, R., Daniels, K. et al. (2000). Clathrin plays a novel role in the regulation of cell polarity, pseudopod formation, uropod stability and motility in Dictyostelium. J Cell Sci, 113(*Pt 1), 21-36.*

Winder, S. J., & Ayscough, K. R. (2005). Actin-binding proteins. J Cell Sci, 118*(Pt 4), 651-654.*

Wu, C., Asokan, S. B., Berginski, M. E., Haynes, E. M., Sharpless, N. E., Griffith, J. D. et al. (2012). Arp2/3 is critical for lamellipodia and response to extracellular matrix cues but is dispensable for chemotaxis. Cell*, 148(5), 973-987.*

Xu, X. S., Lee, E., Chen, T., Kuczmarski, E., Chisholm, R. L., & Knecht, D. A. (2001). During multicellular migration, myosin ii serves a structural role independent of its motor function. Dev Biol*, 232(1), 255-264.*

Xu, Y., Moseley, J. B., Sagot, I., Poy, F., Pellman, D., Goode, B. L. et al. (2004). Crystal structures of a Formin Homology-2 domain reveal a tethered dimer architecture. Cell*, 116(5), 711-723.*

Yang, C., & Svitkina, T. (2011). Visualizing branched actin filaments in lamellipodia by electron tomography. Nat Cell Biol*, 13(9), 1012-3; author reply 1013-4.*

Yoshida, K., & Soldati, T. (2006). Dissection of amoeboid movement into two mechanically distinct modes. J Cell Sci*, 119(Pt 18), 3833-3844.*

Yu, X., Zech, T., McDonald, L., Gonzalez, E. G., Li, A., Macpherson, I. et al. (2012). N-WASP coordinates the delivery and F-actin-mediated capture of MT1-MMP at invasive pseudopods. J Cell Biol*, 199(3), 527-544.*

Yumura, S., Itoh, G., Kikuta, Y., Kikuchi, T., Kitanishi-Yumura, T., & Tsujioka, M. (2013). Cell-scale dynamic recycling and cortical flow of the actin-myosin cytoskeleton for rapid cell migration. Biol Open*, 2(2), 200-209.*

Zang, J. H., Cavet, G., Sabry, J. H., Wagner, P., Moores, S. L., & Spudich, J. A. (1997). On the role of myosin-II in cytokinesis: division of Dictyostelium cells under adhesive and nonadhesive conditions. Mol Biol Cell*, 8(12), 2617-2629.*

Zheng, B., Han, M., Bernier, M., & Wen, J. K. (2009). Nuclear actin and actin-binding proteins in the regulation of transcription and gene expression. FEBS J*, 276(10), 2669-2685.*

Zhuang, C., Tang, H., Dissanaike, S., Cobos, E., Tao, Y., & Dai, Z. (2011). CDK1-mediated phosphorylation of Abi1 attenuates Bcr-Abl-induced F-actin assembly and tyrosine phosphorylation of WAVE complex during mitosis. J Biol Chem*, 286(44), 38614-38626.*

Zuchero, J. B., Coutts, A. S., Quinlan, M. E., Thangue, N. B., & Mullins, R. D. (2009). p53-cofactor JMY is a multifunctional actin nucleation factor. Nat Cell Biol*, 11(4), 451-459.*

Publications arising from this work

Eukaryotic Cell

Abi Is Required for Modulation and Stability but Not Localization or Activation of the SCAR/WAVE Complex

Andrew J. Davidson, Seiji Ura, Peter A. Thomason, Gabriela Kalna and Robert H. Insall

---

Updated information and services can be found at:
http://ec.asm.org/content/12/11/1509

These include:

SUPPLEMENTAL MATERIAL   Supplemental material

REFERENCES   This article cites 24 articles, 11 of which can be accessed free
at: http://ec.asm.org/content/12/11/1509#ref-list-1

CONTENT ALERTS   Receive: RSS Feeds, eTOCs, free email alerts (when new
articles cite this article), more»

Information about commercial reprint orders: http://journals.asm.org/site/misc/reprints.xhtml
To subscribe to to another ASM Journal go to: http://journals.asm.org/site/subscriptions/

Journals.ASM.org

Abi Is Required for Modulation and Stability but Not Localization or Activation of the SCAR/WAVE Complex

Andrew J. Davidson, Seiji Ura, Peter A. Thomason, Gabriela Kalna, Robert H. Insall

Beatson Institute for Cancer Research, Bearsden, Glasgow, United Kingdom

The SCAR/WAVE complex drives actin-based protrusion, cell migration, and cell separation during cytokinesis. However, the contribution of the individual complex members to the activity of the whole remains a mystery. This is primarily because complex members depend on one another for stability, which limits the scope for experimental manipulation. Several studies suggest that Abi, a relatively small complex member, connects signaling to SCAR/WAVE complex localization and activation through its polyproline C-terminal tail. We generated a deletion series of the *Dictyostelium discoideum* Abi to investigate its exact role in regulation of the SCAR complex and identified a minimal fragment that would stabilize the complex. Surprisingly, loss of either the N terminus of Abi or the C-terminal polyproline tail conferred no detectable defect in complex recruitment to the leading edge or the formation of pseudopods. A fragment containing approximately 20% Abi—and none of the sites that couple to known signaling pathways—allowed the SCAR complex to function with normal localization and kinetics. However, expression of N-terminal Abi deletions exacerbated the cytokinesis defect of the *Dictyostelium abi* mutant, which was earlier shown to be caused by the inappropriate activation of SCAR. This demonstrates, unexpectedly, that Abi does not mediate the SCAR complex's ability to make pseudopods, beyond its role in complex stability. Instead, we propose that Abi has a modulatory role when the SCAR complex is activated through other mechanisms.

Cell movement derives from the extension or protrusion of regions at the front of the cell followed by the coordinated retraction of the rear. When this behavior is coupled to the perception of their situation and surroundings, cells gain the ability to migrate with persistence and direction. For instance, during chemotaxis cells display an ability to detect and move along chemical gradients. Another example is during cytokinesis, where dividing cells establish opposing polarity and migrate apart from each other in a precisely coordinated manner so as to aid in the separation of the newly formed daughter cells ([1]). Directed migration requires the integrated activities of a multitude of proteins, ranging from sensory receptors and mediators of intracellular signaling to contractile actomyosin filaments, inducers of membrane curvature, and actin nucleators and their activators.

Dictyostelium discoideum has long been the model of choice in the study of eukaryotic chemotaxis, as its movement is very comparable to that of higher eukaryotic cells, such as neutrophils, and it is extremely amenable to genetic manipulation ([2]). Such traits make *Dictyostelium discoideum* a powerful model for dissecting the fundamental principles underlying chemotaxis.

In *Dictyostelium*, as in all motile eukaryotic cells, coordinated cycles of actin polymerization and depolymerization underlie cell motility. As an actin nucleator, the Arp2/Arp3 complex induces actin polymerization that promotes the formation of cellular protrusions (or pseudopodia [[3], [4]]). This culminates in a dense branched network of actin capable of supporting a growing pseudopod. The Arp2/Arp3 complex alone has a low basal level of activity ([3]). Several activators of the Arp2/Arp3 complex have now been identified, including the WASP family of proteins. Members of the WASP family include WASP, SCAR (also named WAVE), and the recently discovered WASH ([5], [6]). Interactions with the Arp2/Arp3 complex are mediated through a highly conserved C-terminal VCA domain, which is capable of promoting Arp2/Arp3 nucleation activity. The N-terminal regions of WASP family proteins are more varied and comprise the regulatory regions that connect the Arp2/Arp3-activating C termini to intracellular signaling events ([7]).

SCAR has been clearly demonstrated to be important for pseudopod extension and localizes to the extreme front of such protrusions ([8]). *In vivo*, SCAR exists as part of a large heteropentameric complex containing PIR121, Nap1, Abi, SCAR, and HSPC300, which are collectively known as the SCAR complex ([9]). A single, well-conserved homolog of each complex member is found in *Dictyostelium discoideum* ([10]). Recently, the crystal structure of the human SCAR/WAVE1 complex has been solved, revealing the complex architecture ([11]). Sra-1 (also named PIR121) and Nap1 form a platform upon which nestles a trimer composed of the other three complex members. The C-terminal VCA of SCAR/WAVE1 is sequestered within the complex, suggesting a means by which it is inhibited. However, the crystal structure yields little other information as to the purpose of the remaining bulk of the SCAR complex. Attempts to dissect the contributions of the other members to the complex as a whole have been hindered by the inherent instability of the complex to manipulation ([12], [13]).

As revealed by the crystal structure, SCAR/WAVE1 complex member Abi is situated at the entrance to the PIR121/Nap1 cradle wherein SCAR/WAVE1 is found. It was known that Abi interacted strongly with Nap1, and now that the crystal structure is available, it is notable that of the members of the Abi/SCAR/HSPC300

trimer, Abi is the only one to make any substantial contact with Nap1 (14, 15). The long C-terminal proline-rich tail of Abi had to be removed to aid crystallization, presumably because of its intrinsic disorder. However, it is most probable that it protrudes out from the main body of the complex, where it would be free to interact with other factors, including the extended C terminus of SCAR, following its release from the complex (16).

In addition to the above-described structural considerations, it has been reported that Abi directly recruits the SCAR complex to signaling complexes containing its well-known activator, Rac1 (17). Numerous phosphorylation sites have also been identified in Abi, and some of these have been found to be responsive to stimuli, such as epidermal growth factor treatment or serum starvation, in mammalian cells (18). Also, it has been suggested that Abi localizes and activates the complex through its interaction with ABL kinases, from which it originally derived its name (19). Overall, the literature describes Abi to be a fundamental regulator of the SCAR complex.

Previously, our lab reported the phenotype of *Dictyostelium* cells lacking Abi (*abiA*-null cells) (20). Unlike knockouts in any of the other complex members, in which SCAR is no longer stable and barely detectable by Western blotting, *Dictyostelium abiA*-null cells still retain appreciable levels of SCAR protein. It has been demonstrated that cells lacking Abi possess a cytokinesis defect unique to it among the null cells of the SCAR complex members. Since cells devoid of Abi and SCAR (*abiA scrA* double-null cells) have a phenotype equivalent to that of cells lacking SCAR (*scrA*-null cells), this defect has been attributed to the residual SCAR that is still present in *abiA*-null cells and its possible mislocalization or inappropriate activity during cytokinesis.

All of the facts mentioned above strongly imply that Abi is a crucial component of the SCAR complex responsible for its localization and subsequent activation during chemotaxis and cytokinesis. For these reasons, we have undertaken the creation of a comprehensive deletion series of the *Dictyostelium* Abi gene. The resulting truncated proteins were examined for their ability to stabilize the SCAR complex and to rescue different aspects of the *abiA*-null phenotype. We have thus identified the minimal functional fragment of Abi required to restore SCAR complex levels and activity in *abiA*-null cells.

MATERIALS AND METHODS

Cell culture. *Dictyostelium* cells were cultured axenically in HL-5 medium (Formedium) at 22°C in petri dishes, and plasmid selection was maintained with 10 μg/ml of G418. For growth curves, 5×10^4 cells were plated in 6-well petri dishes, with cells of an individual well harvested and a cell count performed for each 12-h time point. Alternatively, for growth in shaking culture, flasks were inoculated with 5×10^4 cells/ml and a cell count was again performed every 12 h. Cell counts were performed with a CASY cell counter and analyzer system, model TT (Innovates AG). Doubling times were derived, and statistical significance and two-tailed P values were calculated through the use of unpaired t tests.

Immunoblotting. For Western blotting, protein lysates were prepared by boiling cells in LDS buffer (Invitrogen) and were separated by electrophoresis on NuPAGE 4 to 12% bis-Tris gels (Invitrogen). Proteins were transferred onto nitrocellulose membranes (Hybond-C-extra; Amersham Biosciences) and then blocked with a solution containing 5% nonfat dried skimmed milk dissolved in Tris-buffered saline. The membranes were then probed with antibodies specific to SCAR, PIR121, or green fluorescent protein (GFP), followed by the use of fluorescence secondary antibodies that were detected using an Odyssey infrared imaging system (LI-COR Biosciences). Quantification of SCAR levels was achieved by

normalization of the SCAR band intensity to the PIR121 band intensity for each sample over four blots. For quantification, unpaired, two-tailed Student t tests were used to determine statistical significance.

For native PAGE, lysates were separated by electrophoresis on Native-PAGE Novex bis-Tris 4 to 16% gels (Invitrogen) according to the manufacturer's protocol. Proteins were transferred onto polyvinylidene difluoride (PVDF) membranes, blocked, probed with anti-SCAR antibody, and detected by chemiluminescence (Hybond-P PVDF membrane [Amersham], horseradish peroxidase [HRP]-conjugated secondary antibodies and Immobilon Western chemiluminescent HRP substrate [Millipore]).

TIRF microscopy. The HL-5 medium from confluent plates was replaced with development buffer (10 mM KNaPO_4, 2 mM MgCl_2, 1 mM CaCl_2, pH 6.5), and cells were starved for 7 h. The cells were then harvested from the plates, seeded in glass-bottom dishes (Iwaki), and then slightly compressed under 0.4% agarose slabs. SCAR complex localization and cell morphology were imaged simultaneously using total internal fluorescence (TIRF) microscopy and differential interference contrast (DIC) microscopy, respectively, on a modified Nikon Eclipse TE 2000-U microscope using a ×100 Nikon TIRF objective (numerical aperture [NA], 1.45). Images were recorded every 2 s. Pseudopodia were counted manually with the aid of ImageJ software (National Institutes of Health). Pseudopodia were defined as large convex, semicircular protrusions devoid of granular cytosol. This definition excluded all but the largest runs of blebs. HSPC300-GFP recruitment to these protrusions was then retrospectively determined. Ten cells (collectively amounting to an hour of cell migration) were analyzed for each of the transformants, and statistical significance and two-tailed P values were calculated through the use of unpaired Student t tests.

DAPI-phalloidin staining. Doubling times were derived from the growth curves prepared as described above, and cells were seeded at a low density on glass coverslips in a staggered fashion so that the transformants underwent approximately 10 divisions. The coverslips were removed, and cells were then fixed for 5 min with a solution containing 6% (wt/vol) formaldehyde, 15% (vol/vol) picric acid, and 10 mM PIPES [piperazine-N,N′-bis(2-ethanesulfonic acid)] adjusted to pH 6.5. Cells were then washed with phosphate-buffered saline (PBS) before permeabilization with 70% ethanol for 2 min. The fixed cells were washed with PBS and then stained with 33 nM Texas Red phalloidin (Invitrogen) for 30 min. Coverslips were washed again in PBS and finally mounted on glass slides with antifade reagent containing DAPI (4′,6-diamidino-2-phenylindole; Prolong Gold; Invitrogen). Cells were imaged using an inverted wide-field microscope (IX81; Olympus) and a ×60 objective (NA, 1.42) or a Nikon A1 confocal microscope with a ×60 objective (NA, 1.4). The number of nuclei per cell was counted for >100 cells for each of the transformants, and the cells were then grouped into those with either 1 or ≥2 nuclei. The chi-square test was used for investigation of the differences between the observed frequencies of nuclei per cell. When the expected counts fell below 5, Yates' correction was applied.

RESULTS

Only a small fragment of Abi is required to stabilize the SCAR complex. From the crystal structure available from the Protein Data Bank (accession number 3P8C; Fig. 1a), it is apparent that Abi2 is incorporated into the mammalian SCAR/WAVE1 complex through the second of its two N-terminal alpha helices (α2; Fig. 1a). This domain was identified in the *Dictyostelium* Abi by protein alignment (Fig. 1b). We reasoned that this alpha helix alone could be sufficient to fully stabilize the complex in *Dictyostelium abiA*-null cells, and so we proceeded to incrementally delete all peripheral sequence on either side of it (Fig. 1c). Deletion of the N terminus of Abi resulted in the loss of the anti-Abi epitope, which confounded detection (see Fig. S1 in the supplemental material). We were reluctant to directly tag Abi because the different relative positions of GFP could interfere differentially with Abi's
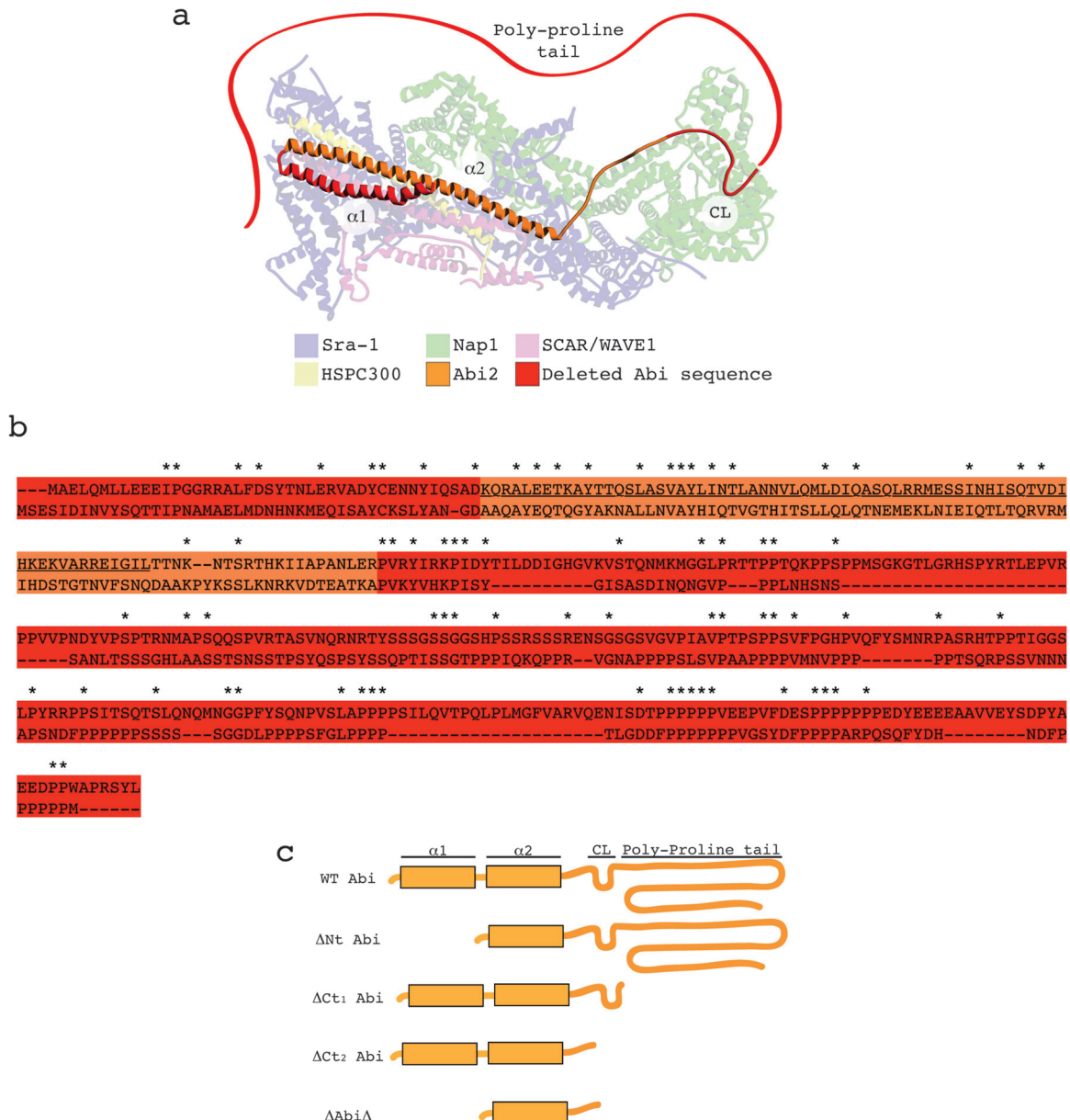
FIG 1 Design and implementation of Abi deletion series. (a) Illustration of human SCAR/WAVE1 complex derived from the recently resolved crystal structure available from the Protein Data Bank (accession number 3P8C). The sequence corresponding to that deleted in the *Dictyostelium* Abi is highlighted in red. Red ribbon, the Abi2 polyproline region that is absent from the crystal structure (not to scale). Labels designate different domains/features of Abi2: α1, 1st alpha helix; α2, 2nd alpha helix; CL, conserved loop. (b) Protein alignment between human Abi2 (above), represented in panel a, and *Dictyostelium* Abi (below) with a color scheme identical to that described for panel a. The sequence corresponding to the C-terminal SH3 domain of human Abi2 was removed to aid alignment, as *Dictyostelium* Abi does not possess this domain. Asterisks, amino acid identities; underlined sequence, amino acids corresponding to the 2nd alpha helix in panel a. (c) Diagrammatic representation of the *Dictyostelium* Abi domain structure and the subsequent deletion series undertaken. WT, full-length Abi; ΔNt, N-terminally truncated Abi; ΔCt₁ and ΔCt₂, C-terminally truncated Abi as shown; ΔAbiΔ, combination of both N-terminally and C-terminally truncated Abi.

normal activity. However, in order to compare the expression of all our constructs, we additionally N-terminally fused our deletion series to GFP, allowing each member of the series to be detected with anti-GFP. Figure 2a demonstrates that all of the Abi constructs were expressed and there were no gross differences in protein levels. Unless otherwise stated, in all subsequent work we coexpressed our untagged deletion series with HSPC300-GFP, an established marker of the SCAR complex (8). The untagged, truncated Abi proteins were then tested for their ability to stabilize the

SCAR complex *in vivo* when expressed in the *abiA*-null cells. The SCAR protein level, as assayed by Western blotting, was initially utilized as a readout of complex integrity (Fig. 2a). We have previously shown that SCAR complex member PIR121 is stable in *abiA*- and *scrA*-null cells, and so we utilized it as a loading control (12). The domains of Abi that proved dispensable for SCAR stabilization included the first alpha helix (N-terminally truncated Abi [ΔNt Abi]) and—as has been shown previously in mammalian cells (14, 21)—the entire C-terminal polyproline tail (C-ter-
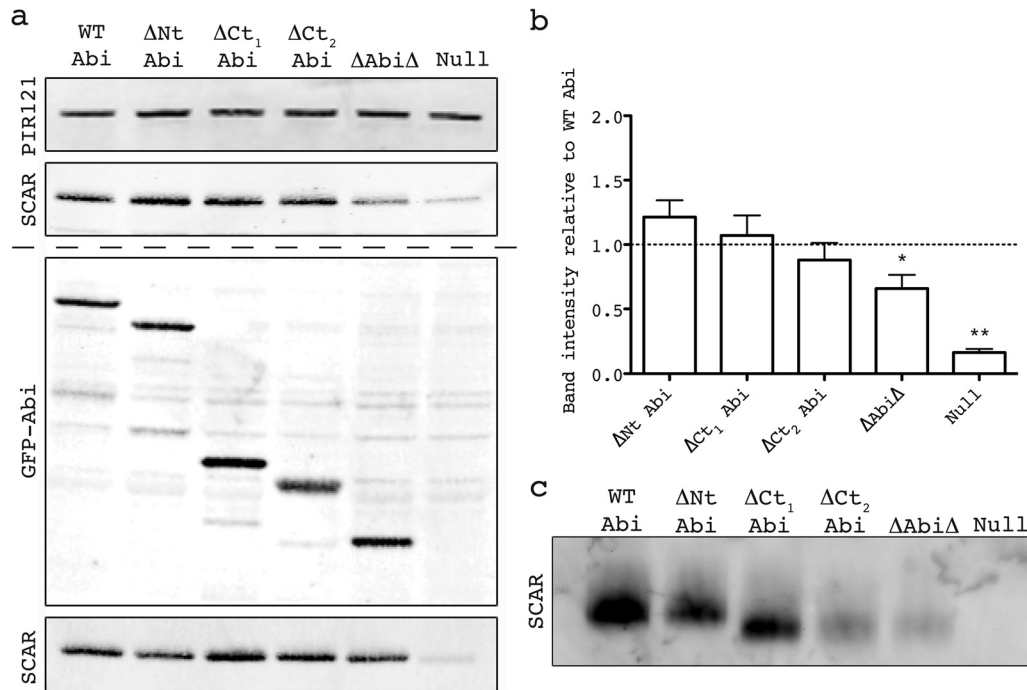
FIG 2 Identification of minimal Abi fragment. (a) Western blot revealing stabilization of SCAR by the untagged/tagged Abi deletion series transformed into an *abiA*-null strain. (Top) Lysates probed with antibody against PIR121, a stable member of the complex that was used as a loading control; (second panel) lysates probed with anti-SCAR antibody demonstrating stabilization of SCAR by different untagged Abi fragments; (third panel) expression of truncated GFP-tagged Abi constructs confirmed by anti-GFP Western blotting; (bottom) lysates probed with anti-SCAR antibody demonstrating stabilization of SCAR by different GFP-tagged Abi fragments. The dashed line divides blots into those derived from cells that possessed untagged Abi deletion series (above the dashed line) and those that possessed GFP-tagged Abi deletion series (below the dashed line). (b) Quantification of SCAR levels was achieved by normalization of the SCAR band intensity to the PIR121 band intensity for each untagged transformant over four blots. *, significantly different from WT Abi SCAR levels (unpaired *t* test, $P < 0.05$); **, significantly different from ΔAbiΔ SCAR levels (unpaired *t* test, $P < 0.0001$). Error bars indicate SEMs. (c) Native PAGE demonstrating the stabilization of the entire SCAR complex by the untagged Abi fragments. Intact protein complexes were separated by native PAGE and probed with anti-SCAR antibody following Western blotting. WT, full-length wild-type Abi; ΔNt, N-terminally truncated Abi; ΔCt$_1$ and ΔCt$_2$, C-terminally truncated Abi as shown in Fig. 1c; ΔAbiΔ, combination of both N-terminally and C-terminally truncated Abi; Null, HSPC300-GFP-only vector/empty GFP vector.

minally truncated Abi1 [ΔCt$_1$ Abi]). The most distal C-terminal Abi2 sequence for which there are crystal structure data available (i.e., immediately before the start of the polyproline tail) was strikingly conserved (Fig. 1b). Following its deletion in combination with the polyproline tail (ΔCt$_2$ Abi), it, too, surprisingly, proved unnecessary for SCAR stabilization (Fig. 2a). Further truncation of the C terminus of Abi yielded fragments that were expressed but did not contribute to SCAR stability (data not shown). Finally, a minimal Abi fragment which had deletions at both termini and consisted of little more than the α2 helix (Abi with a combination of both N-terminal and C-terminal truncations [ΔAbiΔ]) restored SCAR protein levels in *abiA*-null cells, if only partially. Quantification of SCAR levels in these cells demonstrated that ΔAbiΔ restored SCAR significantly less than wild-type (WT) Abi (unpaired *t* test, $P < 0.05$) but restored it to a level significantly more than the basal level found in the null strain expressing HSPC300-GFP alone (unpaired *t* test, $P < 0.001$; Fig. 2b). The Abi constructs tagged with GFP also restored SCAR levels in *abiA*-null cells to a comparable extent (Fig. 2a).

The stabilization of the intact complex was confirmed by native gel electrophoresis, as demonstrated in Fig. 2c. Under these conditions *Dictyostelium* SCAR was found in only one high-molecular-weight complex, the presence of which depended on Abi. Both PIR121 and the GFP-tagged Abi deletion series comigrated with this high-molecular-weight complex, confirming that it was the

intact SCAR complex (data not shown; see Fig. S2 in the supplemental material). Neither monomeric nor complexed SCAR was detected in *abiA*-null strains in native PAGE, which is unsurprising, considering the low sensitivity of the method and the small amount of residual SCAR that is present when *abiA* is deleted. Also of note was the significant band shift in the intact complexes that had lost the C-terminal polyproline domain of Abi. Since Abi does not contribute a large amount to the total mass of the SCAR complex, it is likely that truncation of the disordered polyproline tail allows more efficient passage of the complex through the gel during electrophoresis.

In summary, we were successfully able to delete 239 of the 332 total amino acids comprising *Dictyostelium* Abi and still retain SCAR complex integrity. For the first time, we were in a position to interrogate the contribution of an individual complex member to the activity of the whole. With this in mind, we sought to determine if our Abi constructs restored every aspect of the wild-type SCAR complex in *abiA*-null cells with the aim of identifying functions that could be specifically attributed to Abi.

Abi deletion series rescues the growth defect of *abiA*-null cells in proportion to SCAR stabilization. The SCAR complex is required for the optimal growth of *Dictyostelium discoideum* in liquid medium, presumably due to its involvement in macropinocytosis (22). Therefore, having restored the SCAR protein to wild-type levels, we next sought to determine if the truncated Abi
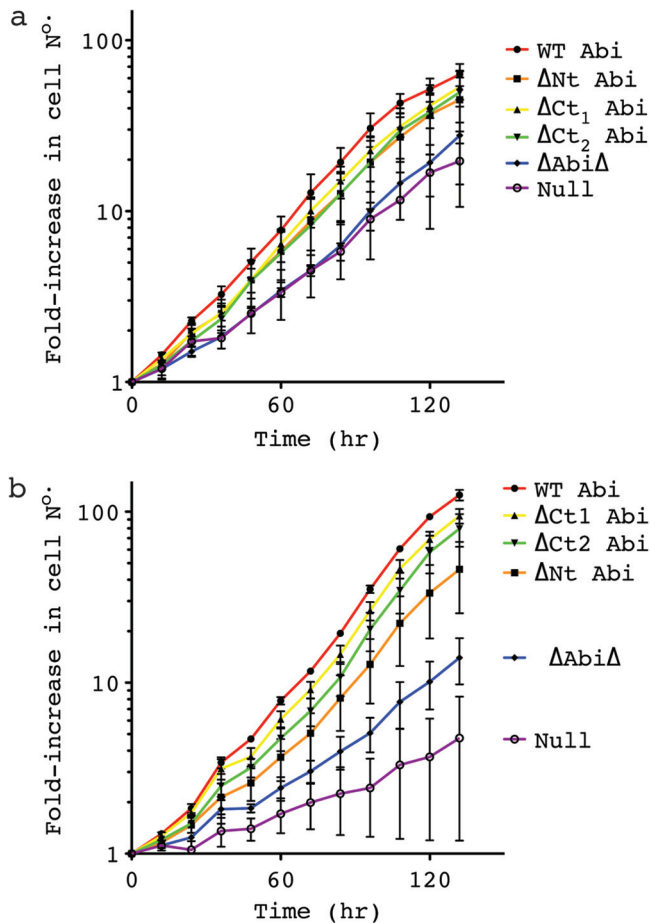
FIG 3 Truncated Abi proteins rescue the growth defect of *abiA*-null cells. (a, b) Growth curves corresponding to transformants cultured on a petri dish (a) or in shaking suspension (b). A cell count was performed every 12 h, and the fold increase was calculated and plotted. Error bars indicate SEMs. WT, full-length Abi; ΔNt, N-terminally truncated Abi; ΔCt₁ and ΔCt₂, C-terminally truncated Abi as shown in Fig. 1c; ΔAbiΔ, combination of both N-terminally and C-terminally truncated Abi; Null, HSPC300-GFP-only vector.

constructs were also capable of rescuing the growth impairment of these cells. As can be seen from Fig. 3a, ΔNt Abi, ΔCt₁ Abi, and ΔCt₂ Abi all restored growth on substrate to a rate comparable to that of *abiA*-null cells rescued with full-length Abi. ΔAbiΔ did not significantly improve the growth of *abiA*-null cells in petri dishes. However, partial rescue was difficult to observe under these conditions, as the defect is relatively small. As shown in Fig. 3b, growth in suspension exacerbated the growth defect of the *abiA*-null cells and revealed an intermediate phenotype of cells rescued with ΔAbiΔ. Under these conditions, cells rescued with ΔAbiΔ doubled significantly more slowly than cells rescued with WT Abi (by 13.9 ± 3.9 h; unpaired *t* test, $P < 0.05$). The severe growth defect of the *abiA*-null cells in suspension led to uneven growth and made it impractical to calculate a doubling time and perform statistical comparisons. However, it is clear that transformation with ΔAbiΔ consistently improved the growth of *abiA*-null cells in suspension.

We have thus demonstrated that loss of either terminus of Abi has no detrimental effect on cell growth. Furthermore, since ΔAbiΔ partially restored SCAR levels and partially restored

growth, the extent to which the growth defect of the *abiA*-null cells was rescued appeared to simply correlate with the SCAR protein levels in these cells. We infer that Abi contributes little to cell growth beyond stabilization of the SCAR complex. This result implies that even when lacking a large proportion of the Abi sequence, the SCAR complex still retains sufficient functionality to support optimal growth and so argues against a central role for Abi in complex recruitment and activation.

This prompted us to investigate the subcellular localization and dynamics of our mutant SCAR complexes, with particular interest in their ability to drive pseudopod extension.

SCAR complex containing truncated Abi localizes normally in migrating cells. Coexpression of GFP-tagged complex member HSPC300 alongside the Abi fragments identified as described above in an *abiA*-null background allowed the localization of the respective mutant complexes to be determined. When visualized by TIRF microscopy, which illuminates only the bottom ~100 nm of a cell, HSPC300-GFP was seen to localize strongly to the leading edge of migrating wild-type cells, correlating with pseudopod extension. No obvious differences in SCAR complex dynamics were observed between any of the Abi fragments and full-length Abi, which all showed robust concentrations of the complex at the leading edge of randomly migrating cells (Fig. 4a; see Movie S1 in the supplemental material). This was accompanied by the smooth extension of cellular protrusions, as illustrated by the kymographs in Fig. 4b. The HSPC300-GFP recruitment was weaker in cells expressing ΔAbiΔ, and they were also more prone to outbreaks of blebbing. Both observations are consistent with there being reduced levels of SCAR in these cells (23). However, SCAR complex-driven pseudopodia were also clearly evident, although the rate of protrusion was seen to be significantly decreased (unpaired *t* test, $P < 0.05$) compared to that of WT Abi-rescued cells (Fig. 4b and c; see Movie S1 in the supplemental material). HSPC300-GFP was essentially completely delocalized in *abiA*-null cells transformed with HSPC300-GFP alone. These cells almost exclusively moved by means of blebbing (Fig. 4b) and rarely extended anything that could be classified as a pseudopod. This was reflected in a significant reduction in the protrusion rate of ~30% compared to that of WT Abi-expressing cells (unpaired *t* test, $P < 0.001$; Fig. 4b). The few pseudopodia that were generated were devoid of concentrated HSPC300-GFP (Fig. 4c) and were likely driven by WASP, as we have previously shown in SCAR complex-deficient cells, including *abiA*-null cells (8). All of this implies that not only is the majority of the Abi sequence unnecessary for SCAR complex stabilization but also it is not essential for normal complex localization. Furthermore, since all the transformants were generating the normal diverse range of pseudopodia, which are suppressed in the *abiA*-null cells, it would appear that the majority of Abi is not required for SCAR complex activation or function either.

Deletion of the α1 helix alone confers a multinucleate phenotype. Our lab has previously shown that *Dictyostelium abiA*-null cells have a tendency to become multinucleate due to a failure in cytokinesis (20). Many *Dictyostelium* mutants accumulate multinucleate cells during growth in shaking culture but can resolve such cells when introduced to a substrate by myosin-independent cytokinesis or by the mitosis-independent process of traction-mediated cytofission (24). However, even in the presence of a substrate, *abiA*-null cells often become multinucleate. The *abiA* constructs generated here were tested to determine which deletions could rescue this phenotype. Doubling times were de-
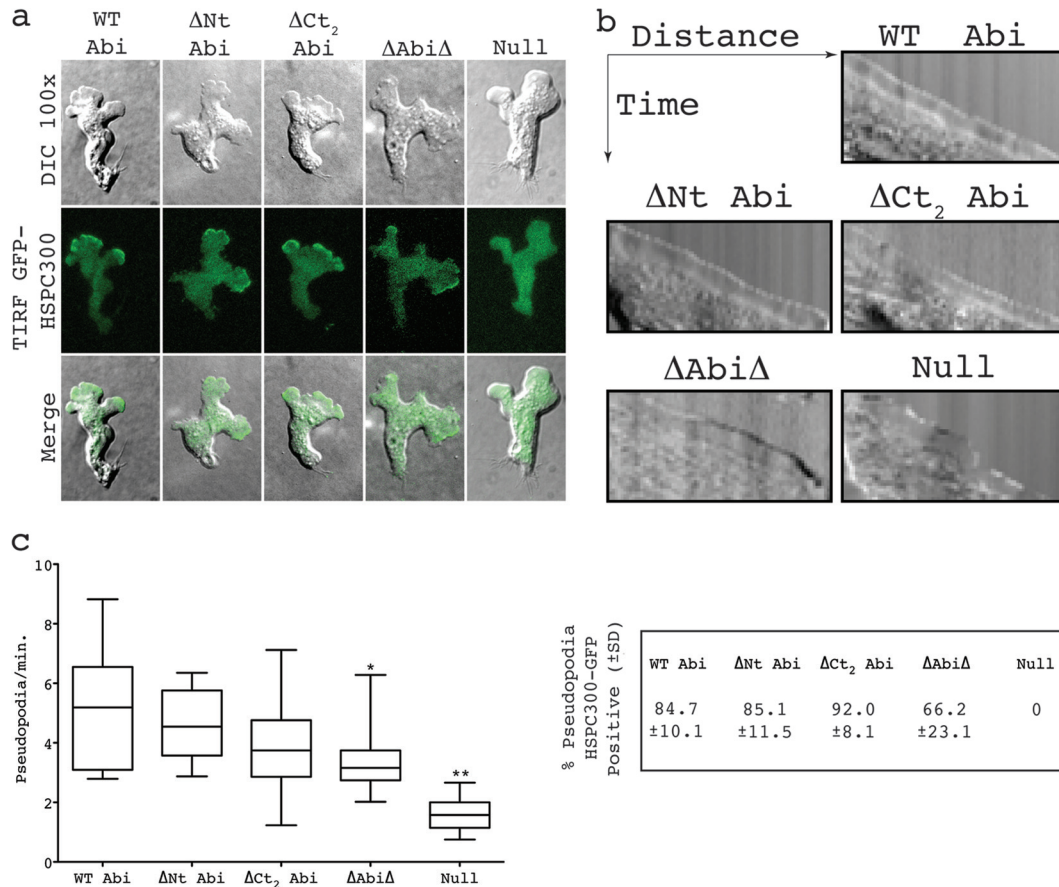
FIG 4 SCAR complexes containing truncated Abi proteins localize normally in migrating cells. (a) Localization of HSPC300-GFP in *abiA*-null cells expressing different Abi fragments. (Top row) DIC images of migrating cells coexpressing Abi-truncated constructs and the SCAR complex marker HSPC300-GFP; (middle row) TIRF images of the same cells revealing localization of mutant SCAR complexes; (bottom row) merged images of the upper two rows. (b) Representative kymographs highlighting smooth progression of advancing protrusions in cells expressing Abi truncations. Null cells present with a ragged slope indicative of blebbing. (c) All truncated Abi proteins rescue the suppressed pseudopod formation of *abiA*-null cells. *, significantly reduced rate of pseudopod formation compared to that for WT Abi-rescued cells (unpaired t test, $P < 0.05$); **, significantly reduced rate of pseudopod formation compared to that for ΔAbiΔ-rescued cells (unpaired t test, $P < 0.001$). The percentages in the box on the right indicate the proportion of pseudopodia with robust HSPC300-GFP localization $\pm$ SD. WT Abi, full-length Abi; ΔNt, N-terminally truncated Abi; ΔCt$_2$, C-terminally truncated Abi; ΔAbiΔ, combination of both N-terminally and C-terminally truncated Abi; Null, HSPC300-GFP-only vector.

rived from the growth curves shown in Fig. 3a. Cells were plated at a low density and cultured for 10 divisions. Following this, the cells were then fixed and stained with DAPI to visualize the nuclei and with Texas Red phalloidin for actin so as to clearly define the cell boundaries (Fig. 5a). The number of nuclei per cell was then counted, and the proportion of multinucleate cells for each of the transformants is shown in Fig. 5b. Cells with ≥ 2 nuclei were rarely seen in *abiA*-null cells rescued with full-length Abi or Abi lacking the C-terminal polyproline tail. The vast majority of these cells were mononucleate, with only a small population of cells having ≥ 2 nuclei (12 and 7% of the total, respectively). As has been previously documented, the *abiA*-null cells expressing only HSPC300-GFP accumulated multinucleate cells, with a significant increase in the number of cells with ≥ 2 nuclei compared to that for the WT Abi controls (26%; chi-squared test, $P < 0.0001$) being detected. Furthermore, there were also more severely multinucleate cells present, including some with as many as 10 nuclei per cell (Fig. 5b). Surprisingly, deletion of the N-terminal α1 helix resulted in a significant increase in the number of cells with ≥ 2 nuclei (42%) even compared to the number of *abiA*-null cells

(chi-square test, $P < 0.0001$). This was also true of ΔAbiΔ-expressing cells (39% of cells with ≥ 2 nuclei). Again, this proved to be a significant increase compared to the results for both the WT Abi controls and the *abiA*-null cells (chi-square test, $P < 0.0001$ and $P < 0.01$, respectively), although there was no statistically significant difference compared to the results for the ΔNt Abi-expressing cells (chi-square test, $P = 0.36$). The different severity in the phenotype observed between the *abiA*-null cells and the ΔAbiΔ- and ΔNt Abi-expressing cells correlates with the increasing SCAR levels in these cells (Fig. 2a and b) and, therefore, presumably, an increasing amount of deregulated SCAR complex.

These data are consistent with our lab's previous conclusion that it is the remaining SCAR in the *abiA*-null cells that is responsible for its multinuclearity. The data presented here identify the α1 helix of Abi as being important for the regulation of the SCAR complex during cytokinesis.

DISCUSSION

Abi is considered a key component of the SCAR complex that is thought to control its activation by acting as a target for phosphor-

SCAR/WAVE

A complex issue

Andrew J Davidson* and Robert H Insall*

The Beatson Institute for Cancer Research; Glasgow, UK

The SCAR/WAVE complex drives the actin polymerisation that underlies protrusion of the front of the cell and thus drives migration. However, it is not understood how the activity of SCAR/WAVE is regulated to generate the infinite range of cellular shape changes observed during cell motility. What are the relative roles of the subunits of the SCAR/WAVE complex? What signaling molecules do they interact with? And how does the complex integrate all this information in order to control the temporal and spatial polymerisation of actin during protrusion formation? Unfortunately, the interdependence of SCAR complex members has made genetic dissection hard. In our recent paper,[1] we describe stabilization of the *Dictyostelium* SCAR complex by a small fragment of Abi. Here we summarize the main findings and discuss how this approach can help reveal the inner workings of this impenetrable complex.

The SCAR/WAVE Complex and its inputs

The highly conserved SCAR complex (also called the "WAVE complex") causes actin-based protrusion during cell migration in a diverse range of eukaryotes including the amoeba *Dictyostelium discoideum*, *Drosophila melanogaster*, and mammalian cells.[2-4] SCAR/WAVE is a WASP family member that induces actin nucleation via recruitment and activation of the Arp2/3 complex.[5,6] In vivo, SCAR activity is regulated by its inclusion within a ~400 kDa regulatory complex consisting of PIR121, Nap1, HSPC300, and Abi.[7-9] This regulatory complex undoubtedly acts as a

signaling hub, where competing inputs are integrated and coupled to the activation of SCAR. However, we still lack even a basic knowledge of what the complex interacts with, never mind how such possible interactions are interpreted and translated into actin polymerisation, motility, and chemotaxis.[10] Confusingly, WASP, which lacks the regulatory complex, can respond to many of the same inputs.[2]

The different roles of SCAR complex members

The recent resolution of the human SCAR complex crystal structure has greatly advanced our understanding of how these proteins interact with SCAR and one another.[11,12] However, the relative contribution of the individual complex members to the activity of the whole remains poorly understood and still awaits elucidation.

Thus far, it has been established that the SCAR complex interacts with its best-known activator, Rac, via PIR121.[11,13] As highlighted in **Figure 1**, Abi has been implicated in the recruitment of the SCAR complex to signaling complexes containing Rac.[14] Furthermore, multiple, stimulus-responsive phosphorylation sites have also been identified across the different SCAR complex members.[15]

In vivo, SCAR is entirely dependent on its regulatory complex for stability, and in the absence of any one complex member, SCAR is rapidly degraded.[3,16] Herein lies the problem that has confounded the study of the individual SCAR complex members: the inability to separate the function of the individual complex members from their requirement for complex stability.

Figure 1. The role of Abi within the SCAR complex. The SCAR complex is composed of PIR121 (blue), Nap1 (green), HSPC300 (hidden in this image), SCAR (magenta), and Abi (orange). The SCAR complex promotes activation of the Arp2/3 complex (magenta arrow). Abi has long been considered a key regulator of the SCAR complex. In combination with the Rac/PIR121 interaction (blue arrow), Abi was thought to activate actin polymerization by coupling SCAR to various signaling and adaptor proteins (orange arrows) via its C-terminal SH3 domain (metazoans only) and polyproline tail (dashed ribbons). However, having deleted the majority of *Dictyostelium* Abi, it is now evident that Abi is not required for SCAR complex activation. Instead, Abi likely acts to tune the activity of the SCAR by integrating both positive and negative signals (dashed lines). One possible negative input could be acting through the N-terminal first α-helix to suppress SCAR activity during mitosis. However, the regulators that bind this domain have yet to be identified.

Numerous studies have endeavored to replace different SCAR complex members with mutant or truncated proteins in order to determine their function.[17,18] However, all too often, the effect on complex stability has been ignored.

Most of Abi is dispensable

Previously, our lab has characterized the individual SCAR complex member gene disruptants in *Dictyostelium discoideum*.[16,19-21] These mutants typically exhibit a *scr*A null phenotype due to the degradation of SCAR. We reasoned that if SCAR complex stability could be restored in the different SCAR complex member nulls, we could finally address the relative role of these proteins to the activity of the complex as a whole. In particular we sought to identify functional domains required for normal SCAR complex recruitment and activity. To achieve this, we set about generating a deletion series of the *Dictyostelium* PIR121, Nap1, and Abi with the objective of identifying minimal fragments of these proteins that could stabilize the complex. This would enable us to assign specific functions to the absent domains. Incremental truncation of both PIR121 and Nap1 failed to yield any fragments that could stabilize SCAR. Although not available at

the time, the SCAR complex crystal structure subsequently revealed the highly convoluted conformation of both PIR121 and Nap1 within the complex, which undoubtedly underlies the failure of this approach in theses cases.

In contrast, in our recent paper we demonstrated that we could successfully delete 239 of the 332 amino acids comprising Abi and retain both SCAR and SCAR complex stability in the *Dictyostelium abi*A null.[1] Surprisingly, we found that none of this sequence was necessary for robust recruitment of the SCAR complex to the tips of pseudopodia. The suppressed rate of pseudopod formation in the *abi*A null was also restored, implying that the majority of Abi sequence is not required for SCAR complex activation either. Although the N-terminus of Abi was specifically involved in regulating the SCAR complex during cytokinesis, apparently negatively, we could find no phenotype associated with a loss of the C-terminal polyproline tail.

What is the true role of Abi within the SCAR complex?

As summarized in **Figure 1**, it was concluded that SCAR complex localization and activity do not depend on any signals that are transduced through Abi.[1] Instead,

we suggest that Abi serves to modulate the activity of SCAR, particularly during events such as cytokinesis. Despite low detailed amino acid identity, a C-terminal polyproline tail is a consistent feature of almost all Abi homologs, which implies that the polyproline domain does have a universal role in the regulation of the SCAR complex. We propose it acts as a non-essential signal integrator that tunes the activity of the SCAR complex after it has been activated by alternate pathways.

Such a role is consistent with the evolutionary recent acquisition of a C-terminal SH3 domain found in metazoan Abi homologs. Even though this domain has been implicated in the regulation of the mammalian SCAR complex, it is not required for SCAR complex recruitment during actin-based protrusion.[14,22]

The attainment of multicellularity in metazoa has been accompanied with a huge increase in regulatory complexity, and cells within a tissue have very different requirements of the SCAR complex in comparison to free-living amoeba. For example, unlike amoebae that are constantly on the move, metazoan cells within a tissue presumably suppress SCAR complex activity until it is required during carefully choreographed events. We propose that Abi is the obvious candidate for

the application of these additional layers of control.

Future directions and conclusions

Although deletion series analysis allowed us to explore the role of Abi within the SCAR complex, this has proved too crude a method to similarly investigate the function of the other complex members such as PIR121 and Nap1. We believe a subtler approach will be required to mutate these complex members while preserving complex stability. For instance, our lab has recently successfully used phosphomimetic mutation to study the activation of SCAR.[23] Few phosphosites have been identified within PIR121 and Nap1. PIR121 and Nap1 are also both so large that systematic alanine scanning mutagenesis is a daunting prospect. However, given the fragility of the SCAR complex, it may prove the only available option.

The intricacy of the SCAR complex continues to block investigation from every angle, and as a result we have barely scratched the surface of how these proteins collectively function. Despite the difficulty, we believe that genetic approaches could still offer the key to unlocking the secrets of the SCAR complex.

Disclosure of Potential Conflicts of Interest

No potential conflicts of interest were disclosed.

References

1. Davidson AJ, Ura S, Thomason PA, Kalna G, Insall RH. Abi is required for modulation and stability of the SCAR/WAVE complex, but not localization or activity. Eukaryot Cell 2013; 12:1509-16; PMID:24036345; http://dx.doi.org/10.1128/EC.00116-13

2. Veltman DM, King JS, Machesky LM, Insall RH. SCAR knockouts in Dictyostelium: WASP assumes SCAR's position and upstream regulators in pseudopods. J Cell Biol 2012; 198:501-8; PMID:22891261; http://dx.doi.org/10.1083/jcb.201205058

3. Kunda P, Craig G, Dominguez V, Baum B. Abi, Sra1, and Kette control the stability and localization of SCAR/WAVE to regulate the formation of actin-based protrusions. Curr Biol 2003; 13:1867-75; PMID:14588242; http://dx.doi.org/10.1016/j.cub.2003.10.005

4. Hahne P, Sechi A, Benesch S, Small JV. Scar/WAVE is localised at the tips of protruding lamellipodia in living cells. FEBS Lett 2001; 492:215-20; PMID:11257497; http://dx.doi.org/10.1016/S0014-5793(01)02239-6

5. Machesky LM, Insall RH. Scar1 and the related Wiskott-Aldrich syndrome protein, WASP, regulate the actin cytoskeleton through the Arp2/3 complex. Curr Biol 1998; 8:1347-56; PMID:9889097; http://dx.doi.org/10.1016/S0960-9822(98)00015-3

6. Machesky LM, Mullins RD, Higgs HN, Kaiser DA, Blanchoin L, May RC, Hall ME, Pollard TD. Scar, a WASp-related protein, activates nucleation of actin filaments by the Arp2/3 complex. Proc Natl Acad Sci U S A 1999; 96:3739-44; PMID:10097107; http://dx.doi.org/10.1073/pnas.96.7.3739

7. Eden S, Rohatgi R, Podtelejnikov AV, Mann M, Kirschner MW. Mechanism of regulation of WAVE1-induced actin nucleation by Rac1 and Nck. Nature 2002; 418:790-3; PMID:12181570; http://dx.doi.org/10.1038/nature00859

8. Ismail AM, Padrick SB, Chen B, Umetani J, Rosen MK. The WAVE regulatory complex is inhibited. Nat Struct Mol Biol 2009; 16:561-3; PMID:19363480; http://dx.doi.org/10.1038/nsmb.1587

9. Pollitt AY, Insall RH. WASP and SCAR/WAVE proteins: the drivers of actin assembly. J Cell Sci 2009; 122:2575-8; PMID:19625501; http://dx.doi.org/10.1242/jcs.023879

10. Insall RH. Understanding eukaryotic chemotaxis: a pseudopod-centred view. Nat Rev Mol Cell Biol 2010; 11:453-8; PMID:20445546; http://dx.doi.org/10.1038/nrm2905

11. Chen Z, Borek D, Padrick SB, Gomez TS, Metlagel Z, Ismail AM, Umetani J, Billadeau DD, Otwinowski Z, Rosen MK. Structure and control of the actin regulatory WAVE complex. Nature 2010; 468:533-8; PMID:21107423; http://dx.doi.org/10.1038/nature09623

12. Davidson AJ, Insall RH. Actin-based motility: WAVE regulatory complex structure reopens old SCARs. Curr Biol 2011; 21:R66-8; PMID:21256435; http://dx.doi.org/10.1016/j.cub.2010.12.001

13. Kobayashi K, Kuroda S, Fukata M, Nakamura T, Nagase T, Nomura N, Matsuura Y, Yoshida-Kubomura N, Iwamatsu A, Kaibuchi K. p140Sra-1 (specifically Rac1-associated protein) is a novel specific target for Rac1 small GTPase. J Biol Chem 1998; 273:291-5; PMID:9417078; http://dx.doi.org/10.1074/jbc.273.1.291

14. Innocenti M, Frittoli E, Ponzanelli I, Falck JR, Brachmann SM, Di Fiore PP, Scita G. Phosphoinositide 3-kinase activates Rac by entering in a complex with Eps8, Abi1, and Sos-1. J Cell Biol 2003; 160:17-23; PMID:12515821; http://dx.doi.org/10.1083/jcb.200206079

15. Lebensohn AM, Kirschner MW. Activation of the WAVE complex by coincident signals controls actin assembly. Mol Cell 2009; 36:512-24; PMID:19917258; http://dx.doi.org/10.1016/j.molcel.2009.10.024

16. Ibarra N, Blagg SL, Vazquez F, Insall RH. Nap1 regulates Dictyostelium cell motility and adhesion through SCAR-dependent and – independent pathways. Curr Biol 2006; 16:717-22; PMID:16581519; http://dx.doi.org/10.1016/j.cub.2006.02.068

17. Leng Y, Zhang J, Badour K, Arpaia E, Freeman S, Cheung P, Siu M, Siminovitch K. Abelson-interactor-1 promotes WAVE2 membrane translocation and Abelson-mediated tyrosine phosphorylation required for WAVE2 activation. Proc Natl Acad Sci U S A 2005; 102:1098-103; PMID:15657136; http://dx.doi.org/10.1073/pnas.0409120102

18. Ring C, Ginsberg MH, Haling J, Pendergast AM. Abl-interactor-1 (Abi1) has a role in cardiovascular and placental development and is a binding partner of the alpha4 integrin. Proc Natl Acad Sci U S A 2011; 108:149-54; PMID:21173240; http://dx.doi.org/10.1073/pnas.1012316108

19. Blagg SL, Stewart M, Sambles C, Insall RH. PIR121 regulates pseudopod dynamics and SCAR activity in Dictyostelium. Curr Biol 2003; 13:1480-7; PMID:12956949; http://dx.doi.org/10.1016/S0960-9822(03)00580-3

20. Pollitt AY, Insall RH. Abi mutants in Dictyostelium reveal specific roles for the SCAR/WAVE complex in cytokinesis. Curr Biol 2008; 18:203-10; PMID:18261908; http://dx.doi.org/10.1016/j.cub.2008.01.026

21. Pollitt AY, Insall RH. Loss of Dictyostelium HSPC300 causes a scar-like phenotype and loss of SCAR protein. BMC Cell Biol 2009; 10:13; PMID:19228419; http://dx.doi.org/10.1186/1471-2121-10-13

22. Stradal T, Courtney KD, Rottner K, Hahne P, Small JV, Pendergast AM. The Abl interactor proteins localize to sites of actin polymerization at the tips of lamellipodia and filopodia. Curr Biol 2001; 11:891-5; PMID:11516653; http://dx.doi.org/10.1016/S0960-9822(01)00239-1

23. Ura S, Pollitt AY, Veltman DM, Morrice NA, Machesky LM, Insall RH. Pseudopod growth and evolution during cell movement is controlled through SCAR/WAVE dephosphorylation. Curr Biol 2012; 22:553-61; PMID:22386315; http://dx.doi.org/10.1016/j.cub.2012.02.020

Actin-Based Motility: WAVE Regulatory Complex Structure Reopens Old SCARs

The SCAR/WAVE complex controls actin polymerization at the leading edges of moving cells, but its mechanism of regulation remains unclear. The recent determination of its crystal structure, and identification of the binding sites for upstream regulators, mean its workings can finally start to be revealed.

Andrew J. Davidson
and Robert H. Insall

The thrust that drives migration of eukaryotic cells comes from polymerizing actin filaments, which push the front edge of the cell forwards. SCAR/WAVE proteins are central coordinators of this process [1]. They catalyze formation of new actin filaments from actin monomers and the Arp2/3 complex, under tight temporal and spatial control from multiple intracellular signals; without SCAR/WAVE proteins, pseudopods — the actin structures at the heart of migration — are greatly diminished or altogether lost [2,3]. Activators of SCAR/WAVE are known, particularly the small GTPase Rac1, but the mechanisms through which they work are poorly understood. It would be fair to say this is the biggest limitation to current progress in the field. Conversely, full understanding of the regulation of SCAR/WAVE would be the most significant advance in the understanding of cell migration in a generation.

Into this gap rides a new paper by Chen *et al.* [4], featuring a high-resolution structure of WAVE1 and its regulators founded on some masterful protein chemistry [4]. While a complete understanding of SCAR/WAVE regulation is some way away, this work is bound to reinvigorate the field and kickstart efforts to understand the mechanisms underlying SCAR/WAVE activation.

Regulation of WAVE1
WAVE1 is a member of the WASP family of actin-nucleation-promoting factors [5]. For all members of this family, actin polymerization is catalysed by a VCA domain, which is small and always found at the carboxyl terminus [6]. The remainder of each protein is mainly thought to regulate the VCA domain. The founding member of this family, WASP, is regulated by autoinhibition. The VCA domain is sequestered and inactivated by a basic region localised near the amino terminus [7]. Activators of WASP destabilize this interaction, which releases the VCA domain for the nucleation of new actin filaments.

Pure WAVE1 is not autoinhibited [8]. However, *in vivo* it exists in a pentameric complex known as the WAVE regulatory complex (WRC), also comprising Sra1, Nap1, Abi2 and HSPC300 [9] (confusingly each of these proteins is known by several names). This complex has remained mysterious, and whether or not its activity is regulated has been a matter of debate [10]. None of the components contains conserved domains, apart from the VCA domain in WAVE1 and a dispensable Src homology 3 (SH3) domain at the end of Abi2. Sra1 and Nap1 are far larger than WAVE, making the complex very large (>400 kDa), yet few functions are known considering the substantial number and size of the subunits. The WRC is unstable in the absence of any individual member, making it tricky to determine the specific contribution of each subunit [3]. One of the few known functional elements was defined by an *in vitro* interaction between the amino terminus of Sra1 and Rac1, the best known activator of the WRC [11].

Several molecules regulate the WRC alongside Rac1. Negatively charged phospholipids are essential for activation of the complex [12], and protein kinases and adaptor proteins like Nck have also been implicated in the activation of the complex [9,13].

The Structure of the WAVE Regulatory Complex
Earlier impressions of the WRC implied that it had a distinctly linear structure. It was believed (despite genetic evidence to the contrary [14]) that the peripheral Pir121 exclusively bound Nap1, which in turn connected to Abi, thence WAVE and HSPC300 at the end [15].

Now, the crystal structure reported in the new study [4] contradicts this simplistic model (Figure 1A). Abi2 in fact sits at the periphery of the complex, forming a trimer with WAVE1 and HSPC300. This trimer nestles in a dimeric cradle formed by the two large subunits — Sra1 and Nap1 — that is unexpectedly almost symmetrical, suggesting a shared origin in the mists of evolution. The catalytic VCA of WAVE1 sits coiled within a conserved recess of Sra1. Chen *et al.* [4] found that perturbation of this interface resulted in constitutively active WRC *in vitro*, suggesting that Sra1 holds WAVE1 in a sequestered, inactive state. This proposed mechanism of WRC regulation shows obvious parallels with the autoinhibition that controls WASP, suggesting a general mechanism of activation for all WASP family members.

Mechanism of Rac1-Mediated Activation
Purified WRC does not stimulate actin polymerization [10]. It must be activated, in particular by Rac1. Similarly, purified WASP is activated by Cdc42. In this better-understood case, the VCA domain of WASP is released when Cdc42 binds competitively to the autoinhibitory site [7]. Chen *et al.* [4] reasoned that, although WAVE1 is not regulated by autoinhibition in the strict sense, direct or indirect competition of activators with the VCA might be a general mechanism of activation for all WASP family members.

One of the strengths of Chen *et al.* [4] is that it includes a direct measurement of Rac1 binding, which has only previously been implied. The reason is apparent from the data – the affinity is very low ($\sim 8\ \mu M$). However, deletion of the VCA domain of WAVE1 increased the affinity of Rac1 closer to 1 μM, implying that Rac1 binding and VCA domain sequestration are competitive, just as previously measured for WASP.
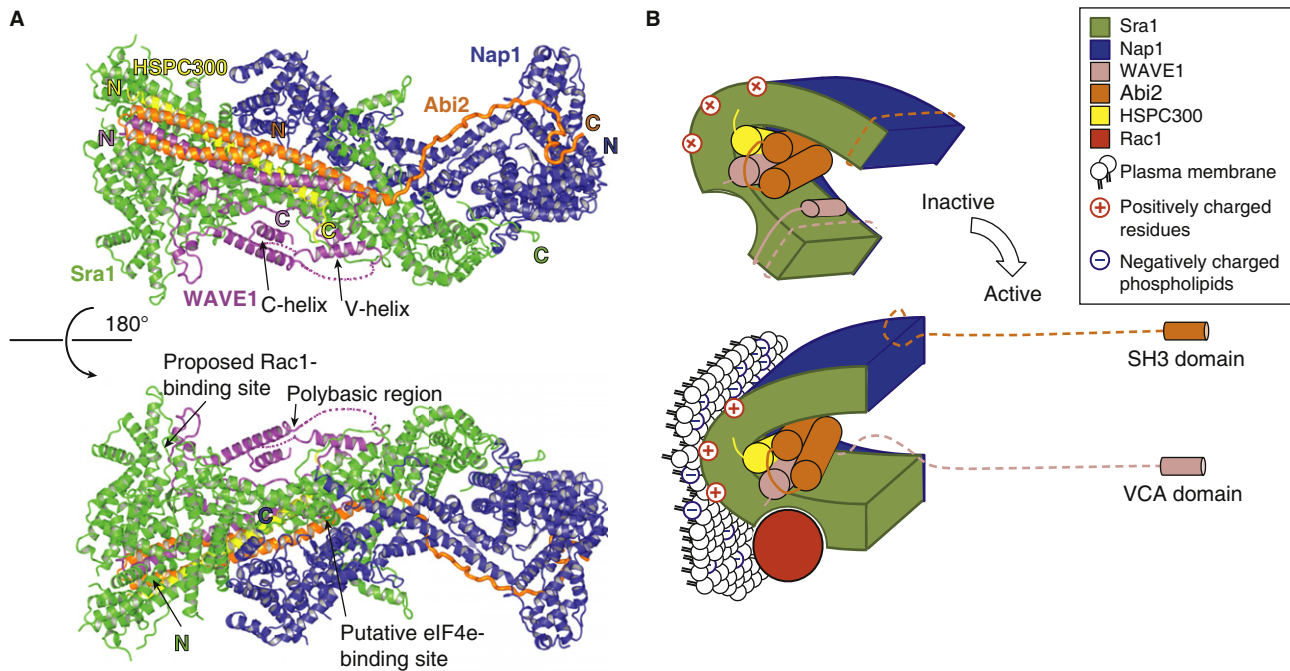
Current Biology

Figure 1. Structure and regulation of the WAVE regulatory complex (WRC).

(A) Structure of the WRC (from [4]). Sra1 (green), Nap1 (blue), HSPC300 (yellow), WAVE1 (magenta) and Abi2 (orange). The complex is complete except for the removal of poly-proline rich regions in WAVE1 and Abi2. In the case of WAVE1, this has been replaced with a short linker (major dashed line). (B) Schematic showing the proposed WRC activation mechanism. Unstimulated WRC sequesters the VCA domain of WAVE1, rendering it inactive. Upon binding of the Sra1 subunit to activated Rac1, the entire WRC is recruited to the plasma membrane and the VCA domain is released from sequestration. The interaction between the positively charged face of the WRC and negatively charged phospholipids in the plasma membrane ensures the VCA domain is oriented in the right way to interact with the actin-polymerizing machinery in the cytoplasm. Proline-rich regions absent from the crystallized WRC are indicated by dashed lines. We speculate that the polyproline regions of Abi2 and WAVE1 may behave in a similar manner, and be freed upon WRC activation to interact with cellular components.

Targeted mutagenesis of Sra1 revealed a Rac1-binding site near the interface with WAVE1's VCA domain. Furthermore, various truncated forms of WAVE1 also led to a decreased affinity for Rac1. Chen et al. [4] conclude that binding of Rac1 to both Sra1 and WAVE1 mediates a conformational change that frees the VCA domain to generate new actin filaments.

Inositol Lipids and Phosphorylation
The members of the WRC, in particular WAVE, are phosphorylated at numerous, physiologically essential sites [16]. Two tyrosines in WAVE1, Tyr125 and Tyr151, are particularly well situated to exert control over the release of the VCA. Chen et al. [4] found that cells expressing phosphomimetic mutations of these tyrosines formed more lamellipodia, suggesting that the mutations indeed cause constitutive activation of the WRC.

The other well-documented activator of SCAR/WAVE activity is negatively charged lipids, in particular inositol phospholipids [12]. Chen et al. [4] mapped the distribution of charge over the surface of the entire WRC, revealing two oppositely charged faces, which the authors suggest aids orientation of the complex at the membrane. They go on to propose that acidic phospholipids cooperate with Rac1 to recruit the WRC to the membrane by binding to its positive face. The negatively charged face is thus pointed away from the membrane, allowing the VCA domain to project into the cytoplasm where actin nucleation is required (Figure 1B). This model fits well with the structure, but implies a relative lack of specificity for particular lipids — phosphatidylinositol (4,5) bisphosphate and even phosphatidylserine are far more appropriate candidates than phosphatidylinositol (3,4,5) triphosphate (PIP_3), in particular, which has been thought to be a key SCAR/WAVE activator [17]. Although highly charged, PIP_3 at low levels contributes relatively little to the total charge of the membrane, and acts more effectively on specific targets like pleckstrin homology domains. This analysis also suggests that lipids play a permissive, rather than a prescriptive role in WRC activation [18].

Remaining Issues
The paper by Chen et al. [4] is undoubtedly a great step forward in understanding how SCAR/WAVE and the WRC work. Like all such advances, it poses many more questions. Exactly how Rac1 binding is translated into VCA release remains to be answered. Furthermore, mutations in the proposed binding site only reduce the affinity of the VCA-deleted WRC for Rac1 from about 1 μM to about 8 μM, in other words returning it to the affinity of the intact complex. However, the fact that wild-type WRC appears to have such low affinity for its activator may also suggest the involvement of other co-factors in vivo. Some complicating issue, perhaps a second binding site, remains to be discovered. Secondly,

there is no indication whether the measured interactions are specific to active, GTP-bound Rac1. This is a key issue; the inactive GDP-bound forms of Rac1 are usually just that — inactive — so the differences between the interactions of the WRC with GDP- and GTP-bound forms will be crucial. And finally, the role of phosphorylation is merely touched upon. It is certain to be more complicated and wide-ranging than can be analyzed in a single paper — but the structure is a crucial starting point.

One interesting and ongoing point is that the function of the majority of the WRC is still unaccounted for. The recombinant complex used to resolve the structure is a masterpiece of protein chemistry, but the large polyproline-rich domains in the carboxyl termini of WAVE1 and Abi2 had to be removed to aid crystallization. The existence of polyproline domains is highly conserved — WAVE1's domains are also seen in all other WASP family members — and thus probably physiologically important. These domains are likely to form extended, unstructured arms that increase the effective size of the complex. Nearly half of Abi2, including an SH3 domain that is important in metazoans but not more distant organisms [19], is absent. The remainder of Abi2 transverses the entire width of the complex, potentially allowing the unseen carboxyl terminus to protrude near the bulk of Nap1.

This leads to the biggest mystery, the function of Nap1. Chen *et al.* [4] like most authors, portray this essential component of the WRC as a structural scaffold. However, it is not only very large, but conserved throughout is length from mammals to *Dictyostelium* and plants [20], implying a more central and specific role. Its conservation is curious, given its apparent separation from the action around Sra1 and the VCA domain, but this just goes to emphasize that the regulation of SCAR/WAVE still holds many secrets.

The structure of the WRC is not the end, or even the beginning of the end, as Winston Churchill said, of understanding how cells make actin protrusions. It is, perhaps, the end of the beginning. The physical arrangement of the subunits and a plausible mechanism for regulation by Rac1 represent a great step forward, but above all they make the prospects for future advances seem much clearer.

References
1. Insall, R.H., and Machesky, L.M. (2009). Actin dynamics at the leading edge: from simple machinery to complex networks. Dev. Cell *17*, 310–322.
2. Steffen, A., Rottner, K., Ehinger, J., Innocenti, M., Scita, G., Wehland, J., and Stradal, T.E. (2004). Sra-1 and Nap1 link Rac to actin assembly driving lamellipodia formation. EMBO J. *23*, 749–759.
3. Kunda, P., Craig, G., Dominguez, V., and Baum, B. (2003). Abi, Sra1, and Kette control the stability and localization of SCAR/WAVE to regulate the formation of actin-based protrusions. Curr. Biol. *13*, 1867–1875.
4. Chen, Z., Borek, D., Padrick, S.B., Gomez, T.S., Metagel, Z., Ismail, A., Umetani, J., Billadeau, D.D., Otwinowski, Z., and Rosen, M.K. (2010). Structure and control of the actin regulatory WAVE complex. Nature *468*, 533–538.
5. Machesky, L.M., and Insall, R.H. (1998). Scar1 and the related Wiskott-Aldrich syndrome protein, WASP, regulate the actin cytoskeleton through the Arp2/3 complex. Curr. Biol. *8*, 1347–1356.
6. Amann, K.J., and Pollard, T.D. (2001). Direct real-time observation of actin filament branching mediated by Arp2/3 complex using total internal reflection fluorescence microscopy. Proc. Natl. Acad. Sci. USA *98*, 15009–15013.
7. Kim, A.S., Kakalis, L.T., Abdul-Manan, N., Liu, G.A., and Rosen, M.K. (2000). Autoinhibition and activation mechanisms of the Wiskott-Aldrich syndrome protein. Nature *404*, 151–158.
8. Machesky, L.M., Mullins, R.D., Higgs, H.N., Kaiser, D.A., Blanchoin, L., May, R.C., Hall, M.E., and Pollard, T.D. (1999). Scar, a WASp-related protein, activates nucleation of actin filaments by the Arp2/3 complex. Proc. Natl. Acad. Sci. USA *96*, 3739–3744.
9. Eden, S., Rohatgi, R., Podtelejnikov, A.V., Mann, M., and Kirschner, M.W. (2002). Mechanism of regulation of WAVE1-induced actin nucleation by Rac1 and Nck. Nature *418*, 790–793.
10. Ismail, A.M., Padrick, S.B., Chen, B., Umetani, J., and Rosen, M.K. (2009). The WAVE regulatory complex is inhibited. Nat. Struct. Mol. Biol. *16*, 561–563.
11. Kobayashi, K., Kuroda, S., Fukata, M., Nakamura, T., Nagase, T., Nomura, N., Matsuura, Y., Yoshida-Kubomura, N., Iwamatsu, A., and Kaibuchi, K. (1998). p140Sra-1 (specifically Rac1-associated protein) is a novel specific target for Rac1 small GTPase. J. Biol. Chem. *273*, 291–295.
12. Lebensohn, A.M., and Kirschner, M.W. (2009). Activation of the WAVE complex by coincident signals controls actin assembly. Mol. Cell *36*, 512–524.
13. Rogers, S.L., Wiedemann, U., Stuurman, N., and Vale, R.D. (2003). Molecular requirements for actin-based lamella formation in Drosophila S2 cells. J. Cell Biol. *162*, 1079–1088.
14. Pollitt, A.Y., and Insall, R.H. (2008). Abi mutants in Dictyostelium reveal specific roles for the SCAR/WAVE complex in cytokinesis. Curr. Biol. *18*, 203–210.
15. Gautreau, A., Ho, H.Y., Li, J., Steen, H., Gygi, S.P., and Kirschner, M.W. (2004). Purification and architecture of the ubiquitous Wave complex. Proc. Natl. Acad. Sci. USA *101*, 4379–4383.
16. Pocha, S.M., and Cory, G.O. (2009). WAVE2 is regulated by multiple phosphorylation events within its VCA domain. Cell Motil. Cytoskeleton *66*, 36–47.
17. Oikawa, T., Yamaguchi, H., Itoh, T., Kato, M., Ijuin, T., Yamazaki, D., Suetsugu, S., and Takenawa, T. (2004). PtdIns(3,4,5)P3 binding is necessary for WAVE2-induced formation of lamellipodia. Nat. Cell Biol. *6*, 420–426.
18. Insall, R.H., and Weiner, O.D. (2001). PIP3, PIP2, and cell movement–similar messages, different meanings? Dev. Cell *1*, 743–747.
19. Veltman, D.M., and Insall, R.H. (2010). WASP family proteins: their evolution and its physiological implications. Mol. Biol. Cell *21*, 2880–2893.
20. Ibarra, N., Blagg, S.L., Vazquez, F., and Insall, R.H. (2006). Nap1 regulates Dictyostelium cell motility and adhesion through SCAR-dependent and -independent pathways. Curr. Biol. *16*, 717–722.

CR-UK Beatson Institute, Bearsden, Glasgow G61 1BD, UK.
E-mail: A.Davidson@beatson.gla.ac.uk, Robert.Insall@glasgow.ac.uk

Protein Dynamics: Moore's Law in Molecular Biology

The millisecond barrier has been broken in molecular dynamics simulations of proteins. Such simulations are increasingly revealing the inner workings of biological systems by generating atomic-level descriptions of their behaviour that make testable predictions about key molecular processes.

Michele Vendruscolo
and Christopher M. Dobson

A fundamental understanding of the manner in which a protein molecule functions depends on a detailed knowledge of not just its structure but also its dynamical behaviour [1]. As molecular dynamics simulations carried out on modern computers make it possible to solve the equations that describe the motion of molecular systems [2], they are a supremely powerful way of providing information at atomic resolution about the way in which protein molecules move and interact with their environments [3]. Indeed, after the initial report of the first application of molecular dynamics simulations to studying the structural